Université d'Ottawa · University of Ottawa

PERMISSION DE REPRODUIRE ET DE DISTRIBUER LA THÈSE

PERMISSION TO REPRODUCE AND DISTRIBUTE THE THESIS

NOM DE L'AUTEUR / NAME OF AUTHOR:	Jason Carey
ADRESSE POSTALE / MAILING ADDRESS:	1407-190 Lees Avenue Ottawa, Ontario K1S 5L5
GRADE / DEGREE:	**ANNÉE D'OBTENTION / YEAR GRANTED**
Ph.D - Mechanical Engineering	2003
TITRE DE LA THÈSE / TITLE OF THESIS: Axial, Flexural and Torsional Rigidities of 2D Braided Fibre Composite Medical Catheters	

L'auteur permet, par la présente, la consultation et le prêt de cette thèse en conformité avec les règlements établis par le bibliothécaire en chef de l'Université d'Ottawa. L'auteur autorise aussi l'Université d'Ottawa, ses successeurs et cessionnaires, à reproduire cet exemplaire par photograhie ou photocopie pour fins de prêt ou de vente au prix coûtant aux bibliothèques ou aux chercheurs qui en feront la demande.

Les droits de publication par tout autre moyen et pour vente au public demeureront la propriété de l'auteur de la thèse sous réserve des règlements de l'Université d'Ottawa en matière de publication de thèses.

The author hereby permits the consultation and the lending of this thesis pursuant to the regulations established by the Chief Librarian of the University of Ottawa. The author also authorizes the University of Ottawa, its successors and assignees, to make reproductions of this copy by photographic means or by photocopying and to lend or sell such reproductions at cost to libraries and to scholars requesting them.

The right to publish the thesis by other means and to sell it to the public is reserved to the author, subject to the regulations of the University of Ottawa governing the publication of theses.

N.B. LE MASCULIN COMPREND ÉGALEMENT LE FÉMININ

06/05/03
DATE

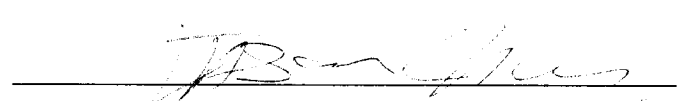
(AUTEUR) SIGNATURE (AUTHOR)

Université d'Ottawa · University of Ottawa

Université d'Ottawa · University of Ottawa

FACULTÉ DES ÉTUDES SUPÉRIEURES ET POSTDOCTORALES

FACULTY OF GRADUATE AND POSTDOCTORAL STUDIES

CAREY, Jason

AUTEUR DE LA THÈSE - AUTHOR OF THESIS

Ph.D. (Mechanical Engineering)

GRADE - DEGREE

Mechanical Engineering

FACULTÉ, ÉCOLE, DÉPARTEMENT - FACULTY, SCHOOL, DEPARTMENT

TITRE DE LA THÈSE - TITLE OF THE THESIS

Axial, Flexural and Torsional Rigidities of 2D Braided Fibre Composite Medical Catheters

Michael Munro and Atef Fahim

DIRECTEUR DE LA THÈSE - THESIS SUPERVISOR

EXAMINATEURS DE LA THÈSE - THESIS EXAMINERS

J. Cameron

M. Liang

D. Redekop

P. Straznicky

J.-M. De Koninck, Ph.D.

LE DOYEN DE LA FACULTÉ DES ÉTUDES SUPÉRIEURES ET POSTDOCTORALES

SIGNATURE

DEAN OF THE FACULTY OF GRADUATE AND POSTDOCTORAL STUDIES

Axial, Flexural and Torsional Rigidities of 2D Braided Fibre Composite Medical Catheters

by

Jason Carey

Thesis submitted to the
Faculty of Graduate and Postdoctoral Studies
in partial fulfillment of the requirements to the degree of

Doctor of Philosophy

Ottawa-Carleton Institute for Mechanical and Aerospace Engineering

Department of Mechanical Engineering
University of Ottawa

Axial, Flexural and Torsional Rigidities of 2D Braided Fibre Composite Medical Catheters

Jason Carey
Department of Mechanical Engineering
University of Ottawa

Cardiovascular catheterization is a common medical procedure. A one-piece braided catheter with different rigidities at the proximal and distal end can, if properly designed, provide the control and flexibility required to replace the current catheter-guidewire catheterization procedure. Such a one-piece catheter would shorten the catheterization procedure and improve catheter control.

An analytical model based on classical laminate plate theory was developed to predict the elastic constants of angle-plied, single overlap two-dimensional fibre composite tubular braids that can be used to produce these catheters. The path of undulating strands can be modelled by a variety of shape functions and solved numerically; a sinusoidal function was selected to model the strand path and a Gauss-Legendre numerical integration method was selected for this work. Predictions are in good agreement with other accepted models and experimental results using large (12.5mm diameter) Kevlar 49/epoxy resin tubes for which the laminar properties had been previously determined. There was also good agreement between experimental and predicted results using Kevlar 49/RP 6443 Polyurethane, an elastomeric resin that could be used for manufacturing catheters. Furthermore, the model, using different fibre and resin materials, was used to design braided composite tubes with rigidities similar to existing cardiovascular catheters. These results are encouraging since they validate the model as a tool for designing braided cardiovascular catheters, which are typically, but not restricted to, 1-2 mm in diameter.

In addition to the catheter work, regression-based practical design equations were developed to predict the elastic moduli of angle-plied composites. These equations can be used for preliminary design of angle-ply composite materials.

SUMMARY

Medical catheters are widely used medical devices and cardiovascular catheters are one of the major types of medical catheters. Surgeons and radiologists require these devices to be sufficiently stiff for control yet flexible enough to navigate through the tortuous cardiovascular system without causing undue discomfort or trauma to the patient. Currently, a two-piece medical catheter-guidewire system is used during most cardiovascular catheterization procedures.

The development of a one-piece braided model catheter with the same rigidities as the combined medical catheter-guidewire system presently employed during cardiovascular catheterization procedures is the principal goal of this research. This will result in a significant reduction in the time required to insert a cardiovascular catheter. This is also the first and fundamental step in the development of optimal rigidity cardiovascular catheters. To begin, the axial, torsional and flexural rigidities of existing medical catheters were reviewed and measured. A model to predict the longitudinal tensile and in-plane shear moduli of 2D braided structures, needed for the calculations of the axial, torsional and flexural rigidities of braided tubes, was developed. The sensitivity of the model to key constituent and laminar properties was analysed. It was concluded that accurate values of E_{f11}, E_m and G_m are required for the micromechanical model; the model is not sensitive to the remaining elastic constants (ν_{f12}, ν_{f23}, G_{f12}, G_{23}).

Oversized braided (Kevlar 49 fibre and thermoset matrix) engineering model composite structures – or model catheters – have been used to verify the model. These model catheters have been produced on an existing braiding machine. Kevlar 49 fibre and

epoxy resin have been used primarily because the laminar mechanical properties have been measured in a previous experimental study by Flanagan and Munro [72]. There was good agreement (approximately 6 %) between the predicted and measured values of the longitudinal elastic modulus of braided tubes which provided confidence in the model. Shear modulus predictions and the range of experimental results also showed reasonable agreement. The results also show that micromechanical models in which accurate values for important elastic constants (E_{f11}, E_m and G_m) are used can accurately predict the experimental results.

The preceding experimental work was carried out for full coverage rigid thermoset matrix braided fibre composites. Actual medical catheters require flexible matrix and an open fibre mesh rather than full fibre coverage; therefore, it was necessary to select the appropriate matrix and reinforcement for an actual medical catheter. The proposed CLPT model was used to select the appropriate fibre and resin to obtain rigidities similar to those of the existing medical catheter-guidewire systems. Laminar elastic constants were estimated using micromechanical models. The proposed CLPT model reasonably predicted the longitudinal elastic and shear moduli of model catheters produced with one of the selected elastomeric resins. The main objective of the thesis was therefore met.

Also, the sensitivity of the proposed classical laminate plate model to undulation region length was also evaluated because of the importance of open mesh braid configurations for medical catheters. It was found that undulation lengths greater than 5.5 times the strand thickness no longer influenced the properties of the undulation region.

Finally, the proposed CLPT model was simplified for practical engineering applications. The proposed CLPT model that was developed was simplified to simple design equations that predict elastic constants for closed and open mesh braid configurations within 95% and 90% of the proposed CLPT model predictions for the materials used in this study.

RÉSUMÉ

Les cathéters, dont une catégorie principale sont les cathéters cardiovasculaires, sont des instruments médicaux grandement utilisés. Il est nécessaire, autant pour les chirurgiens que les radiologistes, que ces instruments soient suffisamment rigides pour faciliter l'emploi, mais aussi suffisamment flexible pour naviguer au travers d'un système cardiovasculaire tortueux et cela, sans causer d'inconfort supplémentaire au patient. Un système à deux pièces, soit le cathéter et le fil-directeur, est utilisé durant une cathétérisation cardiovasculaire

L'objectif principal de cette recherche est le développement d'un cathéter modèle qui posséderait les mêmes rigidités que le système à deux pièces ; ceci réduirait grandement la durée de la cathétérisation cardiovasculaire. De plus, il est à noter que ceci est l'étape fondamentale dans le développement d'un cathéter cardiovasculaire possédant des caractéristiques optimales. En premier lieu, il fut nécessaire de revoir et d'évaluer la rigidité axiale, de torsion ainsi que de flexion de cathéters médicaux existants. Puis, un modèle analytique fut développé afin de prédire le module d'élasticité longitudinal et le module de cisaillement de structures tressées en deux dimensions. Une étude de sensibilité du modèle fut effectuée pour déterminer l'effet des propriétés d'une lamelle de composite et propriétés des composants de base sur les constantes élastiques de la maille élémentaire tressée. Parmi les propriétés utilisées dans l'analyse, seules des valeurs précises de E_{f11}, E_m et G_m sont nécessaires pour les modèles micromécaniques. Le modèle n'est pas sensible aux autres constantes élastiques (ν_{f12}, ν_{f23}, G_{f12}, G_{23}).

Des structures composites sur-dimensionnées (cathéters modèles) ont été utilisées pour faire la vérification du modèle analytique. Les cathéters modèles ont été fabriqués sur

une machine de tressage disponible au département. De la fibre de Kevlar 49 et une résine époxy furent utilisées parce que leurs propriétés mécaniques laminaires avaient été mesurées dans une étude antérieure. Les prédictions du modèle et les résultats expérimentaux du module d'élasticité longitudinale concordèrent (»6 % de différence), ce qui confirme l'approche mathématique. Les prédictions du module de cisaillement et l'intervalle des résultats expérimentaux concordent aussi raisonnablement. De plus, les résultats démontrent que lorsque les constantes élastiques importantes (E_{f11}, E_m et G_m) sont précisément déterminées les modèles micromécaniques prédisent les résultats expérimentaux avec exactitude.

Le travail ci-haut fut effectué pour des tubes de composite à résine thermodurcie tressés ayant un recouvrement complet. De vrais cathéters médicaux nécessitent des résines flexibles et un maillage ouvert de fibre. Il fut donc nécessaire de choisir une fibre et une résine qui seraient appropriées pour un cathéter médical. Le modèle fut utilisé pour sélectionner une combinaison qui possède des rigidités similaires à celles qui furent mesurées pour le système de cathéter et fil-directeur existant. Les modèles micromécaniques furent utilisés pour estimer certaines constantes élastiques de tubes tressés avec de la résine flexible, d'autres constantes furent mesurés par des méthodes expérimentales. Les prédictions du module d'élasticité longitudinal et du module de cisaillement de tubes composites fabriqués de résine flexible étaient raisonnables. Donc, l'objectif principal fut atteint.

De plus, une analyse de sensibilité du modèle à la longueur de la région d'ondulation fut effectuée à cause de l'importance du tressage à maillage ouvert pour la fabrication de cathéters médicaux. Il fut trouvé que la longueur de la région d'ondulation

n'influençait plus les propriétés mécaniques de la région d'ondulation si elle excédait 5.5 fois l'épaisseur de la fibre.

Finalement, le modèle fut simplifié pour des fins d'applications pratiques. De simples équations prédisent les modules élastiques des matériaux utilisés dans cette étude, pour des configurations de tresses à recouvrement complet ou à mailles ouvertes, avec moins de 10 % de différences avec les prédictions du modèle complexe.

ACKNOWLEDGEMENTS

I wish to start by acknowledging the help and contribution of Drs. Munro and Fahim, my thesis supervisors, for investing their time and efforts towards the completion of this body of work. Thank you very much. We were a great team, and hopefully we will be for a long time to come!

I feel that none of this would have been possible without the continuing support and patience of my friends and family; contributions come in many ways and forms. Their contributions cannot be quantified - this is an engineering thesis after all. Thanks Jen for the hard work reading my thesis over and over! Many thanks to the GSAÉD 2001-2003 executives for all the support!

I also wish to thank the members of the defence and proposal committee, Dr. J. Cameron of the Univeristy of Queen's at Kingston, Drs. M. Liang and D. Redekop of the Department of Mechanical Engineering at the University of Ottawa and Professor P. Straznicky of the University of Carleton for investing their time towards the completion of this work.

Finally, the author is grateful to the Natural Sciences and Engineering Research Council of Canada and the Ontario Graduate Scholarship program for financial support. Also, this work would not have been possible without the resources of the Department of Mechanical Engineering.

Cheers!

TABLE OF CONTENTS

LIST OF FIGURES

LIST OF TABLES

GLOSSARY

- **Angle-ply** composite: a composite, such as braids, whose layers, strands, etc., cross at plus or minus equal angles about an axis.
- **Biocompatible:** term inaccurately used to describe the performance of materials within a biological system. (See biological performance)
- **Biological performance:** a material is deemed bioperformant if its biological response is adequate for a specific situation/application; for example, short-term use.
- **Braiding:** a readily automated, versatile and high deposition rate process best used for the production of net shape continuous fibre composite components [25].
- **Catheters:**
  - **Medical catheter:** in this document, the use of medical catheter will signify an actual catheter, currently existing and used, in contrast to "model catheter" defined below.
  - **Model catheter:** in this document, refers to an engineering, over-sized, proof of concept or prototype catheter used to either experimentally or analytically evaluate the proposed model.
- **Catheter distal end:** the end of the catheter that is sent inside body.
- **Catheter proximal end:** the end of the catheter that remains outside the body.
- **Catheterization:** procedure of inserting a catheter.
- **CGWS:** catheter guidewire system.
- **CLPT:** classical laminate plate theory.
- **CVC:** central venous catheterization.

- **Gel time:** time required for a resin's viscosity to increase to the point of becoming a gel.
- **Guidewire:** steel wire used as a guide for a medical catheter.
- **Host response:** other than intended therapeutic local and systemic response of the living system.
- **Jamming:** state defined as the strand position where adjacent strands jam against each other preventing any further movement in that particular direction.
- **Jamming angle:** angle at which jamming occurs.
- **Lamina:** one layer of unidirectional composite.
- **Laminar:** adjective describing an elastic constant or mechanical property related to a lamina.
- **Laminate:** multi-layer composite.
- **Laminate CLPT:** classical laminate plate theory model for laminate materials.
- **Proposed CLPT:** classical laminate plate theory model developed in this work.
- **Lumen:** passageway in medical catheter (i.e. a single lumen catheter is a simple tube; a double lumen catheter has two compartments).
- **Material response:** response of the inserted material in the presence of the biological system. A good material response indicates that the inserted material has a good biological performance.
- **Neat resin:** pure resin.
- **PECF:** pseudo-extracellular fluid.
- **Prepreg:** pre-impregnation of fibres with matrix.

- **PTA and PTCA:** percutaneous transluminal angioplasty and percutaneous transluminal coronary angioplasty.
- **Stent:** Permanent insert in blood vessel to keep it cleared (metallic meshing)
- **Tex:** unit describing the linear density (grams per 1000 meters) of fibres, filaments, tows and yarns.
- **Undulation length:** distance between strand crossovers.
- **Undulation region:** region between strand crossovers during which a strand undulates from one crossover region to the next.
- **Unit cell:** smallest repetitive structure in a braided or woven structure.
- **Vacuolization:** formation of minute cavities in cells containing air or fluid [35]

NOMENCLATURE

The following is the nomenclature used in this thesis.

Finite element analysis

[e]	Displacement transformation matrix
[K']	Stiffness matrix
{q}	Member deformation
{Q}	Force
{r}	Nodal displacement
{R}	Nodal forces
$\underline{q}$	Virtual deformation
$\underline{r}$	Virtual displacement

Fabric geometry model

[C]	Compliance- inverse of stiffness
[Q]	Stiffness matrix of lamina
$[\overline{Q_i}]$	Stiffness matrix of the i^{th} system of strands, global coordinate system
$[\overline{Q_s}]$	Stiffness matrix, global coordinate system
$[T_{\varepsilon,i}]$	Geometric transformation of the i^{th} system of strands
$\{\sigma\}$	Stress
k_i	Fractional volume of i^{th} system of strands

Proposed CLPT model

Greek Symbols

β	Undulation angle
ε^0	Midplane strain
ϕ	Twist angle
γ	Complementary angle of θ
κ^0	Midplane curvature
ν_{21}, ν_{23}	Poisson's ratio
ν_m, ν_f, ν_{12}, ν_{xy}	Major Poisson's ratio of matrix, fibre, lamina and braid, respectively.
θ	Braid angle

Other variables

1"2"3"	Strand coordinate system
1'2'3'	Braid coordinate system
a_u	Undulation length, m
a_{xy}	Area over x and y of region R_1, m^2
d(x,y)	Position in the undulation region
h(d)	Height of the strand measured from the midplane, m
h_c	Thickness of the strand, m

K	Total number of unit cell regions
l_e	Width of a strand at the crossover point of two strands, m
T	Thickness of the unit cell, m
t_m	Thickness of matrix overlaying unit cell, m
x, y, z	Unit cell (global) coordinate system
A	Area, m^2
I	Moment of inertia, m^4
J	Polar moment of inertia, m^4
$[A], [B], [D]$	Extensional, coupling and bending stiffness matrices
$[C]$	Compliance matrix
$[Q]$	Stiffness matrix of lamina
$[Q_{(\theta)}], [Q_{(-\theta)}], [Q_m]$	Stiffness matrix of strands in $+\theta$ and $-\theta$ directions and resin, respectively
$[\overline{Q}]$	Stiffness matrix of lamina, global coordinate system
$[S]$	Overall stiffness of laminate matrix as defined in CLPT with [A], [B], [D]
E_{11}	Lamina longitudinal Young's modulus, GPa
E_{22}	Lamina transverse Young's modulus, GPa
E_{f11}	Fibre longitudinal elastic modulus, GPa
E_m	Elastic modulus of resin or monolithic material, GPa
E_x	Braid longitudinal elastic modulus, GPa
E_y	Braid transverse elastic modulus, GPa
$E_{x\theta}, E_{y\theta}, G_{xy\theta}$	Elastic constants of angle-ply composite at an angle θ
$E_{xlaminate\theta}$, $E_{ylamiante\theta}$, $G_{xylamiante\theta}$	Elastic constants of angle-ply laminate at an angle θ
G_{12}	Lamina shear modulus, Gpa
G_{23}	Lamina out of plane shear modulus, GPa
G_m	Shear modulus of resin or monolithic material, GPa
G_{xy}	Braid shear modulus, GPa
L	Distance between points of angular twist, m
N, M	Stress and moment resultants, GPa-m and GPa-m^2
P_A	Projected area of the unit cell on the midplane, m^2
R_n	Area of the n^{th} region
T	Torque
V_f	Lamina or strand fibre volume fraction
V_{f0}	Unit cell fibre volume fraction
v	Constituent volume, m^3
W_y	Width of the strand, m
X	Width of the unit cell, m
Y	Length of the unit cell, m

CHAPTER 1 : INTRODUCTION

Fibre composite materials have traditionally been used for aerospace and, more recently, sports equipment applications. Growing areas for the application of fibre composites are biomedical and clinical engineering, in which the design of invasive medical products is highly specialized work. Medical catheters are tubes that are used to travel through or inject fluids in the body; they are used in many medical procedures such as angiocardiograms, biopsies, treatment of various urinary track diseases, air exchange, intravenous (IV) infusions, etc. One important trend is to make catheterization procedures more comfortable for the patient. Thus, medical catheters are being produced in smaller sizes and with variable rigidity to provide for easier manipulation and lower discomfort. The objective of this thesis is to develop a model to determine axial, flexural and torsional rigidities that would aid in the design of a single component braided composite model catheter to replace the medical catheter-guidewire combination currently used. The new single-component, braided composite model catheters would simplify the catheterization procedure and reduce patient discomfort.

To that effect, many medical catheter-, predictive model- and design- related concepts were evaluated. Cardiovascular catheters were selected as the principal focus of this study based on specific criteria. It was necessary to assess axial, flexural and torsional rigidities of medical catheters, guidewires and medical catheter-guidewire systems as well as different techniques for varying model catheter-like tube properties; braiding was selected as an appropriate approach for controlling model catheter rigidities.

In order to manufacture future medical catheters, it was necessary to examine possible fibres and flexible matrices as constituent materials as well as consider possible biological performance issues. Since large numbers of possible constituent materials exist and experimental evaluation of the elastic constants of every combination is an unreasonable undertaking, it was necessary to select one of the models that exist in the literature to predict elastic constants of flat and cylindrical woven/braided composites.

A classical laminate plate theory (CLPT) -based predictive model developed for angle-ply composites, such as braids, was selected and the sensitivity of the results to the values used for the constituent properties was performed. The model was validated by comparing predictions to previous theoretical and experimental works as well as compared to in-house experimental data for braid longitudinal elastic and shear moduli of tubes produced with rigid and elastomeric resins. A final selection of constituent materials was performed to illustrate the utility of the proposed tool.

A sensitivity analysis of the proposed CLPT model to different parameters of the undulation region was also done. Finally, regression-based equations were developed for practical and preliminary design purposes.

1.1 Thesis outline

The thesis is divided into chapters that will examine various concepts related to the design and modelling of braided model catheters. In Chapter 2, medical catheter-related concepts are introduced. In Chapter 3, fibres and flexible matrices as constituent materials for medical and model catheter production are examined and discussed in the context of biological performance. Existing predictive models used for flat and cylindrical woven/braided composites are detailed in Chapter 4. In Chapter 5, the proposed classical

laminate plate theory -based predictive model developed for angle-ply composites is described. Sensitivity of the proposed CLPT model to variations in key constituent and laminar properties is found in Chapter 6. A two-part model validation is detailed in Chapter 7 for braid longitudinal elastic and shear moduli. In Chapter 8, the model is used in a preliminary attempt to select constituent materials for medical catheters. Experiments are performed to determine braid longitudinal elastic and shear moduli of the braided tubes produced with the fibre and resins selected in Chapter 9.

For practical design purposes, various simplifications to the model are introduced. First, the effects of undulation region length, strand path definition and consequently open mesh braiding are evaluated in Chapter 10. As a last step, a set of regression-based equations for the longitudinal and transverse elastic moduli as well as shear moduli are developed for practical design use in Chapter 11.

Finally, Chapter 12 contains the conclusions, recommendations for future work and contributions of the thesis to new knowledge.

CHAPTER 2 : MEDICAL CATHETERS

Medical catheters, their characteristics, and uses, are not commonly studied in mechanical engineering. Hence, a brief introduction of key concepts is necessary. The following sections will introduce and discuss various aspects directly related to medical catheters; namely, types of medical catheters, sizes, applications and mechanical properties. Furthermore, improvements required to optimize cardiovascular-related procedures, and different approaches to obtain these improvements, will be discussed.

2.1 Medical Catheters: Market and literature review

Medical catheters are extensively used instruments whose significance is generally understated. In 1996, Ratner [1] estimated that 25 % of all hospitalized patients received intravenous infusions and that there were a growing number of outpatients that required frequent catheterization. He emphasized the importance of medical catheters and intravenous access by stating that modern medicine would be impossible without them. Medical catheter applications are used in task of obtaining data, such as pulmonary artery pressure and gases and blood samples for chemical analysis, and to administering fluids. Medical catheters are also used in more drastic procedures such as cardiovascular, neurological, radiological, surgical and non-surgical applications.

A market intelligence report on medical catheters prepared by FIND/SVP [2], whose main data was obtained from interviews with marketing professionals in the business, is a major document on the subject. Table 2-1 displays the share of the market of each major type of medical catheter in 1995 and a forecast for the year 2000. A 61 %

increase in total worldwide volume was predicted in these five years. It is apparent from the market survey that medical catheters are a financially viable field to investigate.

Table 2-1: Comparative volumes: disposable medical catheter's markets in 1995 vs. year 2000 predicted worldwide volumes and comparative increase [2]

Medical catheter market	Worldwide volume in 1995 (in millions of US$)	Projected worldwide volume in 2000 (in millions of US$)	Increase (%)
Total Balloon	1,376.0	2,109.2	53
PTCA	1,142.0		
PTA	47.0		
Nonvascular	175.0		
Laser	12.0		
Total Atherectomy	160.4	252.4	57
Total Angiography	420.8	699.0	66
Coronary	260.9		
Peripheral	159.9		
Total Neurointerventional	50.0	149.8	200
Total Ultrasound	14.0	29.8	113
Total Electrophysiology	88.4	287.2	225
Mapping	37.4		
RF Ablation	51.0		
Total IV Access	627.8	844.8	35
Standard IV[1]	505.0		
(Needleless)	(101.0)		
CVC	91.0		
PICC/Midline	31.8		
Total Renal	2,725.0	4,642.9	70
Hemodialysis	1,155.0		
Peritoneal Dialysis	1,570.0		
Total Urological Drains	674.8	868.6	29
Foley	645.8		
External	96.0		
Intermittent	14.0		
TOTAL	6,137.1	9,883.6	61

[1] Includes needleless IV catheters

It should be specified that the statistics offered by Ratner and found in Table 2-1 are inflated since they include intravenous needle catheters (IVs). It would not be accurate to state that 25 % of all patients undergo invasive catheterization since intravenous catheters do not enter the body; only the needle is inserted in a vein. Although in the strictest of definition IVs are medical catheters, they are simply tubular extensions for needles inserted into body extremities. To further clarify possible discrepancies with Ratner, Table 2-1 presents the costs of different catheterization. IVs represent 10% of the market in terms of dollars; clearly, cost of a single IV is insignificant as compared to a single balloon catheter and thus, the table does not provide an adequate sense of the yearly number of medical catheters used.

Medical catheters are difficult to categorize since different types of medical catheters can be used for procedures in almost all parts of the body. For the following summary, medical catheters are categorized as follows: (1) cardiovascular, (2) other significant invasive procedures and (3) minimally invasive procedures. Table 2-2 through Table 2-4 detail the types of medical catheters, their various functions, and their constituent materials.

The cardiovascular types of medical catheters are given in Table 2-2 (p8-p10). Balloon catheters are employed during angioplasty procedures to enlarge blocked arteries. Metallic stents are used to permanently keep the artery open after a balloon catheter has opened the blocked artery. Arthrectomy catheters remove obstructions in the blood vessels. Angiography catheters are used to inject a radiopaque fluid in the cardiac region and cardiac arterioles to permit X-rays or other internal-visualization methods to provide real-time imaging of the cardiovascular/blood flow within the blood vessels. Finally,

mapping catheters are used to map the heart during the recording of electrocardiograms and other procedures. Medical catheters for these procedures are all long, hollow and flexible tubes used to deliver the stent, the dye, etc.

Table 2-3 (p11) illustrates the medical catheters that are used in other complex invasive procedures. Ablation catheters remove tissue by various means in every part of the body (cardiovascular, gastro-intestinal, etc.). Others, such as the endotracheal tube, are used for air exchange.

Table 2-4 (p12-p14) contains the medical catheters that are considered less invasive: intravenous, feeding tubes, renal catheters and Foley catheters (urological). Other medical catheters exist; however, the structures resemble those previously listed.

In the following section, the needs pertaining to the improvement of the physical characteristics and the insertion procedure of one specific type of medical catheter selected for this work will be introduced.

Table 2-2: Medical catheters for cardiovascular procedures[1]

Type	Function	Sub-types	Material
Dilatation balloon catheter 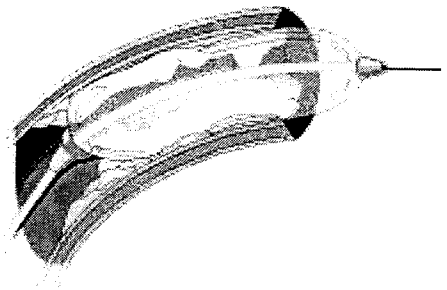 (Balloon catheter [3]) 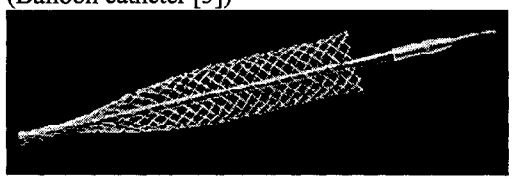 (Braided stent inflated by balloon catheter [4])	- Percutaneous transluminal coronary angioplasty (PTCA) (inflated at pressures of 4-12 atm) 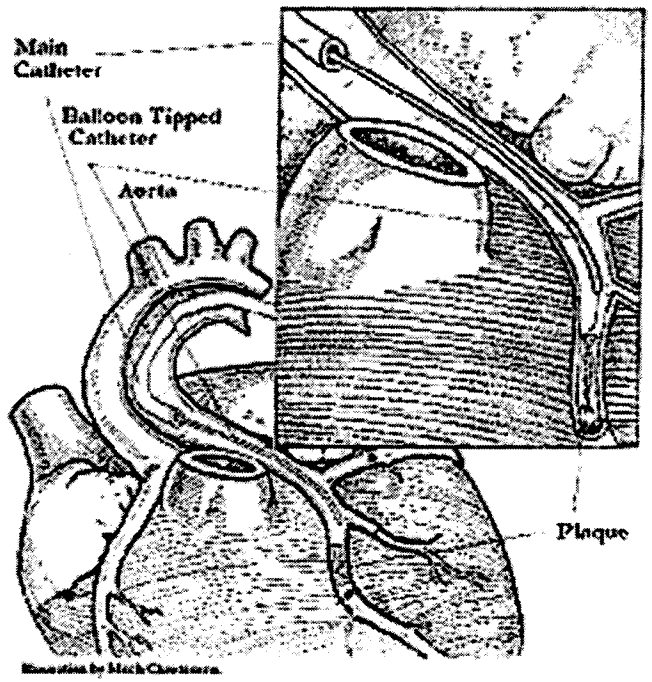 (PCTA procedure [5]) -Percutaneous transluminal angioplasty -Used with stents (braided) -Other nonvascular minimally invasive and traditional procedures	- With and without stents	- Silicone - Some balloon models are made from Polyisoprene.

[1] These catheters can also be used in other procedures.

Type	Function	Sub-types	Material
Arthrectomy catheter 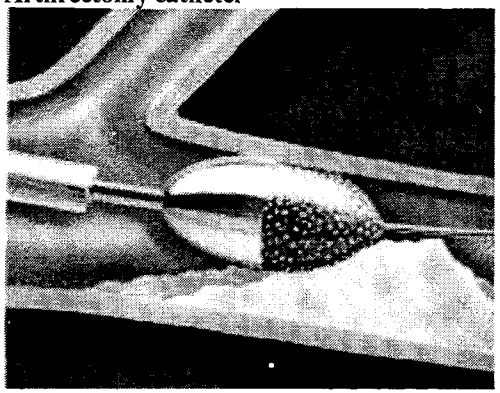 (Rotating head arthrectomy catheter seen here "grinding" fatty tissue [4]) 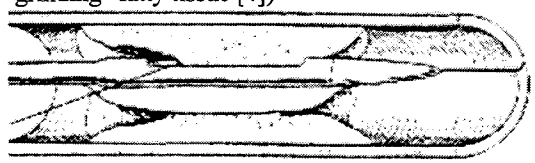 (Blade arthrectomy catheter seen here cutting fatty deposits [6])	Peripheral intraoperative and coronary procedures for [4,6]: -Vascular long lesions -Total occlusion -Ostial lesions -Moderately calcified lesions -Diffuse disease -Saphenous vein grafts -Total blockage	-Rotating -Blade	
Angiography catheter 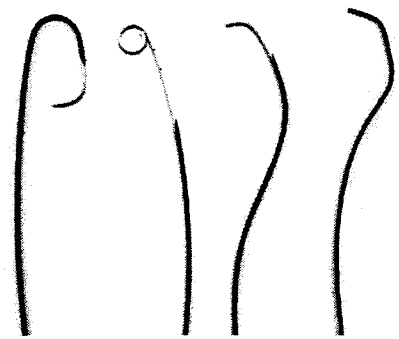 (Various shapes of angiography catheters[5])	Provide real-time imaging of vascular process.	-Radio-graphic imaging -Fluoroscopic imaging -Charge-coupled device imaging	

Type	Function	Sub-types	Material
Electrophysiology catheters: **Mapping catheter** 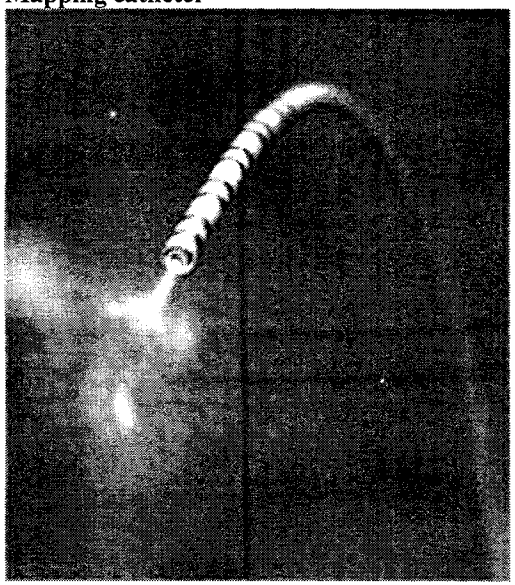 (Mapping catheter seen here injecting contrasting media [7])	-Mapping of the electric field inside the heart to detect arrhythmia 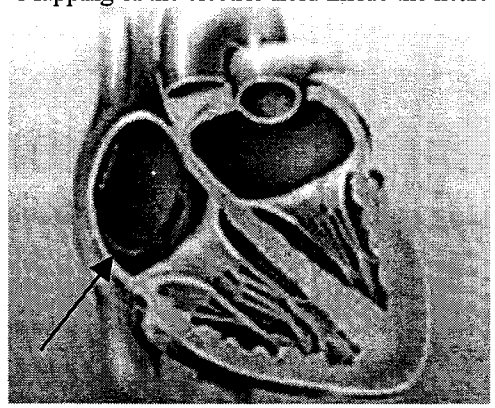 (Mapping catheter inside the heart [7]) -Tachyarrithmia: electrocardiogram -Abdominal (nephrostomy) -Gastric	- Ionizing - Contrasting media injection	- Some models contain stainless steel wire braiding construction, which provides excellent torqueability (see catheter in first column)

Table 2-3: Medical catheters for other invasive procedures

Type	Function	Sub-types	Material
Electrophysiology catheters: Ablation catheter  (Laser angioplasty catheter [4])	- Ablation: removal of body part (burning tissue [8]) 	- Radio frequency - Laser - Microwave - Ultrasound	
Pulmonary catheter 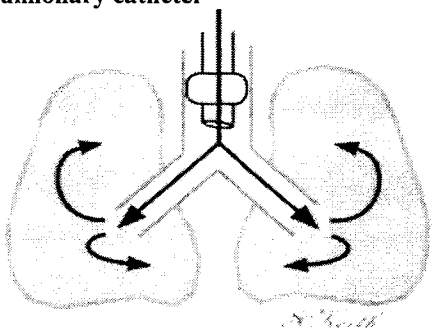 (Endotracheal tube [9])	-Lung catheterization -Airway exchange catheter -Transtracheal - Endotracheal tube (Anesthesia)	-Cook catheter - Grollman pulmonary pigtail catheters	- Polyethylene

Table 2-4: Medical catheters for minimally invasive procedures

Type	Function	Sub-types	Material
Vascular access catheters and IV accessories 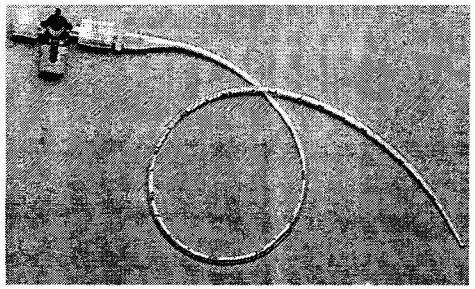 (Single lumen umbilical catheter, typical of other catheters of this section [10]) 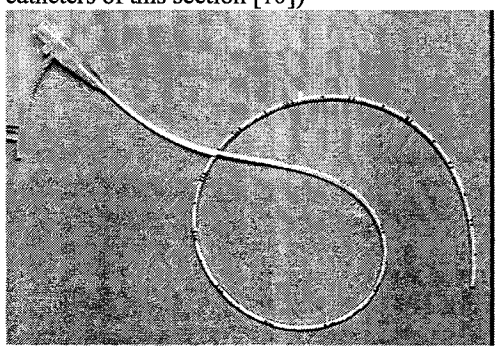 (Feeding tube [11])	For intravenous infusion of fluids and therapies -Antibiotic therapy -Analgesic therapy -Chemotherapy -Total parental nutrition and hydration	-Central venous cath. (CVC) -Subclavian vein cath. (SVC) -Femoral vein cath. (FVC) -Jugular vein cath. (JVC) -Umbilical artery cath. (UAC)	- Silicone

Type	Function	Sub-types	Material
Renal catheter 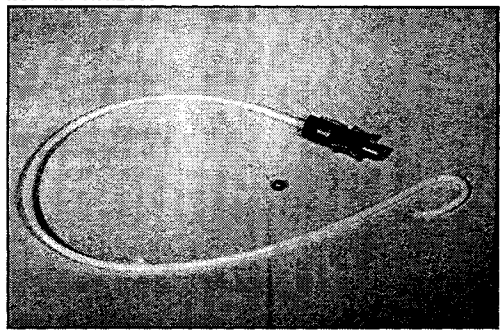 (Kidney drainage catheter [12]) 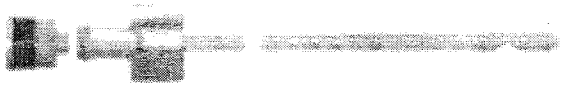 (Bladder filling catheter [13])	Sub-segment of IV and drainage catheter -Hemodialysis (collect and return blood) -Peritoneal (infuse and drain dialysate solution)		

Type	Function	Sub-types	Material
Urological drainage catheter 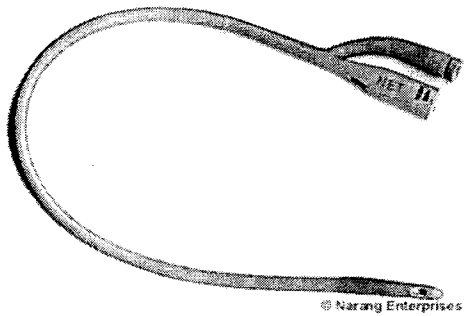 (Foley catheter [14]) 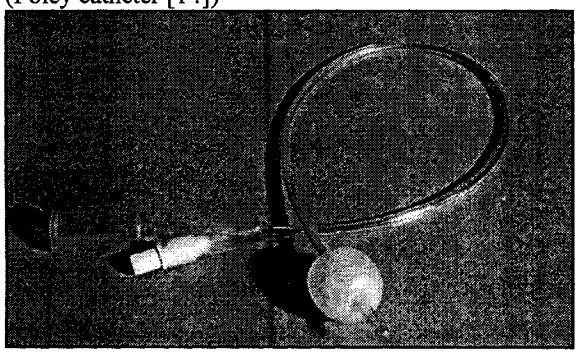 (Foley catheter with inflated balloon [15])	-Incontinence caused by aging, disease or surgical procedure -Urine output measurement for diagnostic purposes	-Foley catheter (main type) -Intermittent catheter -Double-J urethral	-Medical grade polyethylene -Some balloon models are polyisoprene

2.2 Problem definition: The need to improve cardiovascular catheters

Based on the information in the previous section, it is clear that there are many types of medical catheters, all of which are important. However, current cardiovascular catheters have some unique characteristics and rigidity requirements that can be best illustrated by reviewing a typical angiography catheterization process.

The medical procedure of inserting catheters during angiography is considered a minimally invasive cardiovascular procedure. The procedure for angiography catheterization is illustrated in Figure 2-1. A needle is inserted into a vein (A). A guidewire is introduced in the vein through the needle eye (B) and the needle is removed (C). Finally, the catheter is introduced over the guidewire (D) and guided to the appropriate body part. The guidewire is then removed.

During most angiography, the catheter is inserted in the external iliac vein (thigh) as seen in Figure 2-1 (E) and routed to the heart through the inferior vena cava to the right atrium of the heart. A radiologist [16] reported that in areas difficult to manoeuvre, the guidewire is retracted to allow the medical catheter tip to find the passageway; once engaged in the pathway the guidewire is reinserted. Although the positions of the medical catheters in Figure 2-2 are not representative of catheters coming from the groin, they illustrate the possible pathways through which the surgeon can guide the catheters.

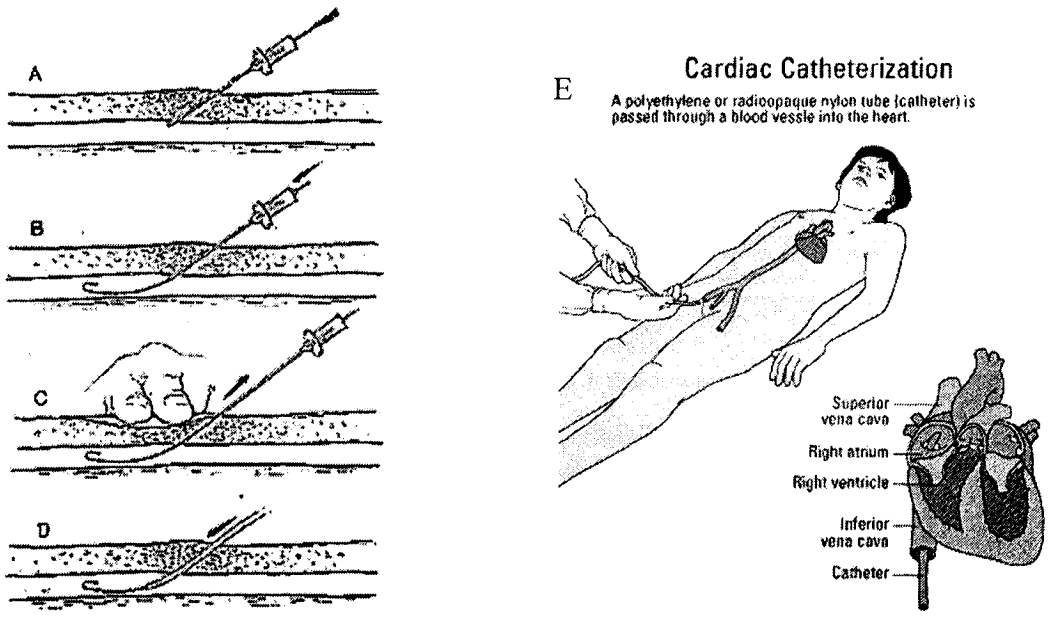

Figure 2-1: Medical catheter insertion procedure for angiography [17]: puncture of the vein (Fig. A); guidewire inserted in vein (Fig. B); the needle is removed with the guidewire remaining in place (Fig. C); catheter slipped over the guidewire (Fig. D). Fig. E: Representative drawing of a heart catheterization through the external iliac vein. [18]

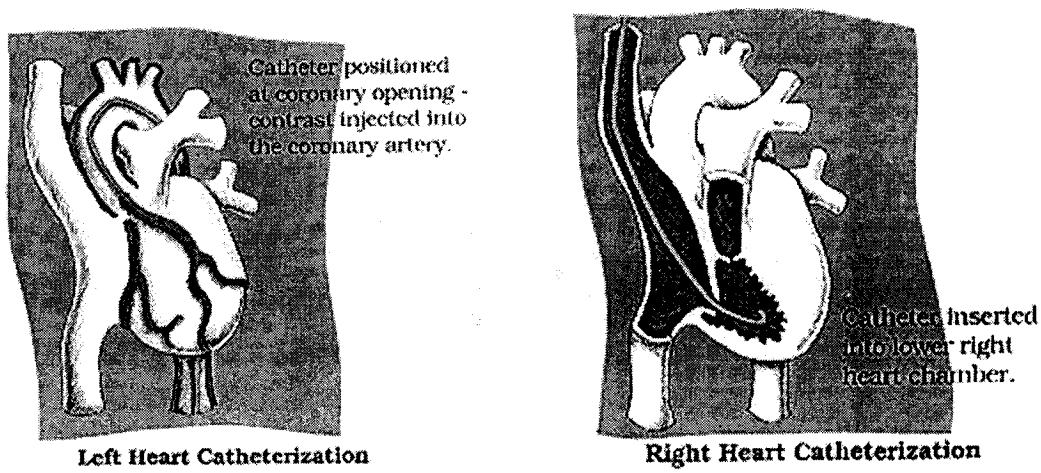

Figure 2-2: Left and right heart catheterization. [19]

During the procedure, the medical catheter-guidewire system (CGWS) may travel through very small multi-branched paths with high curvature sections. Figure 2-3 illustrates the required rigidities. Optimally, the CGWS should have sufficient axial rigidity all along the length for pushing/penetration purposes, and high torsional rigidity to provide a small angle of twist for proper manipulation. As well, the distal end should possess low flexural rigidity to move in the tortuous sections of the cardiovascular system. Since the cardiovascular system gradually becomes less tortuous in the extremities (limbs) and abdomen, decreasing flexural rigidity from proximal to distal is required along the CGWS length. Finally, at the proximal end, the medical catheter should possess high flexural rigidity to prevent buckling when pushed.

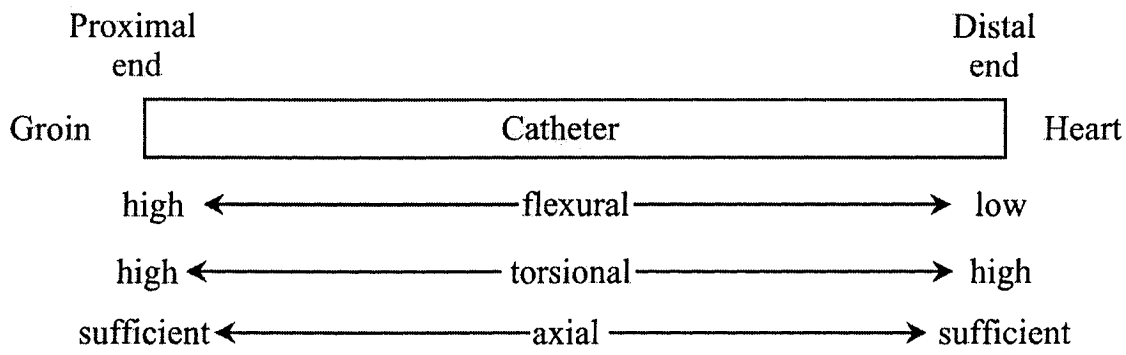

Figure 2-3: Required medical catheter rigidities at proximal and distal ends. Anatomical position given in relation to catheter.

Thus, a cardiovascular catheter should have variable flexural rigidity, high torsional rigidity and sufficient axial rigidity along its length. These requirements are particularly challenging due to the long length (80-120 cm) of some cardiovascular catheters. In order to shorten the time for these procedures, radiologists [16] believe that it would be preferable if the two-piece CGWS were replaced with a single component medical catheter.

It should be noted that only catheter rigidities and not strengths are considered. Medical catheter strengths are not an issue because, practically, catheters should never fail or deform plastically; the applied load levels are not sufficient for failure.

Considering the large number of cardiovascular catheters that are used (Table 2-1) – a $3-billion (US) share of the market – the proposed improvements would have a major positive impact on these procedures and the medical world. Thus, this work will focus on cardiovascular catheters.

2.3 Rigidity of existing cardiovascular catheters and guidewires

In the relevant literature, medical catheter properties are reported in terms of rigidities; thus, for comparative reasons, this work will discuss medical catheter properties in terms of structural rigidity instead of structural stiffness. The difference between the two is that stiffness is also a function of the length of the structure.

If existing CGWSs are to be replaced by a single component medical catheter, then the rigidities of existing medical catheters and guidewires must be determined as benchmarks and as target values. It is also of interest to determine the individual contribution of the medical catheter and guidewire to the overall rigidities of a medical catheter-guidewire system. Only a few sources of information on medical catheter materials and rigidities were found in the literature.

The flexural rigidity, EI, of central venous catheters for adults was evaluated in an early study [20] because it was believed that overly rigid medical catheters might be the principal cause of vascular damage after central venous catheterization. No such conclusion was made, but PVC, silicone or polyurethane medical catheters reduce such incidents [20], probably due to the lower values of flexural rigidities for these materials. The deflection of a cantilevered medical catheter was used to calculate the flexural rigidity of central venous catheters (CVC) of different materials and diameters (Table 2-5). The major conclusion is that a very large range of values of EI (2.8 to 203×10^{-6} Nm^2) for existing medical catheters exists.

Table 2-5: Flexural rigidity of central venous catheters (without guidewires) of different materials and diameters (modified from [20])

Material	Catheter type	Diameter (mm)		Flexural rigidity
		Inner	Outer	EI (Nm^2x10^{-6})
Silicone elastomer	XRO 2181.20	1.2	2.0	5.8
	XRO 2181.20	1.0	2.0	6.9
Polyvinyl chloride	Drum-Cartridge 417.06	1.1	1.65	2.8
Polyurethane	Cavafix Certo-275	0.8	1.4	5.8
	Cavafix Certo-275	1.1	1.7	13.3
	Experimental soft, smooth	1.2	1.8	6.9
	Experimental soft, smooth, heparinized	1.1	1.8	7.8
	Experimental soft, smooth	1.1	1.8	8.0
	Experimental soft	1.1	1.8	8.4
	Experimental high	1.2	1.8	15.3
	Experimental hard	1.2	1.8	15.6
Polyethylene	Cavafix MT-375	1.2	1.7	22.7
	Venen-Katheter	1.2	1.7	23.1
	Cavafix MT-338	1.2	1.7	25.6
	Cavafix MT-345	1.5	2.0	36.7
	Cavafix MT-348	1.5	2.0	45.1
	Venen-Katheter	1.8	2.4	96.4
Polytetrafluoroethylene (Teflon)	Steriflex 167-20	1.5	2.0	55.8
	Leader-cath 101177	1.5	2.0	104.2
	Subclavia-T 1601-4	1.25	1.7	14.4
	Subclavia-T 1602-2	1.5	2.0	203.3

A study in 1989 by Bersten et al. [21] evaluated the flexural rigidity of thirteen different medical catheters, again using a simple cantilever method; one end of a medical catheter section was fixed in position and the other end was loaded to produce small deflections. Table 2-6 contains approximate results estimated from a bar chart for single lumen central venous catheters. As in the case of the medical catheters found in Table 2-5, the range of EI values is quite large.

Table 2-6: Central venous catheter (without guidewire) flexural rigidity – Polyvinyl chloride (PVC); Polyurethane (PU); Silastic (S); Vialon (V); and Polyethylene (PE) (modified from [21])

Manufacturer	Catheter identification	Product number	OD (mm)	Material	EI (10^{-6} Nm^2)
Abbot Ireland Ltd	Drum cartridge	4719	1.65	PVC	4.4
Arrow International Inc		CS-04400	1.65	PU	22.1
Cook		CPUM 50JRS	1.65	PU	5.9
		CPMS 501J	1.65	PE	75.0
Deseret Medical Inc.	Angioguide	380718-1	1.65	V	22.1
	Angioguide	37-720-1	2.10	V	45.6
	Intracath	38-3122-1	1.65	V	19.1
	Subclavian	755	1.65	PVC	13.2
Viggo AB	S-Cath	1705-3	1.65	S	9.6
	Selacon seldy	1780-6	1.65	PU	12.5
Vygon S.A.	Leadercath	120.17	1.65	PE	94.1
	Hemocath	143.17	1.65	PVC	55.1
	Nutricath	2180.20	2.1	S	8.8

Three medical catheters by Deseret Medical Inc [21] used for angiography had flexural rigidities that increased (120 to 280x10^{-6} Nm^2) with increasing diameter (Table 2-7).

Table 2-7: Flexural rigidity of an angiography Teflon catheter without guidewire (modified from [21])

Manufacturer	Catheter identification	Product number	OD (mm)	EI (10^{-6} Nm^2)
Deseret Medical Inc.	Angiocath	2830	2.56	280
	Angiocath	2832	2.10	200
	Intracath	2854	1.65	120

Martin et al. [22] investigated the flexural and torsional rigidities of medical catheters at body temperature using simple cantilever and torsional methods; one end of a medical catheter was fixed in position and the other end was loaded in bending or torsion to produce small linear or torsional deflections, respectively. In addition to the medical catheters made of conventional materials, woven and braided composite medical catheters

were tested. Table 2-8 contains the results of this study. Torsional rigidity was reported as GI instead of the standard GJ, where I is the moment of inertia and J is the polar moment of inertia; thus, the values presented in Table 2-8 have been corrected. As in the previous studies, wide ranges for EI and GJ were found.

Table 2-8: Flexural and torsional rigidity of selected single lumen central venous catheters at body temperature [22]

Material	Catheter type	Outer diameter (mm)	EI (10^{-6} Nm^2)	GJ (10^{-6} Nm^2)
Polyurethane	Cordis (526-844) Commercial Tubing-Xtrutex	2.5	501	49.0
	Tubing-Xtrutex 80A	3.0	154	23.0
	Tubing-Xtrutex 90 A	2.9	214	34.0
	Tubing-Xtrutex 55 D	1.7	126	9.6
	Tubing-Xtrutex 75 D	1.2	219	28.0
PTFE	BD (TTX 042)	1.6	153	22.6
PE	CA (7450)	2.4	188	31.0
PVC	EDW. (Special)	2.4	157	17.0
Braided				
Nylon with Dacron weaving	(7456) Cournand	2.3	441	67
	(5440) NIH	1.9	285	55
	(1264) Lehaman	2.2	349	64
PU with stainless steel Braiding	Cordis (523-854)	2.6	747	97

To further define the problem a Cook ® Torcon Blue braided medical catheter, model number BPS6.0-100-H1 (Figure 2-4), was tested as part of this study. The medical catheter has a stainless steel braided mesh within a polyethylene matrix. The guidewire (model no. TSF-38-145) consists of a central wire (0.5 mm diameter) with a spiral overlap (Figure 2-5). The outer diameter of the guidewire is 0.97 mm.

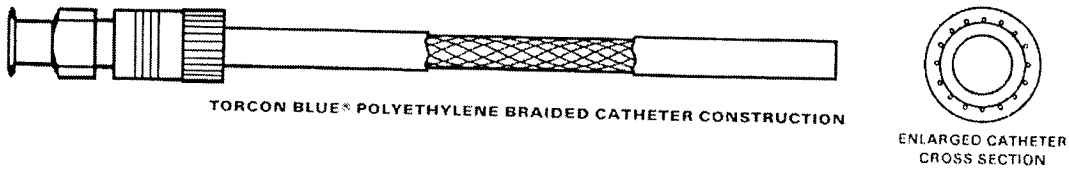

Figure 2-4: Torcon blue medical catheter [23]

Figure 2-5: Guidewire [23]

The flexural rigidities were evaluated using a 3-point bending beam jig. The flexural rigidity of the medical catheter (Table 2-9) was similar to other reported values. The flexural rigidity of the guidewire was higher than that of the medical catheter. Combining the medical catheter and guidewire resulted in a flexural rigidity of nearly 275 % as compared to that of the medical catheter alone.

Table 2-9: Flexural rigidity of Torcon Blue medical catheter, guidewire and CGWS produced by Cook ®

Component	Inner diameter (mm)	Outer diameter (mm)	Span (mm)	Load (N)	Deflection (mm)	EI (10^{-6} Nm^2)
Catheter	0. 965	2	20	5.96	2.85	348
Guidewire	N/A	0.965	20	5.96	2.05	484
CGWS	N/A	2	20	5.96	1.05	945

A static tensile test was performed to obtain the axial rigidity of the medical catheter; it was assumed that it was the same value in compression. A range of axial rigidities for the guidewire was calculated assuming a solid steel rod; the minimum value

was found for the diameter of the inner wire (0.5 mm) and the maximum using the outer diameter of the guidewire (0.97 mm) (Table 2-10).

Table 2-10: Axial rigidity of Torcon blue medical catheter (measured) and guidewire (calculated[1]) produced by Cook ®

Component	Inner diameter (mm)	Outer diameter (mm)	AE (N)
Medical catheter	0.97	2.00	450
Guidewire	N/A	0.50-0.97	39000 - 146000

The torsional rigidity was only measured for the medical catheter since the guidewire turns freely in the CGWS. An evaluation of the torsional rigidity was measured with a torsion system where one end of the medical catheter was clamped and the other only permitted axial and torsional displacement by having one steel tube, which clamped the medical catheter end, slide and turn inside the internal diameter of a larger clamped tube. Torsional load was applied at the free end. The measured torsional stiffness, 1400×10^{-6} Nm^2, was significantly higher than most values in the literature. Torcon Blue medical catheters are designed to have high torsional rigidity; the name Torcon comes from **TOR**que **CON**trol. COOK© would not release exact information on the torsional rigidity of the medical catheter; however, they did state that the medical catheter has a 1 to 1 twist ratio along its length. This implies that the medical catheter was designed with sufficient torsional rigidity to ensure that during catheterization a 30° twist by the operator at the proximal end, for example, will produce a 30° turn of the distal end. This could explain the large difference in torsional rigidity with the previously discussed medical catheters in Table 2-8.

[1] Steel, E = 200GPa; G=83 GPa

Briefly, it can be concluded from the gathered information (Table 2-5, Table 2-6, Table 2-7, Table 2-8, Table 2-9, Table 2-10) that, for medical catheters designed for similar purposes, the flexural, axial and torsional rigidities vary greatly. Therefore, no specific target axial, flexural and torsional rigidity values were found for an optimal one-piece model catheter but rather a range of target values. For design purposes, target ranges of rigidities are of more interest.

2.4 Techniques for varying medical and model catheter rigidity

In Section 2.2, the reasons why an optimal cardiovascular catheter should possess the following structural rigidities' characteristics were given:

- Sufficient axial rigidity and high torsional rigidity all along the length;
- Low flexural rigidity at the distal end to comply with the tortuous anatomy of the vascular system; and
- High flexural rigidity at the proximal end for manipulation.

To evaluate possible techniques for producing variable catheter rigidities, parameters affecting the rigidities were examined. The axial (EA), torsional (GJ) and flexural (EI) rigidities for tubular structures are defined as follows:

$$\begin{aligned} EA &= E\pi\left(r_o^2 - r_i^2\right) \\ GJ &= G\frac{\pi\left(r_o^4 - r_i^4\right)}{2} \\ EI &= E\frac{\pi\left(r_o^4 - r_i^4\right)}{4} \end{aligned} \qquad \textbf{2-1}$$

where r is the radius (o: outer and i: inner), A is the cross-sectional area, I is the area moment of inertia, J is the polar moment of inertia, E is the elastic modulus and G is the shear modulus. If material properties such as E and G are invariable for a particular

medical catheter section, then the rigidities are strictly a function of the tube's inner and outer radii. Conversely, if the critical parameter is a specific medical catheter size, then it becomes necessary to alter the elastic and shear moduli.

Two methods of varying the rigidity of medical catheters have been found in the literature; namely, varying wall thickness and incorporating reinforcing fibres in the wall using two-dimensional braiding. Advanced Polymers, Inc [24] developed variable rigidity medical catheters by increasing the outer diameter of heat shrink tubing along the length of the medical catheter. This allows for varying degrees of flexibility useful for improving the device's control. For variable wall thickness medical catheters made of monolithic materials, the medical catheter inner and outer radii must be varied to obtain the desired rigidities.

Two-dimensional braiding is another well-known method of reinforcing tubular objects (Figure 2-6). By changing the orientation of the fibre bundle angle with respect to the longitudinal axis of the medical catheter, braid angle, the various rigidities of the structure can be altered. The process has been described as "a readily automated, versatile and high fibre deposition rate process best used for the production of net shape continuous fibre composite components" [25]. Briefly, a 2D braiding machine is typically composed of a central pulling device or mandrel and a horizontal or vertical braiding head with a large number of fibre carriers (Figure 2-7(a)). In a standard braider, one-half of the carriers move in the clockwise direction while the other half move in the counter-clockwise direction, both in intersecting serpentine paths (Figure 2-7 (b)). The two paths intertwine, resulting in an interlocked structure (Figure 2-7 (a)).

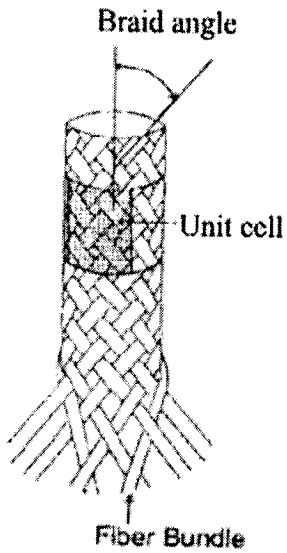

Figure 2-6 Braided tubular structure [modified from 26]

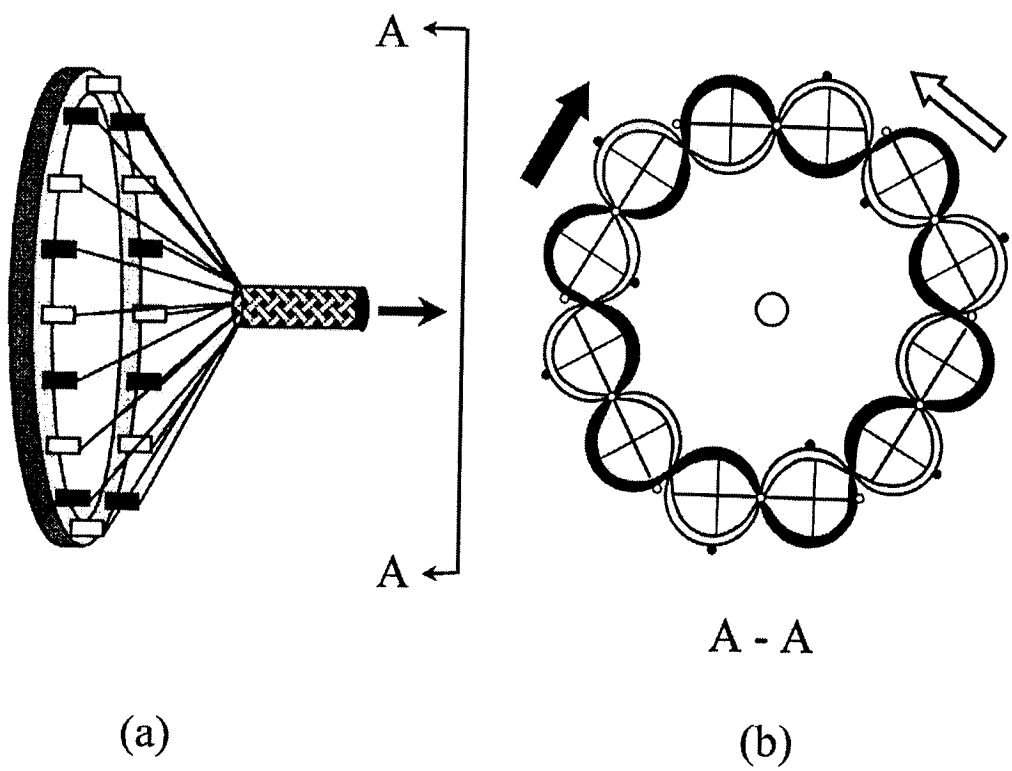

Figure 2-7: (a) Schematic of horizontal tubular braider and braided fabric and (b) representation of serpentine path [27]

Varying the braid angle of fibre reinforcement during the braiding process is another parameter for controlling the rigidities along the length of the medical catheter[2]. Table 2-11 compares the two techniques in general terms, while a numerical example comparing the effect of changing one of the rigidities on the other two rigidities is given in Table 2-12.

For the comparison in Table 2-12, two tubes, with 1 and 2 mm inner and outer diameters, respectively, are assumed. One tube is made of a monolithic plastic material and the other is braided at 45°. It is proposed to double the flexural rigidity of both tubes yet have minimal changes in the axial and torsional rigidities. This can be accomplished by changing the wall thickness of the monolithic tube, thus changing the geometric variables in equation 2-1; or, by changing the braid angle of the braided tube thereby changing E and G in equation 2-1. The monolithic plastic and the braid have different elastic moduli; the changes in rigidity due to modifying the elastic constants or the wall thickness are the conclusions of interest.

The results of Table 2-12 show that changing the thickness of the tube wall will affect axial and torsional rigidities as well as the flexural rigidity. In the case of the torsional and flexural rigidities, the values double, while changing the braid angle only has a small effect on the torsional rigidity while the axial and flexural rigidities are doubled.

---

[2] Details of the calculation of braided tube properties are found in Chapter 5 and Appendix 1.

Table 2-11: Comparison of wall thickness and braid angle variations on model catheter rigidity

Technique	Axial rigidity $EA = E\pi\left(r_o^2 - r_i^2\right)$	Torsional rigidity $GJ = G\frac{\pi\left(r_o^4 - r_i^4\right)}{2}$	Flexural rigidity $EI = E\frac{\pi\left(r_o^4 - r_i^4\right)}{4}$	Comments
Wall thickness	▪ E invariable for specific material ▪ For high rigidity must increase wall thickness substantially⇒ must increase A ▪ Rigidity $\propto r^2$, thickness	▪ G invariable for specific material ▪ For high rigidity must increase wall thickness substantially ⇒ must increase J ▪ Rigidity $\propto r^4$	▪ E invariable for specific material ▪ For high rigidity must increase wall thickness substantially ⇒ must increase I ▪ Rigidity $\propto r^4$	To manipulate properties the size of the catheter must be changed or change the material ⇒ Less flexibility to manipulate properties
Braiding	▪ E can be modified with the braiding angle, fibre type and volume fraction ▪ Not necessary to increase catheter size	▪ G can be modified with the braiding angle, fibre type and volume fraction ▪ Not necessary to increase catheter size	▪ E can be modified with the braiding angle, fibre type and volume fraction ▪ Not necessary to increase catheter size	⇒ More versatile method ⇒ Select one set of constituent materials ⇒ Change braid angle, fibre type and volume fraction not catheter size

Table 2-12: Effect of changing wall thickness of a homogenous material versus changing the braid angle of a braided tube on all structural rigidities

Tube	Braid angle	E_x (GPa)	G_{xy} (GPa)	Inner dia (mm)	Outer dia (mm)	EI (Nm^2)	AE (N)	GJ (Nm^2)
Plastic		3.5	1.3	1	2	0.0026	8250	0.038
		3.5	1.3	1	2.36	0.0052	12560	0.077
Braid[1]	45	6.4	5.5	1	2	0.0047	15080	0.0162
	36.5	12.8	5.3	1	2	0.0094	30160	0.0156

[1] Calculations of the elastic constants were performed with the model proposed in Chapter 5.

Thus, only varying the braid angle can substantially change some rigidities with little effect on other rigidities. Since it is also possible to vary fibre type and strand size, braided medical and model catheters only will be further studied.

2.5 Braided medical catheters: Literature review

The available information on braided medical catheters is limited, as little information has been presented in the open literature. The majority of the detailed engineering information was obtained from patents. The earliest occurrence of braiding used in a medical catheter was in 1976 for a cardiac catheter [28]; however, from studying other patents, it is apparent that the idea originated in a patent by Stevens in 1969 [29]. Table 2-13 lists recent medical catheter patents that employ significantly different braiding patterns and only the different braiding patterns used in the patents described in Table 2-13 are shown in Figure 2-8. The table also contains all factors that should be considered for this research project; namely, the materials used in the construction of the medical catheters, braiding details, geometric configuration and the intended use.

In the available literature, braids are used for a multitude of reasons such as developing high torque, low flexural rigidity, kink resistance and high longitudinal compressive strength. Some patents use fibre reinforcement while others metallic ribbons or wires. The metal meshing was used for greater reinforcement while the fibres were used for reinforcement and smooth transition between medical catheter sections and visibility during x-ray procedures. The different reinforcement, shape and size combinations provide different rigidities. Patents of variable rigidity medical catheters used ribbons, namely in a multi-sectioned medical catheter patent [30] and in a variable diameter braid pattern

[31,32]. In most medical catheter patents, metal ribbons or wires are used except for one [33], which uses aramid or polyester strands. Composite medical catheters previously reported in Table 2-7 by Cournand, NIH and Lehaman were composed of nylon with "Dacron" weaving construction, Cordis medical catheters were composed of stainless steel ribbon braiding with a polyurethane matrix, and Cook© utilized a polyethylene medical catheter with stainless steel reinforcement. However, no study was found comparing the properties of braided tubing produced with flat ribbons or wires.

The patents presented illustrate the versatility of the braiding method. Variable stiffness/rigidity was obtained by two different methods: by joining constant braid sections and by braiding on a variable diameter core. No study or patent was found in which the braid angle was varied continuously along the length of the medical catheter. In addition, no information was found in the literature for controlling all three rigidities simultaneously. This would require a model for the calculation of the axial, torsional and flexural rigidities.

Table 2-13: List of relevant information of Canadian and American medical catheter patents

Patent number	Patent name	Premise of the invention	Procedure/use	Dimensions	Braiding materials and features
US 5,906,606 Chee et al. (1999) [30]	Braided body balloon catheter	Proximal and distal stiffness variations	Angioplasty	Outer dia. range: 0.67-1.67 mm L.[1]: 30-175 cm	-Stiffness variation obtained by connecting differing braid angle tubes (20-60 deg) -Outer lining made of polyethylene, polyvinyl chloride, ethylvinyl acetate, polyethylene terephthalate, and polyurethane, and their mixtures and block or random copolymers -Stainless steel or superelastic alloy ribbons (or wires) with a thickness of 0.0127-0.0508 mm and a width of 0.0254-0.1016 mm. Cross-sections should have an aspect ratio of thickness-width of at least 0.5.
US 5,891,112 Samson, G., (1999) [31]	High performance superelastic alloy braid reinforced catheter	Variable stiffness catheter	Angioplasty	Outer dia. range: 0.67-1.67 mm L.: 60-200 cm	-Variable inner and outer diameter catheter -Braided over variable diameter core -Different braid patterns (diamond, regular) and ribbon size -Polyurethane matrix -Nickel-Titanium superelastic alloy wire or ribbon have been used
US 5,891,114 Chein et al., (1999) [32]	Soft-tip high performance braided catheter	Thin walled, variable stiffness, high kink resistant catheter	Neurovascular conditions	Outer dia. range: 0.67-1.67 mm L.: 60-200 cm	-Stiffness variation obtained by connecting differing braid angle tubes over a continuous polymer inner lining -Polyurethane matrix -Stainless steel or superelastic alloy ribbons with a thickness of .5-2 mils (0.0127-0.0508 mm) and a width of 1 to 4 mils (0.0254-0.1016 mm) -Braid angle is 45° or greater in distal region for greater flexibility and 7.5° over in the proximal region to increase rigidity. Exact braid angles were not provided.

[1] L indicates total length.

Patent number	Patent name	Premise of the invention	Procedure/use	Dimensions	Braiding materials and features	
CA2070452 Macauley et al. (2000) [33]	Intravascular catheter with a nontraumatic distal tip	Smooth transition between tip and shaft unrelated to the braiding components	Guiding catheter for PTCA procedure	Outer dia. range: 0.6-0.85 mm L.: 80-125 cm	-Multifilament polymeric strands (Aramid or Polyester) -Intermixed thermoplastics fibres instead of post braiding impregnating -50-200 denier -2x2 pattern, 16 carriers, one bobbin per carrier -Constant 45° braid angle, no transition zone	
					Covering and impregnating thermoplastic elastomer	Polyurethane[2] matrix -Proximal: RP 6414-3 -Distal: RP 6413-1
WO 95/13110 Jaraczewski, R.S. (1995) [34]	Small diameter, high torque catheter	High torque, flexible, high compressive strength for small catheters	Intercranial selective catheterization	Outer dia. range: 0.3 -4 mm L.: 40-200 cm	-Annealed stainless steel braid used for reinforcement (width: 0.381 mm; thickness: 0.0254 mm) -Outer layer made from polyamide polyether block copolymer, polyurethane, silicone rubber or nylon. -The flexibility is due to the relative lengths and mechanical properties of the inner and outer lining, braid and catheter diameter. -Braid level of reinforcement varied by changing the pic level. Pic should be between 60-100pics/inch - Outer layer hardness between 30A to 72D	

[2] CibaGeigy Corporation.

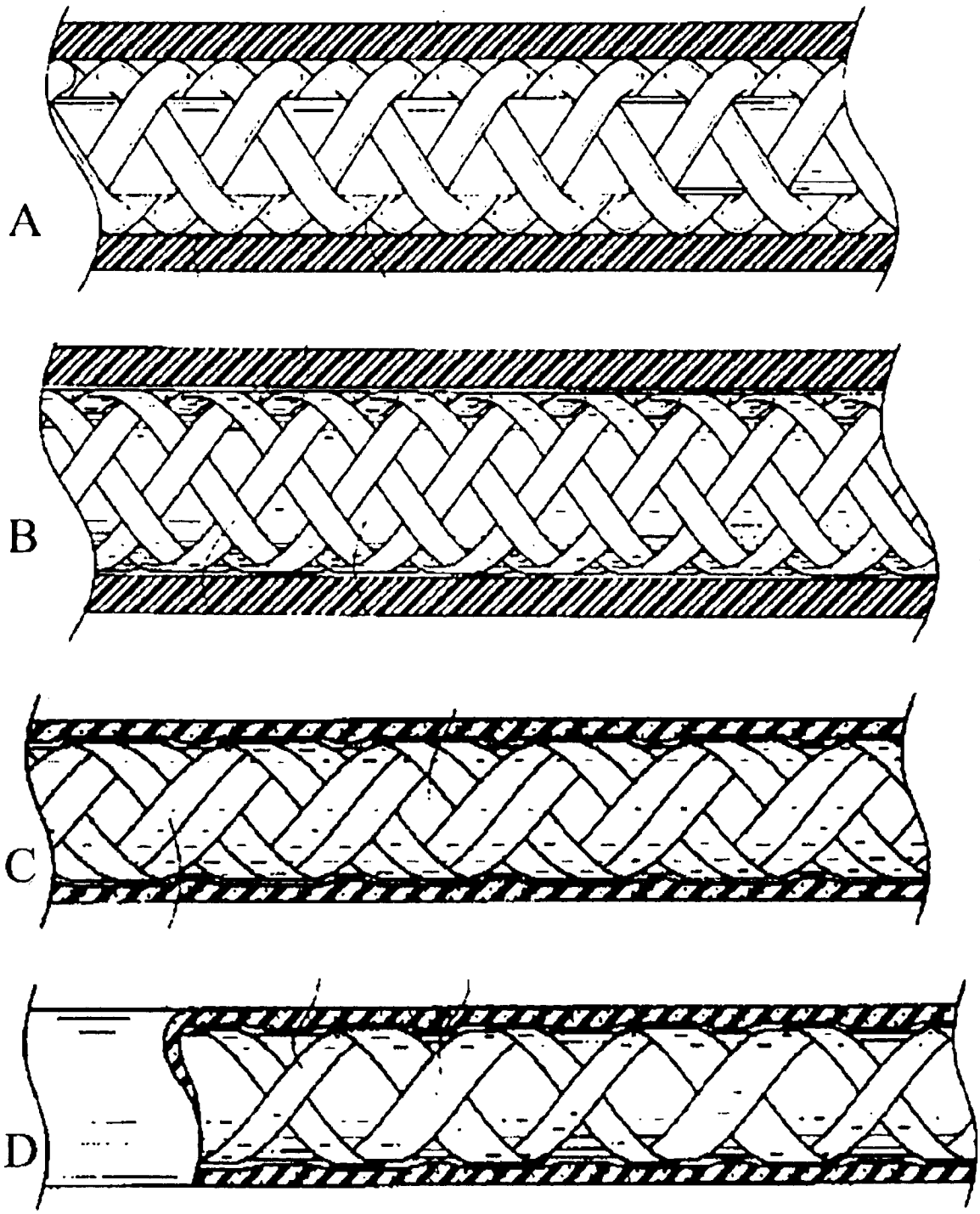

Figure 2-8: Braiding patterns used in medical catheters. A) single wire [30], B) single ribbon [30], C) double fibre [32], D) differing size fibres [32].

2.6 Conclusion

In this chapter, many medical catheter-related concepts were introduced. Both patients and practitioners would welcome improvements to the equipment and procedure. In addition, the vast and expanding market for medical catheters is a clear indication that financially, any conceptual, manufacturing or property control-related improvements would have a significant impact.

From the property control aspect, cardiovascular catheters were selected as the principal focus of this study based on the criteria in Section 2.4. Axial, flexural and torsional rigidities of existing medical catheters, guidewires and medical catheter-guidewire systems were detailed and evaluated. Finally, two techniques for varying medical and model catheter properties, variable diameter monolithic and braided tubes, were introduced. Braiding was selected as an appropriate approach for controlling medical catheter rigidities.

These conclusions made, the next chapter will discuss possible medical catheter materials as well as ways of obtaining laminar and structural elastic constants of medical and model catheters.

CHAPTER 3 : MATERIAL CONSIDERATIONS

Many material aspects were considered during the development of a medical catheter with optimal rigidities. The 2D braiding of fibre composites has been selected as the manufacturing process to produce the one-piece model catheters. When selecting candidate materials for medical catheters, the mechanical properties are of primary importance since these will directly affect medical catheter rigidities; thus, models to obtain laminar properties of fibre composites will be discussed in this chapter. The selection of high bioperformatory resins and fibres will be discussed in the following section. Since this is a very complex issue, it is beyond the scope of this work; however, if the rigidities are similar between candidate materials, then the candidate materials with the greater biological performance will be selected in this work.

3.1 Biological performance of materials

Ratner [1] described the ideal medical catheter as one that, biologically, elicited minimal inflammatory response and inhibited infection; that, structurally, was flexible and able to maintain its flexibility with time; and that was also easily placed, controllable and secure. The following section will examine the biological requirements of the materials that constitute medical catheters by briefly examining the biological system, its response to foreign bodies as well as the importance of this criterion for this work.

The selection of materials for biomedical applications is restricted by their performance in the body. Biological performance is the accepted terminology indicating the level of response of the biological system to a foreign body. Black [35] made a valid case against the use of the term "biocompatibility" since the word "compatible" indicates a

harmonious interaction that no foreign body can have with a biological system. A material is deemed bioperformant if its biological response is adequate for a specific situation/application, for example, short-term use. Ratner [1] reported that the majority of medical catheters are constructed of polyurethane or silicone elastomers because of their good biological performance, but as will be discussed further, other materials could be used.

Many studies have looked at the interaction of materials with biological systems and at the host response and the material response to the biological system. Black [35] described internal biological systems as chemically aggressive environments to foreign bodies. Biological systems also maintain physical conditions and composition with complex control systems easily disrupted by foreign materials such as medical catheters.

The most important factor for biological performance is the level of blood coagulation induced by the foreign body. When a foreign body is introduced in the biological system and causes damage, it begins a process that causes blood clotting. Briefly, what is believed to happen is that when damage occurs to either the blood vessel or the tissue, this releases either platelets or fibrin, which cause thrombosis [1] (Figure 3-1).

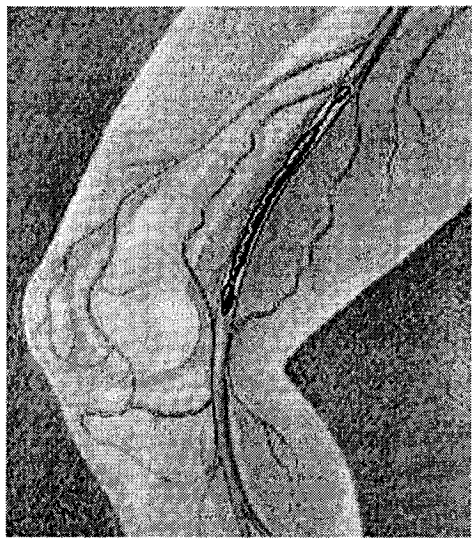

Figure 3-1: Illustration of thrombosis in the leg [4]

Materials used for invasive procedures can cause adverse reactions within the biological system. Therefore, care must be used when selecting materials for bio-insertion. Table 3-1 compares many of the polymeric materials that have been tested for their biological performance. This was done by evaluating their response to pseudo-extracellular fluid (PECF) for 62 hours at 115 °C and 206.8 KPa (abs). Although this table is of importance for biomedical applications with longer exposure times than normally used in cardiovascular procedures, it is important to include in this work for a comprehensive discussion of the subject.

Table 3-1: Correlation between tissue culture to PECF and chemical analysis (polymer exposed to PECF, 62 hr, 115°C, 206.8 KPa) (adapted from [35])

Polymer	Tissue culture response[1]	
Silicone (Silastic)	+1	⇑
Polyurethane (Bayer medical grade)	+1 [36]	Low
Polyethylene	+1	
Fluorinated ethylene propylene	+1 to +2	
Polyphenylene oxide (type 1)	+1 to +2	
Polyethylene	+2	
Acrylic Molding Powder	+2	
Polyphenylene oxide (type 2)	+2	
Fluorinated ethylene propylene	+2	
Ionomer (type 1)	+2	
Polypropylene	+2	
Vinylidene fluoride	+2 to +3	
Nylon	+2 to +3	
Ionomer (type 2)	+2 to +3	
Polyamide (nylon)	+4	
Polyvinyl chloride	+3 to +4	
Polyurethane (type 1) (non-medical grade)	+4	High
Polyurethane (type 2) (non-medical grade)	+4	⇓

[1] Scale: +1 = some vacuolization and growth inhibition, but nominally as control cultures; +2 = moderate vacuolization, morphological changes, and growth inhibition; +3 = severe growth inhibition and vacuolization; and +4 = total growth inhibition.

It is evident from the above table that many materials are available; however, for short-term use (≈ 1hr) devices such as cardiovascular catheters, a greater importance should be placed on candidate material mechanical properties. Moreover, the model catheter can be covered or encapsulated with a thin heat shrink tubing that would not significantly change the structural properties but would increase bio-performance. The following section will examine possible materials of interest based on material properties specifications.

3.2 Selection of fibrous reinforcements for medical catheters

In Chapter 2, different reinforcements used in medical catheters (Table 3-2) were discussed; namely, steel wire and ribbon, Kevlar and polyester fibres. Although Kevlar is not a bioperformant material, it has been used in a catheter [33]. Typical composite fibres, such as carbon fibres and fibreglass are not appropriate for biomedical applications because of poor biological performance with the human body, even if covered by a resin and for a short-term procedure. Nylon fibres could be an appropriate choice for the reinforcing component because they have good biological performance; this is substantiated by their use for sutures and other medical applications.

Table 3-2: Moduli of candidate fibrous reinforcement materials [37, 38, 39]

Material	Tensile modulus, E_f (GPa)	Shear modulus, G_f (GPa)
Polyester	2-4.4	1.232
Kevlar-49	138	2.86
Steel ribbons	200	83
Steel wires	200	83
Nylon 6,6	2.8	0.076

3.3 Selection of matrices for medical catheters

3.3.1 Loading response of elastomeric, flexible and rigid matrices

Matrix resins can have different responses to loading; they can be grouped into elastomeric, flexible and rigid resins materials. Medical catheters have been fabricated using elastomeric resins such as polyurethanes and silicones. In this section, the fundamental difference between elastomeric, flexible and rigid resins will be discussed at the microstructural level.

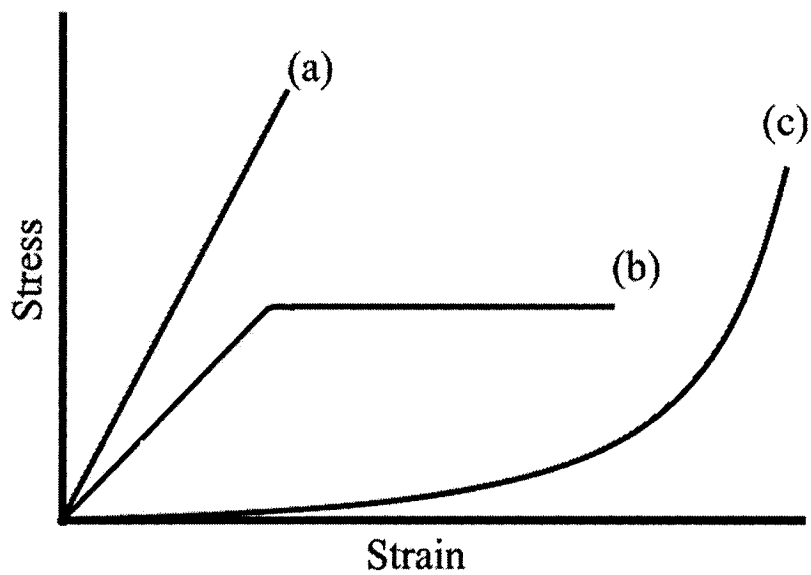

Figure 3-2: Resin stress strain response; (a) elastic response of a rigid resin (b) elastic and low-strain plastic deformation of flexible resins and (c) amorphous uncoiling and elastic response of an elastomeric resin.

In Figure 3-2, typical stress strain curves for elastomeric, flexible and rigid resins are illustrated. The key difference between the polymer stress-strain responses derives from the different polymeric microstructures. Elastic deformation in rigid thermoset resins responds linearly to loading (Figure 3-2 (a)). This reaction is only due to the stretching of the 3D covalent bonds since rigid thermoset resins have highly cross-linked polymeric structures [40].

Flexible resins initially behave in a similar elastic way as their rigid counterparts (Figure 3-2 (b)). A significant drawback to flexible resins is that they plastically deform at low strains. This is due to the lightly crosslinked chains permanently sliding past each other. Finally, flexible resins have high failure strains at low loads.

Elastomeric polymers possess highly coiled and kinked amorphous molecules. The initial low-modulus stage of the elastic response (Figure 3-2 (c)) results from structural changes of the kinked and coiled molecules; there is little or no influence from atomic bonding within the mer. The amorphous distribution and the relatively large spacing between the molecules permit the straightening of the mers; thus, at low stresses, large strains occur while the molecules are straightening. Once straightened, the applied load is resisted by the stiff covalent bond angle of the main chain, sharply increasing the resistance to deformation [40]. The deformation is fully elastic. During typical catheterization procedures, medical catheters deform within the first stage of the elastomeric resin stress-strain curve. The strain experienced by the outer layer of a 2mm diameter tube in flexion for a 100mm radius of curvature is less than 2%. Elastomeric resins undergo elastic deformation for strains above 10%.

3.3.2 Matrix selection for medical catheters

Many materials were considered for the matrix component of the medical catheters based primarily on material properties and, less significantly, on biological performance. Typical medical catheter resin materials discussed in Sections 2.3 and 0 are listed in Table 3-3.

Table 3-3: Nominal tensile modulus of resins used for medical catheters [38, 39]

Resin	Type	Tensile modulus, E_m (MPa)
Polyethylene	Flexible	3400
Polyvinylchloride	Flexible	2500-2600
Nylon 6,6	Flexible	2800
PTFE (Teflon)	Flexible	460-610
Polyurethane (thermoplastics)	Elastic	28-58
Silicone	Elastic	18-29

There are a number of considerations for matrix materials for use in 2D braiding. Matrix materials that must be injection moulded or extruded (PE, PVC, PTFE, nylon) cannot be considered since the processes are incompatible with braiding, as such pressures would change the desired braid angle. Flexible epoxy resins have similar stress-strain curves and are available in liquid form. For complete fibre impregnation, low resin viscosity is required [41]. Resins with viscosities between 350 and 1000cps [39,42,43] and with gel times exceeding 15 to 30 minutes are required to impregnate fibre bundles that are composed of 10μm diameter fibres. Higher viscosity resins will not impregnate fibre bundles because of high flow resistance [41]. However, pourable matrices, having viscosities not exceeding 20,000cps could be used for individual wires, ribbons or large diameter polymeric fibres. In-house experiments showed that it was possible to impregnate small diameter fibre bundles with higher viscosity resins heated to 50°C, (below curing

temperatures), thus decreasing resin viscosity. This manufacturing practice has been well detailed [41]. Consequently, the silicones, polyurethanes and a flexible epoxy (Table 3-4) were selected for further study. For completeness, a rigid epoxy (Epon 825 epoxy resin and Ancamine 1482 hardener) was also selected.

These matrices, together with the candidate fibres (Table 3-2), will be used in the design of the single braided model catheter that possesses similar rigidities as existing medical catheter guidewire systems. A predictive model will be used to calculate the rigidities. However, for reinforcement using fibre composite strands, any predictive models require estimates of elastic constants; these will be discussed in the next section.

Steel ribbons and wires were included for completeness in this section; however, changing the fibre type, fibre volume fraction and strand twist can vary the properties of composite strands much more than for metallic ribbons and wires. Therefore, there will be no further consideration of metallic ribbons or wires.

Table 3-4: Candidate matrix materials[3]

Material	Type	Company	Elongation (%)	Hardness	Tensile modulus (MPa)	Shear modulus[1] (MPa)	Viscosity[2] (Centipoise)	Gel time (min)	Comment
Silicones									
RTV 118	Elastic	GE	325	25A	18.27	7.02	20,000	20	
RTV 11	Elastic	GE		45A	29.2	11.23	12,000	60	
Polyurethanes									
RP 6443	Elastic	REN	475	95±5A	58.28	22.42	2,500	17	Semi-rigid
RP 6434	Elastic	REN	500	35-40A	26.7	10.3	500	19	Very Flexible
Epoxy									
Scotchweld 2216	Flexible	3M	51	35-50D	172	57.3	10 000	120	Flexible
Epon 825	Rigid	Shell Canada Chemicals Co.			3500	1300	300 at 50°C	3hours at 50°C	

[1] $G_m=E_m/2(1+\nu_m)$
[2] At room temperature, unless otherwise specified
[3] Information obtained from material data sheets and manufacturer technical assistance of Ge Silicones and Ren Plastics.

3.4 Determination of elastic constants for fibre composite materials

3.4.1 Introduction

A number of elastic constants of the selected fibre composite materials are required as input for any fibre composite predictive model. The elastic constants are a function of matrix and fibre properties and the fibre volume fraction. Elastic constants can be determined experimentally; however, there are a large number of candidate fibres (Table 3-2) and matrices (Table 3-4) and thus experimental testing would not be a practical approach. Elastic constants can also be predicted with variable accuracy using micromechanical models. Sensitivity of any developed model to elastic constants predicted by micromechanical models will need to be evaluated to ensure that small differences will not significantly affect the final results.

A braided fabric composed of interwoven strands is shown in Figure 3-3. Matrix is added to form the composite. Each fibre/matrix strand is a fibre composite material in which the fibres are primarily aligned, parallel, and oriented along the length of the strand idealized as a unidirectional lamina. Additional laminae-related concepts will be discussed in terms of micromechanical models in the next section.

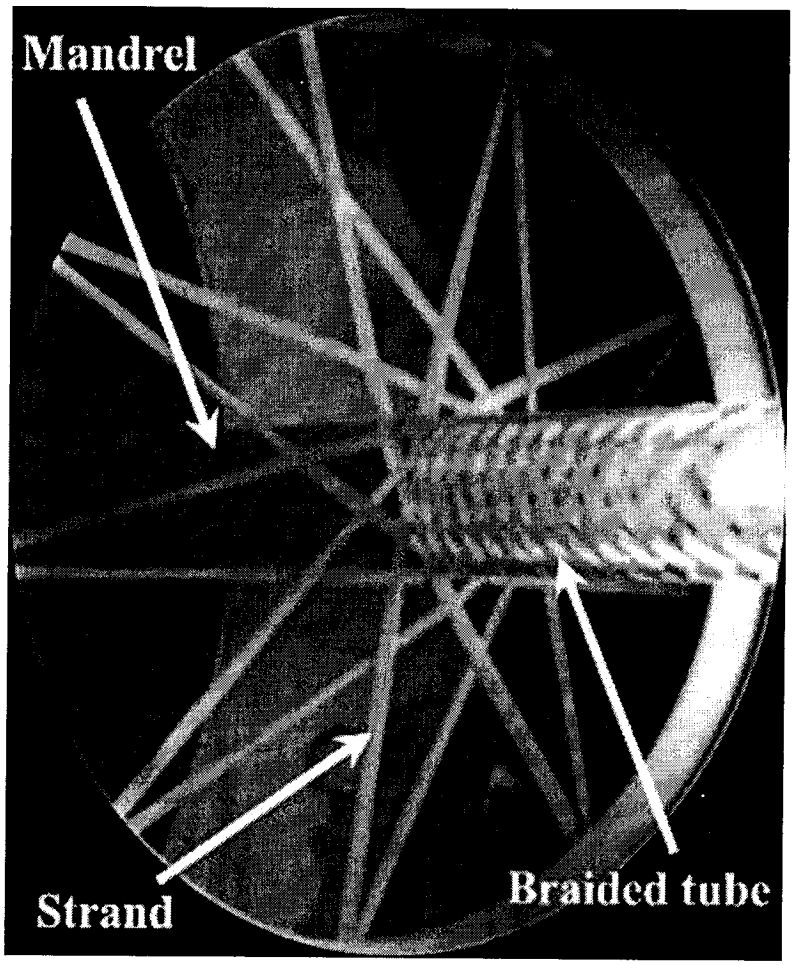

Figure 3-3: Single overlap (diamond) type braiding pattern being produced

3.4.2 Definition of a unidirectional composite

A lamina is composed of stiff, strong, parallel fibres within a less stiff, weaker matrix material. Because of this difference in matrix and fibre properties, and the uniform fibre directionality, the fibre composite exhibits orthotropic behaviour [44]. Figure 3-4 shows a theoretically perfect unidirectional lamina and the conventional material axes. It is, however, important to note that the fibres contained in a lamina are actually more randomly distributed since perfect alignment and distribution is nearly impossible to obtain unless very large fibres are employed [44].

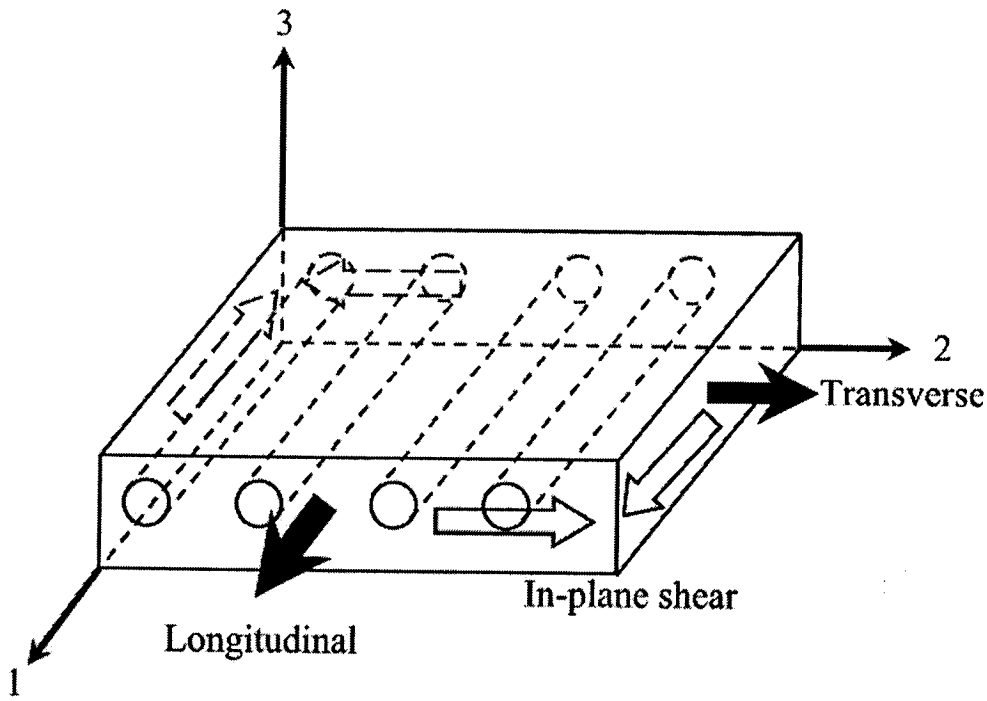

Figure 3-4: Representation of a unidirectional lamina and material directions (1, 2, 3) (adapted from [44])

Although there are many factors that affect the magnitude of lamina elastic constants, the most important one is the relative proportion of fibre and matrix referred to as volume fraction. For the following sections, the subscripts f, m, c will be used for fibre, matrix and composite, respectively.

The volume fractions of the fibre (V_f) and the matrix (V_m) are generically defined as:

$$V_i = \frac{v_i}{v_c}, i = f, m \qquad \textbf{3-1}$$

where v denotes constituent volumes (m^3) and $V_m = 1 - V_f$.

3.4.3 Unidirectional laminar material properties

The required lamina elastic constants for evaluating model catheter rigidities are longitudinal tensile (E_{11T}) and compressive (E_{11C}) moduli; transverse tensile (E_{22T}) and compressive (E_{22C}) moduli; and, in-plane (G_{12}) and transverse (out-of-plane) shear (G_{23}) moduli, as well as major Poisson's ratio (ν_{12}) and out-of-plane Poisson's ratio (ν_{23}). The tensile and compressive values of an elastic constant are evaluated from the same micromechanical model.

The following section will review the literature about micromechanical predictive models used to determine the above elastic constants. For the following analyses, the stress is always transferred from the matrix to the fibres through the fibre-matrix interface; thus, different elastic constants are fibre and/or matrix dependent.

3.4.3.1 Longitudinal elastic modulus, E_{11}

Many models predict elastic constants. The first model examined, for longitudinal modulus of elasticity, is illustrated in Figure 3-5. It is assumed that the fibres are uniform in properties and in diameter, continuous and parallel throughout the composite; that perfect bonding exists between the fibres and the matrix; and finally that no slippage can occur at the interface. Thus the axial strains experienced by the fibres, matrix and lamina are equal. The resulting micromechanical model is:

$$E_{11T,C} = E_f V_f + E_m V_m \qquad \textbf{3-2}$$

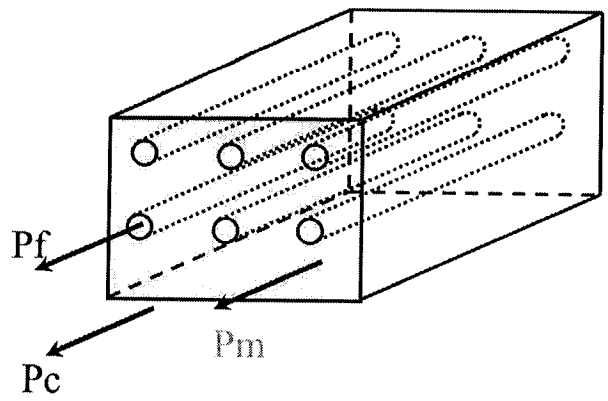

Figure 3-5: Unidirectional model for longitudinal properties (adapted from [44])

This type of relationship is called a "rules of mixtures prediction" (ROM) because the contribution of each constituent is proportional to their volume fraction. The load sharing between the fibres and the matrix increases longitudinal properties as compared to pure matrix. The prediction from this equation is quite accurate and is generally the accepted micromechanical model.

3.4.3.2 Major Poisson's ratio, ν_{12}

The major Poisson's ratio is also generally approximated by a rule of mixtures equation, and can be written as:

$$\nu_{12} = \nu_f V_f + \nu_m V_m \qquad \textbf{3-3}$$

where ν_f, ν_m and ν_{12} are the fibre, matrix and lamina major Poisson's ratio, respectively. Note that the transverse-to-longitudinal Poisson's ratio is found using the following relation:

$$\nu_{21} = \nu_{12} E_{22}/E_{11} \qquad \textbf{3-4}$$

The above models are generally accepted without controversy. In the following sections, models for the other elastic constants listed earlier are reviewed. Different models will be discussed and an individual model will be selected for each elastic constant for use in this work; a selection is required because of the different level of agreement for each model.

3.4.3.3 Transverse elastic modulus, E_{22}

Many models have been developed for the transverse modulus of unidirectional composites, E_{22}. Fibres act as deformation restrictions that result in a higher transverse tensile modulus than the matrix modulus. There are three models generally considered: Rule-of-mixtures, Halpin-Tsai, and Adams and Doner.

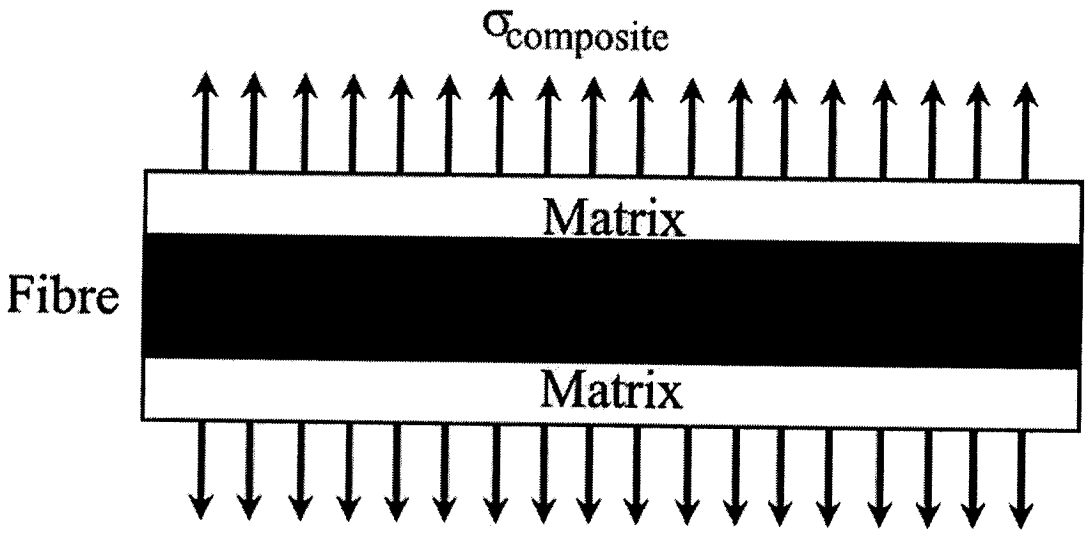

Figure 3-6: Transverse model (adapted from [44])

Figure 3-6, illustrates the ROM model where, again, it is assumed that the fibres have uniform properties and diameter, and are continuous and parallel throughout the composite. The transverse modulus is determined by:

$$\frac{1}{E_{22T,C}} = \frac{V_f}{E_{f_{22}}} + \frac{V_m}{E_m} \qquad \textbf{3-5}$$

where E_{f22} is the transverse fibre modulus, E_m is the matrix elastic modulus, and V_f and V_m are the fibre and matrix volume fractions, respectively.

The Adams and Doner [45] finite difference method was reviewed; however, the predictions must be interpolated from design figures and thus will not be used.

Halpin and Tsai [46] developed regression-based equations that approximate the results of more exact micromechanic analyses [44]. In generalized form, the equations are:

$$\frac{E_{22}}{E_m} = \frac{1+\xi\eta V_f}{1-\eta V_f} \qquad \textbf{3-6}$$

where

$$\eta = \frac{(E_f/E_m)-1}{(E_f/E_m)+\xi} \qquad \textbf{3-7}$$

and where ξ is defined as a measure of reinforcement that depends on fibre and packing geometry and on loading conditions[1]. It has been shown that experimental results are closer to the predictions from the Halpin-Tsai model [46,47]; therefore, the Halpin-Tsai formulation will be used to calculate transverse elastic moduli in this work.

3.4.3.4 In-plane shear modulus, G_{12}

Many in-plane shear properties models were reviewed and compared [48]. As in the previous case, there is a rule of mixtures-based equation suggested by Munro and Lee in 1995 [48] and Barbero [49]:

$$G_{12} = \frac{G_m}{V_m} \qquad \textbf{3-8}$$

[1] $\xi = 2$ for round or square fibres or 2a/b for rectangular cross-sections.

Halpin and Tsai [44] have suggested the following equations, in generalized form:

$$\frac{G_{12}}{G_m} = \frac{1+\eta\xi V_f}{1-\eta V_f} \qquad \textbf{3-9}$$

where

$$\eta = \frac{(G_{f12}/G_m)-1}{(G_{f12}/G_m)+\xi} \qquad \textbf{3-10}$$

where G_{f12}, G_m and G_{12} are the longitudinal shear modulus for the fibre, matrix and lamina, respectively. These equations are in good agreement with the results of Adams and Doner for volume fractions below 55 % [44].

Experimental results by Munro et al. [48] show that the Halpin-Tsai model suitably predicts the in-plane shear modulus. Thus, the Halpin-Tsai model will be used to predict the in-plane shear modulus.

3.4.3.5 Out-of-plane elastic constants

Transverse shear properties have been difficult to predict and to obtain experimentally. Pastore and Yasser [50] suggested the following equation for G_{23}:

$$G_{23} = \frac{E_{22}}{2(1+\nu_{23})} \qquad \textbf{3-11}$$

However, E_{22} and ν_{23} must also be calculated using micromechanical models, thus this method was not deemed appropriate.

Ko et al. [27] defined G_{23} as:

$$G_{23} = \frac{G_m}{\left(1-V_f^{1/2}(G_m/G_{f23})\right)} \qquad \textbf{3-12}$$

while Barbero defined it using the stress-partitioning parameter (SPP) technique [49] as:

$$G_{23} = G_m \frac{V_f + \eta_{23}(1 - V_f)}{\eta_{23}(1 - V_f) + V_f G_m / G_{f12}}$$

$$\eta_{23} = \frac{3 - 4\nu_m + G_m / G_{f12}}{4(1 - \nu_m)} \qquad \text{3-13}$$

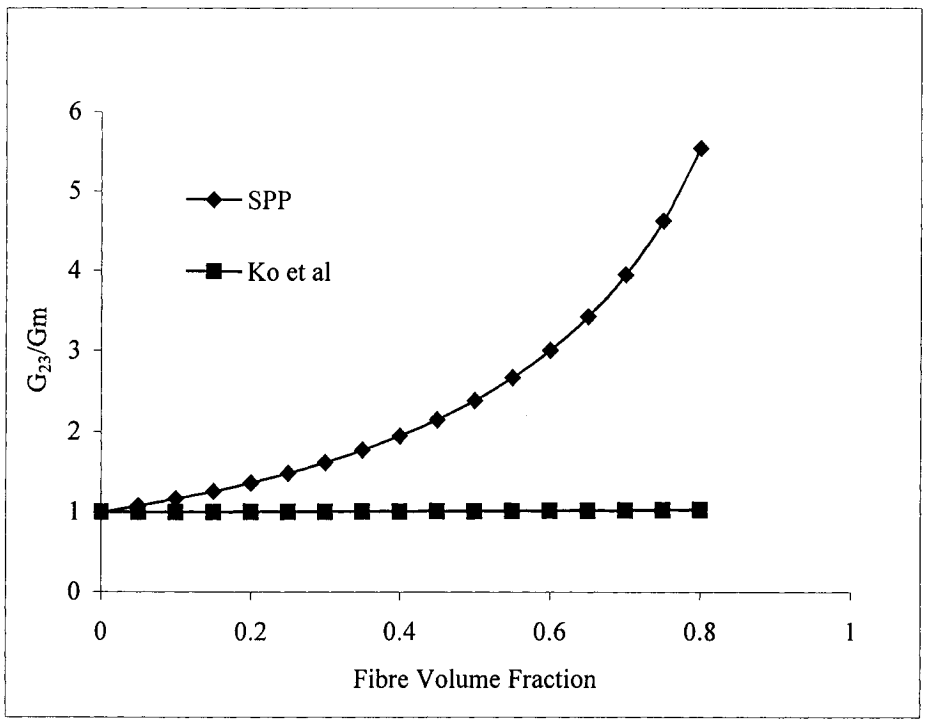

Figure 3-7 Comparison of G_{23}/G_m based on E-glass properties.

The difference between the Ko and Barbero models is seen in Figure 3-7. Clearly, the SPP model is sensitive to changes in fibre volume fraction. Since G_{f23} could not be found, G_f was used for the Ko model; this would not affect the shape of the curve since both values are constant. However, no experimental data was found to validate either one. Since Barbero's model appears to vary with volume fraction, which is in agreement with other micromechanical models, it is selected for this work. It is believed that out-of-plane elastic constants have little to no effect on the overall elastic constants of the structure; this will be shown in a subsequent chapter.

Finally, the out-of-plane Poisson's ratio (ν_{23}) was defined by Ko et al. [27] as:

$$\nu_{23} = V_f \nu_{f23} + V_m (2\nu_m - \nu_{21}) \qquad \textbf{3-14}$$

where ν_{f23} is the fibre out-of-plane Poisson's ratio.

3.5 Conclusion

This chapter introduced candidate fibre and matrix materials. Microstructural and loading response differences between elastomeric, flexible and rigid matrix materials were also presented. Many micromechanical models, which were developed to predict various lamina elastic constants, were discussed and selected for use as inputs to a future predictive model. A rule of mixtures approach was selected for the longitudinal elastic modulus and major Poisson's ratio. The Halpin-Tsai model was selected for the transverse elastic modulus and in-plane shear modulus. Finally, the stress partitioning parameter model was selected for the out-of-plane shear modulus and the Ko approach was chosen for the out-of-plane Poisson's ratio.

Although the most appropriate micromechanical models have been selected to predict elastic constants, there is controversy regarding the selection of the most appropriate model. Therefore, as aforementioned, the sensitivity of the proposed CLPT model to variations in the elastic constants presented in this chapter will be evaluated.

CHAPTER 4 : REVIEW OF ANALYTICAL MODELS

4.1 Introduction

As discussed in Section 2.4, the following rigidities are of interest for medical catheters: axial rigidity, EA, flexural rigidity, EI, torsional rigidity, GJ, where, A, I and J are functions of the medical catheter inner and outer diameters. For isotropic materials, E and G are constant values. For braided composite materials, E and G are substituted for by E_x and G_{xy}, the braid longitudinal elastic modulus along the medical catheter axis and braid shear modulus at right angle to the medical catheter axis, respectively. Both values depend on the matrix and fibre elastic constants, V_f and fibre braid angle. A number of models based on the concept of a unit cell have been developed for woven and braided composites to predict E_x and G_{xy}; these models will be examined in a subsequent section; first, the unit cell geometry of a braided structure is introduced.

4.2 Basic geometric characteristics of braids

Different configurations of braid can be produced (Figure 4-1); namely, the single overlap or diamond braid, the double strand overlap or regular braid, and the triple strand overlap or Hercules braid [51].

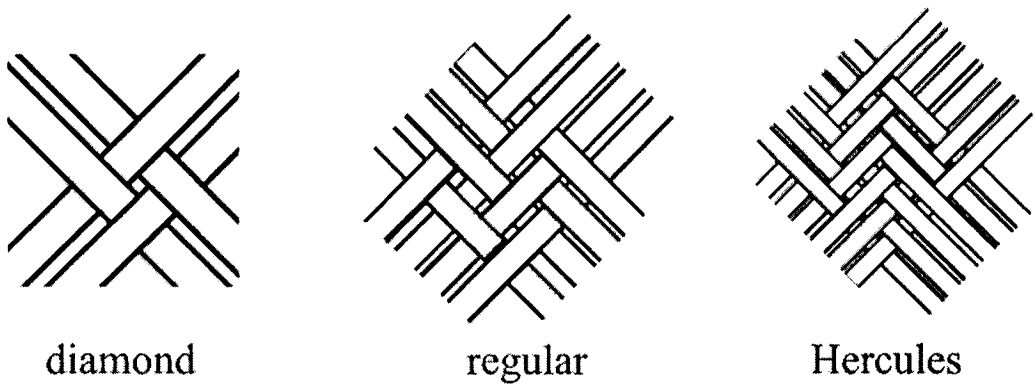

Figure 4-1: Types of braiding patterns; the diamond braid is a single overlap; the regular or 2x2 braid is a double overlap; the Hercules braid is a triple overlap.

This work focuses on the diamond braid configuration for which the repeating pattern or unit cell is shown in Figure 4-2. The braid angle, θ, is the angle between the strand and the mandrel axis; X and Y are the width and height of the unit cell, respectively. W_y is the width of the strand. Woven and braided fabrics will both be discussed in this review since a plain weave fabric unit cell is equivalent in structure to a $\theta=45°$ closed mesh diamond braided fabric unit cell in which the individual strands are adjacent to each other. Furthermore, research work dealing with plain weave fabrics is more prevalent than that for braids. In the general case of an open mesh configuration, matrix only regions (M) separate the individual strands as shown in Figure 4-2. The figure depicts the basic diamond braid unit cell with regions of overlapping fibre composite strands and matrix, of matrix only and of undulating fibre composite strands. The top view of a unit cell does not illustrate the fibre undulation or overlap; thus, changes are required in the unit cell definition of Figure 4-2. Undulations due to the fibre intertwining can significantly reduce the mechanical performance of the braid in-plane stiffness and strength [52].

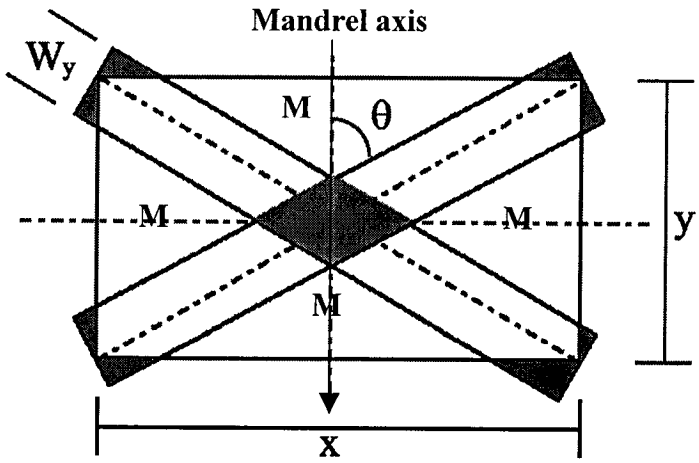

Figure 4-2 Top view of a diamond braid unit cell (adapted from [53]); matrix only regions are marked with an M.

The most pertinent existing analytical models developed to predict stiffness characteristics of woven/braided composite structures will be reviewed. These models require the preliminary analysis of laminar elastic constants presented in Section 3.4.3 and knowledge of unit cell geometry.

Falzon, Herszberg and Baker [54] reviewed and evaluated different methods for predicting elastic properties and strength of flat plain weave fabrics. Three general approaches were examined: finite element (FE) models, elementary models such as the fabric geometry model (FGM), and modified classical laminate plate theory (CLPT). Similar models were also developed specifically for cylindrical composites [55,56].

The following sections will discuss these types of models, emphasizing the capabilities of each to predict elastic constants of woven/braided structures.

4.3 Modelling the stiffness of flat braided structures

4.3.1 Finite element models

In their extensive review, Falzon et al. [54] stated that finite element (FE) models are the most powerful means of analyzing textile materials in two or three dimensions, but are more appropriate for strength predictions.

Figure 4-3 represents a FE model developed by Nakai et al. [26] which analyzes complex braided structures (Figure 4-3 (c), (d)) by reducing the structure to its simplest element, a fibre bundle. The fibre bundle is modelled as a three-dimensional structure composed of longitudinal fibre and diagonal resin truss members (Figure 4-3(a)).

Similarly, Ko et al. [27] used a comparable FE model, the finite cell model (FCM), to analyze braided structures. The FCM is a numerical structural truss analysis of a unit cell structure. The unit cell is defined as the smallest repeated volume and is treated as a 3D space-truss structure having pin-joints with three degrees-of-freedom in translation. The fibres are assumed to travel along the diagonals in the unit cell. The macrostructure is subjected to a virtual displacement and is then analyzed with the principle of virtual work. The governing equations for FE models are based on a force-displacement relationship, as the following example based on the finite cell model defined by Ko et al. [27] demonstrates.

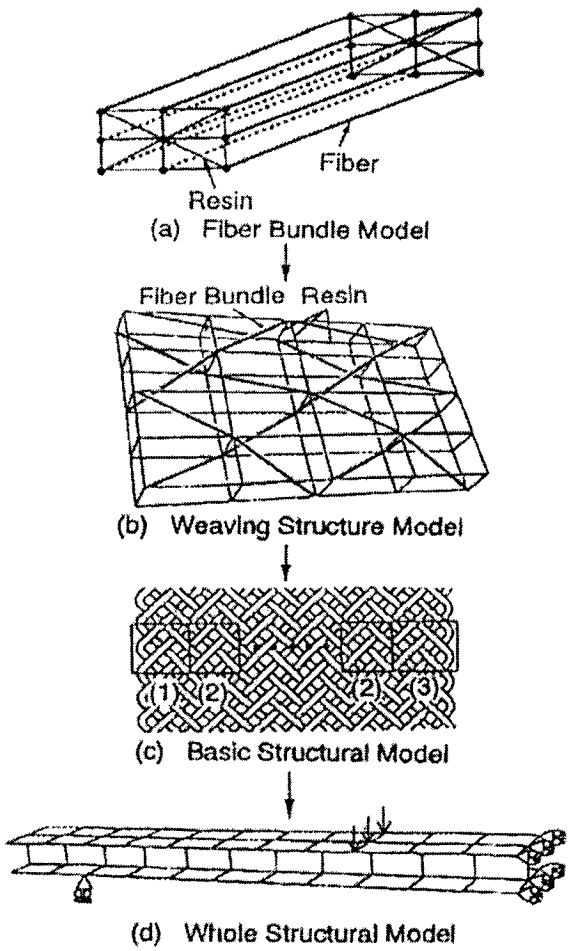

Figure 4-3: FE structure as defined by Nakai et al. [26]

The nodal displacements are defined as:

$$\{q\}=[e]\{r\} \qquad \textbf{4-1}$$

where $\{q\}$ is the member deformation,

$[e]$ is the displacement transformation matrix,

and $\{r\}$ is the nodal displacement.

The force-deformation relationship is given by:

$$\{Q\}=[K']\{q\} \qquad \textbf{4-2}$$

where $[K']$ is the stiffness matrix for a six degrees-of-freedom truss.

The principle of virtual work states that the work done on a system by external forces is equal to the strain energy stored in the system; thus, the principle of virtual work can be written as:

$$W=\{\underline{r}\}^T\{R\}=\{\underline{q}\}^T\{Q\} \quad \textbf{4-3}$$

where {R} are nodal forces

and $\underline{r}$ and $\underline{q}$ are the virtual displacement and deformation, respectively.

Combining the previous equations yields the generalized form of the FE model,

$$\{R\}=[e]^T[K'][e]\{r\} \quad \textbf{4-4}$$

In another related study, Hamada et al. [57], using the Nakai [26] model, analyzed the flexural rigidity of braided composite tubes with FEA. They modelled the system but did not provide any information on any comparison between analytical and experimental results. FE analysis proved capable of predicting torsional rigidity and shear stress of braided tubes [58]; however, the results were far from convincing as the predictive results were approximately one-half of the experiment values.

Foye's analysis, referenced in Falzon et al [54], subdivided the unit cell into subcells comprised of oriented unidirectional composites and matrix and treated them individually as inhomogeneous hexahedral finite elements.

Falzon et al. [54] emphasized that FE models were capable of stiffness predictions as well as strength analysis but that the level of additional complexity to predict stiffness of a unit cell, as compared to other approaches, was significant. In addition, the fibres are assumed to be straight and thus do not accurately account for the fibre undulation in an actual woven/braided fabric.

4.3.2 Elementary models

4.3.2.1 Fabric geometry model

Ko et al. [27] developed the Fabric Geometry Model (FGM) to study the compressive behaviour of braided metal-matrix composites. The FGM is an elementary finite element method, similar in basic structure to the FCM, which defines a stiffness matrix for each strand that depends on the unit cell geometry and lamina elastic constants (Figure 4-4).

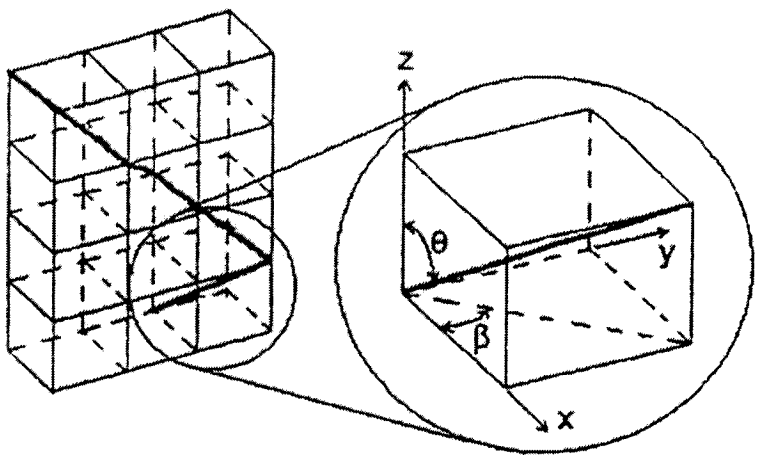

Figure 4-4: FGM structure [27]

FGM assumes isostrain – all parallel strands undergo the same amount of strain – and that the contribution of each strand is proportional to the percentage of the unit cell volume each strand occupies. Therefore, the stiffness of the unit cell is a volumetrically weighted sum of all the strand stiffnesses in the structural coordinate system. Using spatial coordinate transformation, the stiffness tensor can be obtained for appropriate fibre direction.

The stiffness matrix for each strand in the global coordinate system is expressed as:

$$[\overline{Q}_i] = [T_{\varepsilon,i}][Q][T_{\varepsilon,i}]^{-1} \quad \textbf{4-5}$$

where $[\overline{Q}_i]$ is the stiffness of the i^{th} system of strands,

$[T_{\varepsilon,i}]$ is the geometric transformation for the i^{th} system of strands

and [Q] is the stiffness of an equivalent unidirectional composite.

A system stiffness matrix is defined by superimposing the volume-weighted contribution of each strand system such as:

$$[\overline{Q}_s] = \Sigma k_i [\overline{Q}_i] \quad \textbf{4-6}$$

where k_i is the fractional volume of the i^{th} system of strands

and $[\overline{Q}_s]$ is the overall stiffness matrix of the structure.

To account for non-linear behaviour, the system stiffness should be calculated at every new strain level. Therefore, the incremental stress-strain behaviour is determined by:

$$\{\sigma\} = \{\sigma\} + [\overline{Q}_s][\Delta\varepsilon] \quad \textbf{4-7}$$

Soebroto, Hager, Ko and Pastore [59] found agreement (4% error) with preliminary experimental results using this method to predict the hoop strength of tubular fibreglass composites.

Conversely, Pastore and Yasser [50] modified the FGM because of specific drawbacks. They stated that the FGM failed the basic transverse isotropy assumption; in other words, the mathematical derivation produced elastic constants that did not exhibit the transverse isotropy required for unidirectional fibre composite. In addition, the transformation matrices associated with the stiffness calculations were not sufficiently robust to handle all cases. Their self-consistent FGM was developed to improve the

response by reformulating material property conditions on a micromechanical level. This is achieved using:

$$G_{23} = \frac{E_{22}}{2(1+\nu_{23})} \qquad \textbf{4-8}$$

4.3.2.2 Angle ply undulation model

Falzon et al. [54] developed the angle-ply undulation model that models the strand undulation by a single undulation angle ($\pm\psi$) line model. This method was developed to better account for through-the-thickness undulations and the in-plane off-axis orientations, which, according to the authors, were not sufficiently addressed in the FGM. The elastic constants are nonetheless calculated using the FGM analysis.

Although Falzon et al. [54] identified the FGM as adequate for stiffness prediction for shapes of varying complexity, Vandeurzen et al. [60] stated that FGM was incapable of correctly predicting shear moduli for woven-fabric composites. Falzon et al. [54] evaluated the FGM predictive model results to experiments performed on RTM plain weave fabrics made of carbon fibre plain weave fabric (G814) and epoxy resin (GY260). The fibre volume fraction was 58 % and the laminate thickness was 1.88 mm. Unidirectional properties were not provided. Young's modulus (E_x, E_y) and Poisson's ratio (ν_{xy}) were experimentally determined from tensile tests (ASTM D3039-76) and shear moduli (G_{xy}) from the rail shear test (ASTM D 4255-83). The FGM had 4 %, 3 %, 8 % and 40 % errors for E_x, E_y, G_{xy} and ν_{xy}, respectively, with respect to the experimental results.

Overall, FGM-based models appear to predict elastic constants with accuracy; however, the approach does not model undulating strands accurately.

4.3.3 Classical laminate plate theory

The classical laminate plate theory (CLPT), developed to predict in-plane properties of flat laminate composites, was modified by Ishikawa and Chou [61] to predict stiffness and strength behaviour of woven composites. Compared to regular laminates, woven fabrics have undulations that are not accounted for in CLPT. Two early and relevant models were developed: the mosaic model (Figure 4-5), a simplistic method of modelling the undulation by an assemblage of asymmetrical cross-ply laminates; and the fibre undulation model (Figure 4-6), which improved on the single angle approach of FEA (Section 4.3.1) and accounts for continuity and undulation by using a sine function to model the fabric waviness.

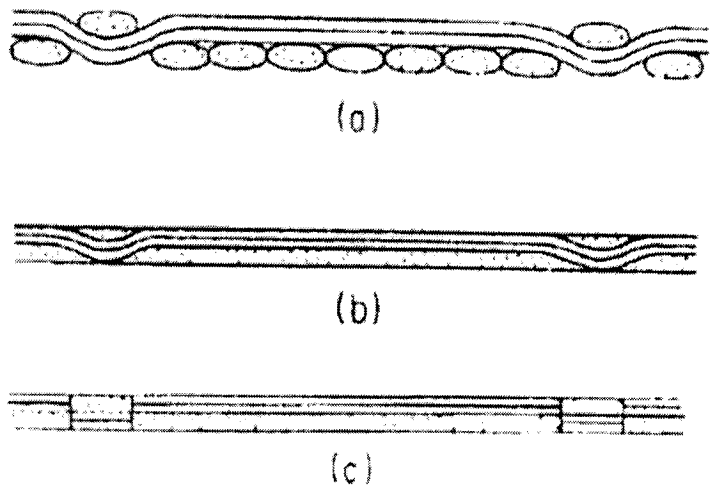

Figure 4-5: Fabric models for mosaic model: (a) actual woven fabric; (b) first simplification: strands are regrouped in regions containing strands going in the same directions and fabric is given the same thickness; (c) all unidirectional sections are divided in rectangular lamina [61].

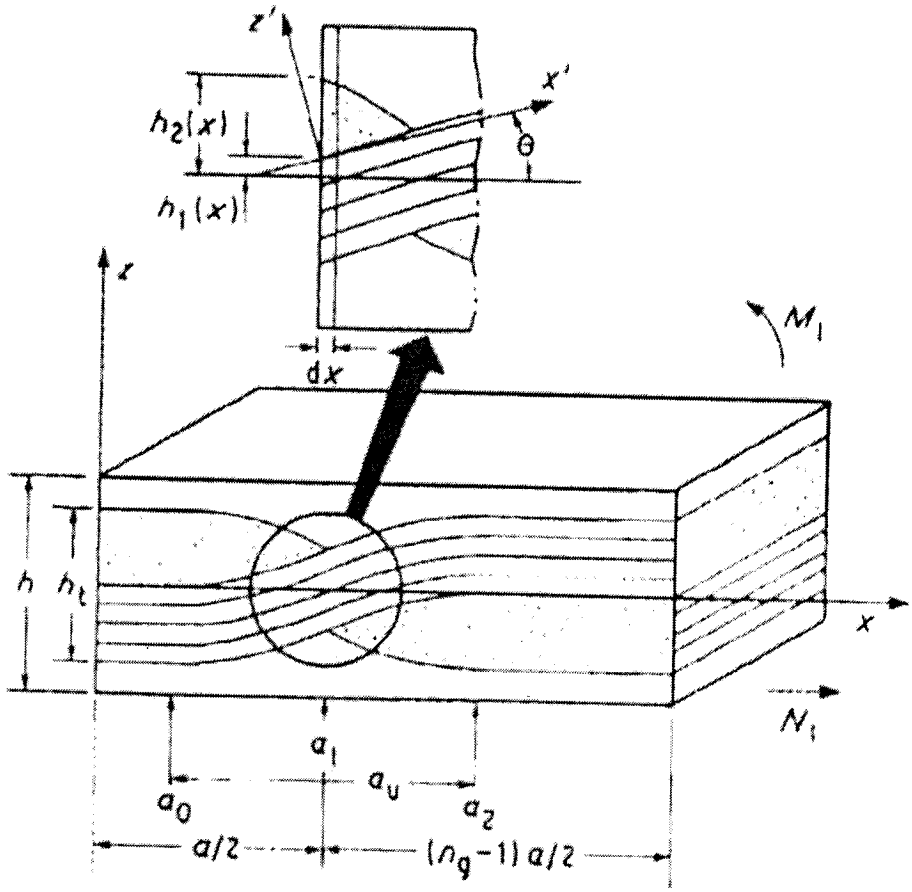

Figure 4-6: Fibre undulation model [61].

Redman et al. [62] developed a "CLT/rule-of-mixtures" based model where the stiffness of each offset fibre is analysed separately and then combined to obtain the overall stiffness of the structure. As in the case of the Falzon's angle ply undulation model (Section 4.3.2.2), Redman's model assumes a single undulation angle, but also assumes open meshing.

Naik and Ganesh [63] predicted thermoelastic properties of woven fabrics with an improved classical laminate plate theory approach. The work focused on a representative unit cell that would account for "strand undulation and continuity, actual strand cross section and weave geometry, strand fibre volume fraction and gaps between the two adjacent strands" [63]. An important part of their work was to compare various approaches

to modelling strand undulation (sinusoidal, circular, element array model with parallel-series combination). The important conclusion was that the sinusoidal approach modelled the undulation path more precisely.

The classical laminate plate theory is based on many concepts and on many assumptions. The first is uniform membrane strain and curvature at the midplane of the unit cell. This assumes perfect inter-laminae bonding in the laminate, therefore resulting in strains being distributed as in typical isotropic structures such as plates, shells and beams [64].

The following are the CLPT assumptions summarized by Gillespie et al. [65]:

- The laminate is in plane stress.
- Plates are constructed of an arbitrary number of layers of orthotropic sheets bonded together. However, the orthotropic axes of material symmetry of an individual layer need not coincide with the x-y axes of the plate.
- Plates are thin compared to the other dimensions.
- The displacements in the x, y and z directions, commonly referred to u, v and w[1] are small compared to the plate thickness.
- In-plane strains are small compared to unity.
- In order to include in-plane force effects, non-linear terms in the equations of motion involving products of stresses and plate slopes are retained. All other non-linear terms are neglected.
- Transverse shear strains are negligible.

---

[1] This common use of u and v as displacement will only be used in this section; for the document, the nomenclature set earlier is correct.

- Tangential displacements in x and y are linear functions of the z coordinate.
- The transverse normal strain is negligible.
- Each ply obeys Hooke's law.
- The plate has constant thickness.
- Rotational inertia terms are negligible.
- There are no body forces.
- Transverse shear stresses vanish on the surfaces.

For a traditional multi-layered laminate, the longitudinal elastic and shear moduli are determined in the following manner[2]. The stress-strain relationship for the laminate is formulated, assuming midplane membrane strain (ε^0) and curvature (κ^0), as:

$$\begin{Bmatrix} N \\ M \end{Bmatrix} = [S] \cdot \begin{Bmatrix} \varepsilon^0 \\ \kappa^0 \end{Bmatrix} \qquad \textbf{4-9}$$

where

$$[S] = \begin{bmatrix} A & B \\ B & D \end{bmatrix}$$

and where N and M are the stress and moment resultants, in GPa-m and GPa-m^2, respectively. A, B and D, the plane stress 3x3 matrices, are respectively called the extensional stiffness matrix, coupling stiffness matrix and bending stiffness matrix for the unit cell configuration. Briefly, the extensional matrix defines axial stiffness; the bending matrix defines the principal bending/torsional effects; while the coupling matrix defines the

[2] Although the method is found in most introductory text on composite materials, the development of these equations is detailed in Appendix 1.

influence that extensional and bending effects can have on the curvature and longitudinal deformations of the structure, respectively.

The longitudinal elastic and shear moduli of the laminate that are used to calculate axial, flexural and torsional rigidities, as detailed in Appendix 1, are:

$$E_x = \frac{1}{a_{11}t}$$
$$G_{xy} = \frac{1}{a_{66}t} \qquad \text{4-10}$$

where a_{11} and a_{66} are found the compliance matrix, [C] which is inverse of the stiffness matrix, [S].

In a braided composite, the fibre strands are woven, resulting in fibre undulation. To account for the undulations, a by-region volumetric analysis of the unit cell must be performed. Raju and Wang [66] defined the unit cell of a woven composite, which is equivalent to a 45° angle-plied full coverage braid, as a multi-layer system with strand undulations within the matrix. They divided the unit cell in a multi-region system with different layers of unidirectional composite and matrix (Figure 4-7) similar to Foye's FE model (Section 4.3.1). Finally, the strand undulation is defined as a sine function as in the Ishikawa and Chou undulation model.

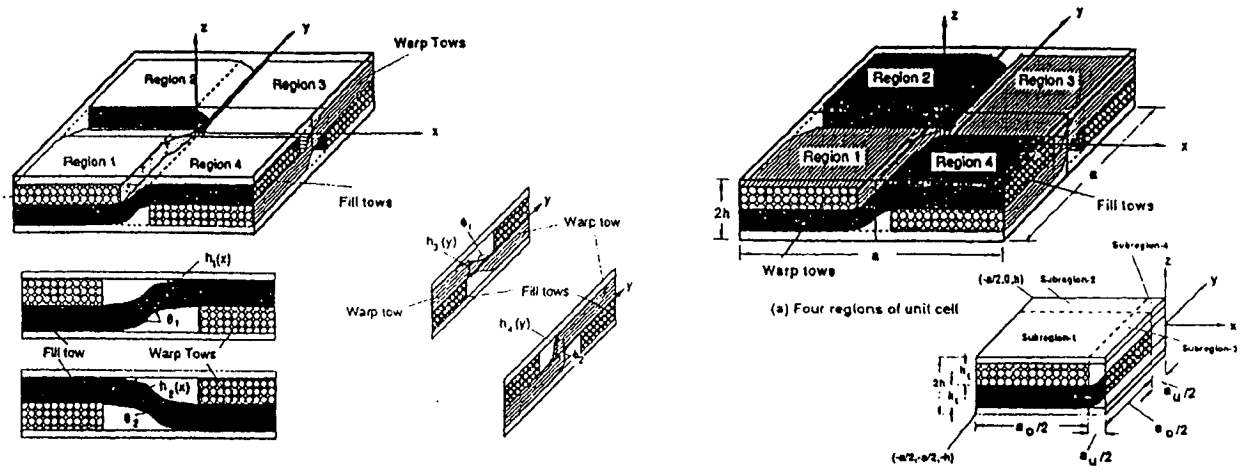

Figure 4-7: Unit cell definition for woven fabric with undulations (modified from [66])

The following modifications to the CLPT were introduced by Raju and Wang [66] to perform the volumetric analysis. The per unit load and moments were defined as:

$$\{N\} = \frac{1}{P_A}\int_{P_A}\{\overline{N}(x,y)\}dxdy$$
$$\{M\} = \frac{1}{P_A}\int_{P_A}\{\overline{M}(x,y)\}dxdy \qquad \text{4-11}$$

where $\overline{N}, \overline{M}$ are the stress and moment resultants on an infinitesimal element area dx·dy. To include the constitutive matrices for all sub-regions of a unit cell, the CLPT equations developed for laminates were expanded as follows:

$$\{N\} = \frac{1}{P_A}\sum_{i=1}^{k}\left[\left(\int_{R_i}[A]_i\,dR_i\right)\{\varepsilon^0\} + \left(\int_{R_i}[B]_i\,dR_i\right)\{\kappa^0\}\right]$$
$$\{M\} = \frac{1}{P_A}\sum_{i=1}^{k}\left[\left(\int_{R_i}[B]_i\,dR_i\right)\{\varepsilon^0\} + \left(\int_{R_i}[D]_i\,dR_i\right)\{\kappa^0\}\right] \qquad \text{4-12}$$

where P_A is the projected area on the midplane of the unit cell, R_i is the area of the i^{th} region, k is the total number of regions in the unit cell and $[A]_i$, $[B]_i$, $[D]_i$ are the constitutive matrices of the individual regions.

Finally, Falzon et al. [54] describe the Ishikawa and Chou models as limited because they only predict in-plane properties and are not suited for complicated structural shapes. However, Raju and Wang [66] found encouraging results between their more complex CLPT undulation zone model for woven fabrics and experimental results from other sources for plane weave structures. They compared their CLPT model predictive results for a plain weave with the experimental results from Foye, which, as aforementioned, also subdivided the unit cell into smaller regions. Fibre properties used are listed in Table 4-1. The properties of the plain weave predictive model and the experimental results are found in Table 4-2. Both methods give similar results.

Table 4-1: Elastic constants [66]

Elastic constants	Value
E_{f11}	144.80 GPa
E_{f22}, E_{f33}	11.73 GPa
ν_{f12}, ν_{f13}	0.23
ν_{f23}	0.30
G_{f12}, G_{f13}, G_{f23}	5.52 GPa
E_m	3.45 GPa
ν_m	0.35
G_m	1.28 GPa

Table 4-2: Experimental and analytical results [66]

Method	E_x (GPa)	G_{xy} (GPa)
Experimental	62.95	-
CLPT (Raju and Wang)	60.61	4.89
FE (Foye)	63.78	4.83

Compared to the experimental results reported for E_x, the CLPT had errors of 3.7 % while the FE models had 1.4 %. The shear modulus results were 4.83 GPa for the FE and 4.89 GPa for the CLPT, which is a 1.4 % difference.

Recent developments of the CLPT model, such as done by Naik and Ganesh, and Raju and Wang, show good capabilities of predicting in-plane response to axial, flexural and torsional loading.

4.4 Modelling of cylindrical braided tubes

All the models discussed previously are for flat plates. Models exist for cylindrical braided tubes but flat plate models are often used to obtain elastic properties for structures of various forms; however, caution must be taken to minimize curvature effects by having a thin cylinder [56] and relatively small unit cell geometry with respect to the cylinder dimensions.

Two analytical methods have been developed specifically for woven/braided tubular composites. Ari-Gur and Krizan [55] presented a model for tubular composites assuming that every woven layer is separated into a representative unidirectional lamina with a thickness proportional to the fibre volume fraction of each individual orientation. A major drawback is that it assumes taut fibres to minimize any curvature effects, neglecting the effect of the undulations. In addition, the result of the model was not compared to experimental results.

The second method is cylindrical classical laminate theory. The constitutive equation is analogous to that of the CLPT; however, the equations are in the cylindrical coordinate system. Most of the theory developed for plates in the preceding section applies to the cylindrical classical laminate theory [56] and will not be repeated. The constitutive matrices are the same in both flat plate and cylindrical approaches; thus, the elastic constants can be found as detailed in Section 4.3.3. Again, this model does not consider

through-the-thickness properties. It does however seem to be able to predict in-plane responses to axial, torsional and bending efforts for tubular sections. Whitney et al. [56] used this method to predict the type of deformation that would occur in 45°, helically filament-wound cylindrical shells. They found that the model predicts the correct mode of deformation under simple and combined loading but they do not present any numerical values, only observations. Again, a major drawback of the model is that it neglects the effect of the undulations.

4.5 Model evaluation

The preceding sections described types of models that could be used to predict the rigidities of braided tubes and compared some results. Table 4-3 summarizes the models and provides the advantages and disadvantages for each. Briefly, finite element methods can predict stiffness and strength but are very complex, and are computer memory consuming. FE models are capable of obtaining through-the-thickness properties, which are not important for medical catheter design. Medical catheters should be designed based on elastic deformation and rigidity requirements and not strength; therefore, an FE method was not selected for this work.

To date, the FGM seems to be the most widely used model. However, it is apparently not geometrically thorough since fibre undulation is not accounted for sufficiently; it is difficult to conceive how better geometric parameters could be incorporated beyond the angle ply undulation model without integrating a more complex unit cell.

The CLPT has weaknesses since it does not account for through-the-thickness properties; but the unit cell can be improved to better reflect the fabric geometry and is appropriate for predicting elastic constants of woven and angle-ply.

It could be argued that a cylindrical model should be used for this work. However, since neither model evaluated in Section 4.4 accounts for fibre undulation, they are inappropriate for this work. In addition, the unit cell size is relatively thin with respect to the tube dimensions; thus, there is little concern in using a flat plate to model a thin, slightly curved section. Moreover, the same elastic constants required for this work can be determined using the classical laminate plate theory developed for flat plates; therefore, it is deemed acceptable to use a less complex model if it will yield the same information.

Table 4-3: Comparison of the capabilities of the predictive models

Method	Fabric type	Basis of model	Unit cell	Equations	Load	Comparison of analytical results with experimental results	Advantages	Disadvantages
Finite Cell Method (FCM) and Finite Element Method (FE)	-3D or 2D -Any type of fabric	-Must calculate homogeneous properties with micromechanics or lamination theory -Multi-level modelling -Based on concept of fabric unit cell and structural truss analysis -Unit cell treated as 3D space truss structure -Virtual work principle -Nodal displacement -Strain energy consideration	Figure 4-3	-Nodal displacement: $\{q\}=[e]\{r\}$ -Force-deformation relationship: $\{Q\}=[K']\{q\}$ -Principle of VW: $\{\underline{r}\}^T\{R\}=\{\underline{q}\}^T\{Q\}$ Leads to: $\{R\}=[e]^T[K'][e]\{r\}$ where: q: member deformation [e]: displacement transformation matrix $\{r\}$: nodal displacement $[K']$: stiffness matrix $\{R\}$: nodal forces	-Axial -Shear -Bending -Torsion	-For woven fabric, Nastran software: Upper bound shows good agreement longitudinal and transverse moduli [54] -Underestimates in-plane shear modulus [54] -50 % difference in major Poisson's ratio [54] -Poor results for torsion of braided tubes [58]	-Best suited for strength analysis -All types of loading	-Lengthy process -Complicated programming -Memory consuming

Method	Fabric type	Basis of model	Unit cell	Equations	Load	Comparison of analytical results with experimental results	Advantages	Disadvantages
Fabric Geometry Model (FGM) and Angle ply undulation model	-3D -Braid -Woven	-Stiffness of each strand calculated with Hooke's law and transformed in the general coordinates. -The fractional volume of the strand determines level of influence of each strand -The total structure stiffness is the sum of the all the volumetrically weighted stiffness components	Figure 4-4	$[\overline{Q_i}] = [T_{\varepsilon,i}][Q][T_{\varepsilon,i}]^{-1}$ $[\overline{Q}_s] = \Sigma k_i [\overline{Q}_i]$ $\{\sigma\} = \{\sigma\} + [\overline{Q}_s][\Delta\varepsilon]$ where: $[Q]$: the strand stiffness matrix $[T_{\varepsilon,i}]$: transformation matrix $[Q_i]$: stiffness matrix in the general coordinate system k_i : fractional volume of the i^{th} system of strands $[Q_s]$:overall stiffness matrix of the structure $\{\sigma\}$: stress $[\Delta\varepsilon]$: strain increment	-Axial -Bending -Torsion	For woven fabric: -Good results for longitudinal and transverse moduli [54] -Good results for in-plane shear modulus [54] -50 % difference in major Poisson's ratio [54] -Provides values for other properties but not compared	-Simple analysis -Adequate accuracy for stiffness predictions -Adaptable to complex architecture	-Does not provide possibility of modelling unit cell -Unsuitable for strength analysis
Classical laminate plate-based theories (CLPT)		-The CLPT assumes uniform membrane strain and uniform curvature at the midplane of the unit cell -Perfect bonding between lamina		The same constitutive equation is at the basis of all the different models of the classical laminate theory. Even the cylindrical version of the model has the same basic equations for the exception of the coordinate system in which the stresses and strains are evaluated. $\begin{Bmatrix} N \\ M \end{Bmatrix} = \begin{bmatrix} A & B \\ B & D \end{bmatrix} \cdot \begin{Bmatrix} \varepsilon^0 \\ \kappa^0 \end{Bmatrix}$			-Simple -Provides desired E and G	-No through-the-thickness properties

Method	Fabric type	Basis of model	Unit cell	Equations	Load	Comparison of analytical results with experimental results	Advantages	Disadvantages
Mosaic model	-2D -Biaxial woven fabrics	Idealize fibre waviness by laminate sections in orthogonal directions ignoring continuity. [7,21]	Figure 4-5	Component of the constitutive matrices $A_{ij} = \sum_{k=1}^{n} (\overline{Q}_{ij})_k (h_k - h_{k-1})$ $B_{ij} = \frac{1}{2} \sum_{k=1}^{n} (\overline{Q}_{ij})_k (h_k^2 - h_{k-1}^2)$ $D_{ij} = \frac{1}{3} \sum_{k=1}^{n} (\overline{Q}_{ij})_k (h_k^3 - h_{k-1}^3)$	Axial	-For woven fabric: Upper bound shows good results for longitudinal and transverse moduli of woven fabric. [54] -Underestimates in-plane shear modulus [54] -Underestimates major Poisson's ratio [54] -Does not predict other properties	-Simple	-In-plane properties only, no though-the-thickness properties -Poor representation of the unit cell -Too simplistic to account for all loading types
Fibre undulation model	-3D -Woven - Braiding	-CLPT that considers the effect of the undulation regions.	Figure 4-6	Expansion of the constitutive equation $\{N\} = \frac{1}{P_A} \sum_{i=1}^{k} \left[\left(\int_{R_i} [A] dR_i \right) \{\varepsilon^0\} + \left(\int_{R_i} [B] dR_i \right) \{\kappa^0\} \right]$ $\{M\} = \frac{1}{P_A} \sum_{i=1}^{k} \left[\left(\int_{R_i} [B] dR_i \right) \{\varepsilon^0\} + \left(\int_{R_i} [D] dR_i \right) \{\kappa^0\} \right]$ Component of the constitutive matrices $(A_i)_{subregion-m} = \int_x \left(\int_y \left[\int_z (\overline{Q}_i)_{subregion-m} dz \right] dy \right) dx$ $(B_i)_{subregion-m} = \int_x \left(\int_y \left[\int_z (\overline{Q}_i)_{subregion-m} \cdot z dz \right] dy \right) dx$ $(D_i)_{subregion-m} = \int_x \left(\int_y \left[\int_z (\overline{Q}_i)_{subregion-m} \cdot z^2 dz \right] dy \right) dx$ See section 4.3.3 for further details	-Axial -Bending -Torsion		-Clearly defines unit cell	-In-plane properties only, no though-the-thickness properties -Do not predict failure
Cylindrical CLPT	-3D -Tubular - Braiding			-Same as fibre undulation; A, B, D are the same as CLPT. -The elastic and shear moduli are calculated the same way	-Axial -Bending -Torsion	-Matched observed response of filament wound cylindrical shells	-Clearly defines unit cell	-In-plane properties only, no though-the-thickness properties -Do not predict failure -No undulation

Method	Fabric type	Basis of model	Unit cell	Equations	Load	Comparison of analytical results with experimental results	Advantages	Disadvantages
Ari-Gur and Krizan [55]	-Tubular - Braiding	-Layers separated in lamina with thickness proportional to fibre volume fraction			-Axial -Bending -Torsion	N/A	-Simple model -Through-the-thickness properties	-Bending equation does not appear appropriate for the compressive side of the cylinder in flexion -No undulation

4.6 Conclusion

The information detailed in the above table, combined with the various comparisons detailed in Section 4.3, provides enough justification to select the CLPT over the other models. In the next chapter, the proposed analytical method for obtaining the longitudinal elastic and shear moduli of a fibre composite braided unit cell is introduced and developed.

CHAPTER 5 : PROPOSED ANALYTICAL MODEL

5.1 Introduction

It was detailed in Section 4.3.3 that the braid longitudinal elastic and shear moduli required to evaluate the rigidities of a braided model catheter could be determined using classical laminate plate theory from equation 4-9. The proposed CLPT model to predict the braid longitudinal elastic and shear modulus is a generalization of the 0°/90° CLPT model developed by Raju and Wang [66] for plain weave fabrics that can account for angle-plied braided structures by determining modified A, B and D matrices. A major difference between 2D braids and plain weave fabrics is the physical limitations of braids in the jammed state. This state is defined as the strand position where adjacent strands jam against each other preventing any further movement in that particular direction [67]. This defines the minimum and maximum braid angles for a specific number of strands and strand width. These limits are not necessary for the Raju and Wang plain weave model; however, the predictions of the proposed braid model are only realistically valid between the maximum and minimum jamming angles.

This work focuses on the single strand overlap braid for which the repeating pattern or unit cell is shown in Figure 5-1. The braid angle, θ, is the angle between the strand and the mandrel axis, y; X and Y are the width and height of the unit cell, respectively. In the general case of an open mesh configuration, matrix only regions separate the individual strands as shown in Figure 5-1. The figure depicts the basic diamond braid unit cell with regions of overlapping fibre composite strands and matrix (R_1-R_5), of matrix only (R_6-R_9) and of undulating fibre composite strands (R_{10}-R_{13}).

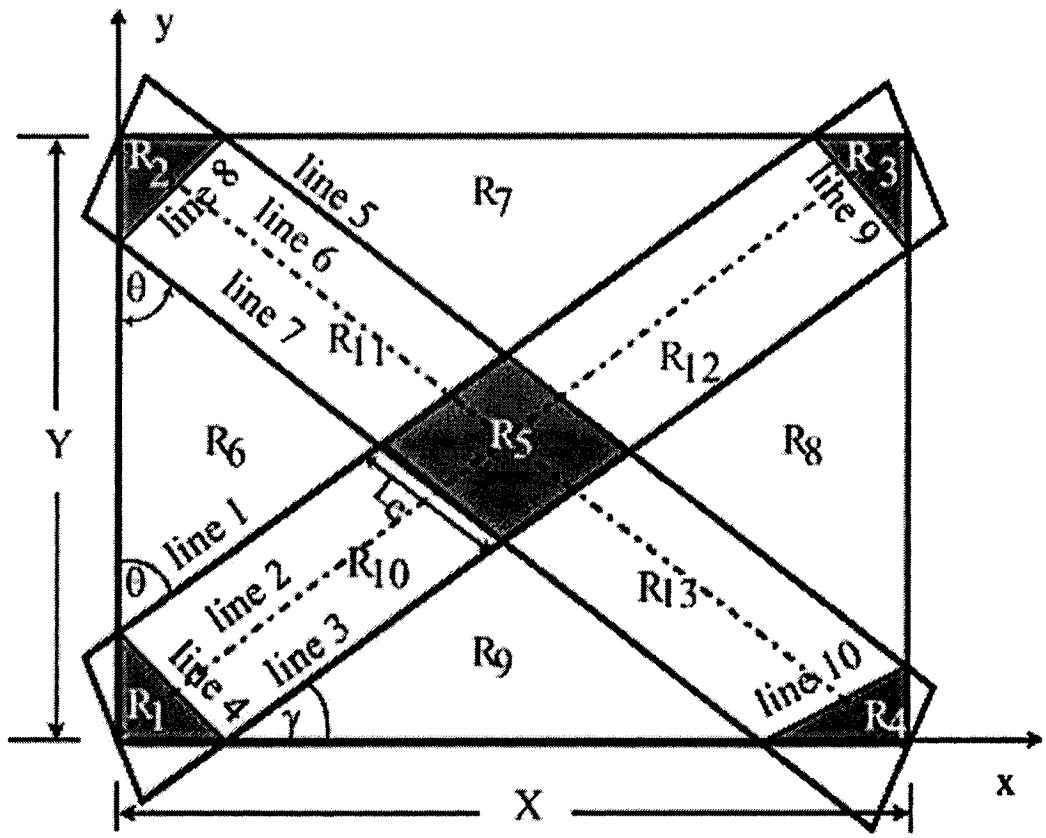

Figure 5-1: Unit cell dimensions and regions of a diamond braid unit cell (top view). Regions R_1-R_5 indicate overlapping fibre composite strands and matrix; Regions R_6-R_9 are matrix only zones, Regions R_{10}-R_{13} are single undulating fibre composite strands.

The braided tube is modelled as a series of repeating unit cells (Figure 5-2(a) and (b)) that all possess the same elastic characteristics if the unit cell geometry remains constant. Figure 5-2 (c) introduce the concept of undulating strands, which will be explained in a subsequent section. Regions R_{10}-R_{13} are composed of overlapping and undulating layers of matrix and fibre composite strands. The proposed approach to model and predict the elastic response of an angle-plied composite structure will be fully defined in terms of the thirteen unit cell regions.

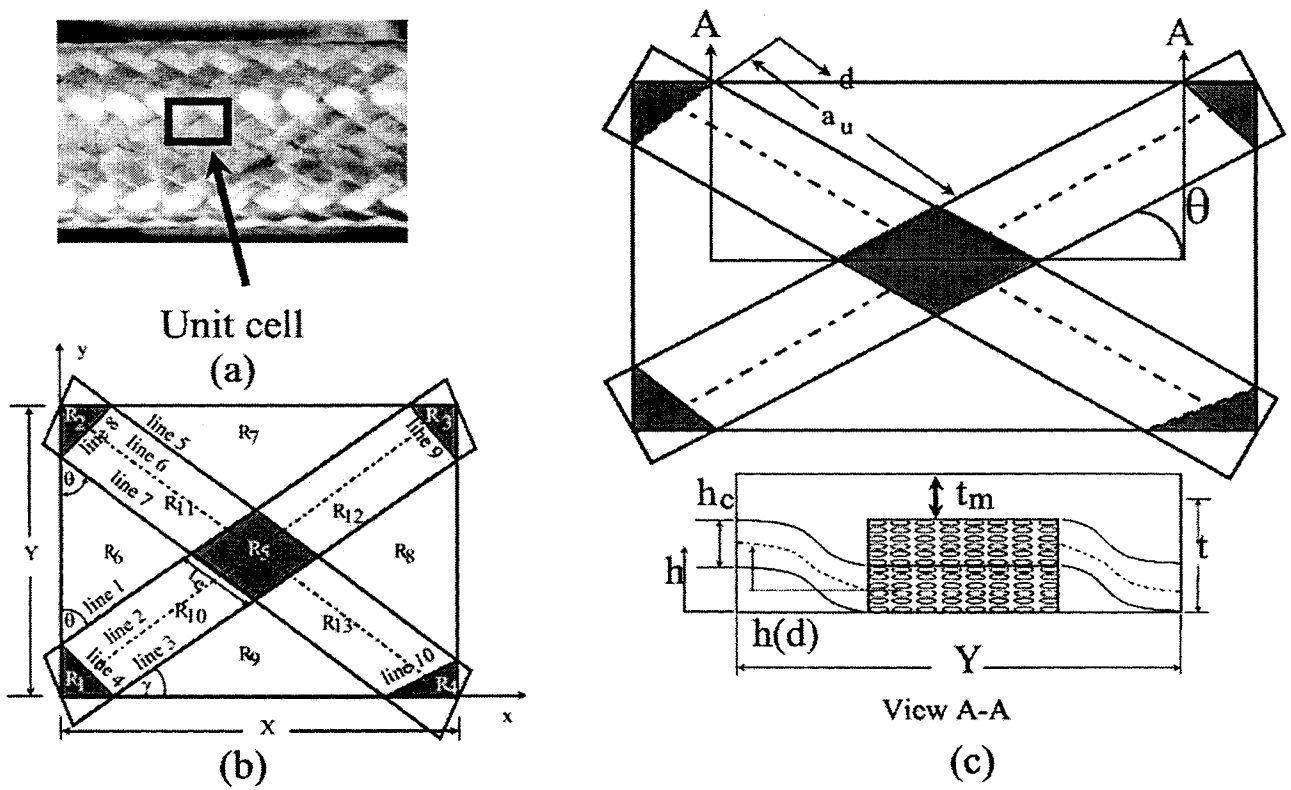

Figure 5-2: Braided tube dissection: (a) braided tube (courtesy of A. Mazzawi); (b) open mesh unit cell; (c) section A-A: cross section view of the unit cell depicting overlapping strands. In figure (c), the resin is assumed clear and is therefore not reflected in the section views.

5.2 Assumptions

Further to the assumptions made to derive the CLPT model and outlined in Section 4.3.3, the following set of assumptions are introduced to facilitate the development of the model for braided tubular structures.

- The matrix-impregnated strands have a fibre volume fraction, V_f, of 60 % as in a typical unidirectional composite.
- The shape of the cross-sections of actual strands varies with manufacturing method. For this work, the strand is assumed to have an invariant rectangular cross-section described by the strand width, Wy, and the wet strand thickness, h_c (Figure 5-2(c)). Within a unit cell, it is further assumed that the strands are parallel.
- The strand undulation geometry is defined as follows: the fibre orientation is assumed to be inclined with respect to the horizontal axis by an angle β (Figure 5-3 (a)). The rectangular cross-section of the unidirectional strand is inclined and always perpendicular to the fibres. The outer edges of the strand undulate as sine functions.
- The rectangular cross-section is inclined with respect to the base plane by an angle ϕ (twist angle).
- Figure 5-3 (b) illustrates the three assumptions defining the strand undulation. Using the strand dimensions defined previously and considering the case of adjacent strands, the twist angle, ϕ, has been estimated by geometry to be approximately 7° (Appendix 2). For any rectangular surface, the axial stiffness will be unaffected since it is independent of the location of the fibre strands. Since the twist of the strand does not change the radial position of the strand, the torsional rigidity will not change. The

effect of the twist angle on flexural rigidity can be estimated by evaluating the moment of inertia. A twist angle of 7° results in a difference of moment of inertia of only 4.7 % as compared to the untwisted state (Appendix 2). Thus, the twist angle, ϕ, is neglected in this work.

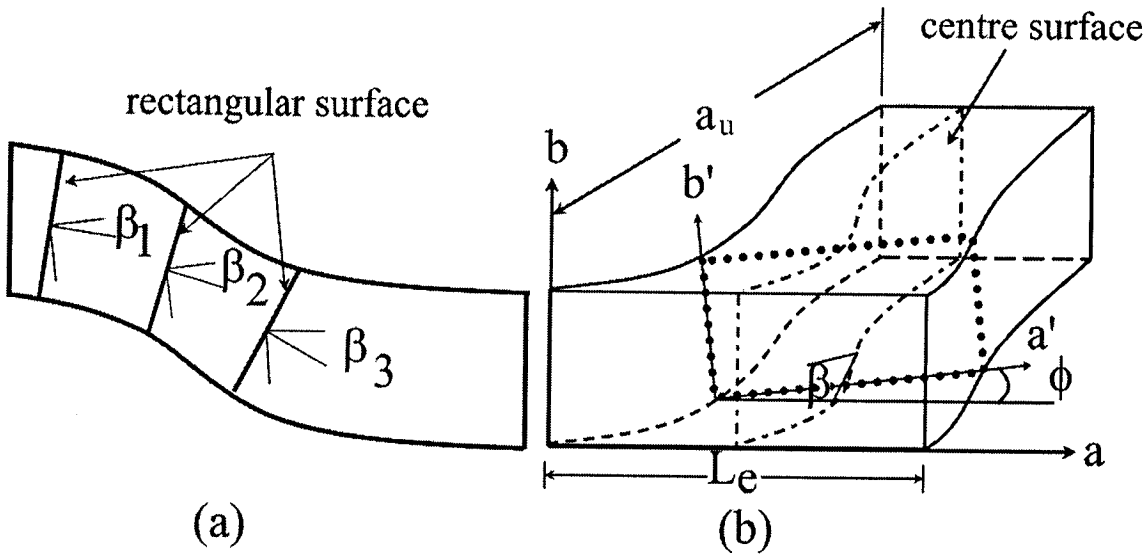

Figure 5-3: (a) Side view of a strand depicting the inclination of the repeating rectangular surface at various inclination angles β, which follows a sinusoidal trajectory; (b) view of an undulating and twisting strand. L_e is the edge length of the strand as defined by equation 5-2.

5.3 Definition of the unit cell geometry

5.3.1 Unit cell regional boundary definition

The unit cell of the diamond braid presented in Figure 5-1 has thirteen regions: five regions of two layers of overlapping fibre composite strands and one of matrix (R_1 - R_5); four of matrix only (R_6 - R_9); and four undulation regions of fibre composite strand (R_{10} -

R_{13}). The following algebraic equations define the boundaries (Figure 5-1) of the thirteen regions.

$$
\begin{aligned}
&\text{line}_1 : y = x\tan(\gamma) + L_e\cos\theta \\
&\text{line}_2 : y = x\tan(\gamma) \\
&\text{line}_3 : y = x\tan(\gamma) - L_e\cos\theta \\
&\text{line}_4 : y = -x\tan(\gamma) + L_e\cos\theta \\
&\text{line}_5 : y = -x\tan(\gamma) + (Y + L_e\cos\theta) \\
&\text{line}_6 : y = -x\tan(\gamma) + Y \\
&\text{line}_7 : y = -x\tan(\gamma) + (Y - L_e\cos\theta) \\
&\text{line}_8 : y = x\tan(\gamma) + (Y - L_e\cos\theta) \\
&\text{line}_9 : y = -x\tan(\gamma) + (2Y - L_e\cos\theta) \\
&\text{line}_{10} : y = x\tan(\gamma) + (L_e\cos\theta - Y)
\end{aligned}
\qquad \textbf{5-1}
$$

The assumptions require that lines 1, 2, 3, 8 and 10 be parallel to each other and that lines 4, 5, 6, 7 and 9 be parallel to each other. Thus, the edges of region R_5 are of equal length as lines 4, 8, 9, and 10. The edge length is denoted as L_e, and is given by:

$$L_e = \frac{W_y}{\cos(2\theta - \pi/2)} \qquad \textbf{5-2}$$

The braid angle, θ, is defined as follows:

$$\theta = \tan^{-1}(X/Y) \qquad \textbf{5-3}$$

The angle gamma, γ, the complementary angle of θ, is defined as

$$\gamma = \tan^{-1}(Y/X) \qquad \textbf{5-4}$$

5.3.2 Strand undulation path definition

In order to effectively define the strand undulation, a section cut of the unit cell is required. Figure 5-2 (c) illustrates a cut view of the unit cell. The illustration presents the parameters related to fibre undulation within the unit cell.

- a_u (top view Figure 5-2 (c)) is the undulation region length;
- h_c is the composite strand thickness;
- t_m is the overlaying matrix thickness;
- t is the unit cell thickness, which is the sum of two composite strand thicknesses (h_c) and the overlaying matrix thickness (t_m); and
- h(d) is the sinusoidal function which defines the undulation strand path. The "d" function, the direction along the strand edge, is dependent on the various limit lines of the region and the braid angle (i.e.: d(x,y)). The undulation is assumed to follow a cosine function such as:

$$h(d) = \left[1 - \cos\{\pi(d/a_u)\}\right]h_c/2 \quad 0 \le d \le a_u \qquad \textbf{5-5}$$

- β, the undulation angle, is defined as:

$$\tan\beta = \frac{dh(d_{(x,y)})}{dd_{(x,y)}} \qquad \textbf{5-6}$$

5.3.3 Undulation region geometry

The geometry of undulating strand regions depends on the undulation length, a_u; this section will examine this relationship. The following example assumes that the undulating strand path follows a cosine function. The undulation length is varied from 1 to 10 units, and h_c is arbitrarily assumed equal to unity. The profile of the strand is defined as follows:

$$h(d) = \left[1 - \cos\left\{\pi\left(\frac{(d - d_1)}{d_2 - d_1}\right)\right\}\right] h_c/2 \qquad \textbf{5-7}$$

The undulation angle, β, derived from the above equation varies along the entire length of the undulation zone. Differentiating the equation gives:

$$\beta = a\tan\left\{\frac{\sin\left\{\pi\left(\frac{(d - d_1)}{d_2 - d_1}\right)\right\}}{d_2 - d_1}\pi h_c/2\right\} \qquad \textbf{5-8}$$

where d_2-d_1 is equivalent to a_u and for the present case d_1 is set to zero. Equations 5-8 and 5-8 are plotted versus 'd' to show the undulation shape of the strand for $0 \le d \le a_u$. Figure 5-4 shows the undulation profile plot for a_u=1...10, and Figure 5-5 shows the undulation angle for the same increments of a_u. Figure 5-6 depicts the maximum value of the undulation angle for the same increments of a_u. The figures show that increasing the undulation length decreases the maximum inclination angle and therefore reduces the off-axis effective property loss. Conversely, a greater undulation length implies a greater amount of matrix rich zones and neat resin content which could be as detrimental to the overall structure stiffness as a steep maximum undulation angle. Total unit cell neat resin content can be

shown to significantly decrease the elastic properties [66]. Further work on the influence of undulation length and neat resin content on regional and unit cell elastic constants will be studied in a subsequent chapter.

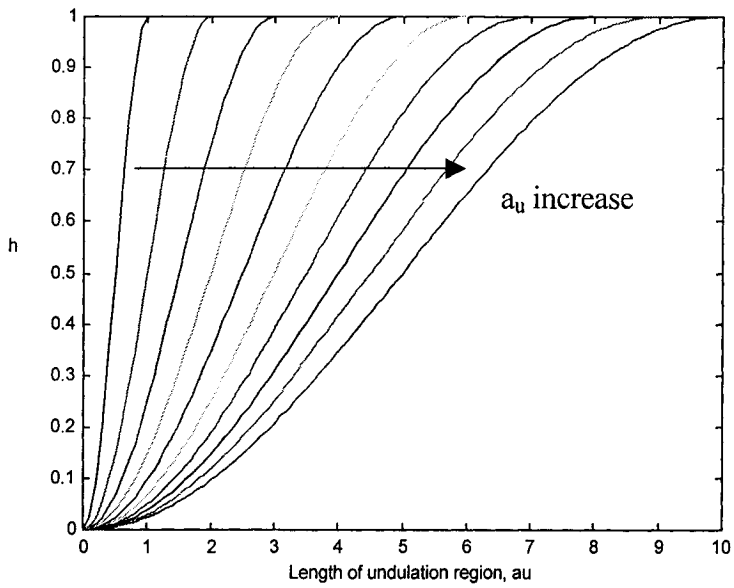

Figure 5-4: Undulation profile, h, in the undulation zone over an increase in undulation length ($1 \le a_u \le 10$).

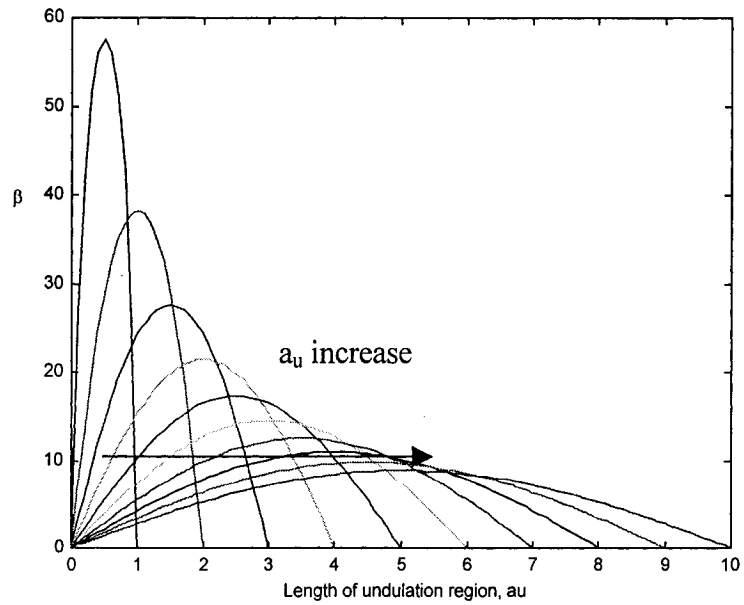

Figure 5-5: Undulation angle, β, versus position in the undulation zone for an increase in undulation length ($1 \le a_u \le 10$).

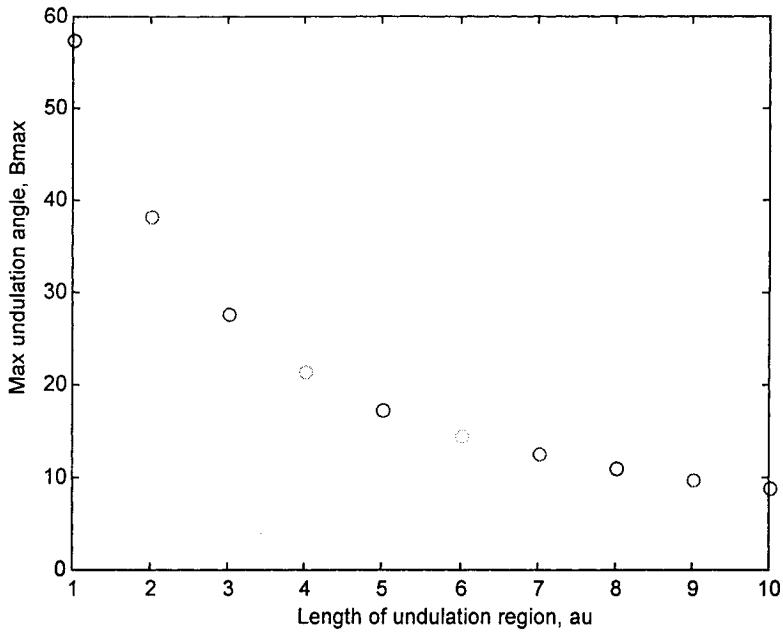

Figure 5-6: Maximum undulation angle, β_{max}, in the undulation zone for an increase in undulation length ($1 \leq a_u \leq 10$).

The preceding example is simplistic; however, it should provide the reader with a better understanding of how the geometry of the undulation zones could affect key parameters on the structure geometry. Furthermore, it serves as an introduction to the development of the equations (Section 5.5.2) that define the classical laminate plate theory as applied to an undulating strand. Unidirectional composites that form the unit cell undergo rotations of β about the braid axis and/or θ about the longitudinal mandrel axis for undulating and non-undulating regions, respectively. The following section will discuss the transformation of unidirectional composite elastic constants from body (strand) to general (unit cell) coordinate systems.

5.4 Transformation of material properties

For the proposed CLPT model, laminar properties are determined using standard micromechanical models developed previously [44, 49, 68] and reviewed in Section 3.4. The longitudinal modulus, E_{11}, and the major Poisson's ratio, ν_{12}, are calculated using the rules of mixtures equations. The transverse, E_{22}, and in-plane shear, G_{12}, moduli are calculated using Halpin-Tsai equations. The out-of-plane shear modulus, G_{23}, is predicted using the semi-empirical stress-partitioning parameter [49] while the out-of-plane Poisson's ratio, ν_{23}, is calculated with an equation previously used by Ko [27]. Transverse isotropy is assumed; therefore, G_{13} is equivalent to G_{12} and ν_{13} equivalent to ν_{12}.

In accordance with the plane stress and the twist angle assumptions (Section 5.2), the following section will define the specific stiffness matrix transformation equations required for the proposed CLPT model. The equations defined in Section 4.3.3 were modified for the preceding assumptions.

Two series of transformation equations were defined: one for regions without undulation (Section 5.4.1) and one for regions with undulations (Section 5.4.3). Figure 5-7 shows the change in the unit cell coordinate system (x, y, z) necessary to be in the strand coordinate system (1", 2", 3"). Stiffness properties are transformed in the opposite order presented in the figure; thus, all strand properties must be transformed to effective strand properties in the unit cell coordinate system. Regions without undulation go though the first transformation only; resin only regions do not undergo transformations; and undulation regions go through both.

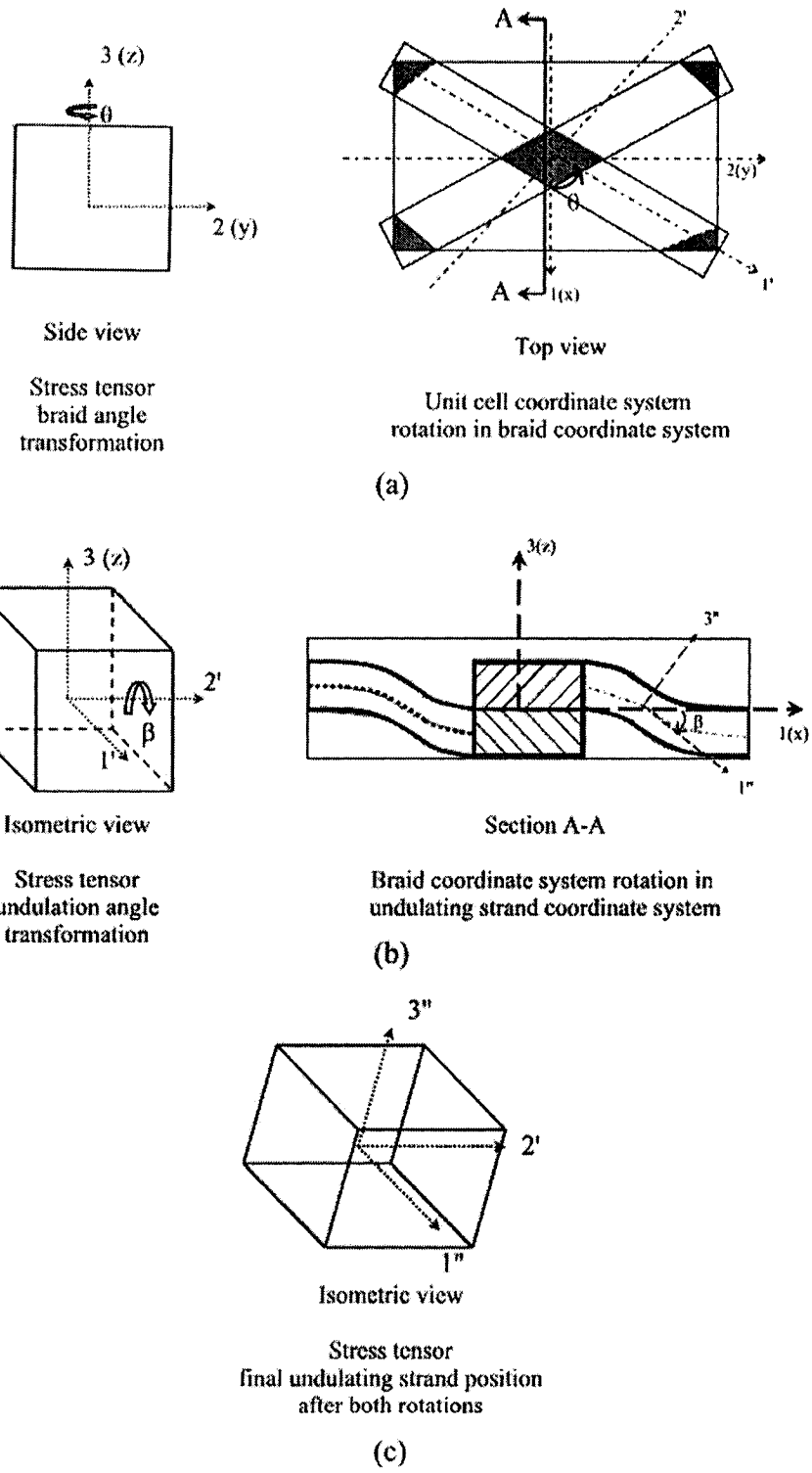

Figure 5-7: Geometric transformation of the stress tensors required for stiffness matrix transformation with accompanied coordinate system on braided structures: (a) braid angle transformation; (b) undulation transformation; (c) final undulating strand direction. The inverse transformation is required to obtain the unit cell stiffness matrix.

5.4.1 Regions without undulation, $R_1 - R_5$

The regions that do not have undulating strands must only be rotated through the braid angle θ to the unit cell coordinate system. Stiffness matrix components, Q_{ij} in the 1' and 2' directions, (as defined in Figure 5-7) are transformed using the following equation [69]:

$$[\overline{Q}] = [T_\theta]^{-1}[Q][T_\theta]^{-T} \qquad \textbf{5-9}$$

where

$$[Q] = \begin{bmatrix} \frac{E_{11}}{1-\nu_{12}\nu_{21}} & \frac{\nu_{21}E_{11}}{1-\nu_{12}\nu_{21}} & 0 \\ \frac{\nu_{12}E_{11}}{1-\nu_{12}\nu_{21}} & \frac{E_{22}}{1-\nu_{12}\nu_{21}} & 0 \\ 0 & 0 & G_{12} \end{bmatrix} \qquad \textbf{5-10}$$

and

$$[T_\theta] = \begin{bmatrix} \cos^2\theta & \sin^2\theta & 2\sin\theta\cos\theta \\ \sin^2\theta & \cos^2\theta & -2\sin\theta\cos\theta \\ -\sin\theta\cos\theta & \sin\theta\cos\theta & \cos^2\theta - \sin^2\theta \end{bmatrix} \qquad \textbf{5-11}$$

5.4.2 Resin only regions, $R_6 - R_9$

Resin only regions do not undergo any transformations since monolithic resin is isotropic and thus elastic constants are the same in all directions. The stiffness matrix for resins, Q_m is defined as:

$$[Q_m] = \begin{bmatrix} \frac{E_m}{1-\nu_m^2} & \frac{\nu_m E_m}{1-\nu_m^2} & 0 \\ \frac{\nu_m E_m}{1-\nu_m^2} & \frac{E_m}{1-\nu_m^2} & 0 \\ 0 & 0 & G_m \end{bmatrix} \qquad \textbf{5-12}$$

5.4.3 Regions with undulation, $R_{10} - R_{13}$

For undulating regions, the stiffness matrix components are initially transformed through the undulation angle, β, from the material axes to the braid angle coordinate system (from coordinate system 1"2"3" to 1'2'3' seen in Figure 5-7). The transformation (equations 5.14 to 5.19) used by Ishikawa and Chou [61] gives the effective stiffness matrix in the braid angle coordinate system $[Q_{(\beta)}]$. The following equation gives the effective stiffness matrix of the undulating strands, $[\overline{Q}_u]$ in the unit cell coordinates:

$$[\overline{Q}_u] = [T_\theta]^{-1}[Q_{(\beta)}][T_\theta]^{-T} \qquad \textbf{5-13}$$

where

$$[Q_{(\beta)}] = \begin{bmatrix} \frac{E_x(\beta)}{D_v} & \frac{E_y(\beta)\nu_{21}(\beta)}{D_y} & 0 \\ \frac{E_y\nu_{21}(\beta)}{D_v} & \frac{E_y(\beta)}{D_v} & 0 \\ 0 & 0 & G_{12}(\beta) \end{bmatrix} \qquad \textbf{5-14}$$

and

$$E_x(\beta) = \frac{1}{\left[\frac{\cos^4\beta}{E_{11}} + \left(\frac{1}{G_{13}} - 2\frac{\nu_{31}}{E_{11}}\right)\cos^2\beta\sin^2\beta + \frac{\sin^4\beta}{E_{33}}\right]} \quad \textbf{5-15}$$

$$\nu_{21}(\beta) = E_x(\beta)\left[\nu_{31}\frac{\cos^2\beta}{E_{11}} + \nu_{23}\frac{\sin^2\beta}{E_{33}}\right] \quad \textbf{5-16}$$

$$G_{12}(\beta) = \left[\frac{\cos^2\beta}{G_{12}} + \frac{\sin^2\beta}{G_{23}}\right]^{-1} \quad \textbf{5-17}$$

$$E_y(\beta) = E_{22} = E_{33} \quad \textbf{5-18}$$

$$D_v = 1 - (\nu_{21}(\beta))^2 \frac{E_{22}}{E_x(\beta)} \quad \textbf{5-19}$$

The unit cell geometry defined earlier (Section 5.3) and the elastic constant transformation procedures are required for the classical laminate plate theory; the complete proposed CLPT model is described in the following section.

5.5 Predictive analysis of mechanical properties of a unit cell

This section will detail the proposed analytical model that will predict the elastic constants (E_x, G_{xy}) of a single unit cell. A modified classical laminate plate theory (CLPT) is the basis for the model. The following are the basic equations of the CLPT for a unit cell (the complete analysis is found in Appendix 1).

$$\begin{Bmatrix} N \\ M \end{Bmatrix} = \begin{bmatrix} A & B \\ B & D \end{bmatrix} \begin{Bmatrix} \varepsilon^0 \\ \kappa^0 \end{Bmatrix} \qquad \textbf{5-20}$$

M and N are the moments and forces per unit length applied to the unit cell, respectively, and ε^0 and κ^0 are the midplane membrane strain and curvature, respectively. Raju and Wang [66] expanded this equation to account for 'n' different regions with the following area-weighted set of equations:

$$\begin{Bmatrix} N \\ M \end{Bmatrix} = \begin{bmatrix} [A^*] & [B^*] \\ [B^*] & [D^*] \end{bmatrix} \begin{Bmatrix} \varepsilon^0 \\ \kappa^0 \end{Bmatrix} \qquad \textbf{5-21}$$

where the weighted equations are:

$$\left.\begin{aligned} [A^*] &= \frac{1}{P_A}\sum_{n=1}^{k}\left(\int_{R_n}[A]_n\,dP_n\right) \\ [B^*] &= \frac{1}{P_A}\sum_{n=1}^{k}\left(\int_{R_n}[B]_n\,dP_n\right) \\ [D^*] &= \frac{1}{P_A}\sum_{n=1}^{k}\left(\int_{R_n}[D]_n\,dP_n\right) \end{aligned}\right\} \text{for } k = 13 \qquad \textbf{5-22}$$

In the above equation, k is equal to 13 because the unit cell is divided in 13 regions, P_A is the projected area of the entire unit cell on the midplane and P_n represents the projected

area of each of the 13 regions of the unit cell on the midplane. Thus, P_A is the sum of all P_n. This observation leads to the following simplification of the equation:

$$\begin{aligned}[A^*] &= \frac{1}{P_A}\sum_{n=1}^{13}[A]_n \\ [B^*] &= \frac{1}{P_A}\sum_{n=1}^{13}[B]_n \\ [D^*] &= \frac{1}{P_A}\sum_{n=1}^{13}[D]_n\end{aligned} \qquad \textbf{5-23}$$

where [A], [B] and [D] are 3x3 matrices found for each of the thirteen regions as:

$$\begin{aligned}[A] &= \int_x\left(\int_y\left(\int_z[\overline{Q}]dz\right)dy\right)dx \\ [B] &= \int_x\left(\int_y\left(\int_z[\overline{Q}]\cdot z dz\right)dy\right)dx \\ [D] &= \int_x\left(\int_y\left([\overline{Q}]\cdot z^2 dz\right)dy\right)dx\end{aligned} \qquad \textbf{5-24}$$

and $[\overline{Q}]$ is the stiffness matrix, in the unit cell coordinate system, of the layer of resin or fibre composite strand. For the following equations, $[Q_c(\theta)]$ is the strand stiffness matrix rotated through the braid angle, $[Q_c(-\theta)]$ is the strand stiffness matrix rotated through the negative braid angle, and $[Q_m]$ is the resin stiffness matrix.

Section 5.3 defined the precise geometry of the unit cell, which includes various layers of composite and matrix materials. It also defined the fibre crossovers and undulation. The following sections will detail the various analytical steps used to obtain the constitutive matrices [A], [B] and [D] of the thirteen regions of the unit cell. The regions without and with undulation will be discussed separately.

5.5.1 Overlapping strands and matrix only regions, R_1 - R_9

Constitutive relationships for regions R_1 to R_9 – without undulation – have been established and can be found in Appendix 3. These relationships were calculated directly, without numerical methods. As an example of a non-undulating region, Equation 5-23 can be solved for region 1 (lower left corner Figure 5-1) as follows:

$$[A] = \int_x \int_y \int_{-(2h_c+t_m)/2}^{(2h_c+t_m)/2} [\bar{Q}] dz dy dx$$
$$= \int_0^{l_e \sin\theta} \int_0^{-x\tan\gamma + l_e\cos\theta} dy dx \left[\int_{-(2h_c+t_m)/2}^{(2h_c+t_m)/2} [\bar{Q}] dz \right] \qquad 5\text{-}25$$

where the first integration can be subdivided for the three layers found in the subsection (Figure 5-8). The bottom strand is at an angle of minus θ with the main axis of the system, the second is at an angle of plus θ.

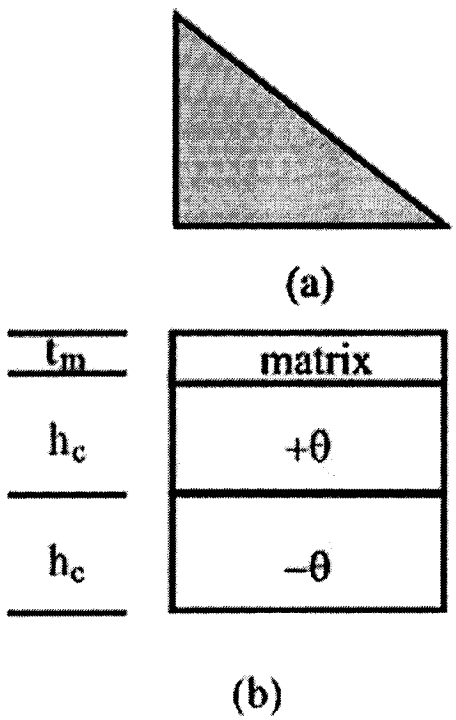

Figure 5-8: Region 1: (a) side view; (b) top view.

The integration of the first term on the right hand side is constant for a non-undulation region since it is the area over xy of region 1 (Figure 5-1). It will be denoted a_{xy}, and is given by:

$$a_{xy} = \int_0^{l_e \sin\theta} \int_0^{-x\tan\gamma + l_e\cos\theta} dydx$$
$$= \left[-\frac{(l_e \sin\theta)^2 \tan\gamma}{2} + {l_e}^2 \sin\theta\cos\theta \right]$$

The integration of the second term of the right hand side is found by expanding the integration over the different layers, which gives:

$$\int_{-(2h_c+t_m)/2}^{(2h_c+t_m)/2} [\overline{Q}]dz = \int_{-(2h_c+t_m)/2}^{-t_m/2} [Q_c(-\theta)]dz + \int_{t_m/2}^{h_c-t_m/2} [Q_c(\theta)]dz + \int_{h_c-t_m/2}^{h_c+t_m/2} [Q_m]dz$$
$$= ([Q_c(-\theta)] + [Q_c(\theta)])h_c + [Q_m]t_m$$

Substituting the results of the integration in Equation 5-25 gives:

$$[A] = \left[-\frac{(l_e \sin\theta)^2 \tan\gamma}{2} + {l_e}^2 \sin\theta\cos\theta \right] [([Q_c(-\theta)] + [Q_c(\theta)])h_c + [Q_m]t_m]$$

[B] and [D] matrices are solved in the same fashion. The final forms for [A], [B] and [D] are:

$$[A] = a_{xy}[([Q_c(-\theta)] + [Q_c(\theta)])h_c + [Q_m]t_m]$$

$$[B] = \frac{1}{2} a_{xy} \begin{Bmatrix} [Q_c(-\theta)]\left(\left(\frac{t_m}{2}\right)^2 - \left(-h_c - \frac{t_m}{2}\right)^2\right) + \dots \\ [Q_c(\theta)]\left(-\left(\frac{t_m}{2}\right)^2 + \left(h_c - \frac{t_m}{2}\right)^2\right) + \dots \\ [Q_m]\left(\left(h_c + \frac{t_m}{2}\right)^2 - \left(h_c - \frac{t_m}{2}\right)^2\right) \end{Bmatrix} \quad \text{5-26}$$

$$[D]=\frac{1}{3}a_{xy}\begin{Bmatrix}[Q_c(-\theta)]\left(\left(\frac{t_m}{2}\right)^3-\left(-h_c-\frac{t_m}{2}\right)^3\right)+\ldots\\ [Q_c(\theta)]\left(-\left(\frac{t_m}{2}\right)^3+\left(h_c-\frac{t_m}{2}\right)^3\right)+\ldots\\ [Q_m]\left(\left(h_c+\frac{t_m}{2}\right)^3-\left(h_c-\frac{t_m}{2}\right)^3\right)\end{Bmatrix}$$

A generalized solution of the elements of the stiffness matrix for all the non-undulating regions is given in the following equation; the upper and lower boundaries of which, established in Figure 5-1, are listed in Table 5-1. Regions R_5, R_7 and R_9 must be separated in two mirror parts for integration purposes (i.e.: R_5 part 1 and part 2, R_7 part 1 and part 2, and R_9 part 1 and part 2). Figure 5-9 shows all of the "regions" and "region parts" found in Table 5-1.

$$A,B,D=\sum_b^a\int_d^c\left[\begin{matrix}\int_g^f Q_{ij}(\theta)z^{0,1,2}dz+\int_g^h Q_{ij}(-\theta)z^{0,1,2}dz+\\ \int_j^i Q_m z^{0,1,2}dz\end{matrix}\right]dydx \qquad \textbf{5-27}$$

The summation sign in the previous equation indicates that there can be many integrals in x and y since regions can have many different upper and lower bounds. Table 5-1 contains all the bounds for the above equation for the nine undulation-less regions.

Table 5-1: Coefficients for equation 5-28 for all non-undulating regions defined in Figure 5-9 ($s\theta = \sin\theta$ and $c\theta = \cos\theta$).

	a	b	c	d	e	f	g	h	i	j
$\mathbf{R_1}$	$L_e s\theta$	0	$-x\tan\gamma + L_e c\theta$	0	$-t_m/2$	$-t_m/2 + h_c$	$-(h_c + t_m/2)$	$-t_m/2$	$t_m/2 + h_c$	$-t_m/2 + h_c$
$\mathbf{R_2}$	$L_e s\theta$	0	Y	$x\tan\gamma + Y - L_e c\theta$	$-t_m/2$	$-t_m/2 + h_c$	$-(h_c + t_m/2)$	$-t_m/2$	$t_m/2 + h_c$	$-t_m/2 + h_c$
$\mathbf{R_3}$	X	$X - L_e s\theta$	$-x\tan\gamma + 2Y - L_e c\theta$	Y	$-t_m/2$	$-t_m/2 + h_c$	$-(h_c + t_m/2)$	$-t_m/2$	$t_m/2 + h_c$	$-t_m/2 + h_c$
$\mathbf{R_4}$	X	$X - L_e s\theta$	$x\tan\gamma - Y + L_e c\theta$	0	$-t_m/2$	$-t_m/2 + h_c$	$-(h_c + t_m/2)$	$-t_m/2$	$t_m/2 + h_c$	$-t_m/2 + h_c$
$\mathbf{R_5}$										
Part 1	X/2	$X/2 - L_e s\theta$	$x\tan\gamma + L_e c\theta$	$-x\tan\gamma + Y - L_e c\theta$	$-(h_c + t_m/2)$	$-t_m/2$	$-t_m/2$	$-t_m/2 + h_c$	$t_m/2 + h_c$	$-t_m/2 + h_c$
Part 2	$X/2 + L_e s\theta$	X/2	$-x\tan\gamma + Y + L_e c\theta$	$x\tan\gamma - L_e c\theta$	$-(h_c + t_m/2)$	$-t_m/2$	$-t_m/2$	$-t_m/2 + h_c$	$t_m/2 + h_c$	$-t_m/2 + h_c$
$\mathbf{R_6}$	$X/2 - L_e s\theta$	0	$-x\tan\gamma + Y - L_e c\theta$	$x\tan\gamma + L_e c\theta$	0	0	0	0	-t/2	t/2
$\mathbf{R_7}$										
Part 1	X/2	$L_e s\theta$	Y	$-x\tan\gamma + Y + L_e c\theta$	0	0	0	0	-t/2	t/2
Part 2	$X - L_e s\theta$	X/2	Y	$x\tan\gamma + L_e c\theta$	0	0	0	0	-t/2	t/2
$\mathbf{R_8}$	X	$X/2 + L_e s\theta$	$x\tan\gamma - L_e c\theta$	$-\tan\gamma + Y + L_e c\theta$	0	0	0	0	-t/2	t/2
$\mathbf{R_9}$										
Part 1	X/2	$L_e s\theta$	$x\tan\gamma - L_e c\theta$	0	0	0	0	0	-t/2	t/2
Part 2	$X - L_e s\theta$	X/2	$-x\tan\gamma + Y - L_e c\theta$	0	0	0	0	0	-t/2	t/2

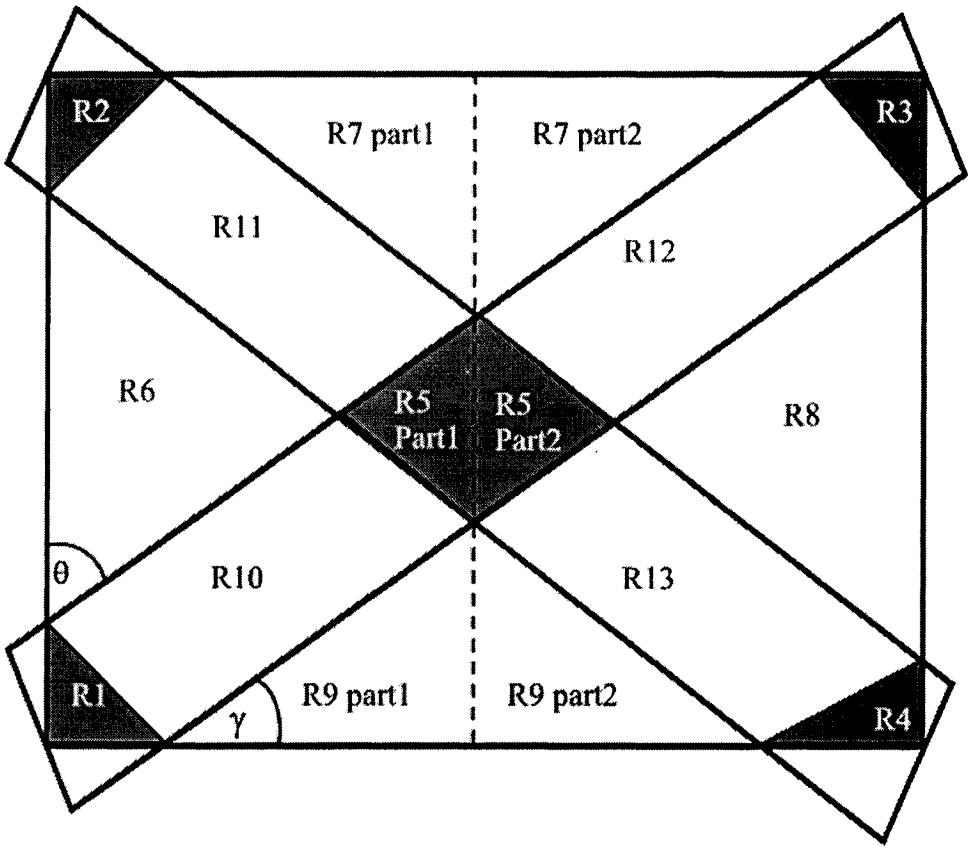

Figure 5-9: Unit cell subdivided in all regions and subsequent integration parts.

5.5.2 Regions with undulation, R_{10}-R_{13}

This section will follow the same development as in Section 5.5.1. In the case of undulating regions, the equations for the stiffness matrices cannot be evaluated directly. Numerical methods must be used to evaluate the stiffness matrix since it is a function of undulation angle, braid angle and x, y and z position in the strand.

Figure 5-10 illustrates how undulating regions were subdivided as well as the surface integration used for the numerical evaluation. A Gauss-Legendre quadrature with n=10 was employed to evaluate the sinusoidal portions of the integral. Since the twist angle is neglected and there is symmetry along the strand cross-section, the integration is constant for every increment along the strand cross-section; therefore, a single evaluation of the Gauss-Legendre quadrature was performed, and the complete integral was found by multiplying the result by L_e, the edge length or thickness of the cross-section. Figure 5-10 shows the direction of evaluation of the quadrature.

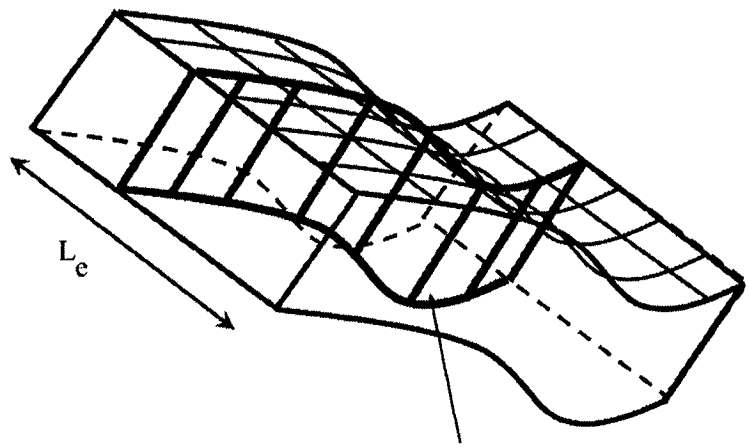

Figure 5-10: Details of undulating strand for numerical calculation purposes (view slanted for comprehension purposes)

Gauss-Legendre quadrature requires that the function be evaluated at unequally spaced nodes along the curve. For the following integral [70,71]

$$I = \int_b^a f(d)dx \qquad \textbf{5-28}$$

the nodes for function evaluations are given by:

$$d_i = \frac{a+b}{2} + \frac{a-b}{2}\xi_i \qquad \textbf{5-29}$$

where a and b are curve bounds and ξ_i are the zeros of the quadrature. The integral is given by:

$$I = \frac{a-b}{2}\sum_{i=1}^{10} w_i f(d_i) \qquad \textbf{5-30}$$

For n=10 the zeros and weights, w_i, are listed below.

Table 5-2: Gauss-Legendre quadrature zeros and weights at n=10

i	Zeros ($\pm\xi_i$)	Weights (w_i)
1, 10	0.1488743390	0.2955242247
2, 9	0.4333953941	0.2692667193
3, 8	0.6794095683	0.2190863625
4, 7	0.8650633667	0.1494513492
5, 6	0.9739065285	0.0666713443

As mentioned earlier (Section 5.3.2), d is measured along the strand direction and is a function of both x and y. In the three above equations, 'a' and 'b' are replaced by 'a_u' and '0', respectively, to reflect the length (a_u) of the sinusoidal curve. In each case, (x_1, y_1) and (x_2, y_2) are the start and end point of the sine function, thus a_u is defined as:

$$a_u = \sqrt{(x_2 - x_1)^2 + (y_2 - y_1)^2} \qquad \textbf{5-31}$$

For each (x_i, y_i) point, the following $f(x_i,y_i)$ functions were evaluated for the A, B and D integrals as follows:

$$\text{For A, } f(x_i, y_i) = Q(\beta)\left[Z_{strand} + h_c - Z_{strand}\right] + Q_m\left[\begin{matrix} Z_{strand} + 2h_c + t_m - \ldots \\ (Z_{strand} + h_c) \end{matrix}\right]$$

$$\text{for B, } f(x_i, y_i) = 1/2\left\{Q(\beta)\left[(Z_{strand} + h_c)^2 - Z_{strand}^{\ 2}\right] + Q_m\left[\begin{matrix} Z_{strand}^{\ 2} + \ldots \\ (2h_c + t_m)^2 - \ldots \\ (Z_{strand} + h_c)^2 \end{matrix}\right]\right\} \qquad \textbf{5-32}$$

$$\text{for D, } f(x_i, y_i) = 1/3\left\{Q(\beta)\left[(Z_{strand} + h_c)^3 - Z_{strand}^{\ 3}\right] + Q_m\left[\begin{matrix} Z_{strand}^{\ 3} + \ldots \\ (2h_c + t_m)^3 - \ldots \\ (Z_{strand} + h_c)^3 \end{matrix}\right]\right\}$$

where β for coordinates (x_i, y_i) is given by:

$$\beta = \tan^{-1}\left(-\frac{h_c \pi}{a_u}\sin\left(\pi\frac{\sqrt{(x_i - x_1)^2 + (y_i - y_1)^2}}{a_u}\right)\right) \qquad \textbf{5-33}$$

and, the height between the bottom of the unit cell to the bottom of the strand is defined as:

$$Z_{strand} = h(d) - \frac{h_c}{2} = h_c \cos\left\{\pi\left(\frac{\sqrt{(x_i - x_1)^2 + (y_i - y_1)^2}}{a_u}\right)\right\} \qquad \textbf{5-34}$$

The result of the numerical integration was multiplied by L_e. Convergence of the Gaussian technique was tested for region R_{10}, assuming similar results for the others, using 8^{th}, 10^{th} and 12^{th} order Gauss-Legendre quadrature. Table 5-3 shows the results of the different numerical methods.

Table 5-3: Comparison between 8th, 10th, and 12th order Gaussian quadrature for region R_{10} [A], [B] and [D] calculations.

	A			B			D (10^{-4})		
Gauss Legendre 8	47.61	53.87	1.38	0.0250	0.0277	0.0007	0.1630	0.1742	0.0041
	53.87	66.34	-7.62	0.0277	0.0344	-0.0038	0.1742	0.2203	-0.0233
	-2.76	15.25	1.81	-0.0014	0.0076	0.0017	-0.0083	0.0465	0.0193
Gauss Legendre 10	47.62	53.88	1.38	0.0250	0.0277	0.0007	0.1630	0.1742	0.0041
	53.88	66.36	-7.62	0.0277	0.0344	-0.0038	0.1742	0.2203	-0.0233
	-2.76	15.25	1.81	-0.0014	0.0076	0.0017	-0.0083	0.0465	0.0193
Gauss Legendre 12	47.62	53.88	1.38	0.0250	0.0277	0.0007	0.1630	0.1742	0.0041
	53.88	66.36	-7.62	0.0277	0.0344	-0.0038	0.1742	0.2203	-0.0233
	-2.76	15.25	1.81	-0.0014	0.0076	0.0017	-0.0083	0.0465	0.0193
Notes	**Invariant between 10 and 12**			**Invariant**			**Invariant**		

The different numerical methods are invariant at the level of significant numbers used in this work and thus an acceptable convergence was obtained. For the B and D matrices no change was found up to the 4th decimal place. Between the 8th and 10th order numerical integration of A, differences were found at the 2nd decimal place (4th significant number). No such change was found between the 10th and 12th order numerical integration. This leads to believe that a 10th order approximation is sufficient for the undertaken engineering work.

5.5.3 Evaluation of E_x and G_{xy}

The unit cell in-plane elastic constants are obtained from the stiffness matrices developed in the previous section with the following matrix manipulation. Subsequent to the overall $[A^*]$, $[B^*]$ and $[D^*]$ matrices being calculated as the summation of [A], [B] and [D] of all thirteen regions, the overall stiffness matrix, a 6x6 matrix, of the unit cell is defined as:

$$[S]=\begin{bmatrix}[A^*] & [B^*]\\ [B^*] & [D^*]\end{bmatrix} \qquad \textbf{5-35}$$

The inverse of the overall stiffness matrix (the compliance matrix) is defined as:

$$[S]^{-1}=[C]$$

$$[C]=\begin{bmatrix}[a] & [b]\\ [b] & [d]\end{bmatrix} \qquad \textbf{5-36}$$

where [a] is defined as:

$$[a]=\begin{bmatrix}a_{1,1} & a_{1,2} & a_{1,3}\\ a_{2,1} & a_{2,2} & a_{2,3}\\ a_{3,1} & a_{3,2} & a_{3,3}\end{bmatrix} \qquad \textbf{5-37}$$

and calculated as follows:

$$[a]=[A^*]^{-1}+[A^*]^{-1}[B^*]^{-1}\left([D^*]-[B^*][A^*]^{-1}[B^*]\right)^{-1}[B^*][A^*]^{-1} \qquad \textbf{5-38}$$

The unit cell elastic constants are found directly from the equations defined in Section 5.1:

$$E_x = 1/(a_{1,1}t)$$
$$E_y = 1/(a_{2,2}t)$$
$$\nu_{x,y} = -a_{1,2}/a_{1,1}$$
$$G_{xy} = 1/(a_{3,3}t)$$

5-39

where t is the total thickness of the unit cell. However, only E_x and G_{xy} are required to determine model catheter axial, flexural and torsional rigidities.

5.6 Conclusion

In this chapter, a predictive model based on a modified classical laminate plate theory was developed to evaluate the longitudinal elastic modulus, E_x, and shear modulus, G_{xy}, of braided composites. This work represents a generalization of the plain weave fabric case, as the angle between the fibre strands is not restricted to 90°.

The geometric characteristics as well as the equations for the stiffness and elastic constants of a braided tubular structure unit cell have been completely defined. A modular Matlab™ program was written to perform all calculations. The following two chapters will determine the sensitivity of the software to changes in the constituent properties, and validate the model by comparing its findings to results predicted by models discussed in Chapter 4 and to experimental results.

CHAPTER 6 : SENSITIVITY ANALYSIS OF THE CLPT MODEL TO MICROMECHANICAL PREDICTIONS FOR RIGID THERMOSET MATRIX COMPOSITES

Laminar elastic constants are required for the model presented in Chapter 5. It would be very advantageous if micromechanical models could be used to predict these constants. Given the very large number of candidate fibres and resins, the modelling approach is more practical than the experimental approach of fabricating and testing of laminae. However, the micromechanical models must be shown to accurately predict laminar properties since there is some level of controversy for certain models. This can be done by comparing micromechanical predictions with experimental results at the laminar level. In this study, a comparison is performed at the structural level (i.e. braided tube) between E_x and G_{xy} values predicted using laminar properties found with micromechanical models and the proposed classical laminate plate theory model, and E_x and G_{xy} values found experimentally (Chapter 7). It is necessary to evaluate the sensitivity of E_x and G_{xy} to variations in constituent fibre and matrix properties, the subject of this chapter. This will indicate which constituent properties must be known accurately.

The sensitivity analysis will be performed for a specific fibre and resin system for which there is high confidence in the elastic constants [72]. An extensive experimental laminar database is available [72] for Kevlar 49, carbon and E-glass fibres in an Epon 825/Ancamine 1482 epoxy resin matrix. Since Kevlar is the only fibre that has been used by others for medical catheters, it will be chosen, together with the Epon 825/Ancamine 1482 epoxy resin matrix, for the sensitivity analysis.

Nominal properties of the selected fibre and matrix can be found in Table 6-1. The table also contains the differences between laminar properties, calculated using micromechanical models and determined experimentally. Very good agreement is found between the micromechanical model predictions and experimental results except in the case of the shear modulus; there is a difference of 37.5 % or 0.6 GPa. The error could stem from the fact that constituent shear moduli were calculated[1] and not determined experimentally.

The predicted braided tube moduli values evaluated using micromechanical models and constituent properties of the matrix and fibre (Table 6-1) are listed in Table 6-2.

Table 6-1: Material elastic constants [72]

Material					
(a) constituent	E_{f11} (GPa)	E_{f22} (GPa)	G_{f12} (GPa)	ν_{f12}	ν_{f23}[2]
Kevlar 49 fibre	130	7.3	2.86	0.35	0.1
	E_m		G_m	ν_m	
Epon 825/Ancamine 1482 matrix	3.5	-	1.3	0.3	
(b) Kevlar/epoxy lamina	E_{11} (GPa)	E_{22} (GPa)	G_{12} (GPa)	ν_{12}	
Experimental	79.7	5.9	1.5 [73]	0.3	
Micromechanical prediction	79.4	5.5	2.1	0.3	
Difference	**0.4 %**	**6.8 %**	**37.5 %**	**0 %**	

Table 6-2: Predicted longitudinal elastic and shear moduli results for closed mesh Kevlar/epoxy braided composite at braid angles of 30, 45 and 60 degrees using the proposed CLPT model. Tube ID 0.97 mm, OD 2 mm, strand width 1.4 mm and thickness 0.1 mm

Braid angle (deg)	E_x (GPa)	G_{xy} (GPa)	V_{f0} (%)
30	6.87	2.51	50
45	4.80	3.27	51
60	3.97	3.70	54

[1] G=E/(2(1+ν)

[2] Typical value for out-of-plane Poisson's ratio; see Section 6.4 for the effect of varying the fibre out-of-plane Poisson's ratio.

Sensitivity of the model at braid angle values of 30°, 45° and 60° was determined by varying, one at a time, the following properties by ± 10 %:

- The fibre longitudinal elastic modulus, E_{f11};
- The fibre shear modulus, G_{f12};
- The fibre major Poisson's ratio, ν_{f12};
- The out-of-plane shear modulus of the fibre, ν_{f23};
- The matrix elastic modulus, $E_{m;}$ and,
- The matrix shear modulus, G_m.

Only the maximum difference found from either a –10% or a +10% error is reported the next sections. As mentioned earlier, it is believed that the out-of-plane shear modulus, G_{23}, had little to no effect on the braid elastic constants. In order to verify this earlier statement, a similar sensitivity analysis was also performed with this laminar constant in a following section.

6.1 *Effect of fibre longitudinal elastic modulus variation*

Varying the fibre longitudinal elastic modulus has a major influence on the braid longitudinal elastic modulus at low braid angles (Figure 6-1). At a braid angle of 30°, a 10 % difference in E_{fl1} results in a maximum difference of 4 % with respect to the predicted value; for the braid shear modulus the worst case is found at 60° with a 6.8 % difference.

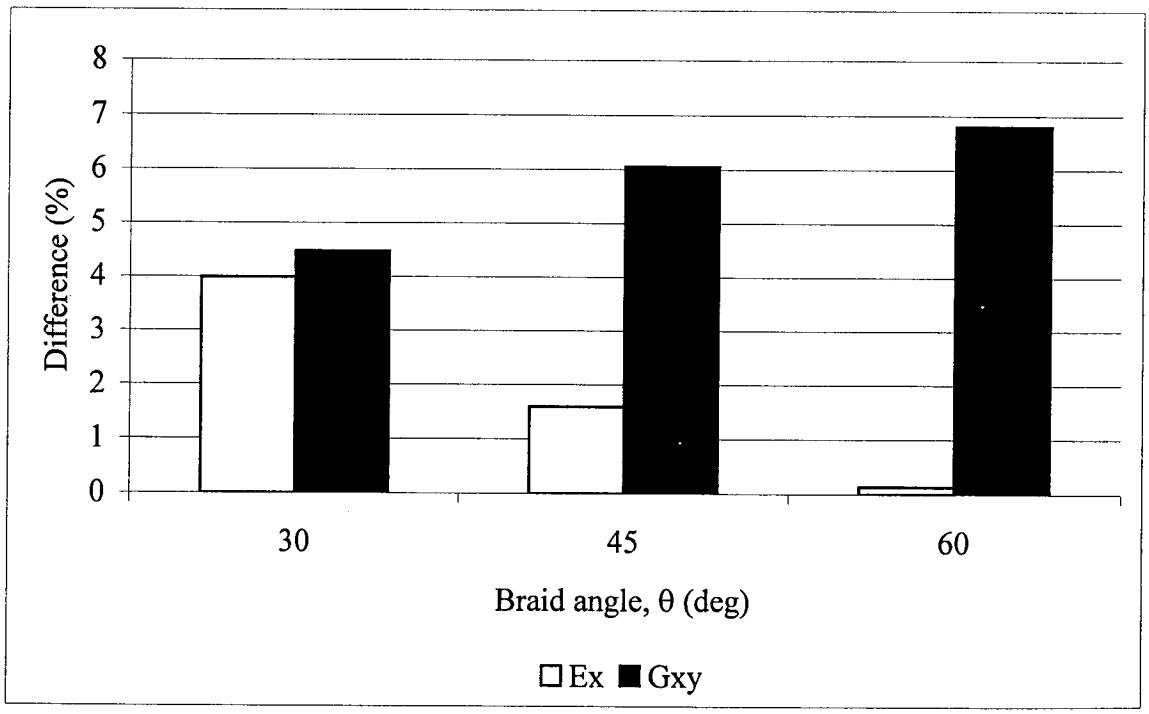

Figure 6-1: Maximum variation (%) in E_x and G_{xy} for a 10 % variation in E_{fl1} at different braid angles

There is a strong influence on the predicted values of braid longitudinal elastic and shear moduli by the input fibre longitudinal elastic modulus, E_{fl1}; therefore, accurate values of the fibre longitudinal elastic modulus are critical to the proposed CLPT model.

6.2 Effect of fibre shear modulus variation

It was found that the variations in fibre shear modulus, G_{f12}, do not have a major effect on the braid longitudinal elastic and shear moduli (Figure 6-2). At all three braid angles, a difference of ± 10 % in the fibre shear modulus results in less than 0.8 % difference in the predicted values.

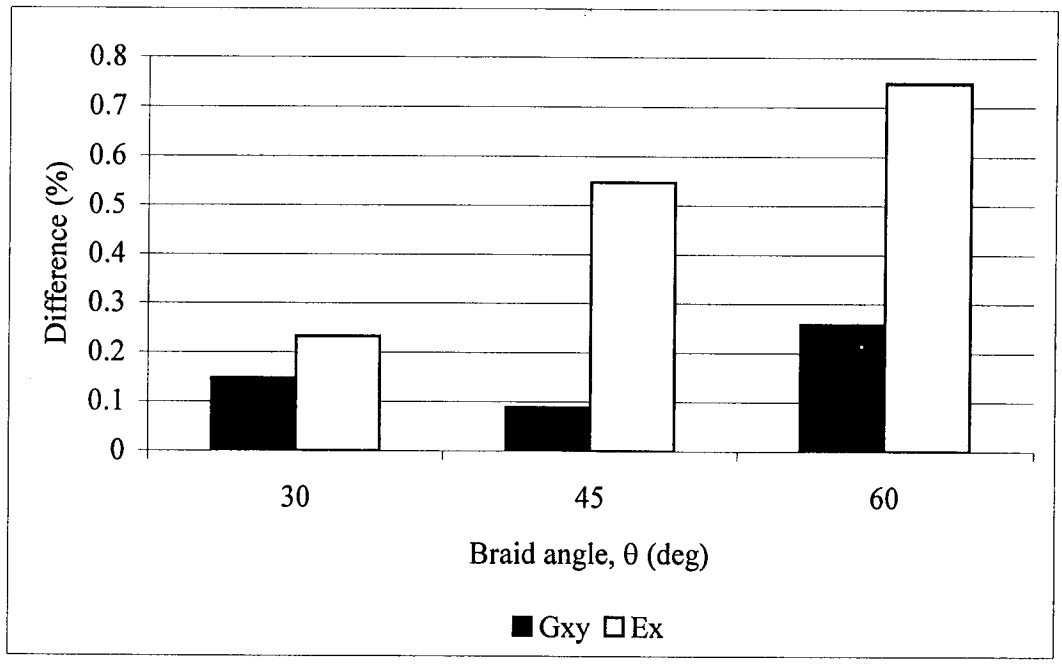

Figure 6-2: Maximum variation (%) in E_x and G_{xy} for a 10 % variation in G_{f12} at different braid angles

There is little effect on the desired elastic constants from a 10 % error in the fibre shear modulus; therefore, small differences in assumed G_{f12} will not affect the accuracy of the proposed CLPT model.

6.3 *Effect of fibre major Poisson's ratio variation*

It was found that variations in the fibre major Poisson's ratio, ν_{f12}, have a minimal effect on the braid longitudinal elastic and shear moduli (Figure 6-3). At all three braid angles, a difference of ± 10 % in the fibre major Poisson's ratio results in less than 0.12 % difference.

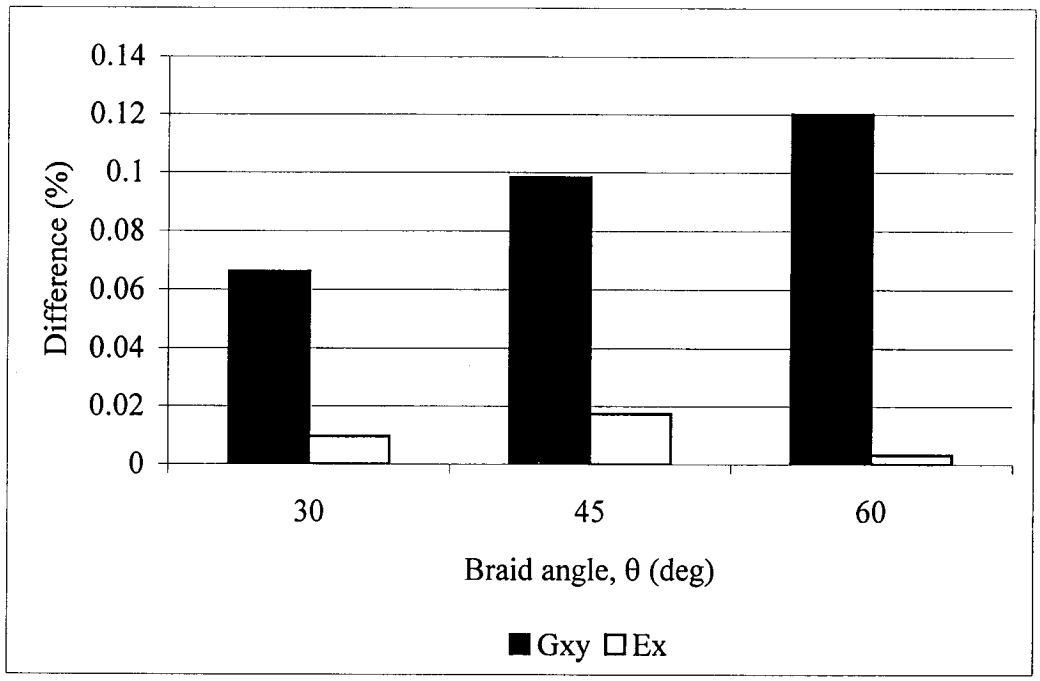

Figure 6-3: Maximum variation (%) in E_x and G_{xy} for a 10 % variation in ν_{f12} at different braid angles

There is little effect on the desired elastic constants from a 10 % error in the fibre Major Poisson's ratio; therefore, small differences in assumed ν_{f12} will not affect the accuracy of the proposed CLPT model.

6.4 Effect of fibre out-of-plane Poisson's ratio variation

Variations in the fibre out-of-plane Poisson's ratio, ν_{f23}, have a negligible influence on the braid longitudinal elastic and shear moduli (Figure 6-4). At all three braid angles, a difference of ± 10 % in the fibre out-of-plane Poisson's ratio results in less than 0.0016 % difference.

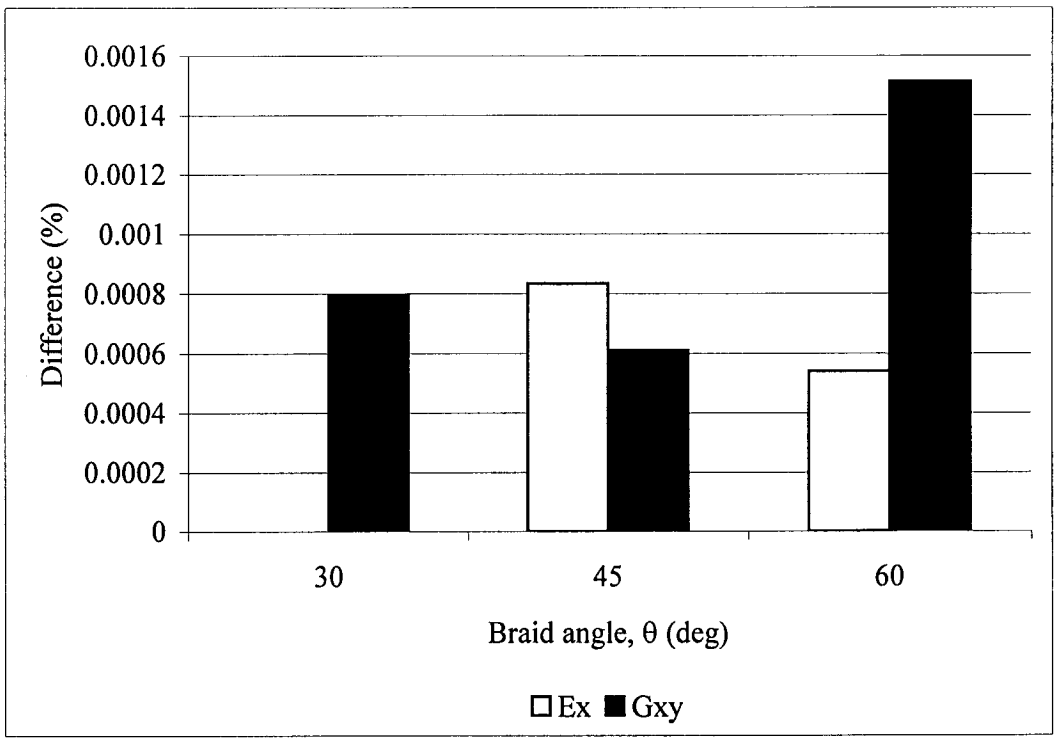

Figure 6-4: Maximum variation (%) in E_x and G_{xy} for a 10 % variation in ν_{f23} at different braid angles

There is little effect on the desired elastic constants from a 10 % error in the fibre out-of-plane Poisson's ratio; therefore, small differences in assumed ν_{f23} will not affect the accuracy of the proposed CLPT model.

6.5 *Effect of resin longitudinal elastic modulus variation*

Variations in resin elastic modulus, E_m, resulted in significant differences in the braid longitudinal elastic and shear moduli (Figure 6-5). Differences between 5.5 and 7.8 % were found for the braid longitudinal elastic modulus while differences between 5.2 and 2.5 % were found for the braid shear modulus. Resin elastic modulus is a dominant material property, thus, differences in the micromechanical predictions could be significant.

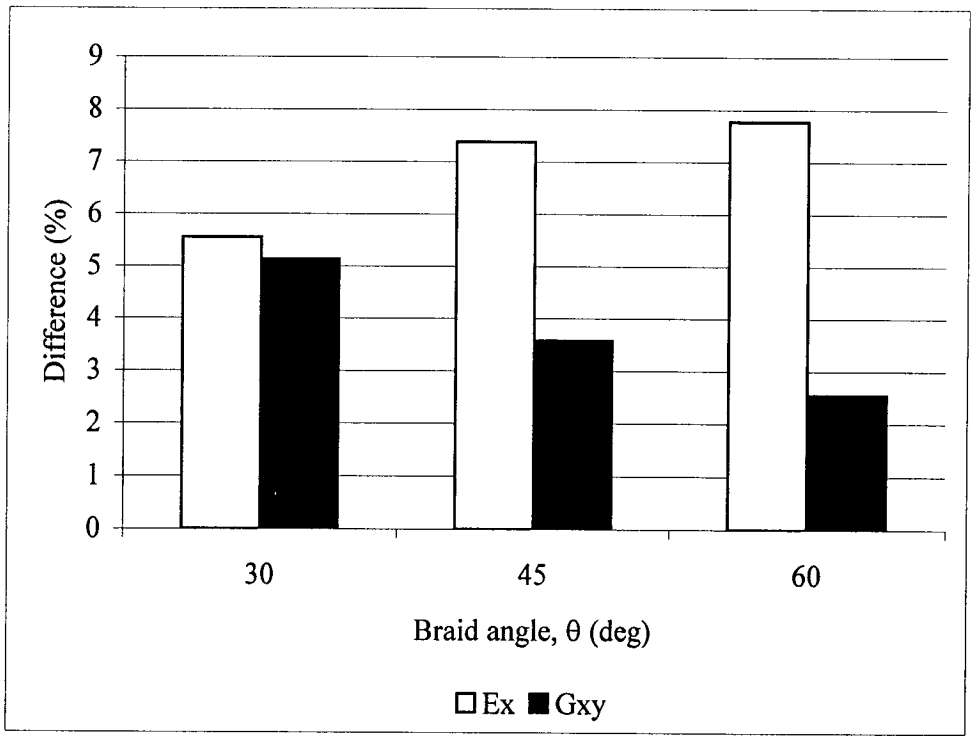

Figure 6-5: Maximum variation (%) in E_x and G_{xy} for a 10 % variation in E_m at different braid angles

There is a strong influence on the predicted values of braid longitudinal elastic and shear moduli by the input resin longitudinal elastic modulus; therefore, an accurate value of the resin longitudinal elastic modulus found experimentally for specific cure conditions is critical to the proposed CLPT model.

6.6 *Effect of resin shear modulus variation*

It was found that the resin shear modulus, G_m, was not a major contributor to the difference in braid longitudinal elastic modulus (Figure 6-6). At all three braid angles, a difference of ± 10 % in the fibre shear modulus results in less than 1 % difference in the predicted values. By contrast, a maximum variation of nearly 5 % and a minimum variation of 2.3 % were found for the braid shear modulus at braid angles of 30° and 60°, respectively.

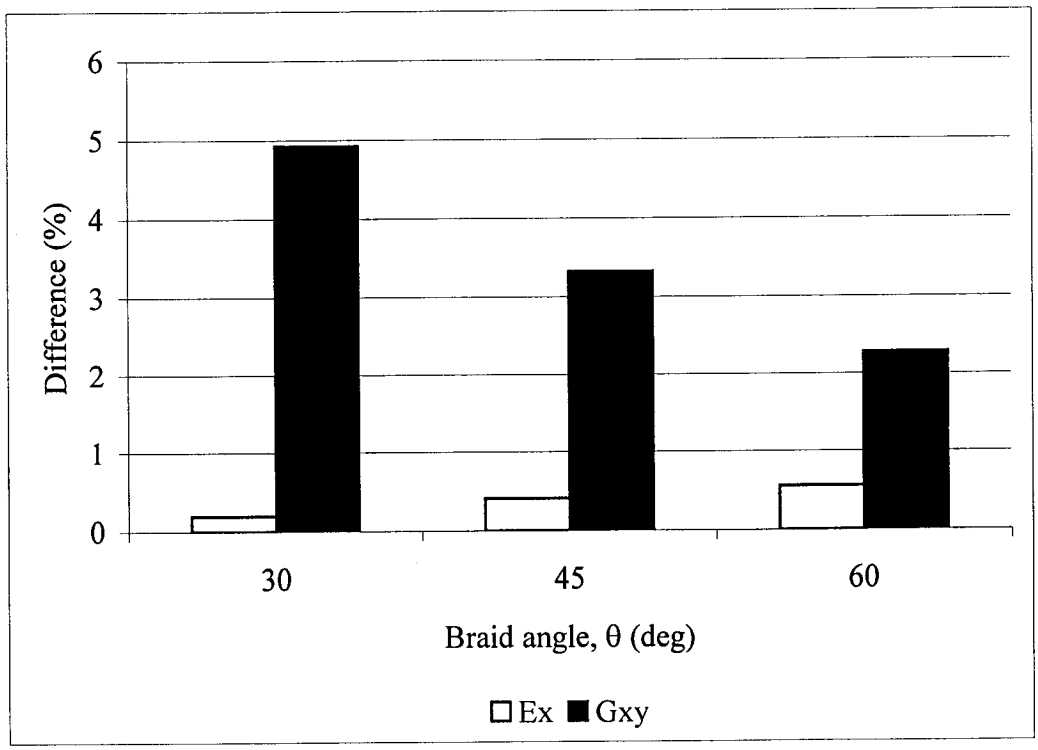

Figure 6-6: Maximum variation (%) in E_x and G_{xy} for a 10 % variation in G_m at different braid angles

There is a strong influence on the predicted value of braid shear modulus by the input resin shear modulus; therefore, an accurate value of this elastic constant found experimentally for specific cure conditions is critical to the proposed CLPT model.

6.7 *Effect of lamina out-of-plane shear modulus*

The final evaluation was for the lamina out-of-plane shear modulus, G_{23}. This laminar property was evaluated since there was some concern as to the accuracy of the micromechanical models evaluated in Section 2.4.3.5.

It was found that lamina out-of-plane shear modulus is not a major contributor to the difference in braid elastic and shear moduli (Figure 6-7). At all three braid angles, a difference of ± 50 % in the out-of-plane shear modulus results in less than 0.02 % difference in the assumed elastic and shear values. Therefore, an accurate value of laminar out-of-plane shear modulus is not critical to the proposed CLPT model.

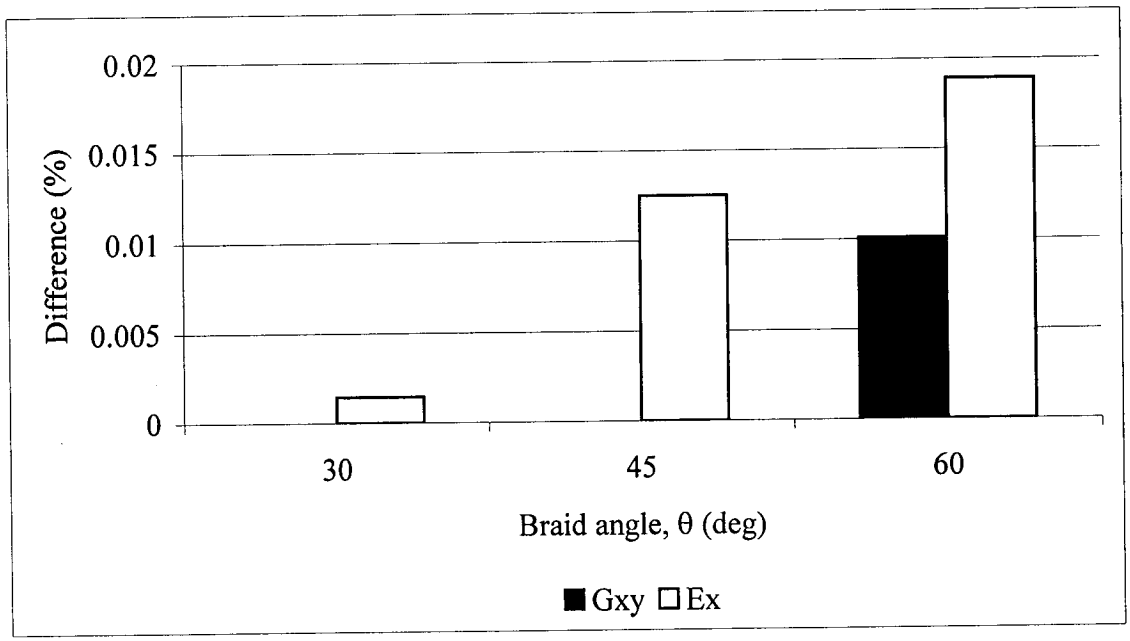

Figure 6-7: Maximal variation (%) in E_x and G_{xy} for a 50 % variation in G_{23} at different braid angles

6.8 Conclusion

After performing a sensitivity analysis of the model, it is clear that some constituent properties must be known accurately in order to give the most accurate micromechanical prediction. This could explain the disparity in the predicted and experimental values of laminar shear modulus seen in Table 6-1. The important constituent elastic constants are the fibre longitudinal elastic modulus, E_{f11}, and the resin longitudinal elastic modulus, E_m, and shear modulus, G_m. A ± 10 % difference in evaluating these properties will lead to differences in E_x and G_{xy} in the order of 2.5 to 8 %. The fibre elastic modulus is well documented by the Kevlar 49 fibre manufacturer (Dupont). The elastic modulus and major Poisson's ratio of epoxy resin/hardener matrix to be used in the experimental study in Chapter 7 have been previously experimentally measured by Flanagan and Munro [72]. The resin matrix shear modulus will be calculated using $G_m = E_m/2(1+\nu_m)$. Thus, the input values are as accurate as possible.

CHAPTER 7 : MODEL COMPARISON AND VALIDATION

7.1 Comparison to existing models

Evaluation of the model is two-fold. As an initial step, to show the accuracy of the model, results were compared to other models developed for braided and woven fabrics. The constituent material properties used for the comparisons are given in Table 7-1.

Table 7-1: Assumed material properties

Material				
Fibres	E_{f11} (GPa)	E_{f22} (GPa)	G_{f12} (GPa)	ν_{f12}
AS4 Carbon	228 [74]	40 [63]	24 [63]	0.26 [63]
E-glass [63]	72	72	27.7	0.3
Polymer resin	E_m (GPa)		G_m (GPa)	ν_m
Epoxy	2.8 - 4.2 [39]	-	1.08-1.62[1]	0.3 [39]
Polyester	2 - 4.4 [39]	-	0.72-1.59[1]	0.38 [39]

Although the proposed CLPT model is based on that of Raju and Wang [66] it cannot be used for 0°/90° fabrics because of the nature of the generalization that is carried out. This model is applicable for angle-plied (±θ) braids about the longitudinal axis; therefore, a 0°/90° configuration creates a discontinuity and thus a direct comparison is impossible.

[1] $G_m=E_m/(2(1+\nu_m))$

For comparison purposes, results for the elastic constants from the proposed CLPT model for a ± 45° braid were rotated 45°, using a method analogous to principal stresses transformations for isotropic materials but adapted for composite materials, to match the orientation of a plain weave composite [44], as follows:

$$\frac{1}{E_x} = \frac{1}{E_{11}}\cos^4\theta + \left(\frac{1}{G_{12}} - \frac{2\nu_{12}}{E_{11}}\right)\sin^2\theta\cos^2\theta + \frac{1}{E_{22}}\sin^4\theta$$

$$\frac{1}{E_y} = \frac{1}{E_{11}}\sin^4\theta + \left(\frac{1}{G_{12}} - \frac{2\nu_{12}}{E_{11}}\right)\sin^2\theta\cos^2\theta + \frac{1}{E_{22}}\cos^4\theta$$

$$\frac{1}{G_{xy}} = 2\left(\frac{2}{E_{11}} + \frac{2}{E_{22}} + \frac{4\nu_{12}}{E_{11}} - \frac{1}{G_{12}}\right)\sin^2\theta\cos^2\theta + \frac{1}{G_{12}}\left(\cos^4\theta + \sin^4\theta\right) \qquad \text{7-1}$$

$$\nu_{xy} = E_x\left[\frac{\nu_{12}}{E_{11}}\left(\cos^4\theta + \sin^4\theta\right) - \left(\frac{1}{E_{11}} + \frac{1}{E_{22}} - \frac{1}{G_{12}}\right)\sin^2\theta\cos^2\theta\right]$$

where, E_x, E_y, G_{xy} and ν_{xy} are the angle-plied braid elastic constants and θ is the transformation angle, 45°. The equations are solved simultaneously for E_{11}, E_{22}, G_{12} and ν_{12}, the 0°/90° fabric elastic constants.

Unidirectional laminar and resin properties were provided in the Raju and Wang paper. Strand dimensions of 0.1 mm and 4.1 mm for the strand thickness and width, respectively, were assumed. For the case of a neat resin content of 3.2 % [66], the proposed CLPT model predicts a longitudinal elastic modulus of 18.57 GPa for a ± 45° braid which, when rotated, is equivalent to 68.48 GPa. This result is 0.13 % different from that of the Raju and Wang prediction of 68.39 GPa, thus providing confirmation of the accuracy of the proposed CLPT model for the woven fabric case detailed in their work. Similar differences were found between both models for the other elastic constants.

The fabric geometry model (FGM) was used by Soebroto, Hager and Pastore [59] to predict the tensile modulus of a biaxially braided E-glass/polyester composite with a reported strand fibre volume fraction, V_f, of 60 % and an inclination angle of three degrees. They stated that the angle was consistent with the unit cell dimensions of the composite. Neither the resin properties nor the strand geometry were provided. Thus, upper and lower bound elastic modulus, E_m, values of 2 and 4.4 GPa, respectively, were used for the polyester resin (Table 7-1) and the shear modulus was determined analytically[2]. The elastic constants for E-glass are also given in Table 7-1. For this model, strand width and thickness were set at 3.1 mm and 0.23 mm, based on a dry strand area of 0.5 mm^2, respectively. The results of the comparison can be seen in Figure 7-1 for a range of braid angles defined by the minimum and maximum strand jamming angles, 30° and 60°, respectively.

[2] $G_m=E_m/(2(1+\nu_m))$

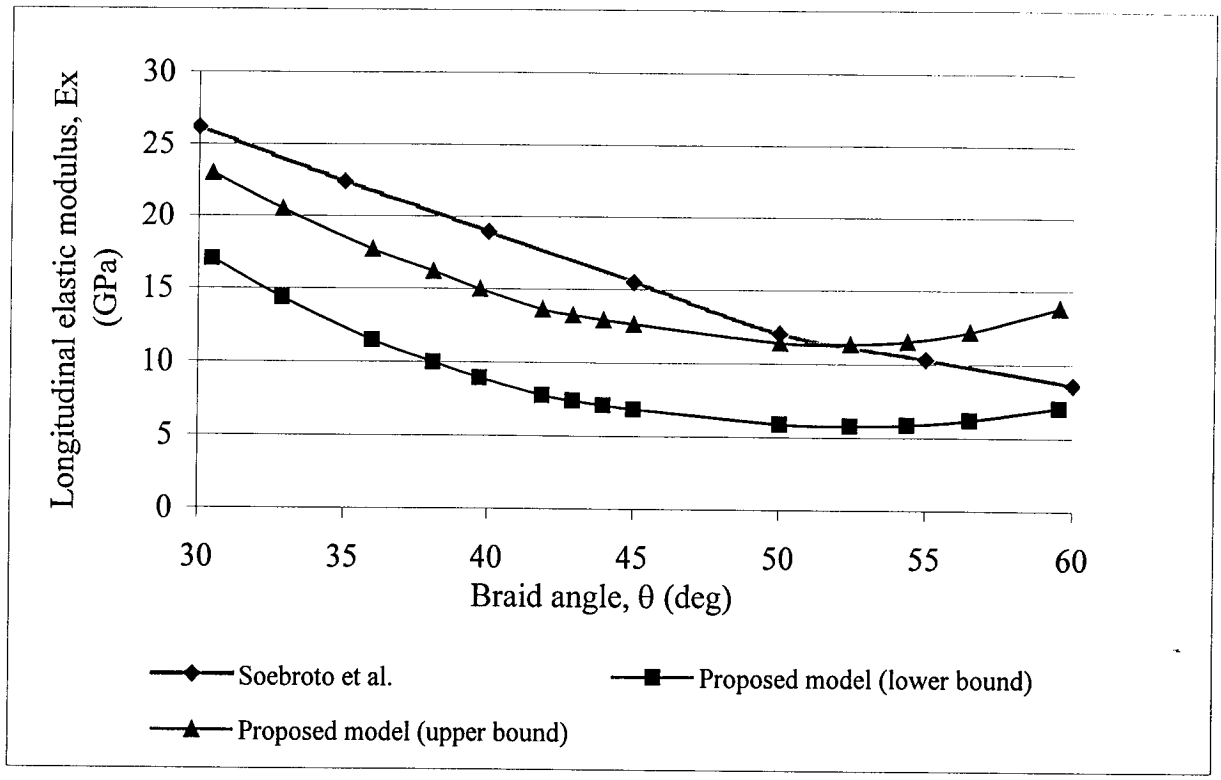

Figure 7-1: Comparison of proposed CLPT model with FGM [59] for an E-glass/polyester braided composite.

The proposed CLPT model generally under-predicts the FGM model between the minimum and maximum jamming angles. A certain contributor to the discrepancy is the shape function used to describe the undulation in both models. The Soebroto et al. model assumes a straight-line function to model the undulation path while the proposed CLPT model assumes a sinusoidal shape. Calculations [63] have shown that the elastic modulus of a strand undulation represented by a single angle is greater than a sinusoidal shape function. The proposed CLPT model's sinusoidal function approach to describing the undulation has also been deemed a more accurate and realistic approach by Naik and Ganesh [63]. Finally, the Soebroto et al. model is linear in the 30-60 degree range (Figure 7-1). This linear behaviour is unexpected since it is believed that the results should be non-

linear as occurs with a biaxial laminate [44]. No experimental results were reported to support the Soebroto et al. findings.

Proposed CLPT model results were also compared to those reported by Redman and Douglas [62] (Figure 7-2). The polymer resin material properties, details of the strand geometry and the inclination angle of the strand were not provided in their paper. Strand width and thickness were assumed at 3.14 mm and 0.16 mm, respectively, based on a dry strand area of 0.22 mm^2 and the reported fibre volume fraction of 0.43. Upper and lower limits for the epoxy elastic modulus were assumed at 2.8 and 4.2 GPa, respectively. The assumed elastic constants for the AS4 carbon fibre are given in Table 7-1.

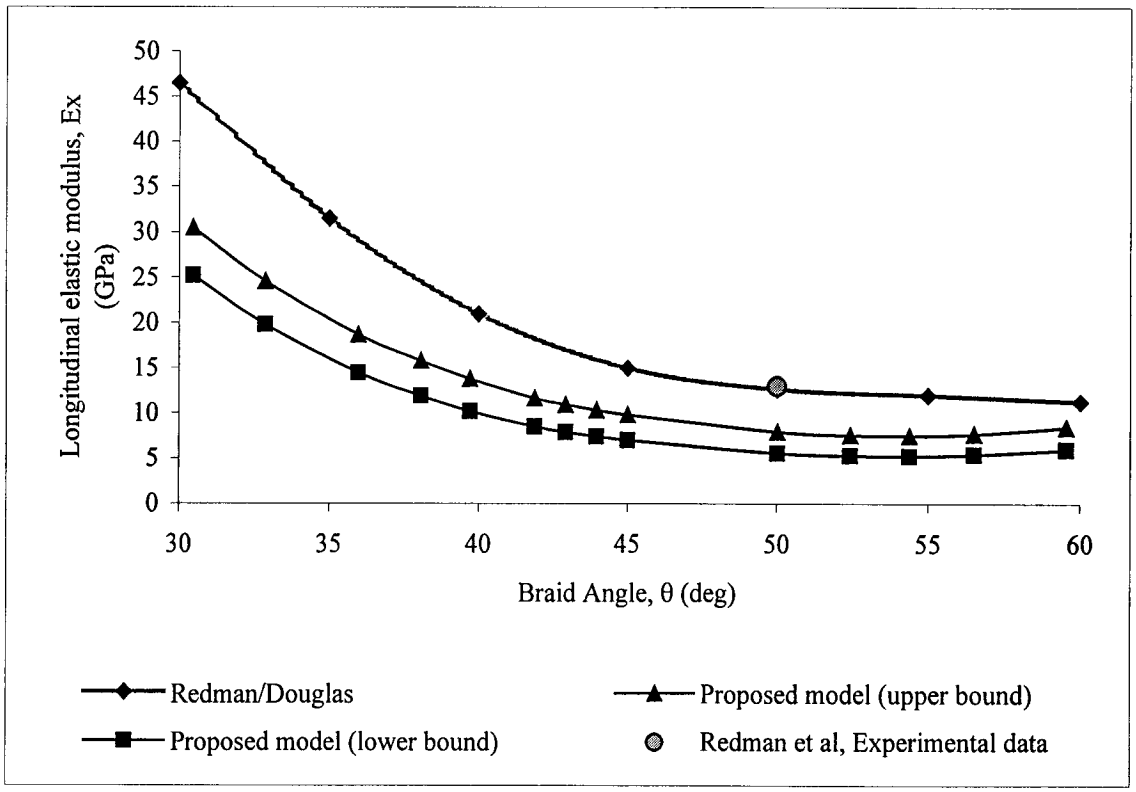

Figure 7-2: Comparison of proposed CLPT model with Redman/Douglas model [62] for carbon/epoxy braided composite.

The discrepancy seen in Figure 7-2 could stem from the possibility that Redman and Douglas reported the unit cell fibre volume fraction, V_{fo} and not the lamina fibre volume fraction, V_f. This is not unexpected since Redman assumes a constant undulation angle because of open meshing, for which a 43 % unit cell volume fraction or neat resin volume content would be expected. Results (Figure 7-2) would be much closer if the lamina fibre volume fraction was in the order of 60 %.

The results shown in Figure 7-2 are similar to those presented in Figure 7-1; however, the prediction by Redman is non-linear and has a very similar trend to the results of the presented model. A single experimental value of longitudinal elastic modulus, E_x, of 13.02 GPa was reported in the Redman et al. paper for a 50° braid angle tube; their model predicted a value of 12.67 GPa resulting in a difference of only 2.7 %. Their model appears accurate based on this comparison; unfortunately, only one experimental result was measured and the material constituent values, which are required to fully assess the accuracy of the proposed CLPT model, were not provided in their paper.

For the case of shear modulus, two cases evaluated by Naik and Ganesh were compared, using material properties and weave geometry provided [63], with the proposed CLPT model and showed very good agreement (Table 7-2). Again, comparison was possible after rotating results 45° to match 0°/90° weave configuration. Results from the proposed CLPT model are lower but still confirm that the proposed approach is valid. Results from the proposed CLPT model are more accurate at predicting most experimental results than the Naik and Ganesh model. Other results from Naik and Ganesh show that it is not unusual to find up to 50 % difference in experimental and predicted results based on the experimental approach [63].

Table 7-2: Comparison between Naik and Ganesh [63] predicted and experimental elastic constants, and current predicted results

Case	GLE1	GLE2	
Elastic Constant	**Ex, GPa**	**Ex, GPa**	**Gxy, GPa (range)**
Experimental results [63]	17.5	20.0	6.25[3] (6.0-6.4) 2.94[4] (2.9-3.0)
Naik and Ganesh Model [63]	14.0	14.5	2.96
Proposed CLPT	17.4	20.3	2.2

7.2 Experimental comparison and validation

7.2.1 Introduction

The second step was the experimental validation of the proposed CLPT model, which involved comparing predicted results with experimental values. Oversized braided engineering model composite structures are used to verify the model. These model catheters are produced on an existing braiding machine. There was high confidence in the input constituent and laminar properties to the model since they had been previously determined for the same fibre volume fraction and curing schedule as used in this work [72]. Thus, similar experimental and predicted results would be a strong basis for validating the proposed CLPT model. Both braided and laminar tubular specimens were fabricated using Kevlar 49 fibres and epoxy resin as the matrix. Braided specimens were used to validate the proposed CLPT model while the laminated specimens were used to confirm the loss of stiffness due to undulating strands.

---

[3] 10° off-axis shear test
[4] ±45° off-axis shear test

7.2.2 Experimental measurement of braid longitudinal elastic modulus

The braided and laminar tubes were made using a Steeger model 4475 36-bobbin braider head and horizontal mandrel drive. Kevlar 49 fibres with a matrix of EPON 825[5] epoxy resin and Ancamine 1482[6] hardener (19phr) were used. Constituent properties can be found in Table 6-1(a).

Both 12.7 mm and 11.1 mm outer diameter mandrels were used to produce the specimens. Tubular specimens were fabricated for braid angles of 42.5° and 50° (Figure 7-3) and of a ± 50° laminate (i.e. three test cases). Braided socks were fabricated (Figure 7-4), placed over 460 mm long mandrels and coated with epoxy resin.

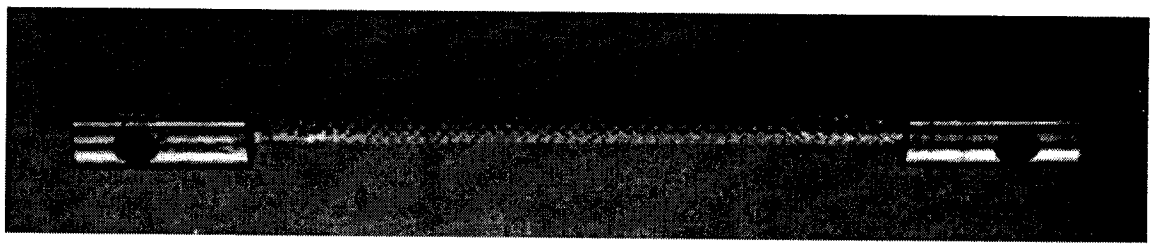

Figure 7-3: Braided tubular specimen with end fittings

[5] Shell Canada Chemicals Co.
[6] Pacific Anchor Inc. (Shell Canada).

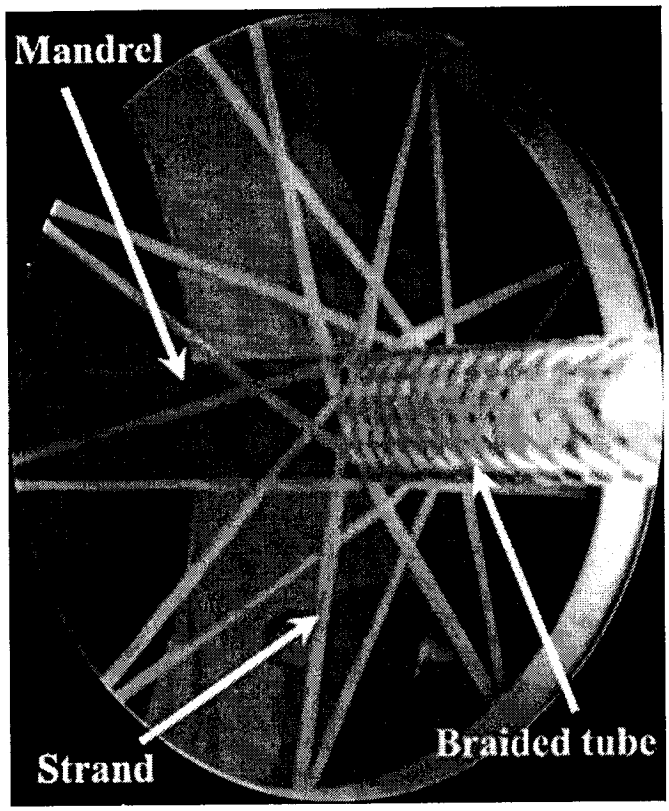

Figure 7-4: Braided tube being manufactured.

The laminate specimens were produced using a two-step procedure. First, the braider head spools that rotate clockwise were removed. Fibre strands were wound over the mandrel for a length of 1000 mm and the dry braid was impregnated with polymer resin. The mandrel was returned to the initial position. The braid head direction was reversed to get the opposite winding angle and the same procedure was repeated. The resulting tubular specimen can be seen in Figure 7-5.

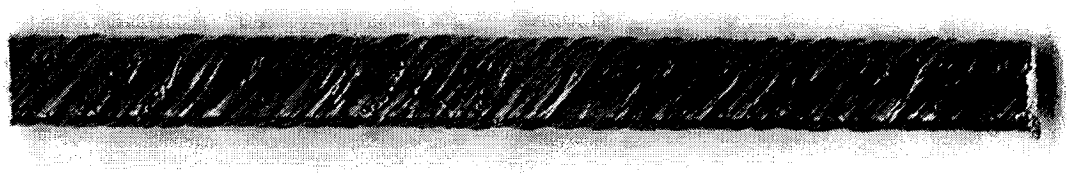

Figure 7-5: Laminate tubular specimen

All specimens were cured at 110°C for one hour. The specimens were removed from the mandrel and cut to a length of 152.4 mm. Three specimens were produced for each of the three test cases. End fittings with a tapered stem [75] were bonded to the inside of the tubes with 3M Scotch-Weld™ Two-Part Epoxy Adhesive 2216 B/A Translucent. A sample end fitting is illustrated in Figure 7-6.

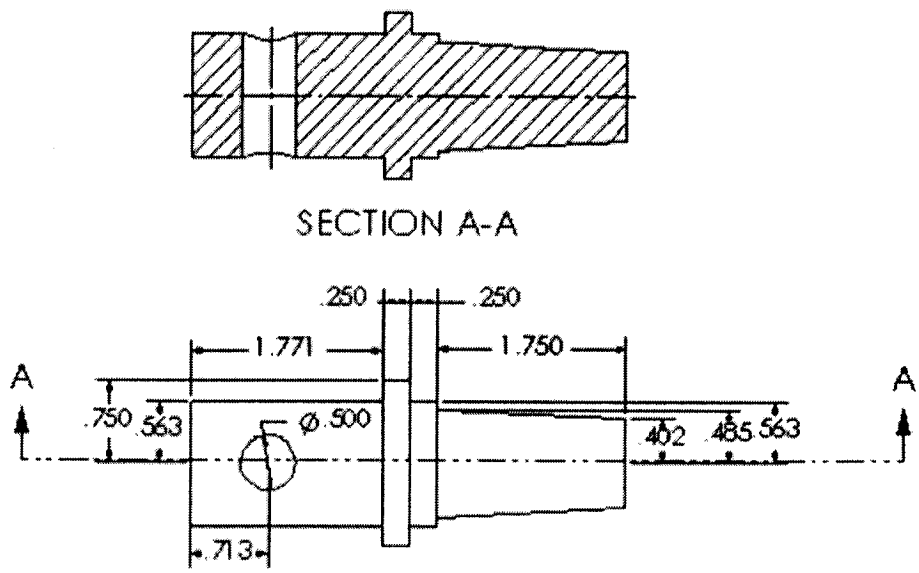

Figure 7-6: Tapered mounting end fitting used for tensile testing braided tubes (25.4 mm ID tube shown, dimensions in inches).

The braid longitudinal elastic modulus, E_x, was determined by performing tensile tests on an Instron testing machine (Model 4482). An Instron extensometer (Model 2620-

530) was used to obtain the longitudinal strain of the specimens. Data was gathered using a LabView ™ virtual instrument. The experimental setup can be seen in Figure 7-7.

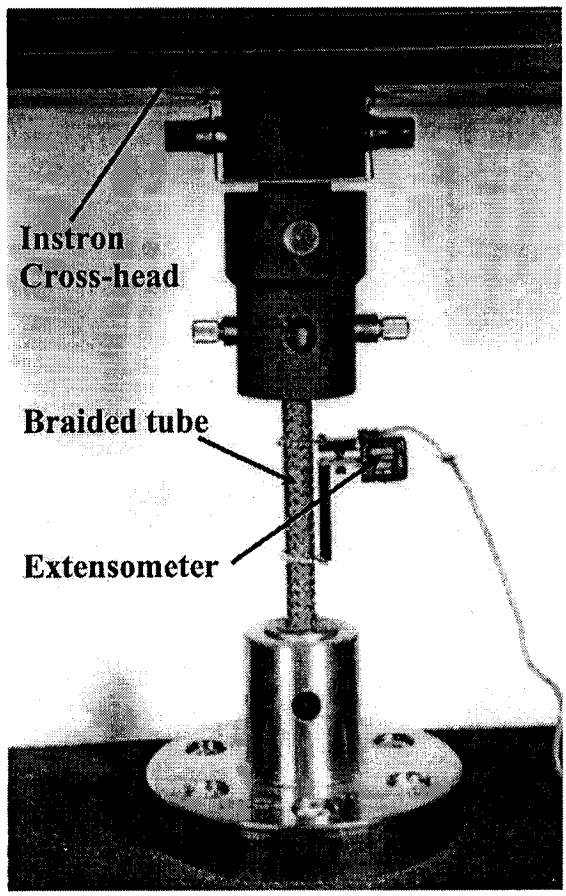

Figure 7-7: Tensile testing setup.

The classical laminate plate theory (laminate CLPT) prediction of the longitudinal elastic modulus for the Kevlar 49/epoxy laminated tube was found to have values between 25 to 5 GPa for angles between 30° and 60°, respectively (Figure 7-8). There is reasonable agreement between the laminate CLPT prediction and the experimental results for the ± 50° laminated tubes; the range of experimental values is 17.6 % of the mean value, 7.9 GPa. There is high confidence in elastic constants that were used as they had been previously measured for the same fibre, epoxy resin and curing schedule. This result does give an

indication of the accuracy of the CLPT when applied to laminated composites fabricated using a 2D braider. The difference between the predicted and experimental values could be due to the varying thickness of the laminated layers produced by a braider as compared to the more uniform thickness of a traditional laminate fabricated using pre-preg.

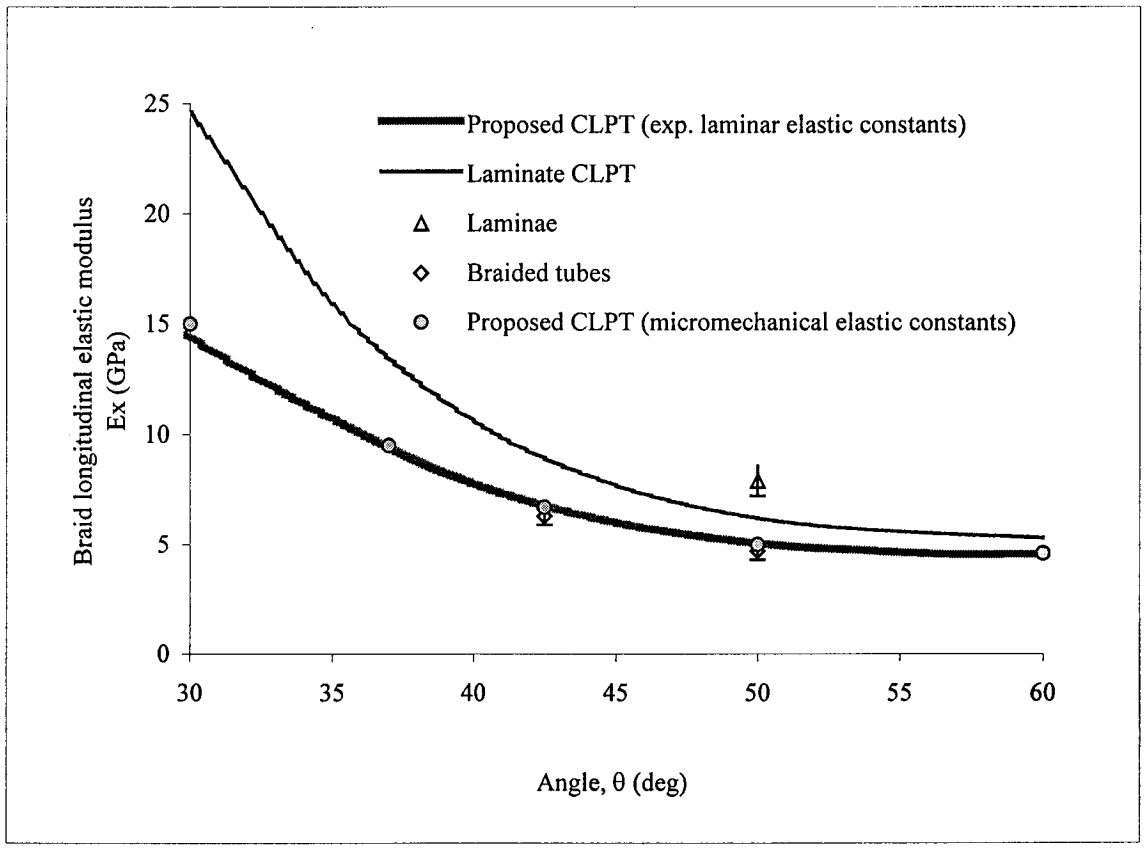

Figure 7-8: Longitudinal elastic modulus for Kevlar49/epoxy composite braided tube as a function of braid angle; unit cell dimensions W_y = 3.1 mm, h_c=0.38 mm and t=0.85 mm; t_m=0.08 mm. Error bars represent the range of the data.

The shape of the curves for the proposed CLPT model for a braided composite and the laminate CLPT model are similar. As expected, the results for the braided composites are lower than laminates due to strand undulation [76]. Strand undulation results in lower

longitudinal elastic modulus values because the strands are off-axis with the longitudinal direction by both the braid and the undulation angles.

The second comparison is between the predictions of the proposed CLPT model and experimental results. For an experimental comparison, the Kevlar 49 strand (7100 Tex) was assumed to be 3.1 mm wide by 0.23 mm thick (0.38 mm impregnated with resin). The resin elastic modulus, E_m, and major Poisson's ratio, ν_m (Table 6-1) had been measured previously [72] and the elastic modulus of the fibre, E_{fl1}, was available from the manufacturer. Thus it is possible to predict E_x using micromechanical constants as inputs.

The mean values for the longitudinal elastic modulus of the 42.5° and 50° braided tubes are 6.3 and 4.7 GPa, respectively (Table 7-3 and Figure 7-8). The ranges of values for the longitudinal elastic modulus of the 42.5° and 50° braided tubes as a percentage of the mean value are 11.1 % and 8.5 %, respectively, thus, there is excellent agreement within each set of data. The proposed CLPT model has good agreement with the experimental results for 42.5° and 50° specimens with errors of 6.3 % and 6.4 %, respectively. This agreement may be due to the use of laminar elastic constants fabricated using the identical fibres, matrix and cure schedule as in a previous study [72].

Table 7-3: Experimental and predicted braid longitudinal elastic modulus, E_x, values

Braid angle, θ (degrees)	Experimental E_x		Theoretical E_x			
	Mean (GPa)	Coefficient of variation (%)	Laminar properties (GPa)	Difference (%)	Micromechanical properties (GPa)	Difference (%)
42.5	6.3	11.1	6.5	3.2	6.7	6.3
50	4.7	8.5	4.9	4.3	5.0	6.4

7.2.3 Micromechanical model predictions

It is important to determine if the model of Chapter 5 essentially predicts the same E_x values whether laminar properties or micromechanical properties are used. The model was therefore used to predict the braid longitudinal elastic modulus with experimentally measured laminar properties [72].

The results are given in Table 7-3 and Figure 7-8. Although the percentage of difference using laminar properties is closer to the experimental values (maximum difference of 4.3 %), using accurate constituent properties in the micromechanical models results in a maximum percentage of difference of only 6.4%. This confirms that micromechanical models can be used with confidence in this specific case to accurately obtain laminar properties.

7.2.4 Experimental measurement of braid shear modulus

Different methods to evaluate shear properties of advanced composite materials were evaluated previously [77]. Typically, Iosipescu, 45° off-axis tensile and 10° off-axis methods are ranked higher than other approaches. The torsion of thin-walled tubes was chosen for this work as the wall of the tube is subjected to a uniform pure shear state over the length of the specimen, if the specimen is free to translate along the tube's longitudinal axis [77, 56]. In addition, the specimen shape (thin-walled tube) matches the geometry of a medical catheter.

The same braided specimens described in the previous section were used for the experimental measurement of the braid shear modulus. The following equation was used to calculate the shear modulus of the braided tubes, G_{xy} [37]:

$$G_{xy} = \frac{TL}{J\phi} \qquad 7\text{-}2$$

where T is the applied torque, L is the distance between points of angular twist measurement (Figure 7-9), ϕ is the difference in angle of twist between both points of measurement and J is the polar moment of inertia.

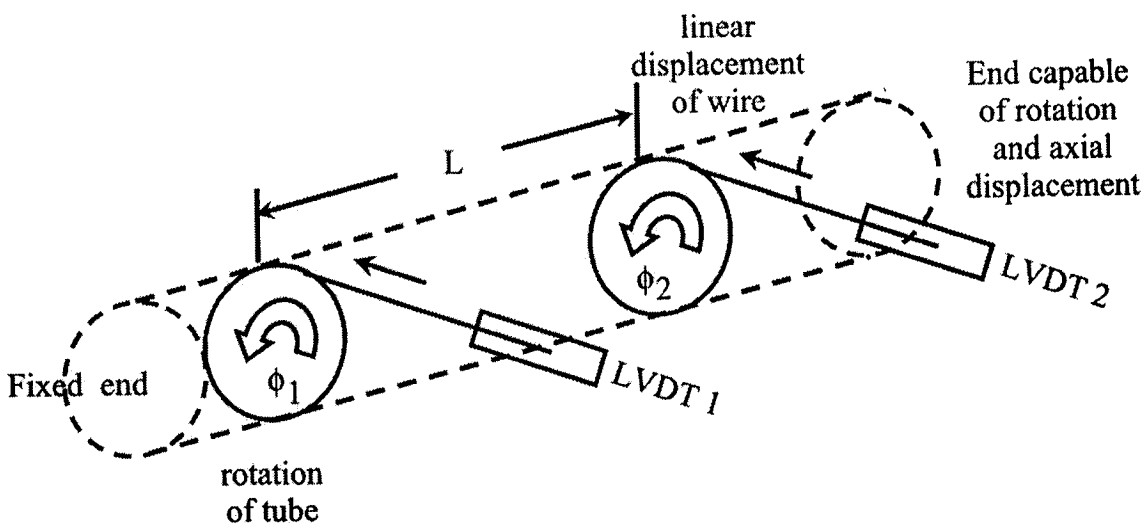

Figure 7-9: Illustration of the twisting of a braided tube (dotted lines). The twist angles taken at two positions separated by a distance L, are shown. Two LVDTs were used to obtain the linear displacement of the tube circumference at positions 1 and 2.

The braid shear modulus was determined using an in-house apparatus (Figure 7-10). One end of the specimen is rigidly fastened to a vertical steel plate while the other end rotates freely about a central rod fixed at both ends of the support structure (Figure 7-10).

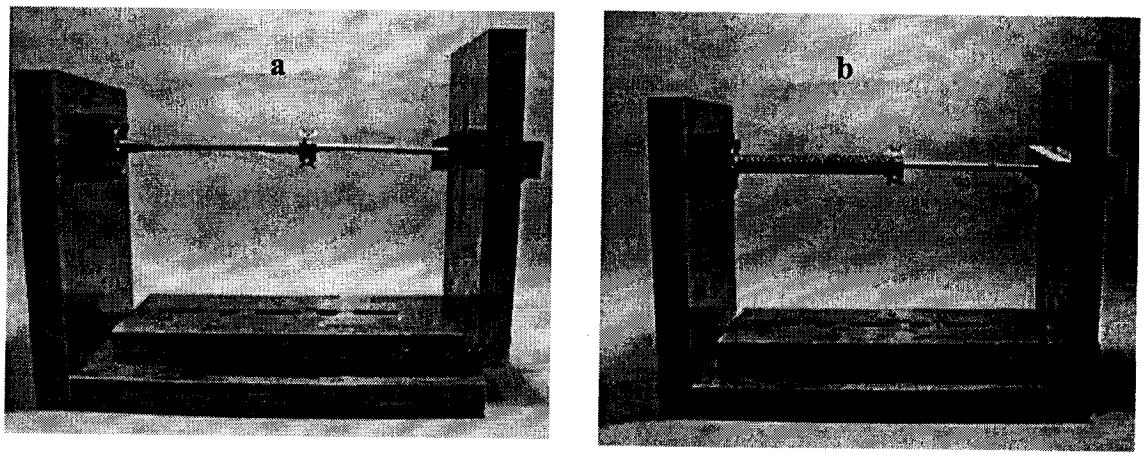

Figure 7-10: Torsion tester without (left) and with (right) a specimen

The braided tube ends are anchored in two different end fittings; one end of the tube is bonded[7] to an end fitting (Figure 7-11 (a)) which is attached to one of the vertical plates of the support structure. The other tube end is bonded to an end fitting with a pulley (Figure 7-11 (b)).

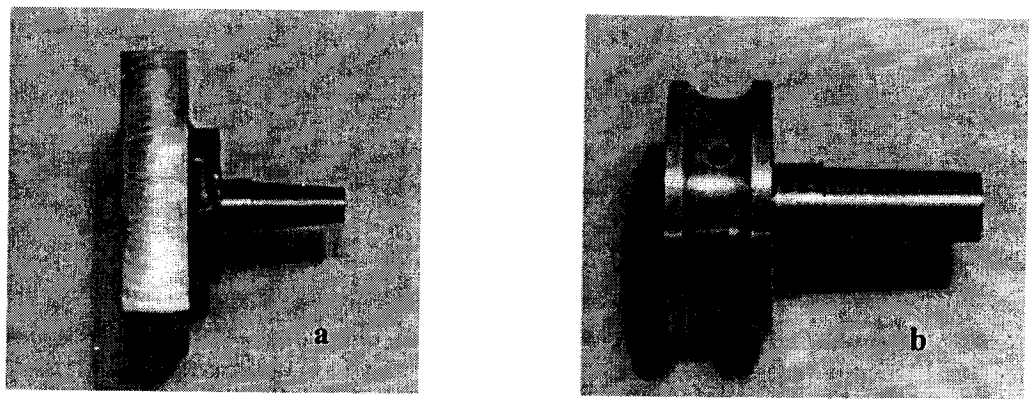

Figure 7-11: Side view of end fittings, fixed end (a); rotating end (b)

[7] 3M Scotch-Weld™ Two-Part Epoxy Adhesive 2216 B/A Translucent.

Angular displacements were measured at two points on the braided tube using two linear variable differential transformers (Intertechnology, Inc. LVDT) connected to flexible wires bonded to the tube (Figure 7-9). The angular displacements were calculated using the relationship for angular rotation, ω, as follows:

$$\omega = \frac{\text{linear displacement of line}}{\text{radius of tube}} \qquad \text{7-3}$$

The difference in angular displacement divided by the distance between the two points between is the angle of twist. The testing fixture was mounted in the frame of an Instron testing machine (Model 4482). A load cell was used to measure the load in the flexible connection fastened to the rotating end fitting. The applied torque is calculated from the load and the minimum radius (Figure 7-11 (b)) of the rotating end fitting.

It was shown in Section 6.6 that variations in resin shear modulus had a significant effect on braid shear modulus; therefore, three neat resin tubes of the same dimensions as the braided tubes were tested. The average shear modulus of the epoxy resin was 1.07 GPa with a range of data of 0.98 – 1.15 GPa. Therefore, for the following work, a shear modulus, G_m, of 1.07 GPa was used in the predictive model.

Experimental and predicted results for braid shear modulus are shown in Figure 7-12. Average experimental values were 4.6 GPa and 4.3 GPa for braid angles of 42.5° and 50°, respectively, with ranges of 3.5 to 5.7 GPa and 2.7 to 5.7 GPa, respectively. Compared to the predicted shear modulus of 5.7 GPa for both braid angles, errors of 19.8% and 24.2 % were found, respectively. This level of difference between predicted and experimental results and experimental variability are not unusual in composite materials.

It is apparent from Figure 7-12 that the experimental results do not show as good agreement with the predicted results as for the braid longitudinal elastic modulus. However, Naik and Ganesh did find discrepancies between predicted and experimental shear modulus results [63] as well as between different experimental approaches. Using the 10° shear test method they found twice the shear modulus results of the ±45° shear test method for the same fabric geometry; again, different testing methods measure significantly different results. Prediction errors were between 0.6 % and 17 % [63].

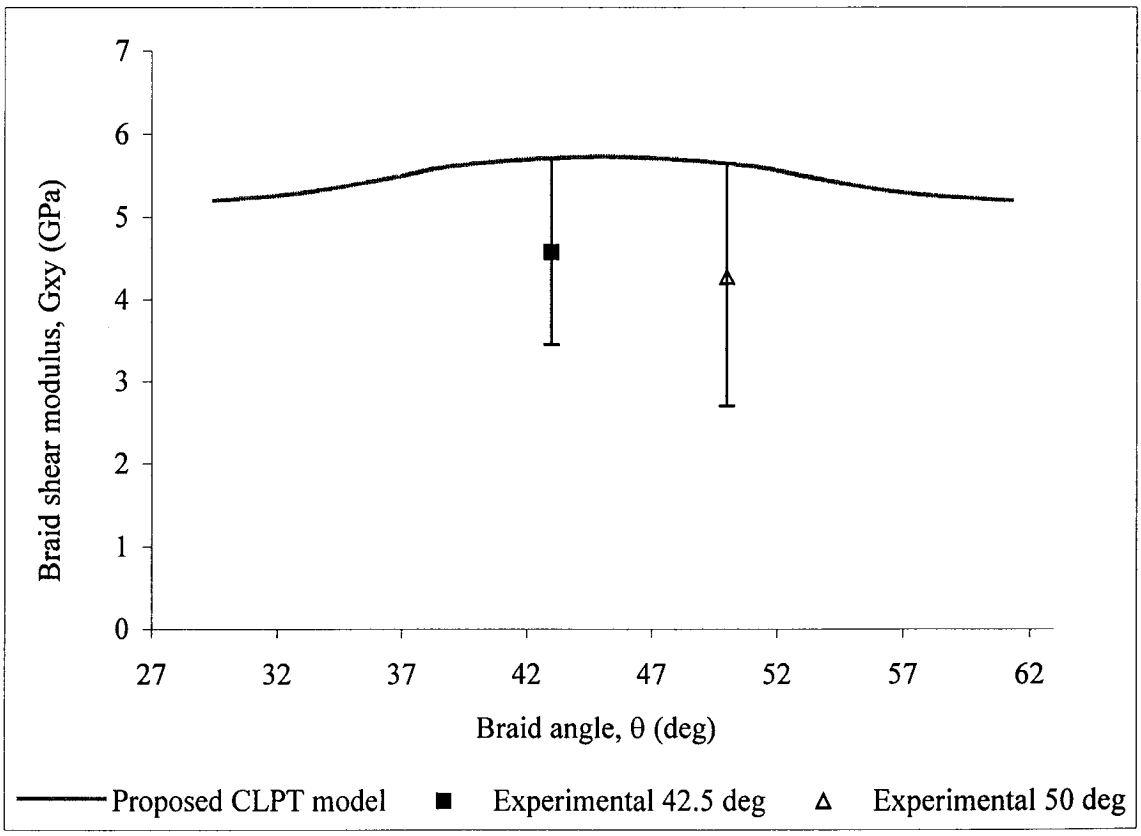

Figure 7-12: Shear modulus for Kevlar49/epoxy composite braided tube as a function of braid angle; unit cell dimensions W_y = 3.1 mm, h_c=0.38 mm and t=0.85 mm. Error bars represent the range of data.

7.3 Conclusions

In this chapter, a model based on a modified classical laminate plate theory developed to predict the longitudinal elastic modulus, E_x, and shear modulus, G_{xy}, of braided tubes was compared to previous models and to experimental results.

It was shown that the proposed CLPT model predicts the same value as the Raju and Wang model for a 0/90° plain weave fabric. It predicts lower E_x values than the FGM model of Soebroto et al and CLPT/ROM model of Redman and Douglas. This could be due to the material and geometric parameters that were necessary for the proposed CLPT model and had to be taken from the published data since they were not reported by the authors. It should be noted that the results of the proposed CLPT model have the same trend as those of the CLP/ROM model. The difference in the trend of the results for the FGM model and the proposed CLPT model could be due to the difference in the modelling of the fibre strand paths. The FGM model assumes a straight path while the proposed CLPT model defines the path as a sinusoidal shape which is a better approximation of the true strand path. In addition to more accurately predicting longitudinal elastic moduli experimental results in this work, a shear moduli comparison between the proposed and Naik and Ganesh models show similar results for two cases reported in their work [63].

Furthermore, the proposed CLPT model is in agreement with experimental results. Differences between the predicted and experimental values of 6.3 % and 6.4 % were found for the braid longitudinal elastic modulus and 19.8 % and 24.2 % for shear modulus, at braid angles of 42.5° and 50°, respectively. This comparison indicates the agreement between the proposed CLPT model and experimental results is essentially as accurate as other models presented for their respective cases. It is believed that the use of a composite

material (Kevlar 49/epoxy) for which laminar material properties had been previously measured and back calculated to constituent elastic constants for use in the proposed CLPT model is a major reason for the high accuracy. The results also indicate that micromechanical models in which accurate values for important elastic constants are used can also accurately predict experimental values; thus, it is not required to measure lamina elastic constants.

As expected, the models confirmed that the laminate CLPT predicts higher results than the proposed CLPT for a braided unit cell; accordingly, the laminate experimental results are greater than the braided results.

In the next chapter, the proposed CLPT model will be used for its primary objective: to select constituent materials and braid angles required to obtain optimal rigidities in a one-piece braided medical catheter for use in cardiovascular catheterization procedures.

CHAPTER 8 : MEDICAL CATHETER MATERIAL EVALUATION AND SELECTION

It was established in Section 2.2 that for an optimal medical catheter there should be sufficient axial rigidity and high torsional rigidity along the length, low flexural rigidity at the distal end to comply with the tortuous anatomy of the vascular system and high flexural rigidity at the proximal end for manipulation. These characteristics were prioritized in the following order: flexural, torsional and finally axial rigidity. The existing literature on medical catheter axial, torsional and flexural rigidities (Table 2-5 to Table 2-8) as well as experimentally determined rigidities of a Torcon Blue medical catheter and CGWS (Table 2-9 and Table 2-10), were previously presented. In Chapter 3, candidate fibre and resin materials (Table 3-2 and Table 3-4) were selected for their appropriate material properties (moduli, viscosity, gel time, etc.) in addition to their previous use in medical catheters.

In this chapter, using the proposed CLPT model, the most appropriate combinations of fibre and resin materials for an optimal medical catheter will be determined. Experimental evaluation of every material combination (Table 3-2 and Table 3-4), at different braid angles, would be a costly process, lengthy, and unreasonable to undertake. Furthermore, appropriate facilities for fabricating medical catheters are not available. The final constituent materials and braid angle combination will be selected based on the level of similarity with the ranges of target rigidities detailed in the next section.

8.1 Candidate materials and rigidity target values

In order to select the candidate fibres and resins, target rigidities (Table 8-1) were selected based on the ranges of values given in Section 2.3. This was especially important for flexural rigidity since different values are required at the proximal and distal ends of the medical catheter.

Table 8-1: Target ranges for rigidities for proposed braided medical catheter

Characteristic	Determined range	Target range	
		Proximal	Distal
Flexural rigidity	126 - 945 (10^{-6} Nm^2)	945	126
Torsional rigidity	17-1400 (10^{-6} Nm^2)	≥1400	≥1400
Axial rigidity	39.4 - 147 (kN)	≥450	

Furthermore, torsional rigidity should be high to provide as for the Torcon Blue medical catheter, a 1:1 ratio of proximal end to distal end rotation angle. Thus, the torsional rigidity results could be above the upper range value ($945x10^{-6}$ Nm^2) if the minimum torsional rigidity is set to coincide with the Torcon Blue medical catheter torsional rigidity.

The candidate fibre and resin materials selected for the comparison are listed in Table 8-2 and Table 8-3, respectively, together with the fibre and unit cell dimensions.

Table 8-2: Candidate fibre materials (modified from Table 3-2)

Material	Tensile modulus, E_{f1} (GPa)	Shear modulus, G_{f12} (GPa)	Reinforcement Dimensions		Unit cell Dimension[1]	
			Thickness (mm)	Width (mm)	Width (mm)	Height (mm)
Polyester[2]	2-4.4	1.232	0.1	1.4	3.6	width/tan(θ)
Kevlar-49	138	2.86	0.1	1.4	3.6	width/tan(θ)
Nylon 6,6[3]	2.8	0.076	0.1	1.4	3.6	width/tan(θ)

Table 8-3: Candidate resin materials (modified from Table 3-4)

Material	Type	Hardness	Tensile modulus, E_m (MPa)	Shear modulus, G_m (MPa)	Viscosity (Centipoise)	Gel time (min)
Silicones						
RTV 118	Elastomeric	25A	18.27	7.02	20,000	20
RTV 11	Elastomeric	45A	29.2	11.23	12,000	60
Polyurethanes						
RP 6443	Elastomeric	95±5A	58.28	22.42	2,500	17
RP 6434	Elastomeric	35-40A	26.7	10.3	500	19
Epoxy						
Scotchweld 2216	Flexible	35-50D	172	57.3	10 000	120
Epon 825	Rigid		3500	1300	300 at 50°C	3hr at 50°C

The predictions of the proposed CLPT model for every combination of fibre and resin at various braid angles for a theoretical medical catheter (0.97 mm inner and 2 mm outer diameter) are found in Appendix 4. Each type of rigidity is examined for each resin system with different reinforcements and at different braid angles. The figures contain, with the exception of the axial rigidities figures, the lower and upper limits as given in Table 8-1.

---

[1] Based on the 3.6mm circumference of an actual medical catheter average diameter (OD 2mm and ID 0.97mm).

[2] Set to have the same dimension as Kevlar; can be extruded to size.

[3] Based on 10 filaments of 0.161 Tex to get same dimension as Kevlar strand.

A process of elimination approach was taken to reduce the number of possible combinations of fibre and resins. Thus the elimination procedure considered rigidities in the following order: flexural, torsional, axial. The braid angles for acceptable combinations of fibre and resin, for axial and flexural rigidities, are found for values within these limits or greater than the upper range value in the case of torsional rigidity.

8.2 Predicted results

The results from the figures found in Appendix 4 are tabulated in Table 8-4; the table is also a decision matrix for selecting the best fibre and resin combinations. Only composites with Kevlar fibres reached both the maximum and minimum flexural rigidity values with the RTV11, RTV118, RP6443 and RP6434 (Figures 2 – 5 in Appendix 4, respectively) resins at different ranges of braid angle. The Scotchweld 2216 epoxy did not reach the lower limit (Figure 1) and the Epon 825 epoxy was altogether above the range (Figure 6). Therefore both Scotchweld 2216 and Epon 825 epoxies were eliminated from further consideration. The combination of Kevlar 49 fibre with the RP6443 polyurethane was ranked first since it matched the desired maximum and minimum flexural rigidities at a greater range of braid angles (25°). This provides more sensitivity for controlling the flexural rigidity. The combination of Kevlar 49 fibre with the RTV11 silicone was ranked second because of it has the second best sensitivity (range of 15°).

For the case of the torsional rigidity, it was found that polyester and nylon fibres could not provide sufficient torsional rigidity (Figures 7-10). Although above the required range, only Kevlar provided sufficiently high torsional rigidity when combined with RTV11, RTV118, RP6443 and RP6434 resins (Figures 7-10).

Table 8-4: Results comparison for fibre and resin selection[4]

Resin	Fibre	Braid angle			Rank	Comments
		Max Rigidity value	Min Rigidity Value	Range		
Flexural Rigidity						
Scotchweld 2216	Kevlar Polyester Nylon	39° DNM DNM	DNM	N/A	X	Eliminated
RTV11	Kevlar Polyester Nylon	27° DNM DNM	42° 35° 35	15° N/A N/A	#2	
RTV118	Kevlar Polyester Nylon	25° DNM DNM	37° 32° 30°	12° N/A N/A	#4	
RP6443	Kevlar Polyester Nylon	30° DNM DNM	55° 43° 43°	25° N/A N/A	#1	Largest braid angle range
RP6434	Kevlar Polyester Nylon	27° DNM DNM	40° 35° 32°	13° N/A N/A	#3	
Epon 825	N/A	Outside range		N/A	X	Eliminated
Torsional Rigidity						
RTV11	Kevlar Polyester Nylon	Over range Too low Too low		N/A	Tied #1 X X	Polyester and Nylon are eliminated; Kevlar is more rigid than necessary but acceptable.
RTV118	Kevlar Polyester Nylon	Over range Too low Too low		N/A	Tied #1 X X	
RP6443	Kevlar Polyester Nylon	Over range Too low Too low		N/A	Tied #1 X X	
RP6434	Kevlar Polyester Nylon	Over range Too low Too low		N/A	Tied #1 X X	
Axial Rigidity						
All combination possesses axial rigidities below the range						

[4] X: eliminated; N/A: not applicable; DNM: Did not meet.

The axial rigidity results for Kevlar fibre with the four resins are shown in Figure 8-1. All axial rigidities for the resins were between 2500 and 5000 N which is significantly above the 450 N target value. However, it can be lowered if necessary by increasing the braid angle at the distal end. As compared to the Torcon Blue medical catheter axial rigidity of 450N, the axial rigidities are greater at low braid angles for the combinations of Kevlar-49 fibres with either RTV11, RTV118, RP6443 and RP6434 resins (Table 8-1). The combination of Kevlar 49 fibre with RP6443 has the highest axial rigidity. For completeness, a comparison between the axial rigidity of GGWS and composites composed of RTV11, RP6343, RP6443 and RTV118 resins and Kevlar-49 at various braid angles can be found in Appendix 4. Axial rigidity results for all four fibre/resin combinations are much lower than the axial rigidity of CGWS.

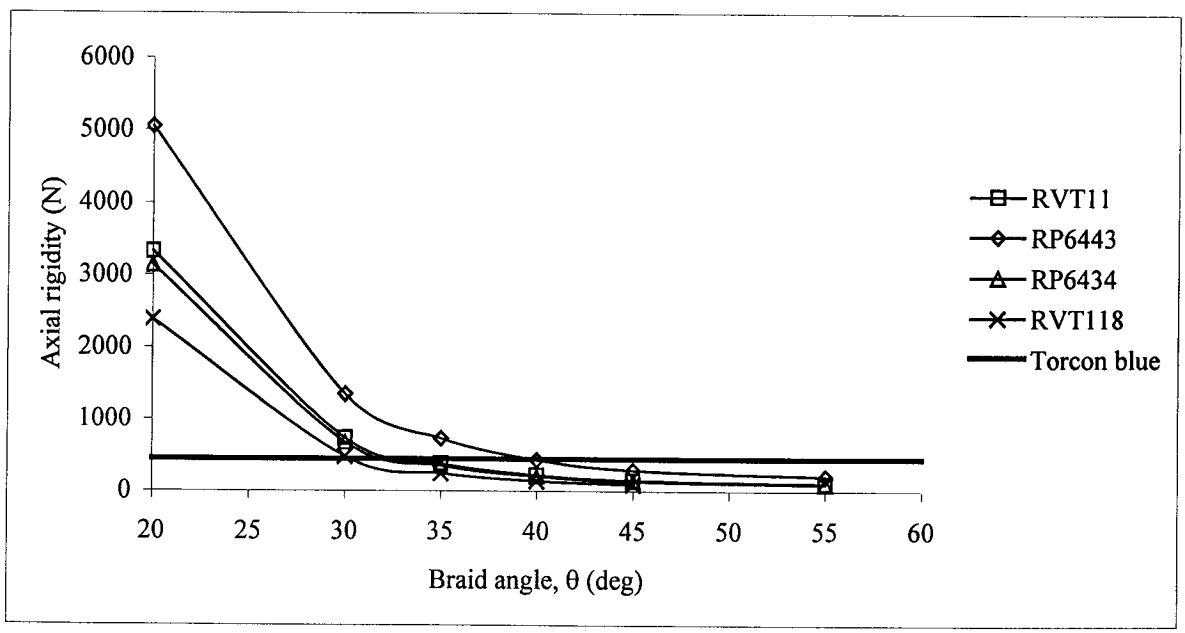

Figure 8-1: Axial rigidity of a composite composed of RTV11, RP6343, RP6443 and RTV118 resins and Kevlar-49 at various braid angles and of the Torcon blue medical catheter. The Torcon Blue Catheter axial rigidity is presented as a baseline and is not a function of the braid angle.

8.3 Conclusion

The predictions from the proposed CLPT model for the many combinations of fibres and resins selected in Chapter 3 were evaluated in this chapter. Epon 825 and Scotchweld 2216 epoxies were eliminated since they were did not meet the flexural rigidity requirements with any fibre type. Nylon and polyester fibres were eliminated since they did not meet the minimal torsional rigidity requirements with any of the resin types.

Based on the results, using Kevlar fibre and either RTV11 or RTV118 silicone[5] resins or RP6443 or RP6434 polyurethane[6] resins can provide adequate flexural and torsional rigidity. All combinations provide similar axial rigidity for a braided medical catheter. Considering the viscosity and gel time for each of these resins (Table 3-4), RTV118 is eliminated since its viscosity is 20,000 centipoises which makes it highly viscous and inappropriate for manufacturing purposes. Of the remaining three resins, RP6443 was selected in combination with Kevlar-49 fibres because it, more than the other resins, met all required characteristics. In addition, RTV11 in combination with Kevlar-49 fibres was selected for further study to evaluate a silicone resin. Both resins also have acceptable viscosities and gel times for fibre wetting purposes.

The following chapter will evaluate the capability of the proposed CLPT model to predict longitudinal elastic and shear moduli model catheters fabricated of Kevlar-49 fibres and both selected resins.

---

[5] General Electric.
[6] Freeman Ren polyurethane.

CHAPTER 9 : COMPARISON OF PREDICTED AND EXPERIMENTAL ELASTIC CONSTANTS OF ELASTOMERIC RESIN COMPOSITE TUBES

9.1 Introduction

It was shown in Chapter 7 that the model predicts the braid longitudinal and in-plane shear elastic moduli for Kevlar 49/epoxy braided model catheters with reasonable agreement. In Chapter 8, the model was used to select candidate constituent materials for a cardiovascular catheter with specific rigidities. Experimental results or analytical predictions for elastic constants of elastomeric braided tubes could not be found in the literature. Thus model catheters fabricated with elastomeric resins will be used to validate the proposed CLPT model. A sensitivity analysis of the model to constituent elastic constants, as performed in Chapter 6, was performed for RP6443 polyurethane. Similar conclusions were found, a 10% error in the fibre and longitudinal elastic modulus, E_{f11} and E_m, respectively, as well as the resin shear modulus, G_m, have significant effects (Table 9-1).

Table 9-1: Difference between baseline braid elastic constants and braid elastic constants evaluated with a 10% difference in constituent elastic constant at different braid angles for RP6443 polyurethane. Significant effects are bolded.

Constituent elastic constant		Difference (%) with baseline longitudinal elastic or shear moduli at specified braid angle		
		30°	45°	60°
E_{f1}	Ex	1.14	0.56	0
	Gxy	**10**	**10**	**9.82**
G_{f12}	Ex		Insignificant	
	Gxy		Insignificant	
ν_{f12}	Ex		Insignificant	
	Gxy		Insignificant	
ν_{f23}	Ex		Insignificant	
	Gxy		Insignificant	
E_m	Ex	**5.32**	0.56	**6.12**
	Gxy		Insignificant	
G_m	Ex	**3.42**	**9.22**	**3.36**
	Gxy		Insignificant	

9.2 Predicted and experimental results

The following sections present the experimental results for braid longitudinal elastic and shear moduli of model catheters fabricated with the selected elastomeric resins, RP6443 polyurethane and RTV11 silicone, both with Kevlar 49 fibres. Each set of experiments was performed using three specimens. Results were used to evaluate the capability of the model to accurately predict elastic constants of elastomeric resin-based composite tubes. Experimental procedures were detailed in Sections 7.2.2 and 7.2.4.

Elastic properties of Kevlar 49 fibre are found in Table 7-1. Resin properties reported in Chapter 8 (Table 8-3) were obtained from manufacturer data sheets. In order to obtain greater accuracy for the following investigation, the elastic moduli, E_m, of both elastomeric resins were evaluated experimentally using ASTM standard D638-02M (Table 8-3). It should be noted that the experimentally determined elastic modulus for RTV11

silicone was approximately 1 MPa, which is significantly different than the value of 29.2 MPa (Table 3-4) provided by the manufacturer[1] (Table 9-2). However, Christiaen [78] reported experimental results of 1 MPa for the elastic modulus of RTV11 that coincides with the experimental results reported in this work.

Table 9-2: Literature and experimentally evaluated resin elastic constants used for comparison between predicted and experimental elastic constants of elastomeric resin composite tubes. $G_m=E_m/2(1+\nu_m)$

Material	Tensile modulus, E_m (MPa)		Shear modulus, G_m (MPa)	
	Literature	Experimental	Literature	Experimental
RTV11	1 [78]	$\cong 1$	11.23[1]	$\cong 0.3$
RP6443	58.28[1]	72.19 ± 4.25	22.42[1]	36.59

For completeness and comparison purposes, predictions of experimental results are presented using both experimental and literature (published or manufacturer's data) resin elastic constants.

[1] Information provided by GE Silicones technical services.

9.2.1 Kevlar/RP6443 polyurethane

9.2.1.1 Longitudinal elastic modulus, E_x

Figure 9-1 shows the experimental and predicted results of the braid longitudinal elastic modulus, E_x, of Kevlar/RP6443 polyurethane braided composite tubes using experimental and literature data for RTV11 elastic constants. The mean values for the experimental longitudinal elastic modulus of the 42.5° and 50° braided tubes are 0.366 and 0.250 GPa, respectively. The ranges of values for the longitudinal elastic modulus of the 42.5° and 50° braided tubes as a percentage of the mean value are 5.8 and 8.3 %, respectively; thus, there is excellent agreement between specimens with the same braid configuration. The difference between the experimental and predicted results using literature values for 42.5° and 50° specimens are 14 % and 8 %, respectively.

The predictions using measured experimental elastic constants are also in Figure 9-1. Larger differences are found (19% and 15%) between predicted and experimental results than when using manufacturer provided resin elastic constants. The experimental data points lie between both curves (Figure 9-1) and differences less than 20 % are found using either experimental or literature (manufacturer) resin elastic constant data in the proposed CLPT model.

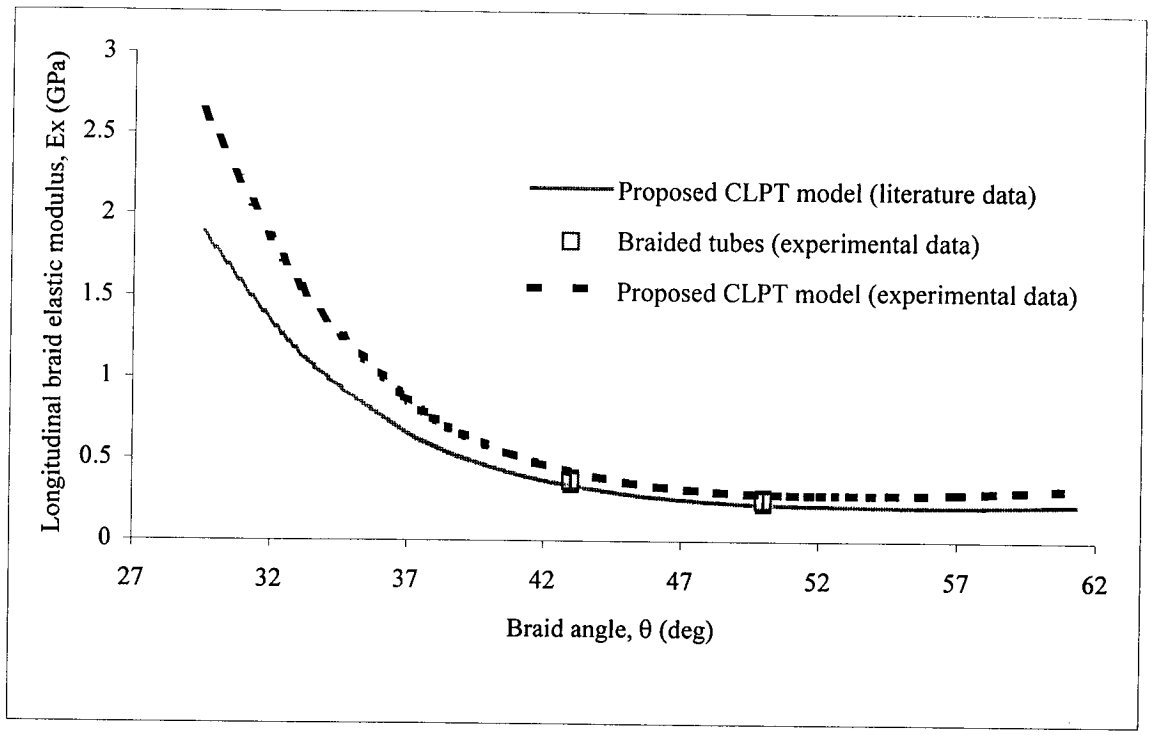

Figure 9-1: Longitudinal elastic modulus for Kevlar49/RP6443 composite braided tube as a function of braid angle; unit cell dimensions W_y = 3.1 mm, h_c=0.48 mm and t=0.96 mm. Error bars represent the range of the data.

9.2.1.2 Shear modulus, G_{xy}

Typical experimental results for the tensile stress-strain response of RP6443 resin specimens and torsion tests of Kevlar 49/RP6443 model catheters are given in Appendix 5. Figure 9-2 compares the experimental and predicted braid shear modulus results. The experimental data ranges were 1.0 to 4.6 GPa and 2.5 to 7.9 GPa for the 42.5° and 50° braids, respectively. A difference of 1.5 GPa was found between the predicted and average experimental results; differences of 52.2 % and 36.0 %, respectively. The predicted results lie within the range of data (Figure 9-2). Less than 1.0 % difference was found between

predictions using literature and experimental resin elastic constants and thus was not reported here.

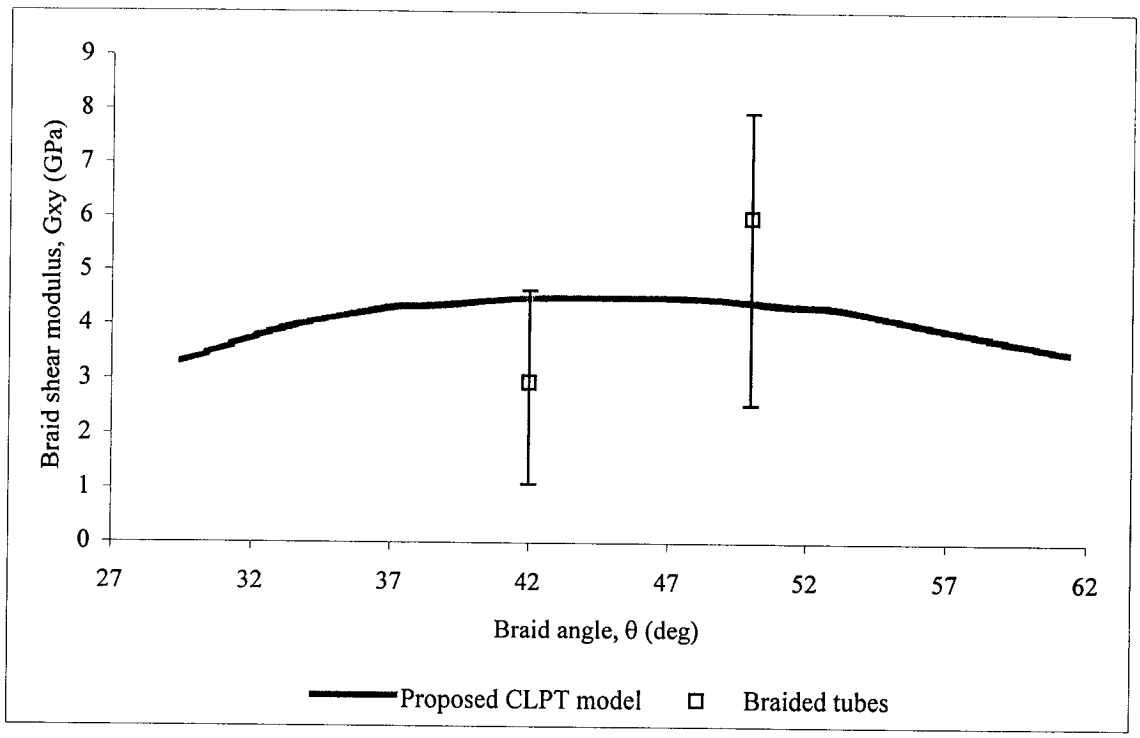

Figure 9-2: Braid shear modulus for Kevlar49/RP6443 composite braided tube as a function of braid angle; unit cell dimensions Wy = 3.1 mm, hc=0.48 mm and t=0.96 mm. Error bars represent the range of the data.

It should be noted that the outer tube walls appeared to slightly collapse at twist angles greater than those used to calculate braid shear modulus results (< 2.57°); this phenomenon is attributable to buckling as the tube length decreases with increased torque. The differences between the predicted and experimental values are greater than those found for the rigid thermoset resin (Figure 7-12).

9.2.2 Kevlar/RTV11 silicone

9.2.2.1 Longitudinal elastic modulus, E_x

The proposed CLPT model did not predict the braid longitudinal elastic modulus of Kevlar/RTV11 silicone specimens as accurately as for the other tested resin/fibre combinations. Large differences were found between the experimental and predicted results for the longitudinal elastic modulus of 42.5° and 50° braided tubes (Figure 9-3); there was approximately a 67 % difference between experimental and predicted results at both braid angles. The results were appreciably better (10 times) than those found using the elastic constants provided by the manufacturer (Figure 9-4), thus suggesting that the experimental results for the elastic modulus of the RTV 11 resin found by Christiaen [78] and in this work are more realistic.

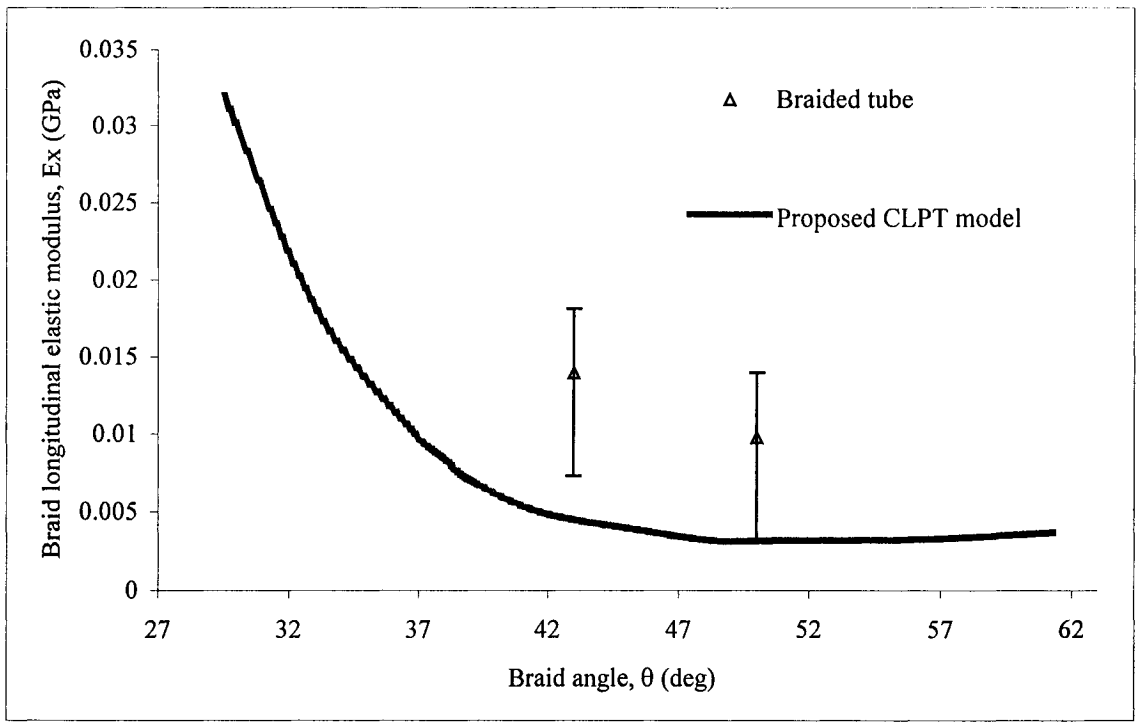

Figure 9-3: Longitudinal elastic modulus for Kevlar49/RTV11 composite braided tube as a function of braid angle; unit cell dimensions W_y = 3.1 mm, h_c=0.46 mm and t=0.92 mm. Error bars represent the range of the data. RTV11 elastic constants were determined experimentally.

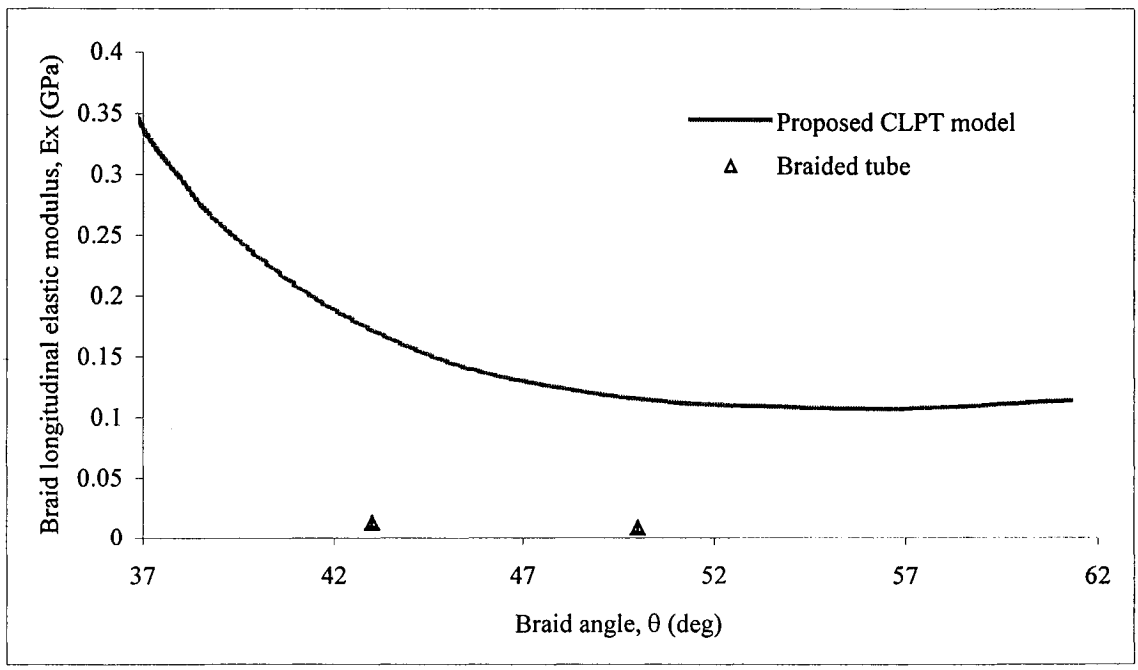

Figure 9-4: Longitudinal elastic modulus for Kevlar49/RTV11 composite braided tube as a function of braid angle; unit cell dimensions Wy = 3.1 mm, hc=0.46 mm and t=0.92 mm. Error bars represent the range of the data. Manufacturer provided elastic constants.

It should be noted that the braided tube outer diameter significantly decreased in the early stage of the experiments. This is an effect that was not found with the other fibre/resin specimens (Epoxy, RP6443).

9.2.2.2 Shear modulus, G_{xy}

Torsion tests to determine the braid shear modulus of Kevlar/RTV11 braided tubes were not performed. Specimen walls collapsed in torsional buckling at very low torques during operator handling, making evaluation of the twist angle impossible with the equipment developed.

The above findings lead to the conclusion to eliminate the Kevlar/RTV11 combination. It possesses elastic constants that result in rigidities significantly lower than required, resulting in considerable deformations at low loads, an undesirable characteristic for a medical catheter.

9.3 Conclusion

In this chapter, the proposed CLPT model was evaluated for model catheters produced using elastomeric resins. Experimental results show good agreement between specimens and are reasonably predicted by the model. In general, the model provides reasonable information for design and material selection purposes.

Having been compared to previous models, experimental results for rigid thermoset and elastomeric resins, the model was shown to meet the goals of this work. It was shown to be a useful tool for predicting the elastic constants of angle-ply braided and woven

composites and, ultimately for this research, selecting fibre/resin combinations that demonstrate the required axial, flexural and torsional rigidities for the future design of an optimal one-piece medical catheter. Further work must be done, in the medical field to determine exactly what are optimal catheter rigidities all along the length of the tube.

The effects of undulation region length, strand path geometry and neat resin content were introduced in Section 5.3.3 as important issues for unit cell-based and other predictive models. In Chapter 10 additional concepts related to the proposed CLPT model such as undulation region parameters as they relate to undulation region elastic constants are presented.

CHAPTER 10 : EFFECT OF THE UNDULATION REGION STRAND PATH MODELLING METHOD

In Chapter 5, the strand path in the undulation region was modelled using a sinusoidal function. Whitcomb [79] showed that a 5-fold increase in the undulation region length (Figure 5-4) with respect to the strand width caused up to a 15 % difference in a normalized unit cell moduli with no apparent sign of levelling off. In the Redman and Douglas model [62], it was assumed the undulation path could be simplified to a single inclination angle if the undulation region length was large compared to the strand thickness. This is a reasonable approximation even for more complex models since sinusoidal curves flatten out over longer distances (Figure 5-4).

Naik and Ganesh [63] evaluated different methods of modelling undulation strand path and found that a sinusoidal representation was the most geometrically accurate. To evaluate the sensitivity of the proposed CLPT model to the selected undulation strand path, two simplifications to the sinusoidal strand path approach are introduced and their effects discussed in the following sections.

Furthermore, in the proposed CLPT model, a numerical integration routine was written to evaluate undulation length region contributions to the unit cell elastic constants. Numerical integration routines are lengthy to program. The two proposed strand path simplifications would not require such time consuming programming.

Finally for completeness, the effect of different braid angles on the undulation region length as well as elastic constants will be examined in the context of open and closed mesh braids.

10.1 Strand path simplifications

10.1.1 Undulation model with a constant undulation angle as a function of undulating region length

The first simplification requires, as with the proposed CLPT model, that the geometry be thoroughly evaluated to obtain the undulation angle. Assuming the strand path is a straight line (Figure 10-1) allows the direct evaluation of the undulation angle, β, from the geometry, as:

$$\beta = \mathrm{Tan}^{-1}\left(\frac{h_c}{a_u}\right) \qquad \textbf{10-1}$$

where, h_c is the strand thickness and a_u is the undulation region length.

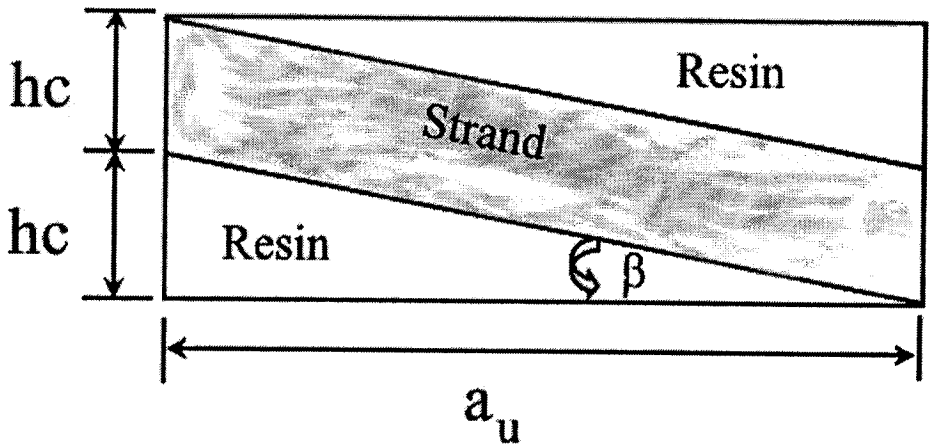

Figure 10-1: Simplified strand path model; the strand is assumed to be straight.

10.1.2 Undulation model with a constant undulation angle of 45 degrees

In order to evaluate the necessity of having precise undulation region dimensions, a further simplification is made by assuming that the undulation angle is 45° for all braid configurations. Referring to Figure 10-1, this means that the undulation length is equal to the strand thickness for all unit cell geometries ($a_u = h_c$).

10.2 Comparison between the proposed and simplified models

A Kevlar/epoxy composite braid with a strand thickness, h_c, of 0.16 mm and a width, W_y, of 3.14 mm was used for the following evaluations. It was further assumed that there were no pure resin layers below or above the unit cell. Elastic constants of open and closed braid configurations will be evaluated using the models described in Sections 10.1.1 and 10.1.2. The longitudinal elastic and shear moduli of the undulation region as predicted by the proposed CLPT model, using a sinusoidal strand path, are tabulated in Table 10-1 for comparison purposes with the two simplified models. These will be compared with open and closed mesh braid configurations independently.

Table 10-1: Undulation region elastic constant predictions from the proposed CLPT model for various braid angles (closed mesh)

Braid angle (Deg)	Ex (GPa)	Ey (GPa)	Gxy (GPa)
29.5	7.7	5.4	2.9
33	6.4	5.1	2.7
37	5.7	4.9	2.7
39	5.6	4.9	2.8
42	5.2	4.9	2.7
45	5.0	5.0	2.8
52	4.9	5.6	2.7
61.5	5.3	7.7	2.9

10.2.1 Closed mesh braids

The following tables (Table 10-2 and Table 10-3) contain the predicted elastic constants for the undulation region evaluated with both simplified models for closed mesh braids; therefore, undulation region lengths are not substantially greater than the strand thickness ($a_u \geq h_c$). Figure 10-2 compares the longitudinal elastic modulus of the undulation region as predicted by the proposed CLPT model and both simplifications mentioned above.

Table 10-2: Undulation region elastic constant predictions, using a constant undulation angle as calculated with the simplified model of Section 10.1.1 for various braid angles

Braid Angle (Deg)	Undulation region length a_u (mm)	Undulation angle (deg)	Ex (GPa)	Ey (GPa)	Gxy (GPa)
29.5	0.22	35.6	6.18	4.01	2.34
33	0.16	44.6	5.35	4.10	2.30
37	0.15	46.1	4.91	4.16	2.39
39	0.17	43.6	4.76	4.17	2.56
42	0.17	43.7	4.56	4.24	2.62
45	0.17	42.9	4.37	4.37	2.69
52	0.16	44.8	4.16	4.83	2.48
61.5	0.22	35.6	4.01	6.18	2.34

Table 10-3: Undulation region elastic constant predictions, using a constant 45° undulation angle, for various braid angles (Section 10.1.2)

Braid Angle (Deg)	E_x (GPa)	E_y (GPa)	G_{xy} (GPa)
29.5	5.80	4.11	2.13
33	5.33	4.11	2.28
37	4.92	4.15	2.44
39	4.75	4.18	2.50
42	4.56	4.25	2.56
45	4.38	4.38	2.55
52	4.16	4.83	2.47
61.5	4.12	5.96	2.09

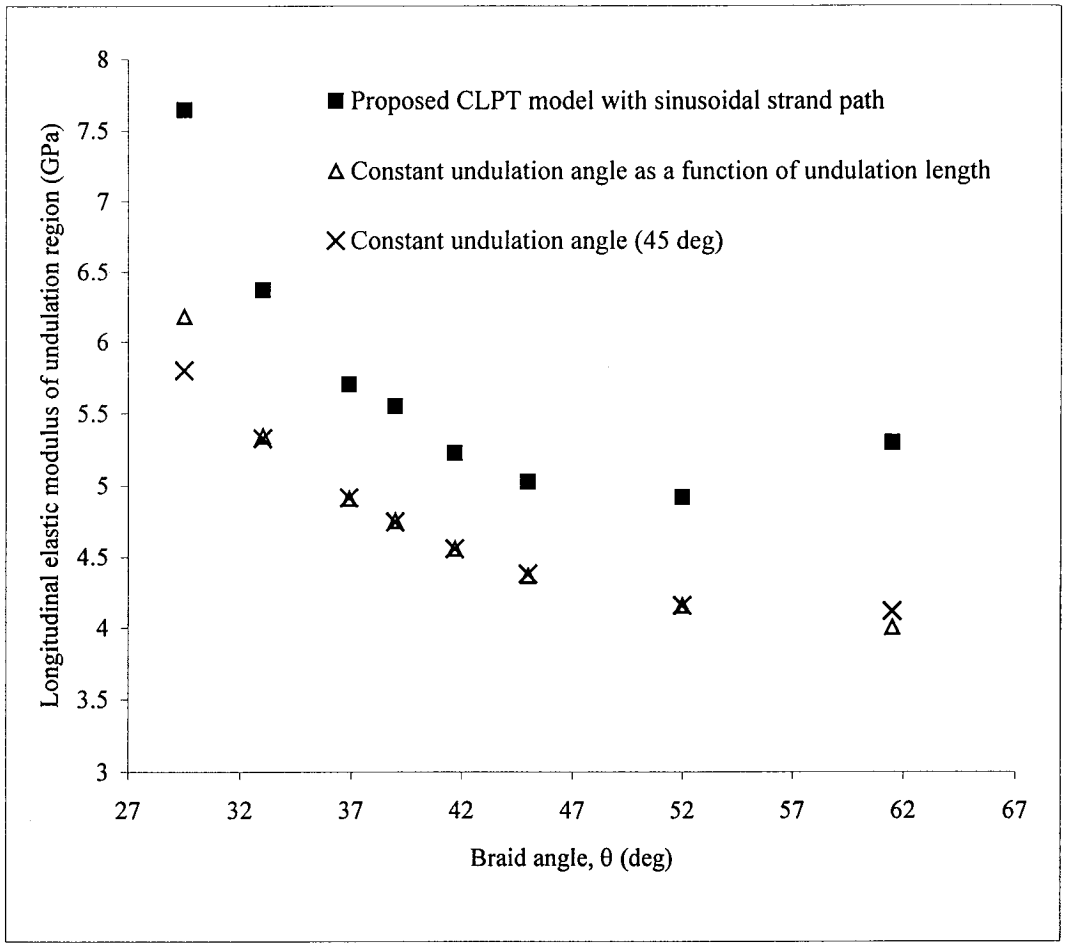

Figure 10-2: Comparison between the longitudinal elastic modulus of the undulation region of the proposed and both simplified models (closed mesh)

The figure shows that the simplifications give lower results than the proposed sinusoidal strand path approach; the results of Figure 10-2 are also representative of the findings for transverse elastic and shear moduli. The results using the simplifications are an average 16.2 % (13 % to 24 %) lower than the results from the more complete model. Between braid angles of 37° and 52°, the difference between the sinusoidal and simplified models is nearly constant at 7 GPa. Both simplification methods give very similar results for a closed mesh braid. This is to be expected since the minimum hypothetical undulation

region length of a closed mesh is the strand thickness, h_c, resulting in an undulation angle of 45° (Figure 10-1 and Table 10-2).

Greater differences are noticeable at 29.5° and 61.5° braid angles. This can be attributed to the fact that at extreme braid angles, undulation lengths cannot physically be as small as the hypothetical minimal value. Near the jamming angles (29.5° and 61.5°), the strand must travel a longer distance before reaching the next overlap and thus cannot form closed mesh composites and β is 35.6° (Table 10-2).

It can be concluded that for closed mesh braids both simplifications provide similar results at intermediate braid angles. To obtain approximate results for the overall braid elastic constants of closed mesh braids, these simplifications can be used since the overall influence of such small differences is minor. An average difference of 16.2 % in undulation region elastic constants was found using one of the simplified models and the sinusoidal strand path; resulting in less than a 1.1 % difference between braid elastic constants predicted with or without the simplifications. The simplification model used for the undulation strand path has little effect on closed mesh configurations; however, greater accuracy and realistic geometry is provided by the used of a sinusoidal strand path in the proposed CLPT model.

10.2.2 Open mesh braids

Contrary to closed mesh braids, the undulation region length for open mesh braids can be substantially larger than the thickness of the strand ($a_u >> h_c$). Since medical catheters may have an open mesh of reinforcing fibres, this aspect was studied. This section will evaluate the influence of undulation region length, at different braid angles, on the undulation region elastic constants. Figure 10-3 shows that, as the undulation region length increases, the undulation angle decreases. An undulation region length of 0.16 mm is the limit used in this work, at this point the strand path is 45° with the horizontal and forms a closed mesh composite.

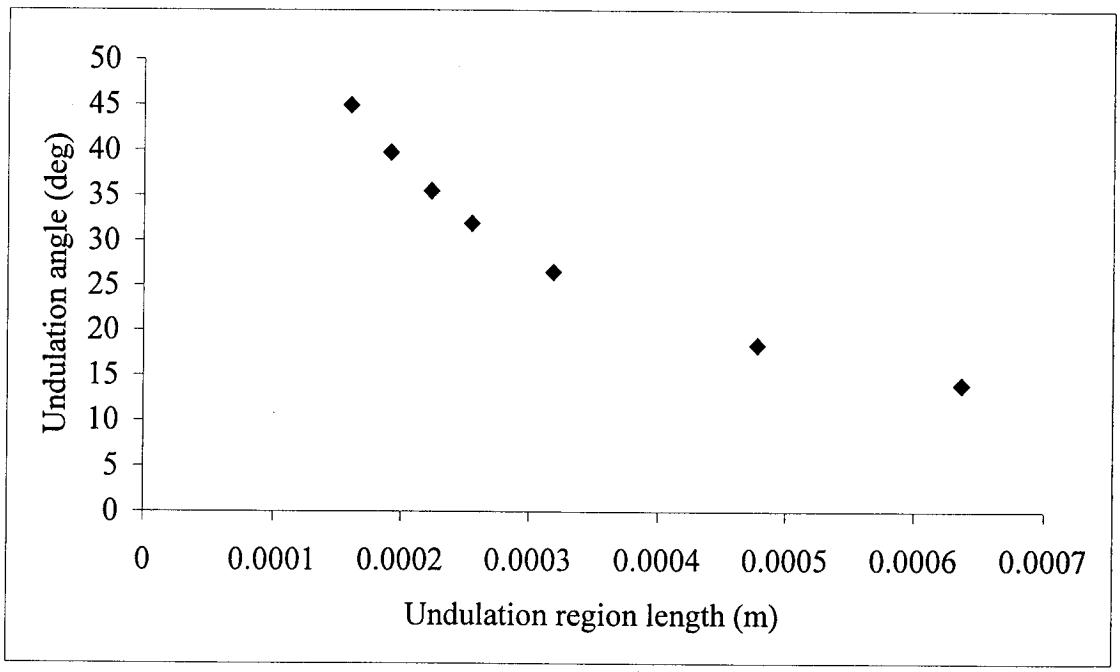

Figure 10-3: Undulation angle as a function of the undulation region length (adapted from Figure 5-6)

The influence of an open mesh on the elastic constants, E_x and G_{xy}, of undulation regions was evaluated by varying the undulation region length at various braid angles. The findings for the elastic constants were normalized with respect to the elastic constant of the closed mesh braid at the specified braid angle (i.e. moduli results for a 45° braid angle composite found with different a_u values were normalized using the moduli results of a 45° braid angle closed mesh composite).

Figure 10-4 shows no significant difference between the findings for various undulation region lengths on the longitudinal elastic modulus. A seven-fold variation of a_u resulted in a maximum difference of 8 % with the closed mesh value. Similar results were found for the transverse elastic modulus (Figure 10-5). The differences remain approximately constant once the undulation region length reaches roughly $5.5h_c$.

In the case of longitudinal elastic modulus, changes in a_u have a lesser effect on the higher braid angle elastic constants. This is due to the small change in longitudinal elastic modulus at higher braid angles [44]. As would be expected, the transverse elastic modulus reacted similarly for low braid angles [44].

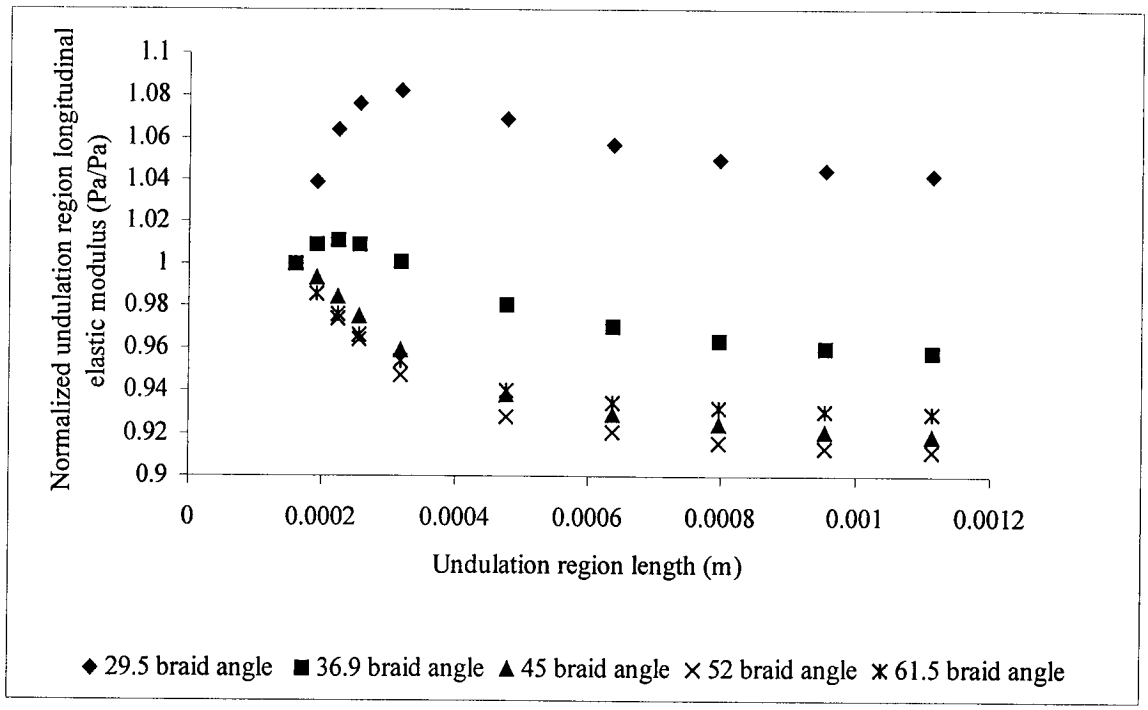

Figure 10-4: Normalized undulation region longitudinal elastic modulus as a function of undulation region length, a_u, at different braid angles.

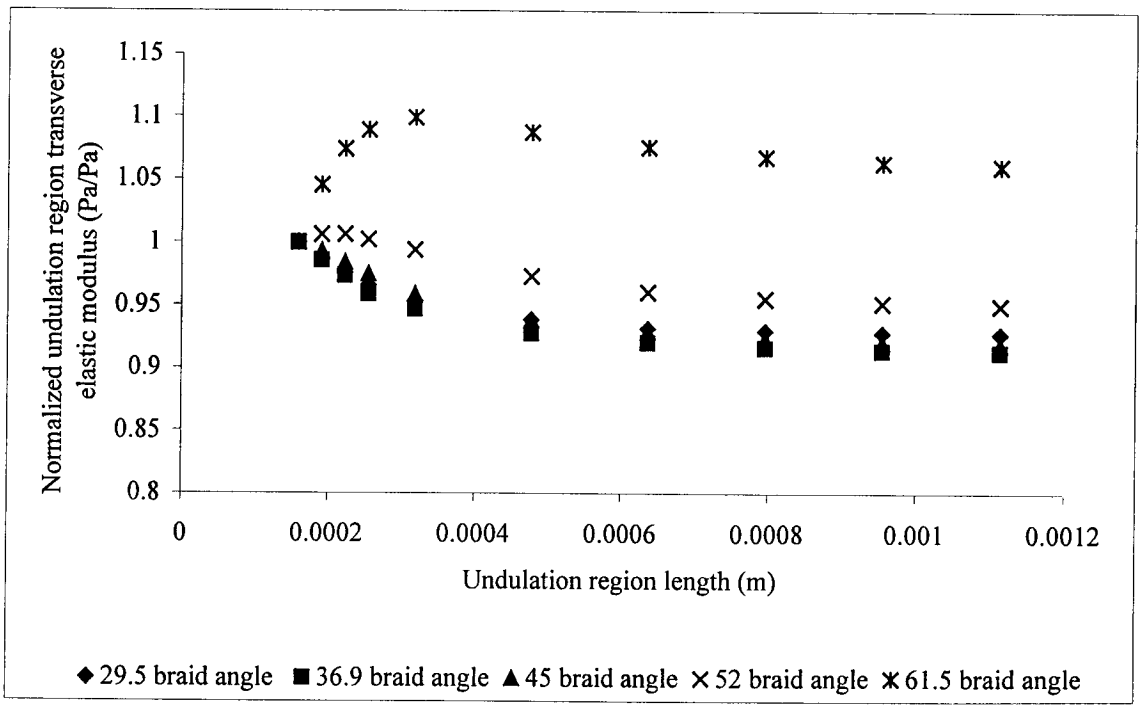

Figure 10-5: Normalized undulation region transverse elastic modulus as a function of undulation region length, a_u, at different braid angles.

Results show that the shear modulus had the largest change. For a seven-fold change in a_u the shear modulus changed by up to 60 % (Figure 10-6). The differences were more pronounced at a braid angle of 45°. This is not unexpected since the shear modulus is significantly higher at this braid angle [44]. The highest and lowest braid angles, 29.5° and 61.5°, are the least influenced by a change in a_u. Again, the difference remained nearly constant once the undulation region length reached 5.5 times the strand thickness.

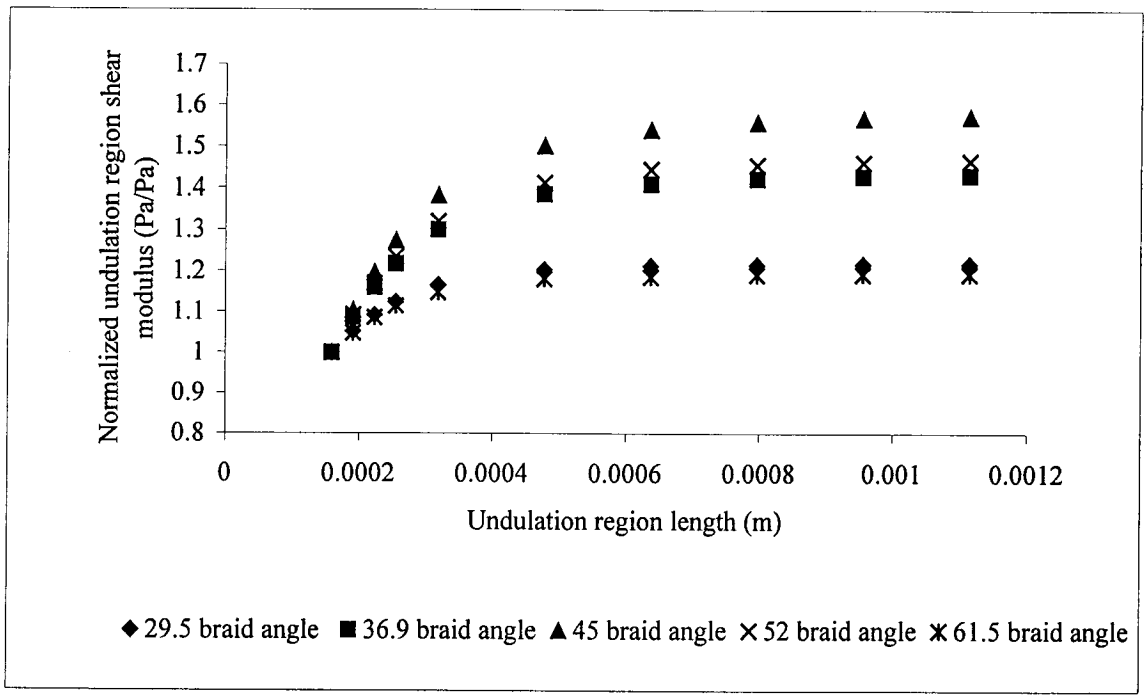

Figure 10-6: Normalized undulation region shear modulus as a function of undulation region length, a_u, at different braid angles.

The findings in the above three figures all level off asymptotically, which can be attributed to a theoretical geometric configuration of the undulation region. When undulation length increases, the inclination angle of the composite strand tends towards zero. As such, at the limit, the structure described in Figure 10-1 can be modeled as a lamina with over and underlying resin layers and no undulation angle (Figure 10-7).

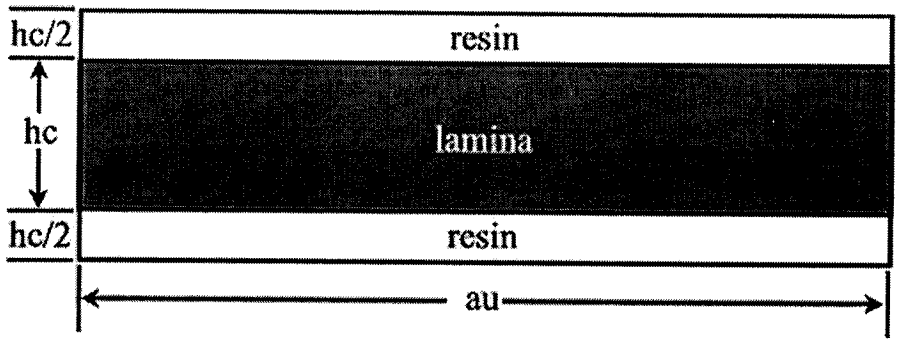

Figure 10-7: Theoretical geometric configuration acting as an asymptote for Figure 10-4, Figure 10-5 and Figure 10-6

In Figure 10-8, the elastic constants (E_x, E_y and G_{xy}), found at various braid angles for the undulating region at large values of undulation length ($a_u = 7h_c$) and the asymptotic theoretical geometric configuration of Figure 10-7, are shown. The results for all elastic constants at all braid angles overlap (small solid symbols within larger open symbols). This indicates that the choice of asymptotic value is correct.

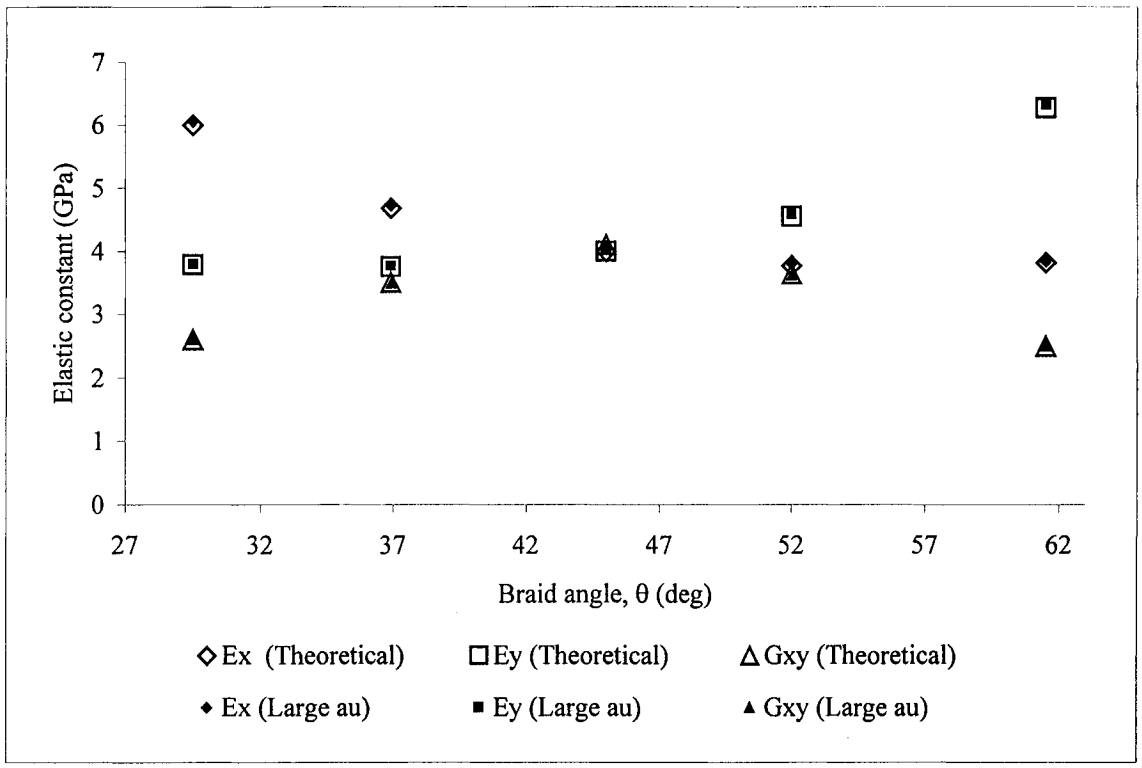

Figure 10-8: Elastic constants of the undulating region at large values of a_u and for theoretical geometric configuration (Figure 10-7), at different braid angles

10.3 Conclusion

In addition to understanding the influence of using simpler strand path models other than the sinusoidal, which requires extensive programming, the intention of this chapter was to quantify the effect of simplifying the undulation region strand path model and undulation region length on undulation regions elastic constants.

Modelling the strand path as a sinusoidal curve is the recommended option; however, depending on braid geometry, different avenues are available. In the case of closed mesh braids, both discussed simplifications provide similar results at intermediate braid angles but not at braid angles nearing the jamming angles. In these cases, the

undulation region length increases; therefore, modelling the strand path as a function of undulation length is more appropriate.

To predict more accurate elastic constants of open mesh braids, it would be wiser to either use the sinusoidal or the undulation angle as a function of undulation length approach (Section 10.1.1) to model the undulation path since the undulation region length has a significant influence on the elastic constants. If the undulation region length is very large compared to strand thickness (a_u >5.5hc), a sinusoidal strand path can be assumed to be straight. This strengthens the argument of using the undulation angle as a function of undulation length approach, if it is the intent to avoid a lengthy numerical methods approach to modelling the strand path and elastic constants.

Furthermore, at very large open mesh configurations (a_u >7hc), the undulation region can be further simplified to a lamina with over and underlying resin layers that have a combined thickness of h_c, therefore, the concept that the neat resin content has a dominant effect on regional elastic constants was introduced in this chapter. This will be important for the development of the design equations, which greatly simplify the proposed CLPT model, as detailed in the next chapter.

CHAPTER 11 : MODEL FOR PRACTICAL DESIGN APPLICATIONS

In earlier chapters, the effects of the undulating strands on braided/woven fabric elastic constants and the importance of precisely predicting their paths were discussed. The previous chapter determined that strand path modelling could be simplified with little effect on the individual contribution of the undulation region and that neat resin content could be a dominant factor for unit cell elastic constants.

In this chapter, the effect of using a simpler regression-based approach to predict the elastic constants of an angle-ply composite with undulating regions (braid) from angle-ply laminate composite elastic constants will be discussed and evaluated for practical design purposes. This will be done for the general cases of practical closed and open mesh angle-ply composites with undulating regions and verified with different fibre/resin combinations.

Similar simplifications have been done previously. Halpin and Tsai [46] developed regression-based equations to predict the numerical results of Adams and Doner [45] for lamina micromechanical properties. Other simpler approaches have been adopted for models of complex composite structures [52, 63]. The Halpin-Tsai formulation is an extensively used micromechanical model for elastic constants of composite lamina at practical fibre volume fractions. The model was fitted to match the Adams and Doner results for a lamina fibre volume fraction of 55%, however, at other fibre volume fractions, the accuracy of the Halpin-Tsai model diminishes.

11.1 Closed mesh braids and angle-plied laminates

As an introductory comparison to illustrate the influence of undulating strands and neat resin content, elastic constants of closed mesh braids and angle-plied laminates are evaluated.

A Kevlar/epoxy composite braid with a strand thickness, h_c, of 0.16 mm and a width, W_y, of 3.14 mm was used for the following evaluations. Laminar elastic constants were reported in Table 6-1. It will be further assumed that there are no layers of neat resin.

Figure 11-1 shows the influence of different braid angles on the longitudinal, transverse and shear moduli of a laminate predicted using the laminate CLPT model. These findings have been reported previously [44]. At higher angles the longitudinal elastic modulus does not vary significantly. Conversely, at lower braid angles, the transverse elastic modulus exhibits little change. In contrast, the shear modulus is greater than the longitudinal and traverse elastic moduli at mid-range angles. Also, the shear modulus is relatively high at the jam angles.

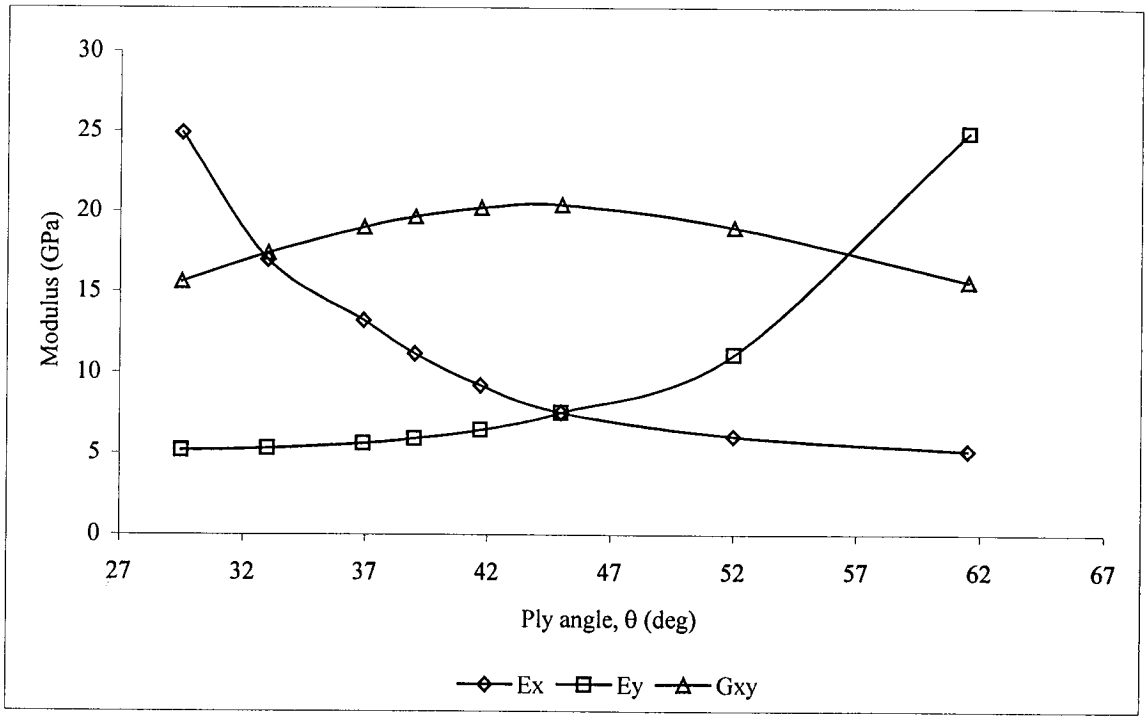

Figure 11-1: Angle-ply laminate longitudinal (E_x), traverse (E_y) and shear (G_{xy}) modulus as a function of ply angle (modified from [44]).

Unit cell elastic constants, as calculated by the proposed CLPT model, are tabulated in Table 11-1 for closed mesh braids for comparison with the laminate elastic constants tabulated in Table 11-2. Elastic constants of braids are lower than the laminates, to different degrees at different braid angles, due to the undulating strands, undulation region length and thus, neat resin content.

Table 11-1: Closed mesh braid elastic constant predicted by the proposed CLPT model at various braid angles

Braid angle (Deg)	E_x (GPa)	E_y (GPa)	G_{xy} (GPa)
29.5	20.2	4.5	11.7
33	15.7	4.8	13.9
37	11.5	5.0	15.0
39	9.6	5.2	15.2
42	7.9	5.7	15.5
45	6.5	6.5	15.6
52	5.1	10.5	15.1
61.5	4.8	23.4	12.6

Table 11-2: CLPT predictions of elastic constants at various braid angles

Braid angle (Deg)	E_x (GPa)	E_y (GPa)	G_{xy} (GPa)
29.5	24.9	5.2	15.6
33	17.0	5.3	17.4
37	13.2	5.6	19.0
39	11.1	5.9	19.7
42	9.2	6.5	20.2
45	7.5	7.5	20.4
52	6.1	11.1	19.0
61.5	5.2	24.9	15.6

Figure 11-2 illustrates the difference between the predicted longitudinal elastic modulus of an angle-ply braid using the proposed CLPT model and a laminate using CLPT. An average ratio between the braid and laminate longitudinal elastic modulus of 0.87 with a range of 0.92 to 0.81 was found. The same level of difference is found for the transverse modulus (Figure 11-3): a range of 0.95 to 0.87 with an average of 0.90. Shear modulus differences which are greater but nearly constant as compared to the longitudinal and transverse moduli can be seen in Figure 11-4. The average ratio between braid and laminate is 0.78 with a range of 0.81 to 0.75. Many variables are expected to affect the results; for example, strand thickness, undulation region length and braid angle will influence the difference between the laminate and braid elastic constants since they directly affect the amount of neat resin content.

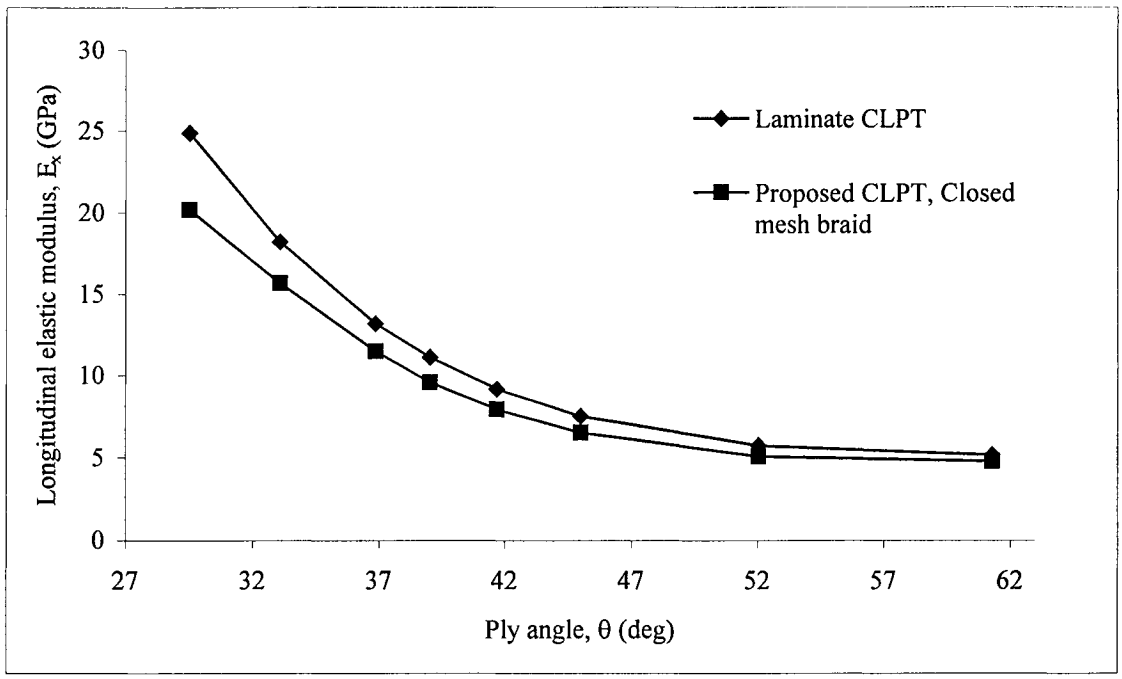

Figure 11-2: Predicted longitudinal elastic modulus of an angle-ply closed mesh composite with undulation regions and a laminate

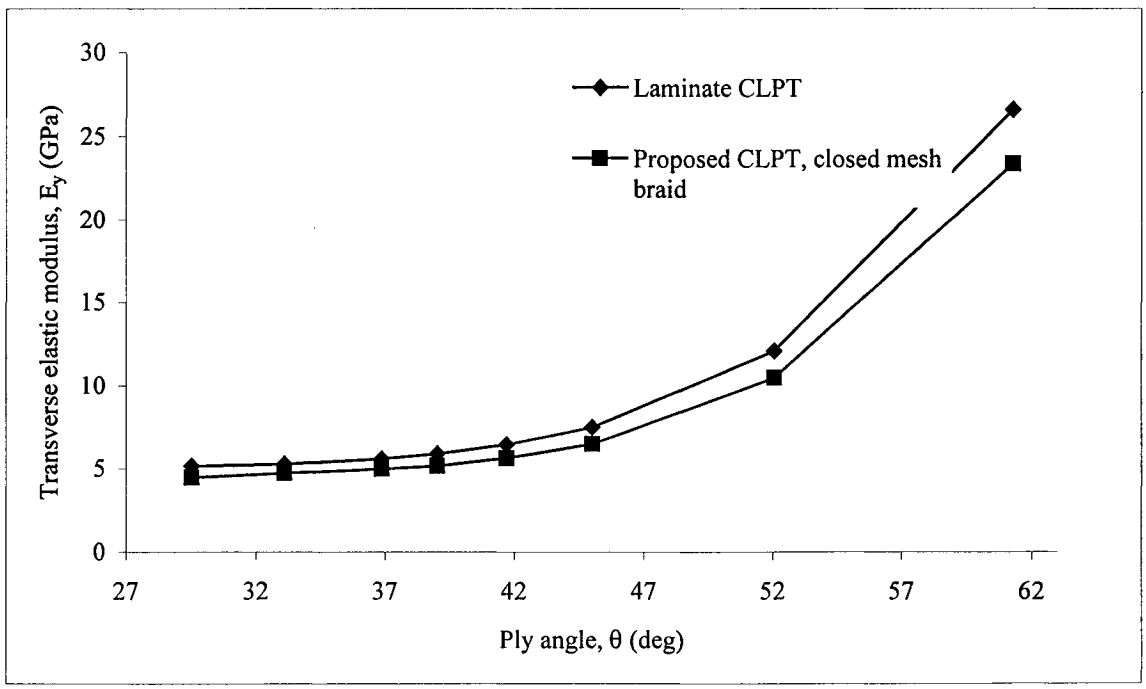

Figure 11-3: Predicted transverse elastic modulus of an angle-ply closed mesh composite with undulation regions and a laminate

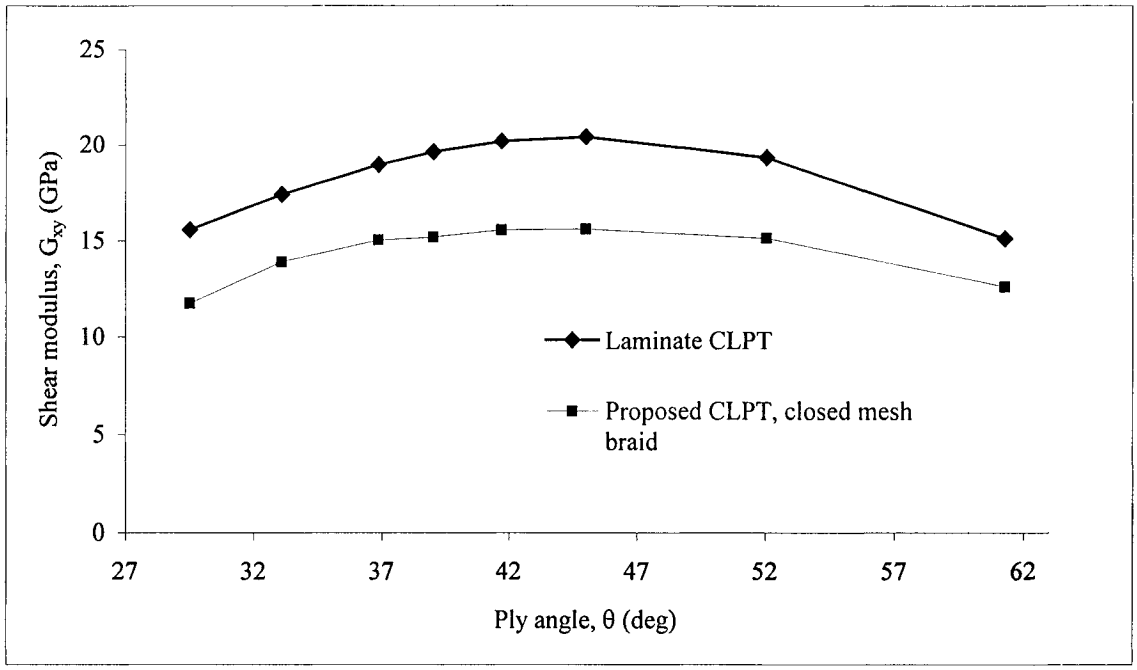

Figure 11-4: Predicted shear modulus of an angle-ply closed mesh composite with undulation regions and a laminate

11.2 Regression equations for evaluating braid elastic constants

It was presented earlier that, contrary to closed mesh braids, the undulation region length of open mesh braids is substantially larger than the thickness of the strand ($a_u >> h_c$). In this section the influence of undulation region length, at different braid angles, on the unit cell elastic constants will be evaluated. Furthermore, simple equations to obtain the elastic constants of open and closed mesh angle-ply braided composites from elastic constants of similar laminates will be presented.

The following three sections illustrate the effect of the undulation region length on the unit cell longitudinal, transverse and shear moduli. For this investigation, the open and closed mesh composite elastic constants discussed are all normalized with respect to laminate elastic constants at the respective braid angle.

11.2.1 Longitudinal elastic modulus

To determine which factors had an influence on braid elastic constants, the ratio of braid to laminate longitudinal elastic modulus was plotted versus three geometric parameters: undulation region length, a_u, unit cell volume fraction, V_{fo}, and unit cell volume fraction ratio, V_{fo}/V_f. As mentioned in Chapter 10, undulation length and fibre volume fraction were believed to have a significant influence on braid elastic constants.

Initially, the influence of open mesh on braid normalized longitudinal elastic modulus was evaluated by varying the undulation region length, a_u, at various braid angles (Figure 11-5). In Figure 11-5, the normalized longitudinal elastic modulus decreases up to 50 % with a 6-fold increase in undulation region length from 0.0005 m to 0.003m with

no apparent sign of levelling off at a braid angle of 29.5°. At a braid angle of 61.5°, the difference is less pronounced; only a 32 % decrease is found. These results were not important since a direct correlation could not be made. The findings were then compared based on the unit cell fibre volume fraction (Figure 11-6) calculated in this work as:

$$V_{fo} = \frac{V_f}{XYh_c}\left[4a_u W_y h_c + 4h_c\left\{-2(\tan\gamma)(L_e \sin\theta)^2\right\} + 4h_c L_e{}^2 \cos\theta \sin\theta\right] \qquad \textbf{11-1}$$

where, V_{f0} is the unit cell fibre volume fraction, V_f is the fibre volume fraction, W_y is the strand width, h_c is the strand thickness, γ is the complementary angle of θ, the braid angle, and L_e, the edge length. From Figure 11-6, the decrease in normalized longitudinal elastic modulus appears nearly linear with the drop in unit cell fibre volume fraction.

To verify this, the ratio of normalized longitudinal elastic modulus was plotted versus the normalized fibre volume fraction (V_{fo}/V_f), which is evaluated from equation 11-1 as follows:

$$\frac{V_{fo}}{V_f} = \frac{1}{XYh_c}\left[4a_u W_y h_c + 4h_c\left\{-2(\tan\gamma)(L_e \sin\theta)^2\right\} + 4h_c L_e{}^2 \cos\theta \sin\theta\right] \qquad \textbf{11-2}$$

The findings (Figure 11-7) show that there is a linear relationship, with intercept at zero, between moduli and volume fraction ratios. As seen in the figure, the slopes range from 1.05 to 0.95. Correlation coefficients, R^2, are greater than 0.9.

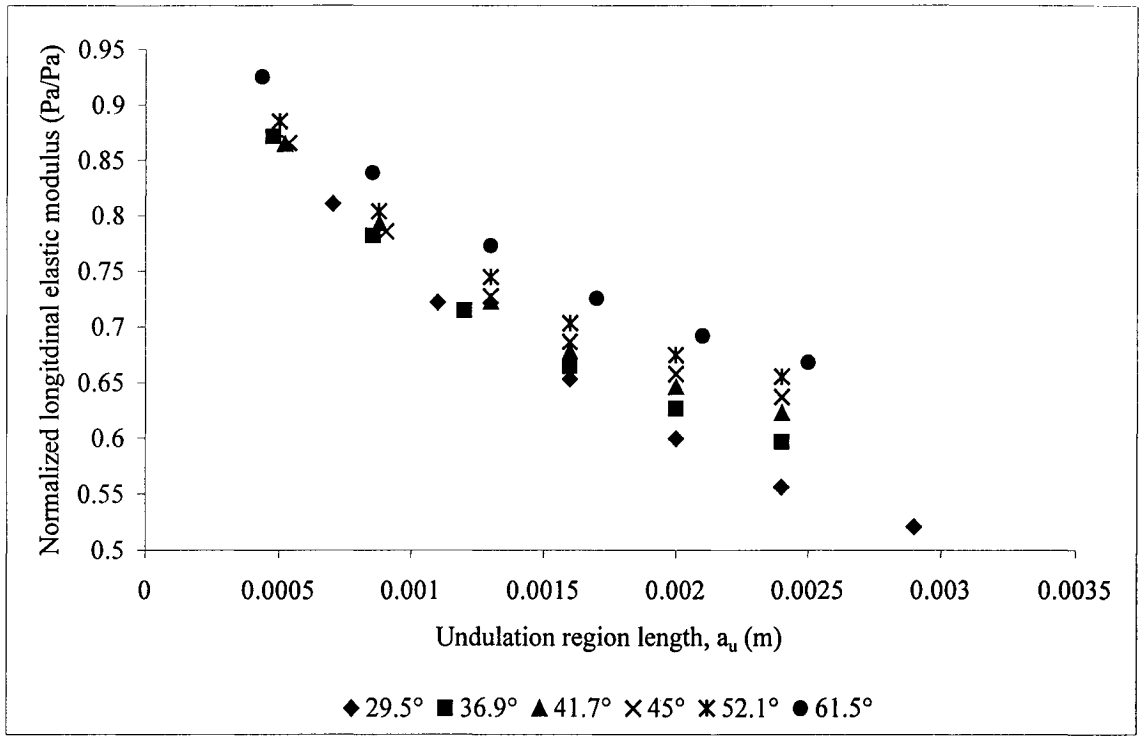

Figure 11-5: Normalized unit cell longitudinal elastic modulus as a function of undulation region length, a_u, at different braid angles.

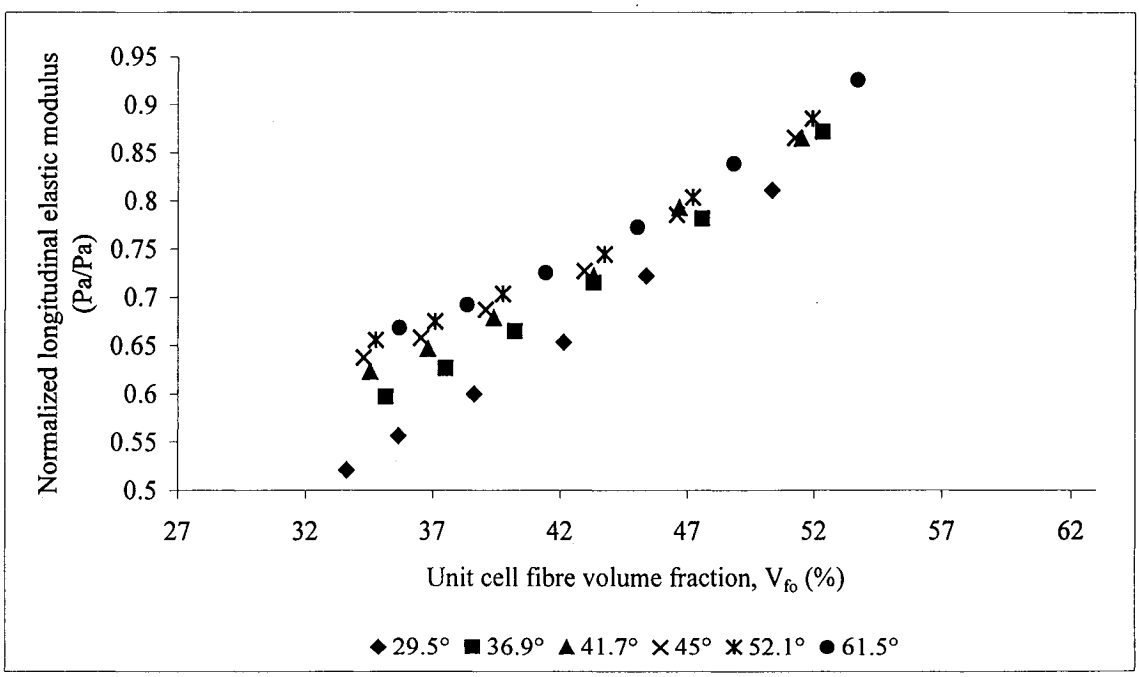

Figure 11-6: Normalized unit cell longitudinal elastic modulus as a function of unit cell fibre volume fraction at different braid angles.

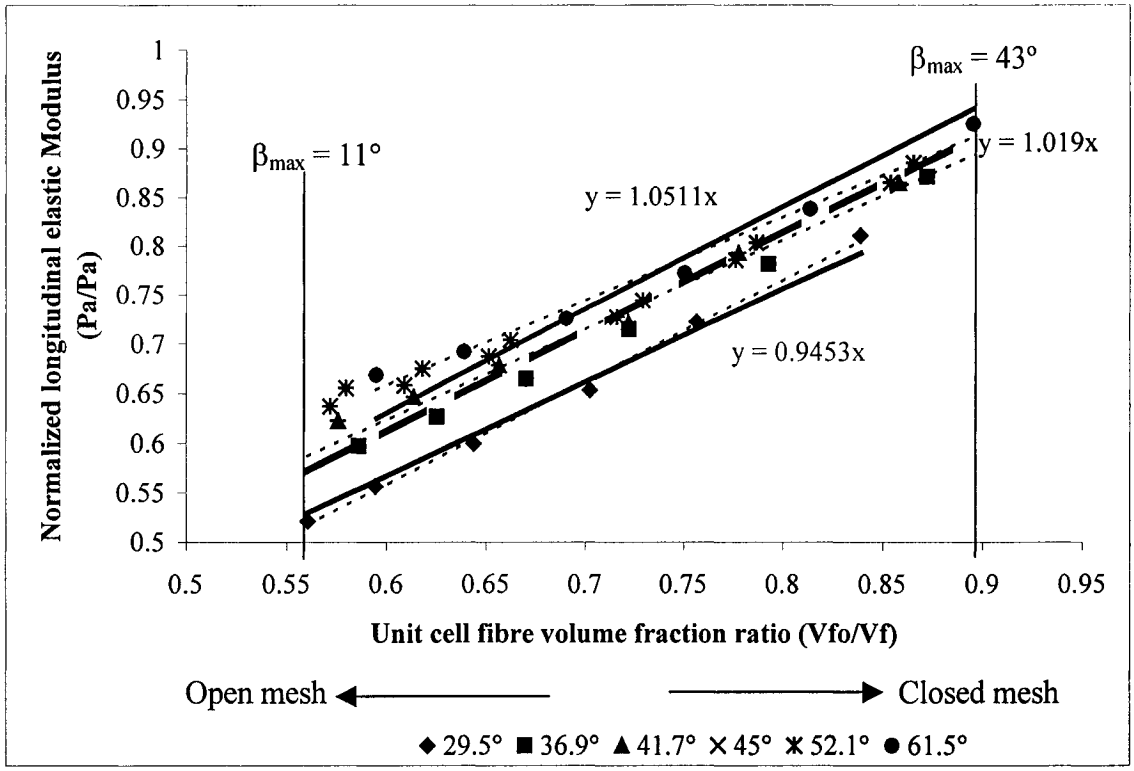

Figure 11-7: Normalized unit cell longitudinal elastic modulus as a function of normalized unit cell fibre volume fraction at different braid angles. Dotted line is the regression of all data. Vertical lines provide the maximum undulation angle for open mesh and closed mesh braids. Practical range of unit cell fibre volume fraction ratio lies approximately between 0.65 and 0.85. Full lines denote regression curves forced through zero for (top to bottom) 61.5°, all data and 29.5°; dotted lines denote actual regression curves for the previous forced curves.

For design purposes, a strong argument can be made to predict the longitudinal elastic modulus of an angle-ply composite in the practical unit cell fibre volume fraction range (approximately 0.65 to 0.85), within ± 5%, as follows:

$$E_{x\theta} = E_{xla\,min\,ate\theta}\left(\frac{V_{fo}}{V_f}\right) \qquad \textbf{11-3}$$

where, $E_{x\theta}$ and $E_{xlaminate\theta}$ are the longitudinal elastic modulus for a braided and similar angle-ply laminate at a braid angle of θ, respectively. It was also determined that only this last comparison (modulus ratio vs. volume fraction ratio) was required for the other elastic constants as shown in the following sections. The level of agreement is similar and more

reasonable in many aspects to the Halpin-Tsai micromechanical model. A further argument can be made for this approach if found applicable to any fibre and resin combination. This will be evaluated in Section 11.3

Experimental results for tube braid longitudinal elastic modulus found in previous chapters are shown in for 42.5° and 50° braid angles; since both data point fall between the upper and lower regression lines they confirm the accuracy of the method. V_{f0} is calculated based on geometry, the lamina longitudinal elastic moduli are evaluated using Classical Laminate plate theory while the braid longitudinal elastic moduli are found experimentally.

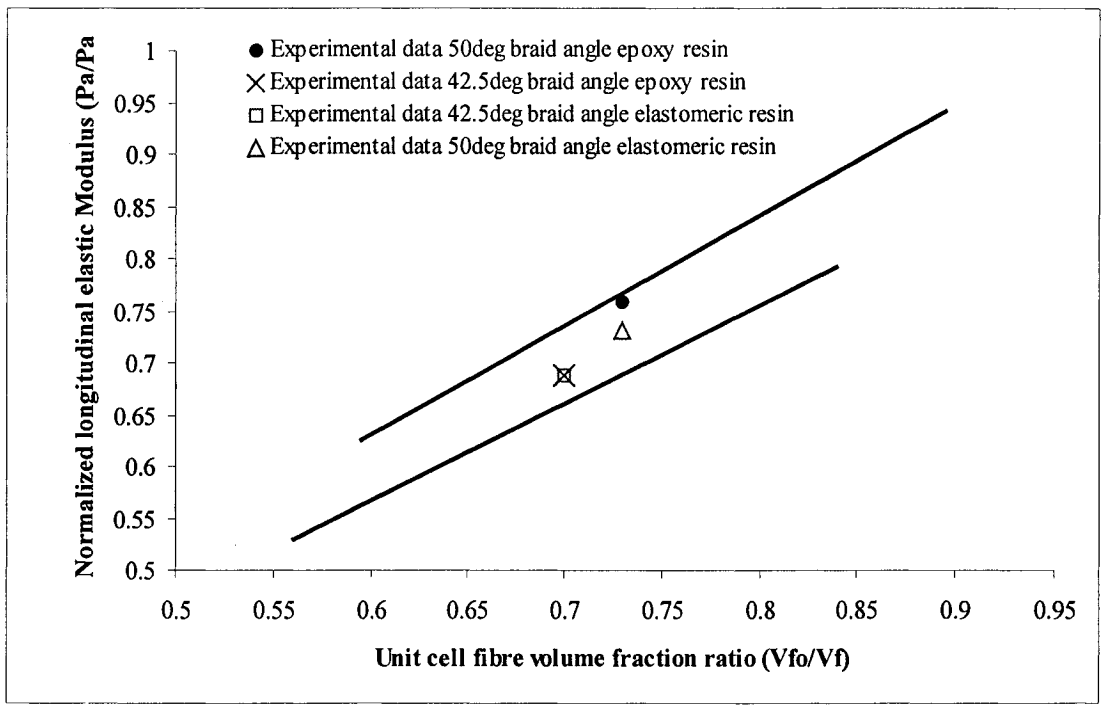

Figure 11-8: Normalized longitudinal elastic modulus versus unit cell volume fraction ratio of experimental data for braided tubes (rigid and elastomeric polymeric resins) with 42.5° and 50° braid angle within the regression limits established in Figure 11-7.

11.2.2 Transverse elastic modulus

The same evaluation as in the previous section was performed for the transverse elastic modulus. Regression curves are used to match the normalized moduli and fibre volume fractions (Figure 11-9).

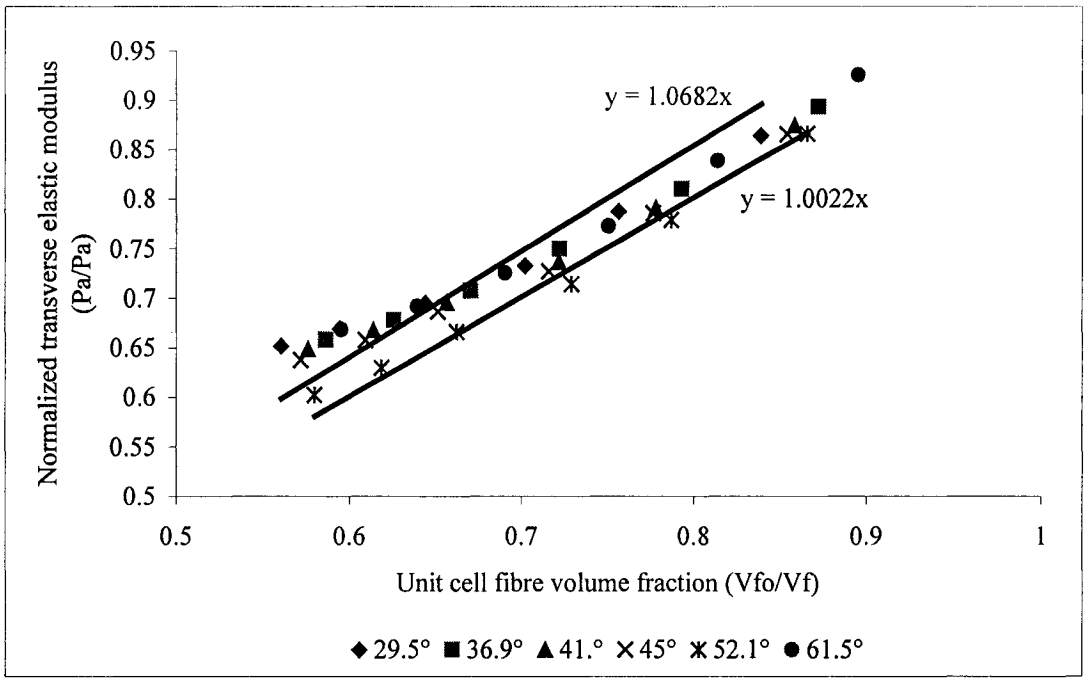

Figure 11-9: Normalized unit cell longitudinal elastic modulus as a function of normalized unit cell fibre volume fraction at different braid angles.

Again, the same type of design equation can be developed to predict the braid transverse elastic modulus from the laminate transverse modulus based on the linear regression analysis shown in Figure 11-9. The transverse elastic modulus for a braid at an angle of θ, $E_{y\theta}$, is found, for the same practical unit cell fibre volume fractions, as follows:

$$E_{y\theta} = E_{yla\,min\,ate\theta}\left(\frac{V_{fo}}{V_f}\right) \qquad \textbf{11-4}$$

where, $E_{ylaminate\theta}$ is an angle-ply laminate at an angle of θ. Again, the correlation coefficients, R^2, are greater than 0.9.

Compared to equation 11-2, there is slightly less accuracy in this method. The slope ranges from 1 to 1.07. However, for practical purposes, there is very reasonable agreement.

11.2.3 Shear modulus

A linear relationship of the form y = mx as found for the other elastic constants did not result for the shear modulus, even if Figure 11-10 shows excellent linearity (R^2 = 0.9974) and very little spread in data. The relationship that resulted was:

$$\frac{G_{xy\theta}}{G_{xylaminate\theta}} = \left[1.23\left(\frac{V_{fo}}{V_f}\right) - 0.3\right] \qquad \textbf{11-5}$$

where $G_{xy\theta}$ and $G_{xylaminate\theta}$ are the shear modulus for a braided and angle-ply laminate at an angle of θ, respectively.

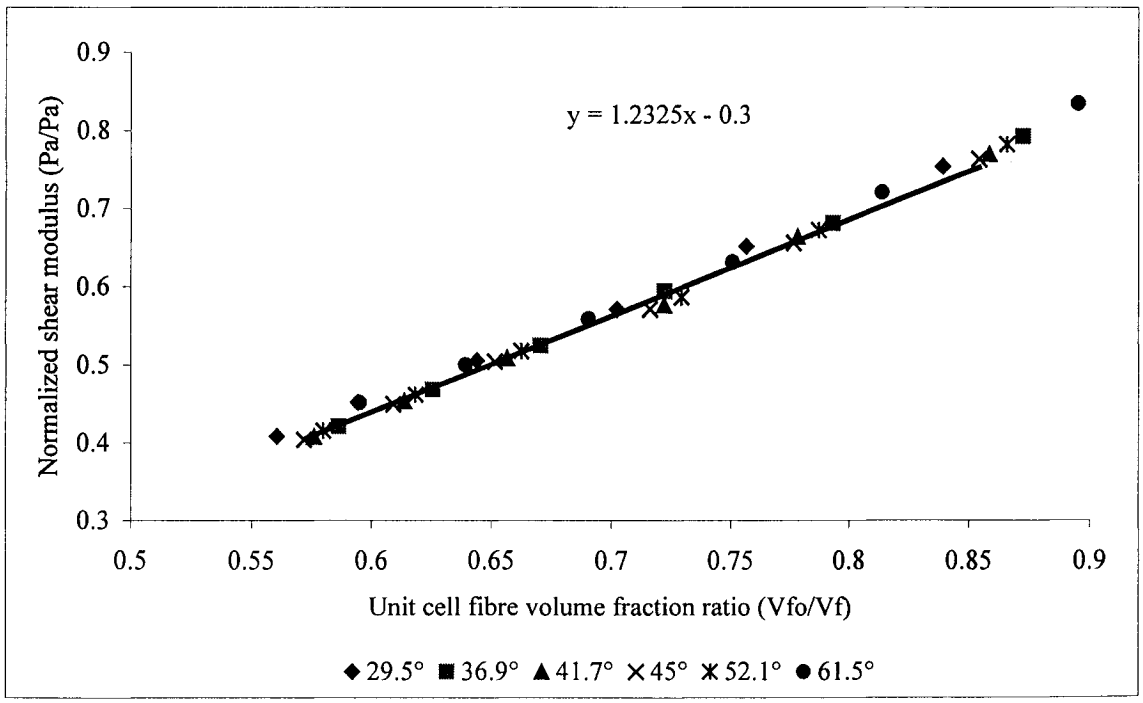

Figure 11-10: Normalized unit cell shear modulus as a function of unit cell fibre volume fraction ratio at different braid angles.

Experimental results for tube braid shear modulus found in a previous chapter are shown and compared to regression equation predictions in Figure 11-11 for 42.5° and 50° braid angles. Differences between experimental and predicted shear modulus results were 20% and 24%, respectively, which are the same level of differences found in other works [63]. Similar differences were found between the experimental results and the regression equations.

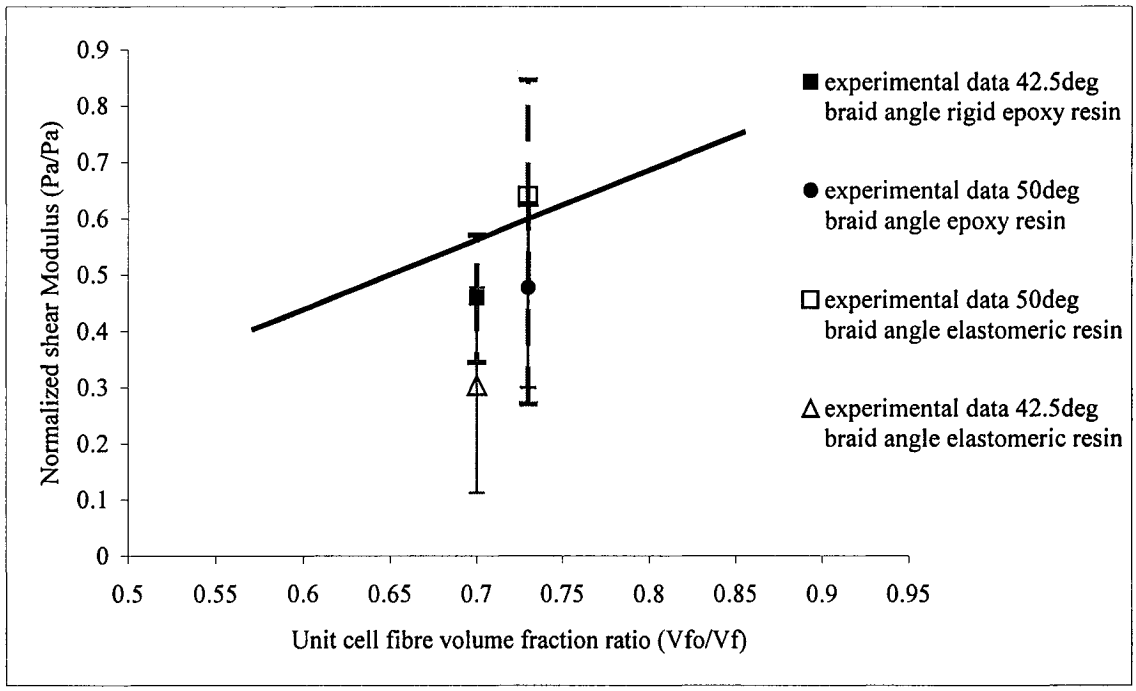

Figure 11-11: Normalized shear modulus versus unit cell volume fraction ratio of experimental data for braided tubes with 42.5° and 50° braid angle within the regression limits established in Figure 11-10.

This result is for a specific fibre/resin combination and would be of very little interest unless the coefficients of 1.23 and –0.3 could be explained as functions of known properties or variables. Since the correlation coefficient was very high (R^2 = 0.9974), an attempt was made to relate the coefficients to known variables. One possibility to explain the slope (1.23) is to use a curve fitting formulation similar to that of Halpin-Tsai (equation 11-6). However, in this work the effect of jam angle was not considered. It is proposed to

model the slope as a function of the laminate shear modulus at the jam angle, similar at both extreme values, and the maximal value found at a 45° braid angle; this is introduced in equation 11-7.

$$\text{slope} = \frac{1 + \eta \dfrac{V_{fo}}{V_f}}{1 - \eta \dfrac{V_{fo}}{V_f}} \qquad \textbf{11-6}$$

where, V_{fo}/V_f is the fibre volume fraction ratio of the closed mesh braid at the jam angle to the angle-ply laminate and η is defined as

$$\eta = \left\{ \frac{\left(\dfrac{G_{xylaminate45}}{G_{xylaminate\_jam\_angle}} \right) - 1}{\left(\dfrac{G_{xylaminate45}}{G_{xylaminate\_jam\_angle}} \right) + 1} \right\} \qquad \textbf{11-7}$$

and $G_{xylaminate45}$ and $G_{xylaminate\_jam\_angle}$ are the shear moduli of the angle-ply laminate at a 45° and jam angle, respectively. For the case being studied in this section, these values are 20.2 GPa and 15.6 GPa. The fibre volume fraction ratio, V_{fo}/V_f, is 0.85. The slope is thus evaluated as 1.26, a difference of 2.4 % with the slope evaluated in the regression analysis.

11.3 Other fibre-resin, open and closed mesh braids combinations

To confirm the design equations developed in the previous sections, the same analysis was performed with carbon/epoxy, E-glass/epoxy and Kevlar/RP6443 combinations. The design equations can all be simplified to the following linear equation form:

$$y = mx + b \qquad \textbf{11-8}$$

where y is the ratio of braid to laminate elastic constant ratio, m is the slope of the regression, x is the fibre volume fraction ratio and b is the intercept. The parameters found for each fibre/epoxy combination, including Kevlar-49/epoxy used in the previous sections, are tabulated below (Table 11-3).

Table 11-3: Design equation parameters for different fibre/epoxy combinations.

Fibre	Elastic constant	Slope, m	Intercept, b	Correlation factor, R^2
Kevlar				
	E_x	1.0	0	0.99-0.94
	E_y	1.0	0	0.98-0.90
	G_{xy}	1.23	-0.3	0.9974
Carbon				
	E_x	0.9531	0	0.96
	E_y	0.9418	0	0.97
	G_{xy}	1.22	-0.3	0.9964
E-glass				
	E_x	0.9414	0	0.95
	E_y	0.9267	0	0.96
	G_{xy}	1.27	-0.3	0.9983
RP6443 Polyurethane				
	E_x	0.9393	0	0.96
	E_y	0.9395	0	0.96
	G_{xy}	1.36	-0.428	0.9948

Similar results were found for all four combinations. Regression coefficient values are all above or equal to 0.9. Carbon and E-glass longitudinal and transverse elastic normalized moduli have a 5 % difference with the normalized fibre volume fraction. For practical and preliminary design purposes, a one to one ratio could be used for both elastic constants (i.e. m = 1).

Shear modulus results were similar for all combinations. Equations 11-5 and 11-6 did show good agreement with all combinations. The predicted slope for carbon was 1.25, which is a 2.5 % difference with 1.22; the E-glass prediction was 1.18, which is a 7.3 % difference with 1.27. The predicted slope for the elastomeric polyurethane with Kevlar 49 was 1.34, which is a 1.6% difference with 1.36.

A possible explanation for some level of discrepancy is the use of micromechanical models to evaluate laminar elastic constants and the use of simple equations to evaluate the shear modulus of some of the fibres as opposed to experimental evaluation.

Although a proper physical explanation of equation 11-4 could not be found, the design equations for the longitudinal elastic (equation 11-2), transverse elastic (equation 11-3) and shear (equation 11-4) moduli are adequate for design purposes.

11.4 Conclusion

Design equations based on braid angle, undulation region length, unit cell size and strand fibre volume fraction were developed to predict the longitudinal and transverse elastic as well as shear moduli of angle-ply braided composites as a function of similar angle-ply laminate elastic constants; good agreement was found with the predictive model of Chapter 5. The simplified expressions could be used for practical engineering design purposes with the same confidence as other regression-based formulations as the Halpin-Tsai micromechanical models.

The shear modulus design equation requires further work; however, similar results were found for different fibre/resin combinations. This suggests that the equations are correct but not fully defined in terms of constituent elastic constants or other parameters. It is believed that the work should be a valuable basis for future investigation and can be used for three fibre/resin combinations, with good agreement, in preliminary engineering design work.

CHAPTER 12 THESIS CONCLUSIONS, CONTRIBUTIONS AND FUTURE DIRECTION

12.1 Conclusions and contributions

The aim of this doctoral thesis was, through an engineering approach, to simplify the catheterization procedure and improve catheter technology; firstly, for clinicians, by reducing the number of components in a medical catheter guidewire system (CGWS) to a single medical catheter that possesses the physical characteristics of an optimized CGWS; and secondly, for the patient, by providing a more comfortable procedure by shortening the catheterization time. To that end, a classical laminate plate theory-based model to predict the elastic constants of angle-plied composite structures, such as braids, was developed, compared to previous models, and experimentally validated. The model was shown to accurately predict the experimental results of braid longitudinal elastic modulus and shear modulus of model catheters produced with a rigid thermoset resin and Kevlar fibre reinforcement. The model also reasonably predicted the elastic constants of braided tubes produced with elastomeric resins.

The principal goal of this work was not to design an optimal one-piece medical catheter. To meet such a goal, measuring exact rigidities, either in-vivo or in-vitro, required along the length of the medical catheter must be performed. Such a task should be done with co-operators in the medical field. Rather, once this step will have been completed, this work provides the tool to calculate equivalent optimal rigidities required at the proximal, medial and distal portions of a one-piece medical catheter by selecting fibre, resin and different braid angle combinations. Preliminary efforts to find medical catheter

rigidities in the literature and measure them experimentally were used to validate the proposed design methodology.

Future production of a one-piece variable braid angle medical catheter can be done on any braider since changing the mandrel and crosshead velocities changes the braid angle. The relationship between velocities has been thoroughly evaluated. The different velocities required to obtain the braid angles for optimum rigidity along the catheter tube are thus selected prior to production and changed at the appropriate time intervals.

It is hoped that the contributions of this work to the body of knowledge are original, substantial and theoretically and practically useful.

First, this document contains a thorough review of basic medical catheter-related knowledge and could be used by other researchers in the fields of engineering or biomechanical/biomedical engineering. Such information as medical catheter/guidewire materials and rigidities was gathered and supplemented with experimental measurement of a catheter and these two sets of data were analysed.

Secondly, a generalized model was developed to predict the elastic constants of angle-plied braided/woven composite materials. For accurate results, the model requires accurate measurement of braid unit cell dimensions and constituent or laminar elastic constants. In these conditions, the model showed excellent agreement with experimental data. The model was developed for the design of medical catheters but can be used for any braided/woven structure, thus broadening the scope and value of the model.

In addition, this work has increased the available experimental data on composite material elastic constants. Longitudinal elastic and shear moduli properties of rigid and elastomeric braided tubes as well as rigid laminar tubes were experimentally evaluated. To

do so, a low-cost and simple test rig to determine the shear modulus of tubular specimens was developed based on existing equipment. The apparatus provides reasonable experimental results.

The effect of strand undulation on the elastic constants of braided composites was confirmed through experimental testing. Simpler approaches to model the strand path in the undulation region were evaluated and recommendations were made based on braid configuration. It was found that the maximum undulation length effect, reached once the undulation length attained $5.5h_c$, was equivalent to the properties of a lamina with overlying and underlying resin layers. The role of neat resin content was also confirmed in this evaluation.

A further contribution, significant for practical design purposes, was the simplification of the proposed CLPT model to equations relating the elastic constants and unit cell fibre volume fractions of braids and angle-ply laminates at equivalent angles. While such design equations are reasonably accurate, they have greater potential for industrial use than the theoretical model developed earlier in Chapter 5.

Finally, this work presents financial benefits in terms of the design process. Starting from three fibres and four resins as candidates for medical catheter constituent materials, the model was used to eliminate combinations incapable of mimicking the required medical catheter rigidities without extensive, and resource - and time-consuming experimental testing. The model was proven to be very useful to select constituent materials when manufacturer-provided data was accurate.

12.2 Future Work

The work that was undertaken opened many viable areas of continuing research from a practical composite- and biomedical- engineering perspective and from theoretical perspective.

The next direction for this work should be to produce actual size medical catheters and test for longitudinal elastic and shear moduli. Further work should be done using materials with high biological performance to ultimately test the model catheters in vitro and then in vivo. Such work requires access to cadavers, biohazard rated rooms and strict preventive contamination procedures and ethical evaluation as well as cooperate with the medical field to determine optimal catheter rigidities.

Also, further work should be done to fully explain the shear modulus design equations developed in Chapter 11 in terms of lamina or constituent characteristics. The Halpin-Tsai approach used to define terms of the regression equations and provides acceptable results has not been related to the physical situation.

The applications of the work discussed in this document are not limited to the biomedical field; any use of braided or other angle-ply composites can be analysed with the proposed CLPT model, be it in the field of aerospace technology or sports equipment design to name but a few. Therefore, the model should be written in a different language that permits user interface and not strictly in-house use.

The issue of the non-linear behaviour of elastomeric and flexible resin elastic constants could be addressed in future developments of the proposed CLPT model to better predict elastic constants of flexible or elastomeric resin-based braids for other non-catheter related applications which could have larger practical working stress-strain ranges.

Finally, the model should be expanded to predict elastic constants of different unit cell geometries (regular, Hercules and triaxial braids, filament wound, etc.) and finally to perform analyses for applications other than medical catheters.

REFERENCES

1. Ratner, B.D., Hoffman, A.S., Schoen, F.J. and Lemons J.E. (eds.), Biomaterial Science: An Introduction to Materials in Medicine, Toronto, Academic Press, 1996.
2. FIND/SVP, The Market for Disposable Catheters and Supplies: A market intelligence report. New York, FIND/SVP, Inc, 1996.
3. Anonymous, Balloon angioplasty, http://johns.largnet.uwo.ca/shine/health/balloon.htm, September 9, 1996.
4. Martín Rubio & Associates, Peripheral Vascular Disease: Diagnostic & Treatment: Arteriogram/Aortogram, Percutaneous Transluminal Angioplasty, http://www.hgcardio.com/pvd_d%26t.htm, 26 October 1998.
5. Medidyne, Home page, http://www.catheter.com/Angiography.htm, March 6, 2000.
6. ViaHealth, atherectomy, http://www.viahealth.org/rgh/departments/cardiac/atherectomy.htm, 1999.
7. Cordis Webster inc., http://www.cordiswebster.com/04products/index.htm, March 6, 2000.
8. Cardima, Atrial Fibrillation, http://www.cardima.com/af_ablation.html, Feb 10 1999.
9. Keith, S.C., MD, Southeast Anesthesiology Consultants, Thoracic anesthesia, http://seanesthesiology.com/thoracic.htm, March 6, 2000.
10. Neocare, Umbilical catheters, http://www.neocare.com/uvc.htm, January 21, 2000.
11. Neocare, Feeding tubes, http://www.neocare.com/ft.htm, January 21, 2000.
12. Moore, N.J., Elemental design, Figure-Four Catheter, http://www.merseyworld.com/elementaldesign/figfour.html, January 6, 1997.

13. Mediplus, MedWeb UK ltd., single lumen cystometry, http://www.mediplus.co.uk/html/body_single_lumen_cystometry.html, February 28, 2000.

14. Narang Enterprises, Foley's catheter, http://www.narang.com/foleyscatheter.html, March 6, 2000.

15. Moore, N.J., Elemental design, Foley Catheter, http://www.merseyworld.com/elementaldesign/foley.html, December 13, 1996

16. Massoud, S., Radiologist, personal communications, 2000.

17. GCM Radiology, James B. Spies, M.D. Drs. Groover, Christie & Merritt, P.C., GCM Radiology: Diagnostic Angiography - Introduction and Procedure Description http://www.gcmnet.com/anintrpt.htm, March 6, 2000.

18. Health central, © A.D.A.M. http://www.healthcentral.com/mhc/img/img1080.cfm, 1998.

19. Bard, C.R., Patient's Guide to Cardiac Catheterization, http://www.holyname.org/brochure/cathguid.htm#cardcath, July 16, 1997.

20. Stenqvist, O., Curelaru, I., Linder, L.-E. and Gustavsson, B., Stiffness of Central Venous Catheters, Acta Anaesthesiol Scand., Vol. 27: 153-157, 1983.

21. Bersten A.D., Williams, D.R.G and Phillips, G.D., Central Venous Catheter Stiffness and its Relation to Vascular Perforation, Anaesth Intens Care, Vol. 16: 342-357, 1988.

22. Martin, R.W. and Johnson, C.C., Engineering Considerations of Catheters for Intravascular Ultrasonic Measurements, SPIE Vol. 1068: 198-206, 1989.

23. Cook© catalogue, p.20-49, 2001.

24. Porto, V.L., Advanced Polymers Inc., http://www.advpoly.com/, December 17, 1999.

25. Munro, M. and Fahim, A., Review of Braiding of Fibre Composite Components, Course notes for MCG 5180, Handout #6, Department of Mechanical Engineering, University of Ottawa, unpublished

26. Nakai A., Fujita A., Yokoyama A. and Hamada H., Design Methodology for a Braided Cylinder, Composite Structures, No. 32, p. 501-509, 1995.

27. Ko, F., Pastore, C. and Head, A., Atkins and Pearce Handbook of Industrial Braiding, Atkins and Pearce, Covington, Kentucky, 1989.

28. Co, E.D., Cardiac Catheter, US 3,935,857, 1976.

29. Stevens, R.C., Tubular Products and Method of Making Same, Cordis Corporation, US 3,485,234, 1969.

30. Chee, U.H., Engelson, E.T. and Samson, G., Braided Body Balloon Catheter, Target Therapeutics, Inc, US 5,906,606, 1999.

31. Samson, G., High Performance Superelastic Alloy Braid Reinforced Catheter, Target Therapeutics, Inc., US 5,891,112, 1999.

32. Chein, T.Y.H., Jansen, L.P., Nita, H. and Sarge, J.A., Soft-tip High Performance Braided Catheter, Target Therapeutics, Inc, US 5,891,114, 1999.

33. Macauley, P.E., Wasicek, L.D., Bayot, A. and Klemm, K., Intravascular Catheter with a Nontraumatic Distal Tip, Advanced Cardiovascular Systems, Inc, CA2070452, 2000.

34. Jaraczewski, R.S. and McQurk, E., Small Diameter, High Torque Catheter, Micro Interventional Systems, WO 95/13110, 1995.

35. Black, J., Biological Performance of Materials, Fundamentals of Biocompatibility, Marcel Dekker, Inc., New York, NY, 1981.

36. Kaplan, W.A., Modern Plastics Encyclopaedia 97, Mid-November, McGraw-Hill companies, 1996.

37. Popov, E.P., Engineering Mechanics of Solids, Prentice Hall, Toronto, Ontario, P. A-3, 1990.

38. MatWeb, The Online Materials Information Resource, http://www.matweb.com/, 2001.

39. Lubin, G., Handbook of Composites, Van Nostrand Reinhold Co, Toronto, Ontario, 1982.

40. Van Vlack, L.H., Elements of Materials Science and Engineering, 6th edition, Series in Metallurgy and Materials Engineering, Addison Wesley, Don Mills, Ontario, 1989.

41. Gutowski, T.G., Advanced Composites Manufacturing, John Wiley & Sons, Inc., Toronto, Ontario, 1997.

42. Peters, S.T., Humphrey, W.D. and Foral, R.F., Filament Winding Composite Structure Fabrication, SAMPE, Covina, CA, 1991.

43. Schwartz, M.M., Composite Materials Handbook, McGraw-Hill, Toronto, Ontario, 1984.

44. Agarwal, B.D. and Broutman L.J., Analysis and Performance of Fiber Composites, Wiley-Interscience, Toronto, Ontario, 1980.

45. Adams, D.F. and Doner, D.R., Transverse Normal Loading of a Unidirectional Composite, Journal of Composite Materials 1: 152-164, 1967.

46. Halpin, J.C. and Tsai, S.W., Effects of Environmental Factors on Composite Materials, AFML-TR 67(June): 423, 1969.

47. McCullough, R.L., Concept of Fibre-Resin Composites, Moral Dekker, Inc., NY, NY, 1971.

48. Munro, M. and Lee, S., Modelling of In-Plane Shear Modulus of Composite Materials for Aerospace Applications, Journal of Reinforced Plastics and Composites, 14: 471-494, 1995.

49. Barbero, J., Introduction to Composite Materials Design, Taylor and Francis, Philadelphia, PA, 1999.

50. Pastore, C.M. and Yasser, A.G., Self-Consistent Fabric Geometry Model: Modification and Application of a Fabric Geometry Model to Predict the Elastic Properties of Textile Composites, Journal of Composites Technology & Research 16(1): 32-36, 1994.

51. Brunnschweiller, D., Braids and Braiding, Journal of the Textile Institute, 45: 668-686, 1953.

52. Naik, N.K. and Shembekar, P.S., Elastic Behavior of Woven Fabric Composites: I-Lamina Analysis, Journal of Composite Materials, 26(15): 2196-2225, 1992.

53. Pastore, C., and Ko, F., CIM of Braided Preforms for Composites, Computer Aided Design in Material Technology, Computational Mechanics Publications: 142-147, 1988.

54. Falzon, P. J., Herzberg, I. and Baker, A.A., Stiffness Analysis of Textile Composites, 5th Australian Aeronautical Conference, Melbourne, Australia, IE Australia, 1993.

55. Ari-Gur, J. and Krizan, J.A., Atkins and Pearce Handbook of Industrial Braiding, Atkins and Pearce, Covington, Kentucky, p. RR-jag-3 to RR-jag-9, 1990.

56. Whitney, J.M., Halpin, J.C., Analysis of Laminated Anisotropic Tubes Under Combined Loading, Journal of Composite Materials, Vol. 2(3), p. 360-367, 1968.

57. Hamada, H., Fujita, A., Maekawa, Z., Kakai, A. and Yokohama, A., Design of Braided Composite Tubes by Numerical Analysis Method, Composites for the Pressure Vessel Industry, 202: 69-73, 1995.

58. Nakai, A., Hamada, H., and Hoa, S.V., Influence of Braiding Structure on Torsional Properties of Braided Composite Tube, Computer Technology: Applications and Methodology, ASME, PVP-Vol.326, P.125-130, 1996.

59. Soebroto, H.B., Hager, T., Pastore, C.M., and Ko F.K., Engineering Design of Braided Structural Fiberglas Composites. National SAMPE Symposium and Exhibition (Proceedings), SAMPE, Covina, CA, USA, p.687-696, 1990.

60. Vandeurzen, P., Ivens, J., and Verpoest, I., Three-Dimensional Micromechanical Analysis of Woven-Fabric Composites: II. Elastic Analysis, Composites Science & Technology, 56(11, Nov): 1317-1327, 1996.

61. Ishikawa, T. and Chou, T.-W., Stiffness and Strength Behavior of Woven Fabric Composites, Journal of Materials Science 17: 3211-3220, 1982.

62. Redman, C.J. and Douglas, C.D., Theoretical Prediction of the Tensile Elastic Properties of Braided Composites, 38th International SAMPE Symposium: 719-727, 1993.

63. Naik, N.K. and Ganesh, V.K., An Analytical Method for Plain Weave Fabric Composites, Composites, 26(4): 281-289, 1995.

64. Advanced Composites Inc, Custom Manufacturing of Composites: Filament Winding of Fiberglas Tubing, Graphite Tubes, Radomes, Custom Fabrication of Aerospace Composites, Carbon Fiber Tubes, Graphite Tubing, Kevlar, and FRP Pipe Composites, http://advancedcomposites.com/custom.htm, 1999

65. Gillespie, J. et al., Laminate property analysis, http://www.ccm.udel.edu/www.ccm.udel.edu/Techsite/Pages/LPA/LPA_Basis.html, July 24, 2000

66. Raju, I.S. and Wang, J.T., Classical Laminate Theory Models for Woven Fabric Composites, Journal of Composites Technology and Research 16(4): 289-303, 1994.

67. Brunschweiller, D., The Structure and Tensile Properties of Braids. Journal of the Textile Institute, 45: T55-T87, 1954.

68. Tsai, S.W. and Hahn, H.T., Introduction to Composite Materials, Westport, CT: Technomic Publishing Co., Inc, 1980.

69. Jones, R., Mechanics of Composite Materials, McGraw-Hill, Toronto, 1975.

70. Horneck R.W., Numerical Methods, Quantum Publishers, Inc, NY, NY, P.154-160, 1975.

71. Burden, R.L, Faires, J.D. and Reynolds, A.C., Numerical Analysis, Second Edition, Prindle, Weber & Schmidt, Boston Massachusetts, Chapter 4.7, 1981.

72. Flanagan, R.C., Munro M. et al., High Energy Density Fibre Composite Rotors, Volume 2, Department of Mechanical Engineering, University of Ottawa, Technical Report no UOME-FP-8603-1, 1986.

73. Quenneville, G.-M., Determination of Shear Properties of Fibre Composite Materials, Fourth Year Undergraduate Thesis, Department of Mechanical Engineering, University of Ottawa, 1986.

74. Hexcel Fibers, Continuous Fibre, http://www.hexcelfibers.com/Markets/Products/Continuous/_Productlist.htm, 2002.

75. Dickson, T., Munro, M. and Lee, S., Torsion Testing of Thin-Walled Fibre Composite Tubes for Determining In-Plane Shear Modulus, not published.

76. Jensen D.W. and Pai S.P., Proceedings of the 7th Conference on Composite Materials, American Society for Composites, University Park, PA, 1992.

77. Lee, S. and Munro, M., Evaluation of In-Plane Shear Test Methods for Advanced Composite Materials by the Decision Analysis Technique, Composites, 17(1), Jan, 13-22, 1986

78. Christiaen, Anne-Claire, Evaluation of the Durability of Elastomeric easy-release coatings, Ph.D. Dissertation, Virginia Polytechnic Institute and State University, Blacksburg, Virginia, July 1998

79. Whitcomb J.D., Three-Dimensional Stress Analysis of Plain Weave Composites, Composite Materials: Fatigue and Fracture (Third Volume), ASTM STP 1110, American Society for Testing and Materials, Philadelphia, pp.417-438, 1991

APPENDIX 1: CLASSICAL LAMINATE PLATE THEORY CONSTITUTIVE EQUATIONS

Strain-displacement relationship

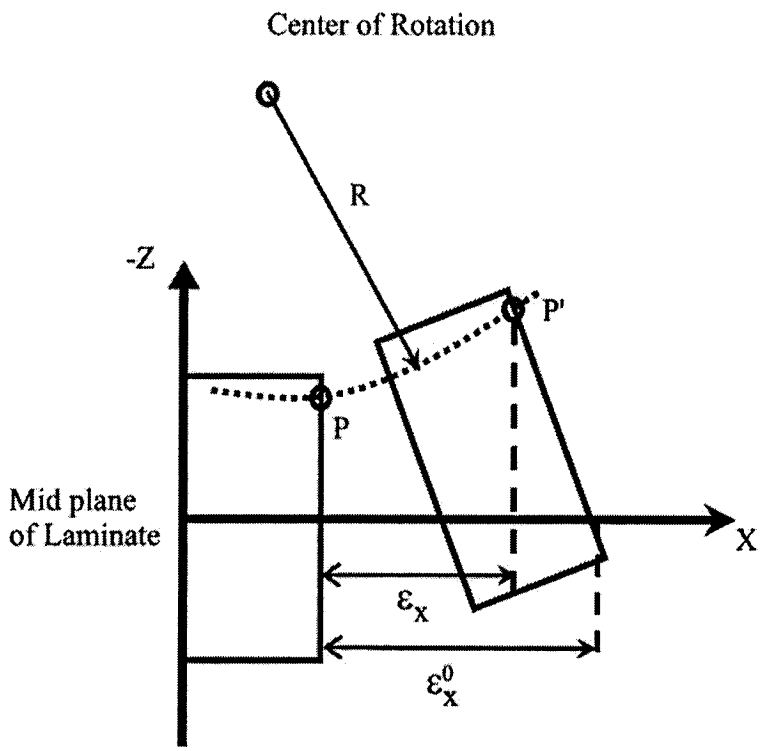

From the above figure, the strain displacement is defined as:

$$\begin{bmatrix} \varepsilon_x \\ \varepsilon_y \\ \gamma_{xy} \end{bmatrix} = \begin{bmatrix} \varepsilon_x^0 \\ \varepsilon_x^0 \\ \gamma_{xy}^0 \end{bmatrix} + z \begin{bmatrix} k_x \\ k_y \\ k_{xy} \end{bmatrix} \quad (1)$$

where, with reference to the radius of curvature illustrated in the figure

$$k = \frac{1}{R} \tag{2}$$

The stresses in a lamina if the laminate midplane strain and curvature are know are calculated as:

$$\begin{bmatrix} \sigma_x \\ \sigma_y \\ \tau_{xy} \end{bmatrix} = \begin{bmatrix} \overline{Q}_{11} & \overline{Q}_{12} & \overline{Q}_{16} \\ \overline{Q}_{21} & \overline{Q}_{22} & \overline{Q}_{26} \\ \overline{Q}_{31} & \overline{Q}_{23} & \overline{Q}_{66} \end{bmatrix} \begin{bmatrix} \varepsilon_x^0 \\ \varepsilon_x^0 \\ \gamma_{xy}^0 \end{bmatrix} + z \begin{bmatrix} \overline{Q}_{11} & \overline{Q}_{12} & \overline{Q}_{16} \\ \overline{Q}_{21} & \overline{Q}_{22} & \overline{Q}_{26} \\ \overline{Q}_{31} & \overline{Q}_{23} & \overline{Q}_{66} \end{bmatrix} \begin{bmatrix} k_x \\ k_y \\ k_{xy} \end{bmatrix} \tag{3}$$

Stress and moment resultants

The load per unit length and moment per unit length, calculated as the integral of the stress over the length are respectively:

$$\begin{aligned} N_x &= \int_{-h/2}^{h/2} \sigma_x dz \\ N_y &= \int_{-h/2}^{h/2} \sigma_{yx} dz \\ N_{xy} &= \int_{-h/2}^{h/2} \tau_{xy} dz \end{aligned} \tag{4}$$

and

$$M_x = \int_{-h/2}^{h/2} \sigma_x z dz$$
$$M_y = \int_{-h/2}^{h/2} \sigma_{yx} z dz \quad (5)$$
$$M_{xy} = \int_{-h/2}^{h/2} \tau_{xy} z dz$$

Combining equations 3 and 4 gives:

$$\begin{bmatrix} N_x \\ N_y \\ N_{xy} \end{bmatrix} = \begin{bmatrix} A_{11} & A_{12} & A_{16} \\ A_{21} & A_{22} & A_{26} \\ A_{31} & A_{23} & A_{66} \end{bmatrix} \begin{bmatrix} \varepsilon_x^0 \\ \varepsilon_x^0 \\ \gamma_{xy}^0 \end{bmatrix} + \begin{bmatrix} B_{11} & B_{12} & B_{16} \\ B_{21} & B_{22} & B_{26} \\ B_{31} & B_{23} & B_{66} \end{bmatrix} \begin{bmatrix} k_x \\ k_y \\ k_{xy} \end{bmatrix} \quad (6)$$

$$A_{ij} = \sum_{k=1}^{n} \left(\overline{Q}_{ij}\right)_k \left(h_k - h_{k-1}\right) \quad (7)$$

$$B_{ij} = \frac{1}{2} \sum_{k=1}^{n} \left(\overline{Q}_{ij}\right)_k \left(h_k^2 - h_{k-1}^2\right) \quad (8)$$

where h_k is the thickness of plate k. Combining equations 3 and 5 gives:

$$\begin{bmatrix} M_x \\ M_y \\ M_{xy} \end{bmatrix} = \begin{bmatrix} B_{11} & B_{12} & B_{16} \\ B_{21} & B_{22} & B_{26} \\ B_{31} & B_{23} & B_{66} \end{bmatrix} \begin{bmatrix} \varepsilon_x^0 \\ \varepsilon_x^0 \\ \gamma_{xy}^0 \end{bmatrix} + \begin{bmatrix} D_{11} & D_{12} & D_{16} \\ D_{21} & D_{22} & D_{26} \\ D_{31} & D_{23} & D_{66} \end{bmatrix} \begin{bmatrix} k_x \\ k_y \\ k_{xy} \end{bmatrix} \quad (9)$$

$$D_{ij} = \frac{1}{3} \sum_{k=1}^{n} \left(\overline{Q}_{ij}\right)_k \left(h_k^3 - h_{k-1}^3\right) \quad (10)$$

The generalized CLPT constitutive equation is thus defined as:

$$\begin{bmatrix} N_x \\ N_y \\ N_{xy} \\ M_x \\ M_y \\ M_{xy} \end{bmatrix} = \begin{bmatrix} A_{11} & A_{12} & A_{16} & B_{11} & B_{12} & B_{16} \\ A_{21} & A_{22} & A_{26} & B_{21} & B_{22} & B_{26} \\ A_{31} & A_{23} & A_{66} & B_{31} & B_{23} & B_{66} \\ B_{11} & B_{12} & B_{16} & D_{11} & D_{12} & D_{16} \\ B_{21} & B_{22} & B_{26} & D_{21} & D_{22} & D_{26} \\ B_{31} & B_{23} & B_{66} & D_{31} & D_{23} & D_{66} \end{bmatrix} \begin{bmatrix} \varepsilon_X^0 \\ \varepsilon_Y^0 \\ \gamma_{XY}^0 \\ k_x \\ k_y \\ k_{xy} \end{bmatrix} \quad (11)$$

In compact form, equation 11 is expressed as:

$$\begin{bmatrix} N_x \\ N_y \\ N_{xy} \\ M_x \\ M_y \\ M_{xy} \end{bmatrix} = [S] \begin{bmatrix} \varepsilon_X^0 \\ \varepsilon_Y^0 \\ \gamma_{XY}^0 \\ k_x \\ k_y \\ k_{xy} \end{bmatrix} \quad (12)$$

where [S] is given by:

$$[S] = \begin{bmatrix} A_{11} & A_{12} & A_{16} & B_{11} & B_{12} & B_{16} \\ A_{21} & A_{22} & A_{26} & B_{21} & B_{22} & B_{26} \\ A_{31} & A_{23} & A_{66} & B_{31} & B_{23} & B_{66} \\ B_{11} & B_{12} & B_{16} & D_{11} & D_{12} & D_{16} \\ B_{21} & B_{22} & B_{26} & D_{21} & D_{22} & D_{26} \\ B_{31} & B_{23} & B_{66} & D_{31} & D_{23} & D_{66} \end{bmatrix} \quad (13)$$

and the compliance matrix, the inverse of [S] is given by:

$$[C] = \begin{bmatrix} a_{11} & a_{12} & a_{16} & b_{11} & b_{12} & b_{16} \\ a_{21} & a_{22} & a_{26} & b_{21} & b_{22} & b_{26} \\ a_{31} & a_{23} & a_{66} & b_{31} & b_{23} & b_{66} \\ b_{11} & b_{12} & b_{16} & d_{11} & d_{12} & d_{16} \\ b_{21} & b_{22} & b_{26} & d_{21} & d_{22} & d_{26} \\ b_{31} & b_{23} & b_{66} & d_{31} & d_{23} & d_{66} \end{bmatrix} \quad (14)$$

Braid elastic constants are found from the compliance matrix as follows:

$$E_x = \frac{1}{a_{11}t} \tag{15}$$

$$G_{xy} = \frac{1}{a_{66}t} \tag{16}$$

APPENDIX 2: TWIST ANGLE EFFECT

The twist angle effect was found assuming strand undulation length and geometry. The strand width (W_y) and thickness (h_c) were assumed to be 1.37 mm and 0.17 mm, respectively; the undulation length (l_{und}) was assumed to be 0.17 mm, which is the limit case. The angle can be found as the arctangent of the vertical displacement, dh, between the top two points (1 and 2) of the strand cross-sectional area found on the sinusoidal curves that describe the strand path (Figure 1(a)) and the edge length, L_e.

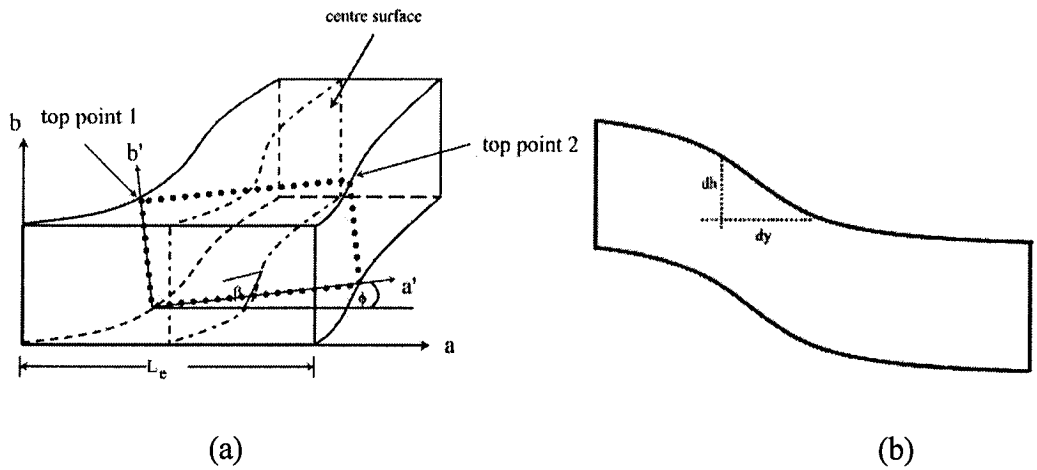

Figure 1: Undulation parameter: (a) position of points required for twist angle calculations; (b) displacement between points.

From configuration geometry, the horizontal displacement is found as:

$$dy = W_y \sqrt{\frac{1}{\cos\left(2\theta - \frac{\pi}{2}\right)} - 1} \qquad (1)$$

The vertical displacement is found by calculating the difference between the values of the sinusoidal function at points 1 and 2 separated be a distance dy, as follow:

$$dh = \frac{h_c}{2}\left\{\left(1+\cos\left(\frac{y+dy}{a_u}\right)\right)-\left(1+\cos\left(\frac{y}{a_u}\right)\right)\right\} \quad (2)$$

where y is the horizontal distance from the end to the first point. The twist angle is found as:

$$\phi = a\tan\left(\frac{dh}{L_e}\right) \quad (3)$$

The highest twist angle for this geometry, 7°, was found at a braid angle of 40°. Calculating the difference in polar moment of inertia[1] between 0 and 7° twist angles resulted in a 4.7 % error.

[1] Equations for the polar moment of inertia for rectangular cross-sections can be found in most standard dynamics textbooks.

APPENDIX 3: DEVELOPED EQUATIONS FOR A, B AND D FOR REGIONS R_1 - R_9

Classical laminate theory stiffness matrices [A], [B] and [D]

section 1

$$As1 := \frac{1}{2} \cdot ledge^2 \cdot \sin(\theta) \cdot (-\tan(\gamma) \cdot \sin(\theta) + 2 \cdot \cos(\theta)) \cdot (Q2 \cdot hc + Q(\theta) \cdot hc + Qm \cdot tm) \ *$$

$$Bs1 := \frac{1}{4} \cdot hc \cdot ledge^2 \cdot \sin(\theta) \cdot (-2 \cdot \cos(\theta) + \sin(\theta) \cdot \tan(\gamma)) \cdot (Q2 \cdot hc + Q2 \cdot tm + Q(\theta) \cdot tm - Q(\theta) \cdot hc - 2 \cdot Qm \cdot tm) \ *$$

$$Ds1 := \frac{-1}{24} \cdot ledge^2 \cdot (-2 \cdot \cos(\theta) + \sin(\theta) \cdot \tan(\gamma)) \cdot \sin(\theta) \cdot (3 \cdot Q(\theta) \cdot hc \cdot tm^2 + 4 \cdot Q(\theta) \cdot hc^3 + 12 \cdot Qm \cdot hc^2 \cdot tm + Qm \cdot tm^3 - 6 \cdot Q(\theta) \cdot hc^2 \cdot tm + 4 \cdot Q2 \cdot hc^3 + 6 \cdot Q2 \cdot hc^2 \cdot tm + 3 \cdot Q2 \cdot hc \cdot tm^2) \ *$$

section 2

$$As2 := \frac{-1}{2} \cdot \sin(\theta) \cdot ledge^2 \cdot (Q2 \cdot hc + Q(\theta) \cdot hc + Qm \cdot tm) \cdot (-2 \cdot \cos(\theta) + \sin(\theta) \cdot \tan(\gamma)) \ *$$

$$Bs2 := \frac{-1}{4} \cdot hc \cdot ledge^2 \cdot \sin(\theta) \cdot (\sin(\theta) \cdot \tan(\gamma) - 2 \cdot \cos(\theta)) \cdot (Q(\theta) \cdot hc - Q2 \cdot hc + 2 \cdot Qm \cdot tm - Q2 \cdot tm - Q(\theta) \cdot tm) \ *$$

$$Ds2 := \frac{-1}{24} \cdot \sin(\theta) \cdot ledge^2 \cdot (-2 \cdot \cos(\theta) + \sin(\theta) \cdot \tan(\gamma)) \cdot (3 \cdot Q(\theta) \cdot hc \cdot tm^2 + 4 \cdot Q(\theta) \cdot hc^3 + 12 \cdot Qm \cdot hc^2 \cdot tm + Qm \cdot tm^3 - 6 \cdot Q(\theta) \cdot hc^2 \cdot tm + 4 \cdot Q2 \cdot hc^3 + 6 \cdot Q2 \cdot hc^2 \cdot tm + 3 \cdot Q2 \cdot hc \cdot tm^2) \ *$$

section 3

$$As3 := \frac{-1}{2} \cdot ledge \cdot \sin(\theta) \cdot (Q2 \cdot hc + Q(\theta) \cdot hc + Qm \cdot tm) \cdot (-\tan(\gamma) \cdot ledge \cdot \sin(\theta) + 2 \cdot ledge \cdot \cos(\theta) + 2 \cdot \tan(\gamma) \cdot X - 2 \cdot Y) \ *$$

$$Bs3 := \frac{-1}{4} \cdot hc \cdot ledge \cdot \sin(\theta) \cdot (Q(\theta) \cdot hc - Q2 \cdot hc + 2 \cdot Qm \cdot tm - Q2 \cdot tm - Q(\theta) \cdot tm) \cdot (-\tan(\gamma) \cdot ledge \cdot \sin(\theta) + 2 \cdot ledge \cdot \cos(\theta) - 2 \cdot Y + 2 \cdot \tan(\gamma) \cdot X) \ *$$

$$Ds3 := \frac{-1}{24} \cdot \sin(\theta) \cdot ledge \cdot (4 \cdot Q(\theta) \cdot hc^3 + Qm \cdot tm^3 + 12 \cdot Qm \cdot hc^2 \cdot tm + 6 \cdot Q2 \cdot hc^2 \cdot tm + 3 \cdot Q2 \cdot hc \cdot tm^2 + 4 \cdot Q2 \cdot hc^3 + 3 \cdot Q(\theta) \cdot hc \cdot tm^2 - 6 \cdot Q(\theta) \cdot hc^2 \cdot tm) \cdot (-\tan(\gamma) \cdot ledge \cdot \sin(\theta) + 2 \cdot ledge \cdot \cos(\theta) + 2 \cdot \tan(\gamma) \cdot X - 2 \cdot Y) \ *$$

section 4

$$As4 := \frac{1}{2} \cdot (Q2 \cdot hc + Q(\theta) \cdot hc + Qm \cdot tm) \cdot ledge \cdot \sin(\theta) \cdot (-\tan(\gamma) \cdot ledge \cdot \sin(\theta) + 2 \cdot ledge \cdot \cos(\theta) + 2 \cdot \tan(\gamma) \cdot X - 2 \cdot Y) \ *$$

$$Bs4 := \frac{1}{4} \cdot hc \cdot ledge \cdot \sin(\theta) \cdot (Q(\theta) \cdot hc - Q2 \cdot hc + 2 \cdot Qm \cdot tm - Q2 \cdot tm - Q(\theta) \cdot tm) \cdot (-\tan(\gamma) \cdot ledge \cdot \sin(\theta) + 2 \cdot ledge \cdot \cos(\theta) - 2 \cdot Y + 2 \cdot \tan(\gamma) \cdot X) \ *$$

$$Ds4 := \frac{1}{24} \cdot ledge \cdot \sin(\theta) \cdot (3 \cdot Q(\theta) \cdot hc \cdot tm^2 + 4 \cdot Q(\theta) \cdot hc^3 + 12 \cdot Qm \cdot hc^2 \cdot tm + Qm \cdot tm^3 - 6 \cdot Q(\theta) \cdot hc^2 \cdot tm + 4 \cdot Q2 \cdot hc^3 + 6 \cdot Q2 \cdot hc^2 \cdot tm + 3 \cdot Q2 \cdot hc \cdot tm^2) \cdot (-\tan(\gamma) \cdot ledge \cdot \sin(\theta) + 2 \cdot ledge \cdot \cos(\theta) + 2 \cdot \tan(\gamma) \cdot X - 2 \cdot Y) \ *$$

section 5

$$As5 := 2 \cdot ledge^2 \cdot \sin(\theta) \cdot (-\tan(\gamma) \cdot \sin(\theta) + 2 \cdot \cos(\theta)) \cdot (Q2 \cdot hc + Q(\theta) \cdot hc + Qm \cdot tm) \ *$$

$$Bs5 := -ledge^2 \cdot \sin(\theta) \cdot hc \cdot (\sin(\theta) \cdot \tan(\gamma) - 2 \cdot \cos(\theta)) \cdot (Q2 \cdot hc - Q(\theta) \cdot hc + 2 \cdot Qm \cdot tm - Q(\theta) \cdot tm - Q2 \cdot tm) \ *$$

$$Ds5 := \frac{-1}{6} \cdot ledge^2 \cdot \sin(\theta) \cdot (\sin(\theta) \cdot \tan(\gamma) - 2 \cdot \cos(\theta)) \cdot (4 \cdot Q(\theta) \cdot hc^3 + 3 \cdot Q2 \cdot hc \cdot tm^2 + 12 \cdot Qm \cdot hc^2 \cdot tm + 3 \cdot Q(\theta) \cdot hc \cdot tm^2 - 6 \cdot Q2 \cdot hc^2 \cdot tm + 4 \cdot Q2 \cdot hc^3 + Qm \cdot tm^3 + 6 \cdot Q(\theta) \cdot hc^2 \cdot tm) \ *$$

section 6

$$As6 := \frac{-1}{4} \cdot t \cdot Qm \cdot ledge \cdot X \cdot \sin(\theta) \cdot (\tan(\gamma) \cdot X \cdot ledge \cdot \sin(\theta) - 4 \cdot ledge \cdot \cos(\theta) + 2 \cdot Y) \ *$$

$$Bs6 := 0$$

$$Ds6 := \frac{-1}{48} \cdot t^3 \cdot Qm \cdot ledge \cdot X \cdot \sin(\theta) \cdot (\tan(\gamma) \cdot X \cdot ledge \cdot \sin(\theta) - 4 \cdot ledge \cdot \cos(\theta) + 2 \cdot Y) \ *$$

section 7

$$As7 := \frac{-1}{4} \cdot t \cdot Qm \cdot (2 \cdot ledge \cdot \sin(\theta) - X) \cdot (2 \cdot ledge \cdot \tan(\gamma) \cdot \sin(\theta) - 4 \cdot ledge \cdot \cos(\theta) + 2 \cdot Y - \tan(\gamma) \cdot X) \ *$$

$$Bs7 := 0$$

$$Ds7 := \frac{1}{48} \cdot t^3 \cdot Qm \cdot (2 \cdot ledge \cdot \sin(\theta) - X) \cdot (-2 \cdot ledge \cdot \tan(\gamma) \cdot \sin(\theta) + 4 \cdot ledge \cdot \cos(\theta) - 2 \cdot Y + \tan(\gamma) \cdot X) \ *$$

section 8

$$As8 := \frac{1}{4} \cdot t \cdot Qm \cdot (-X + 2 \cdot ledge \cdot \sin(\theta)) \cdot (-2 \cdot ledge \cdot \tan(\gamma) \cdot \sin(\theta) + 4 \cdot ledge \cdot \cos(\theta) - 3 \cdot \tan(\gamma) \cdot X + 2 \cdot Y) \ *$$

$$Bs8 := 0$$

$$Ds8 := \frac{-1}{48} \cdot t^3 \cdot Qm \cdot (-X + 2 \cdot ledge \cdot \sin(\theta)) \cdot (2 \cdot ledge \cdot \tan(\gamma) \cdot \sin(\theta) - 4 \cdot ledge \cdot \cos(\theta) + 3 \cdot X \cdot \tan(\gamma) - 2 \cdot Y) \ *$$

section 9

$$As9 := \frac{1}{4} \cdot t \cdot Qm \cdot (2 \cdot ledge \cdot \sin(\theta) - X) \cdot (-2 \cdot ledge \cdot \tan(\gamma) \cdot \sin(\theta) + 4 \cdot ledge \cdot \cos(\theta) - 4 \cdot Y + \tan(\gamma) \cdot X) \ *$$

$$Bs9 := 0$$

$$Ds9 := \frac{1}{48} \cdot t^3 \cdot Qm \cdot (2 \cdot ledge \cdot \sin(\theta) - X) \cdot (-2 \cdot ledge \cdot \tan(\gamma) \cdot \sin(\theta) + 4 \cdot ledge \cdot \cos(\theta) - 4 \cdot Y + \tan(\gamma) \cdot X) \ *$$

APPENDIX 4: PROPOSED CLPT MODEL RESULTS FOR AXIAL, FLEXURAL AND TORSIONAL RIGIDITIES FROM CHAPTER 8

The following figures are the predicted flexural, torsional and axial rigidities used to decide of the most appropriate fibre/resin combinations to manufacture medical catheters (Section 8.2). The appendix is separated into three sections. The first contains the figures that were used with the decision matrix (Table 8-4); the second contains, for completeness, the rigidity figures of the combinations that were eliminated; finally the last section contains the comparison between CGWS and predicted axial rigidities of Kevlar 49 with silicone and polyurethane resins model catheters.

To review the conclusions of Chapter 8, based on the results, using Kevlar fibre and either RTV11 or RTV118 silicone resins or RP6443 or RP6434 polyurethane resins can provide adequate flexural and torsional rigidity while RP6443 and RTV11 resins provide the maximum axial rigidity for a braided medical catheter.

Considering such factors as viscosity and gel time, RTV118 was eliminated since its viscosity is 20,000 centipoises. Of the remaining three resins, RP6443 and RTV11 were selected for further study since they possessed the two highest axial and torsional rigidities in combination with Kevlar-49 fibres. Both resins also have acceptable viscosities and gel times for fibre wetting purposes.

Figures used in the elimination process

Flexural rigidity

The following figures illustrate the flexural rigidity of all fibre and resin combinations.

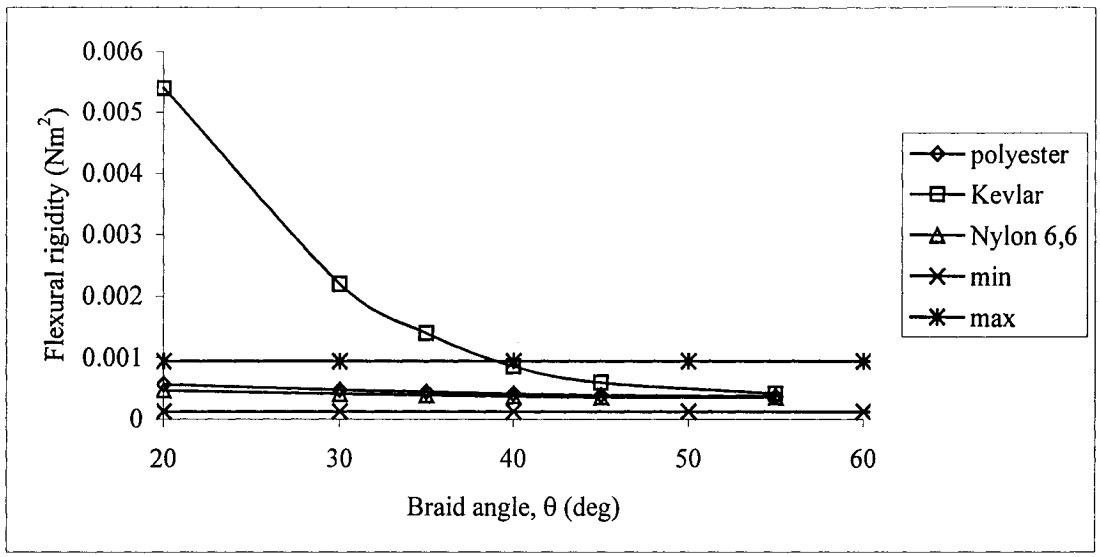

Figure 1: Flexural rigidity of a composite composed of Scotchweld 2216 resin for all three fibres at various braid angles

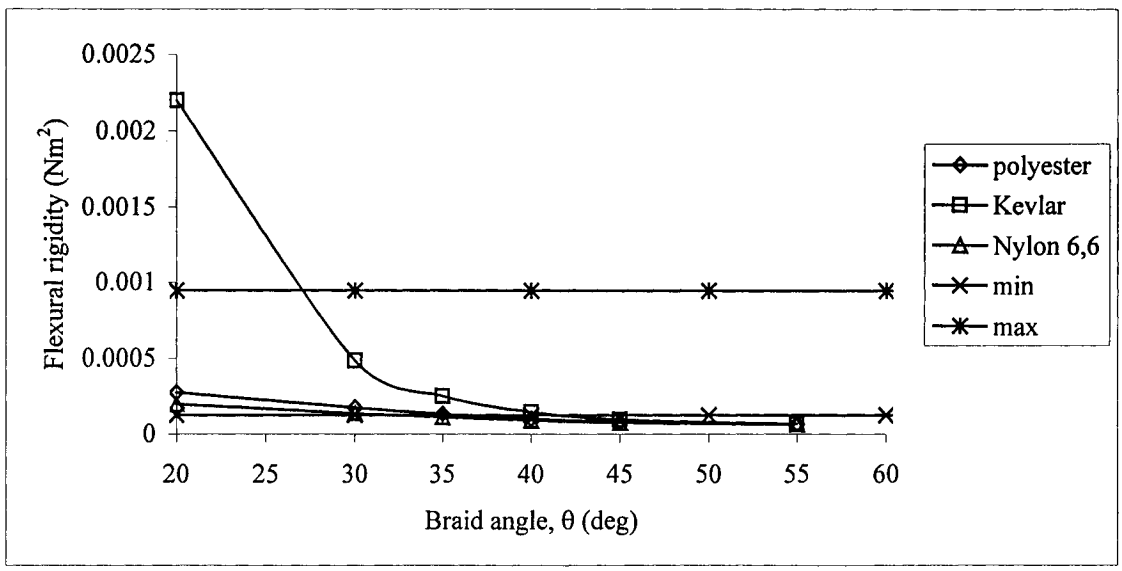

Figure 2: Flexural rigidity of a composite composed of RTV11 resin for all three fibres at various braid angles

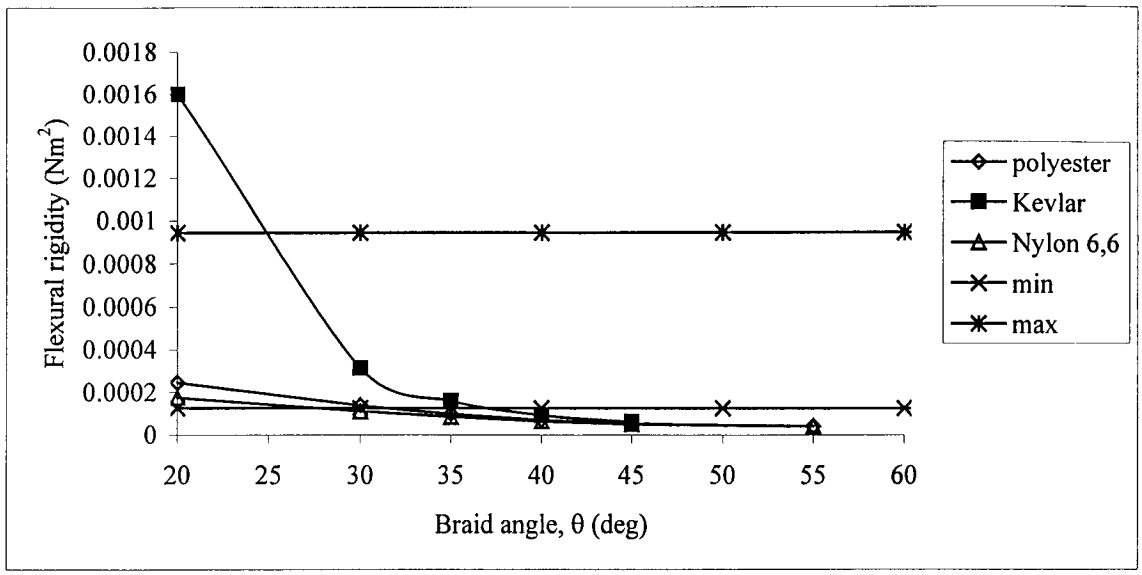

Figure 3: Flexural rigidity of a composite composed of RTV118 resin for all three fibres at various braid angles

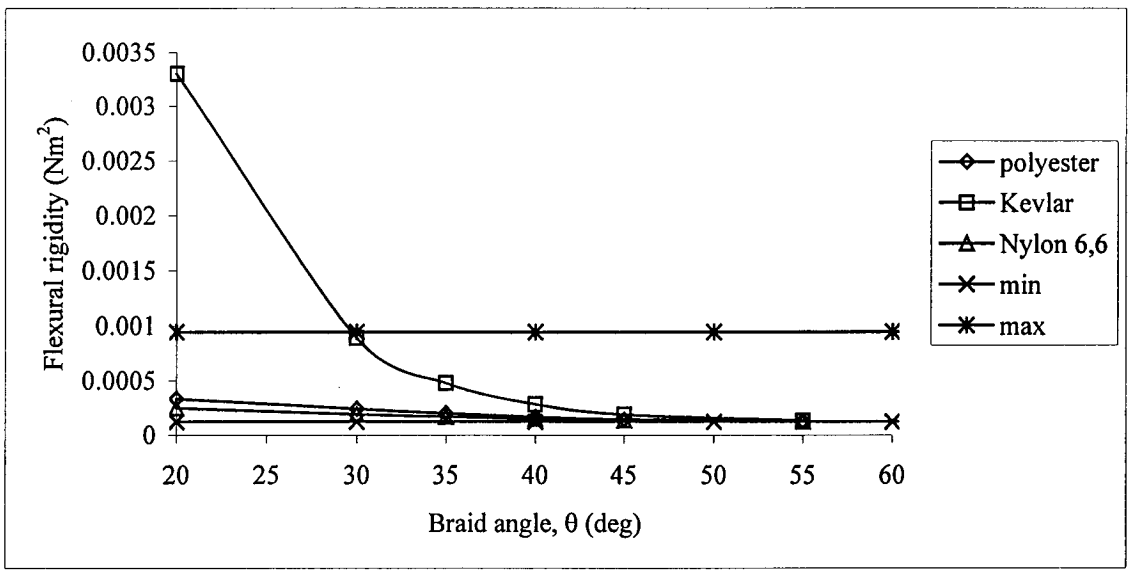

Figure 4: Flexural rigidity of a composite composed of RP6443 resin for all three fibres at various braid angles

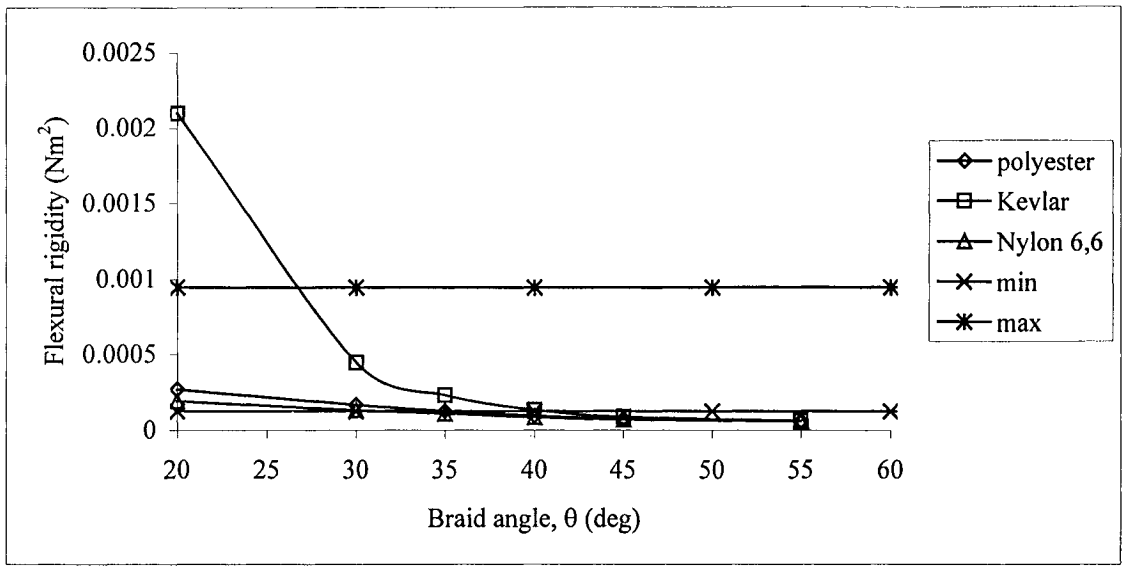

Figure 5: Flexural rigidity of a composite composed of RP6434 resin for all three fibres at various braid angles

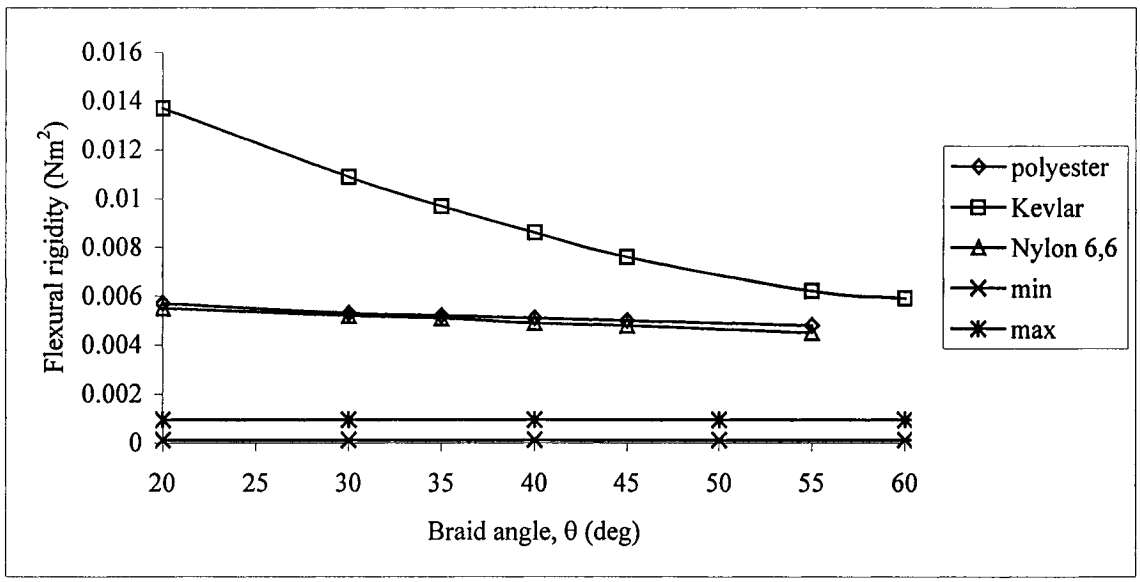

Figure 6: Flexural rigidity of a composite composed of Epon 825/A1482 resin for all three fibres at various braid angles

Torsional rigidity

The following figures illustrate the torsional rigidity of all fibre and resin combinations after both epoxies were eliminated.

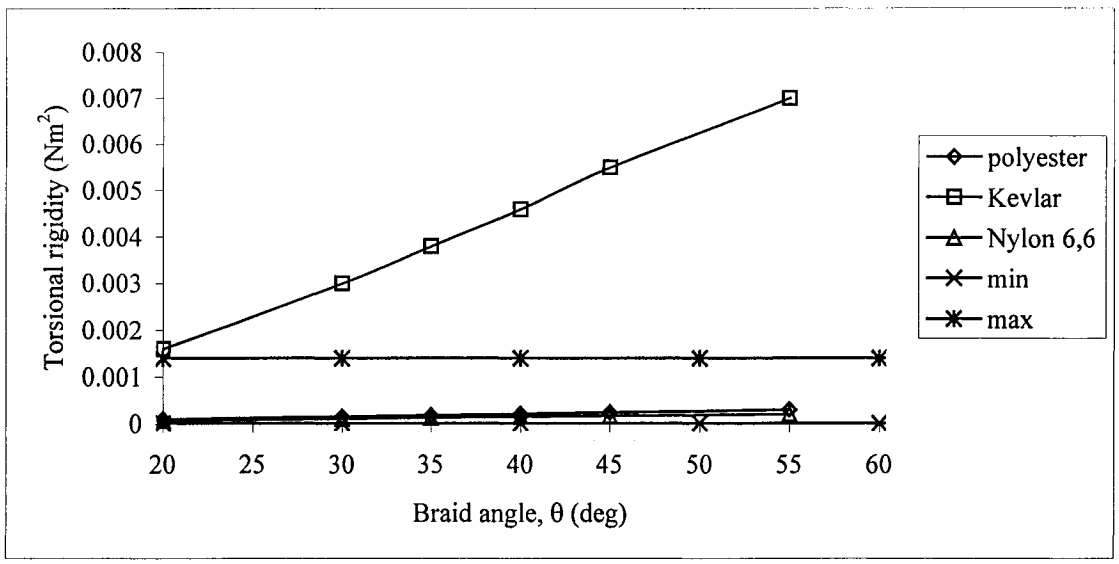

Figure 7: Torsional rigidity of a composite composed of RTV11 resin for all three fibres at various braid angles

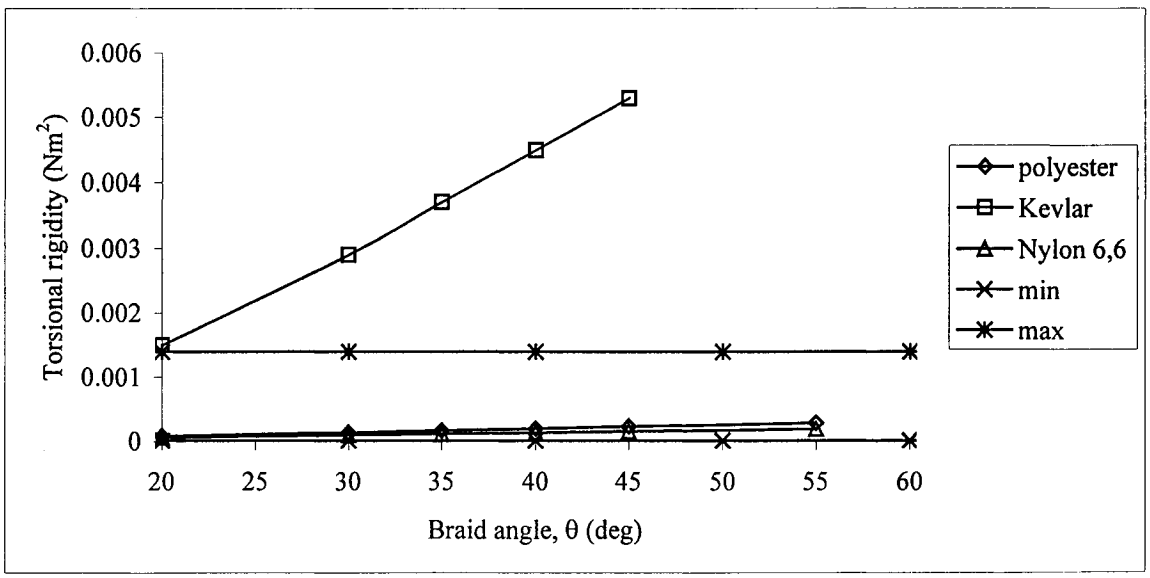

Figure 8: Torsional rigidity of a composite composed of RTV118 resin for all three fibres at various braid angles

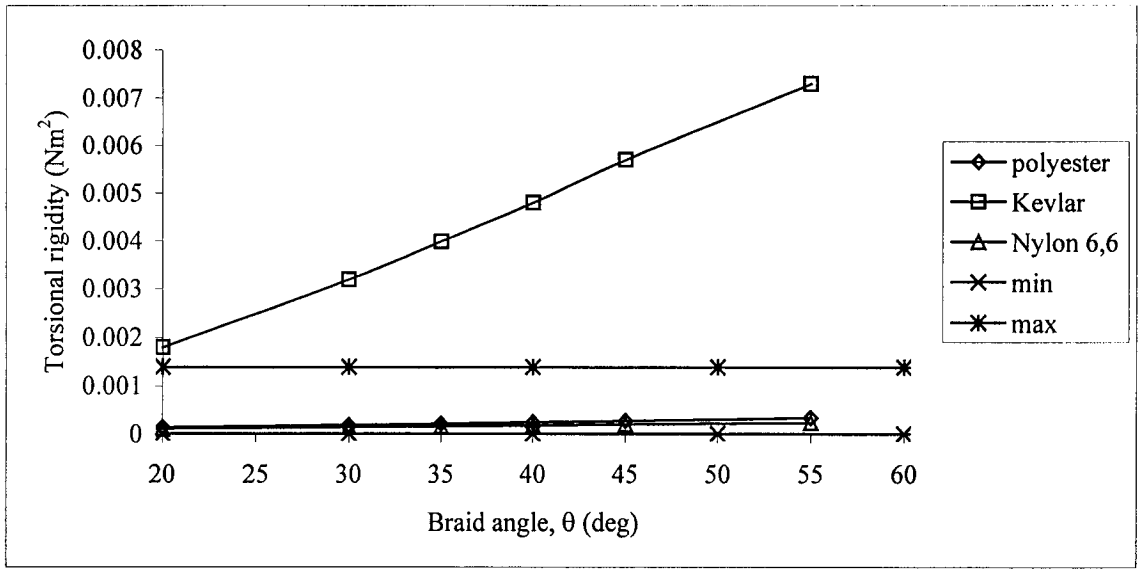

Figure 9: Torsional rigidity of a composite composed of RP6443 resin for all three fibres at various braid angles

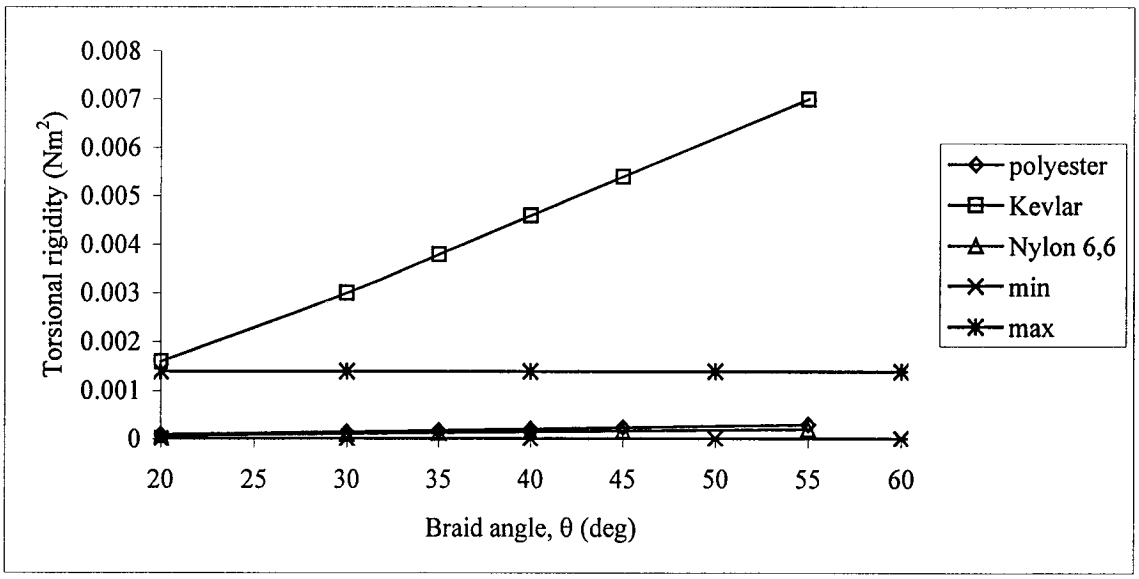

Figure 10: Torsional rigidity of a composite composed of RP6434 resin for all three fibres at various braid angles

Axial rigidity

The following figures illustrate the axial rigidity of all fibre and resin combinations. Polyester and Nylon fibres are eliminated, but are kept in the figure for comparison purposes.

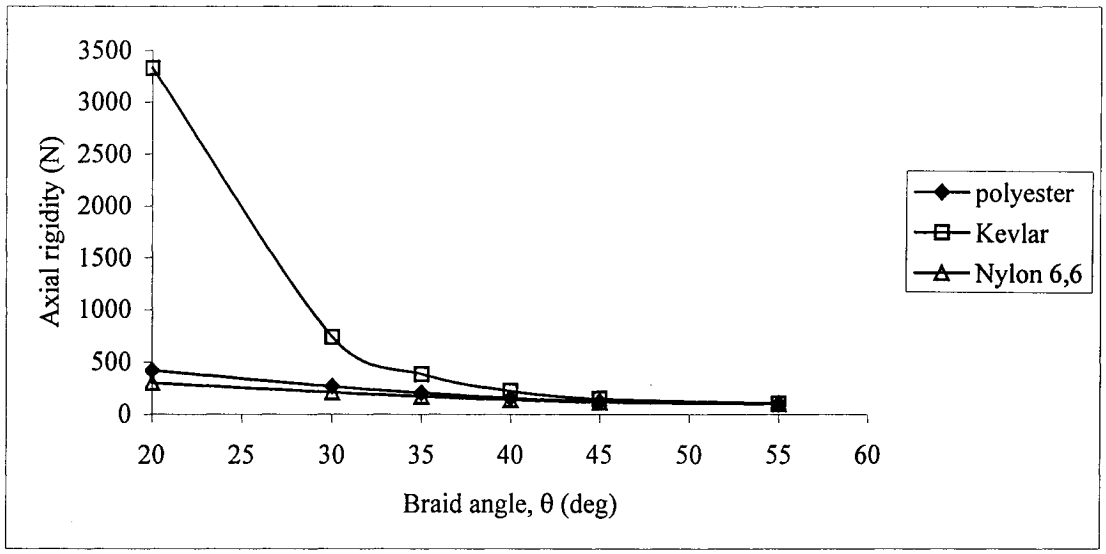

Figure 11: Axial rigidity of a composite composed of RTV11 resin for all three fibres at various braid angles

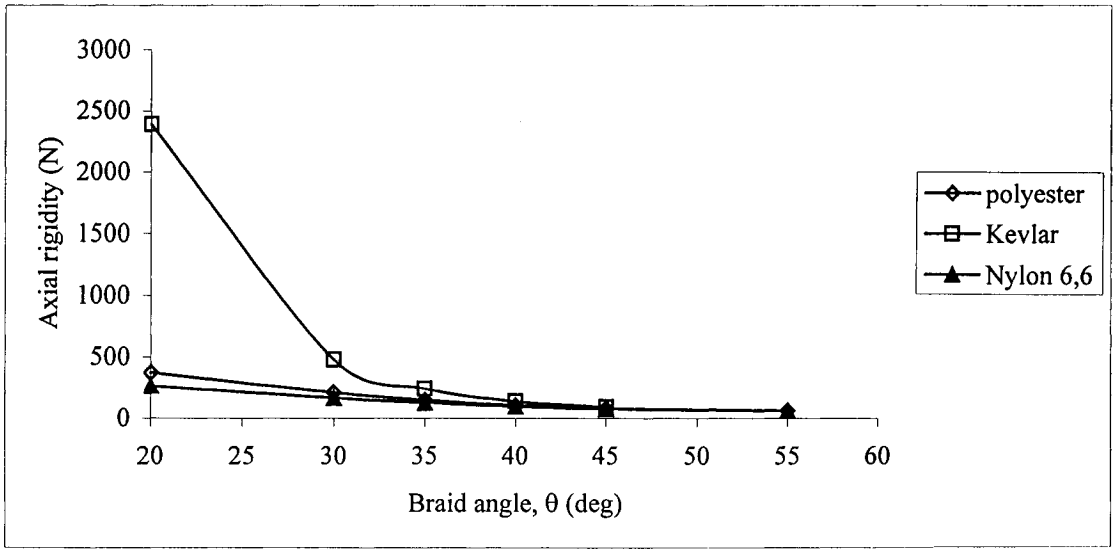

Figure 12: Axial rigidity of a composite composed of RTV118 resin for all three fibres at various braid angles

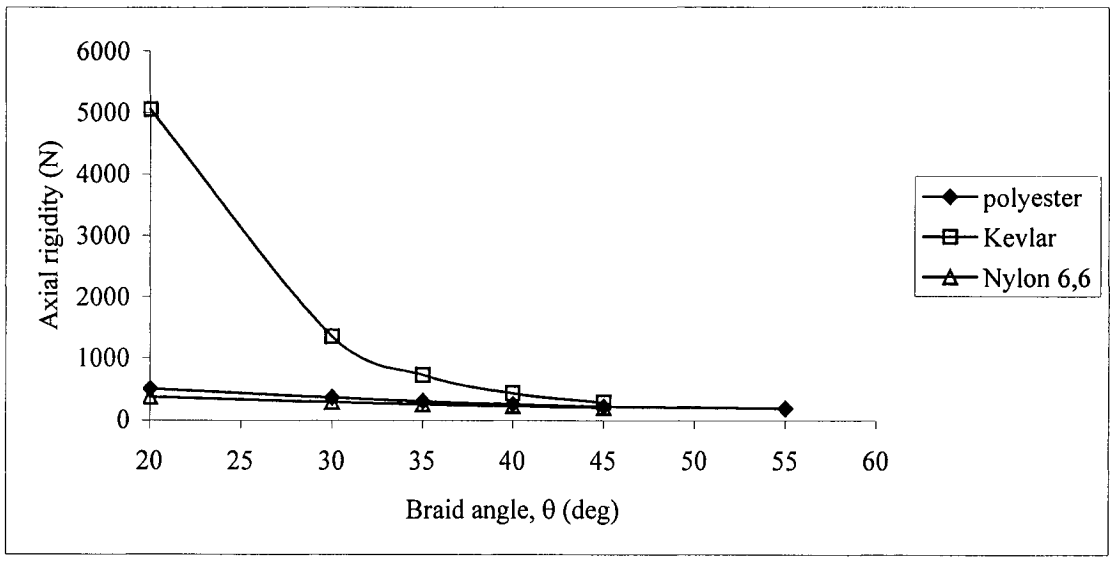

Figure 13: Axial rigidity of a composite composed of RP6443 resin for all three fibres at various braid angles

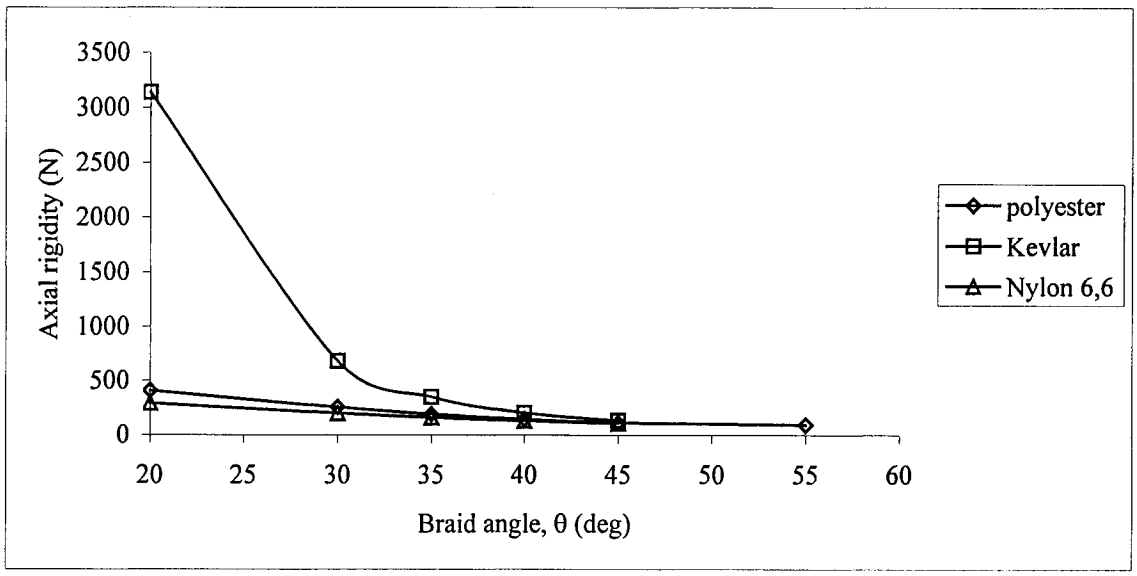

Figure 14: Axial rigidity of a composite composed of RP6434 resin for all three fibres at various braid angles

Rigidity figures of eliminated combinations

The following figures illustrate the torsional and axial rigidity of all fibres with both epoxy resin combinations.

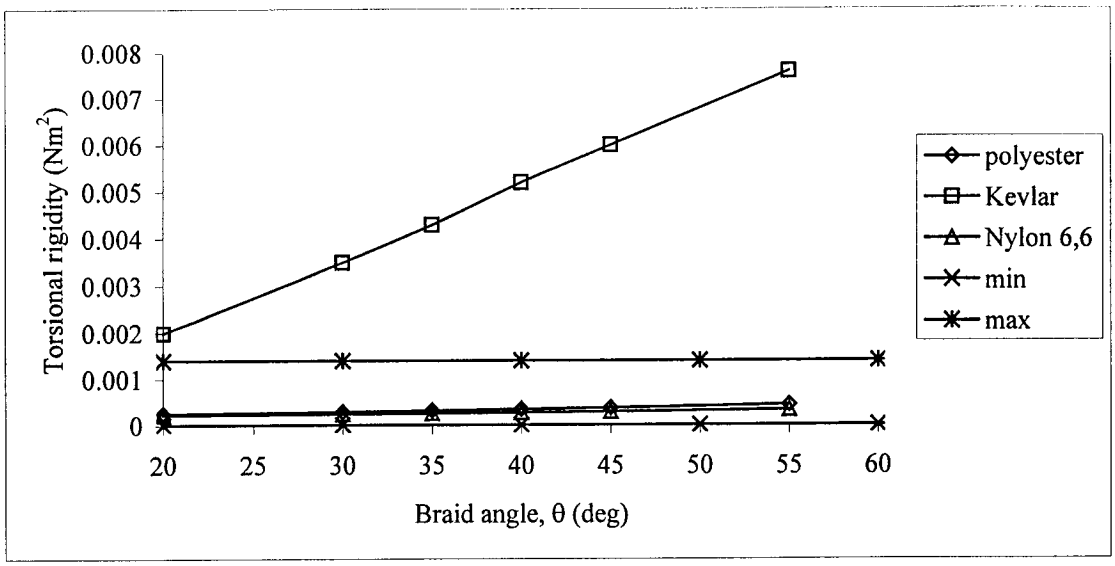

Figure 15: Torsional rigidity of a composite composed of Scotchweld 2216 resin for all three fibres at various braid angles

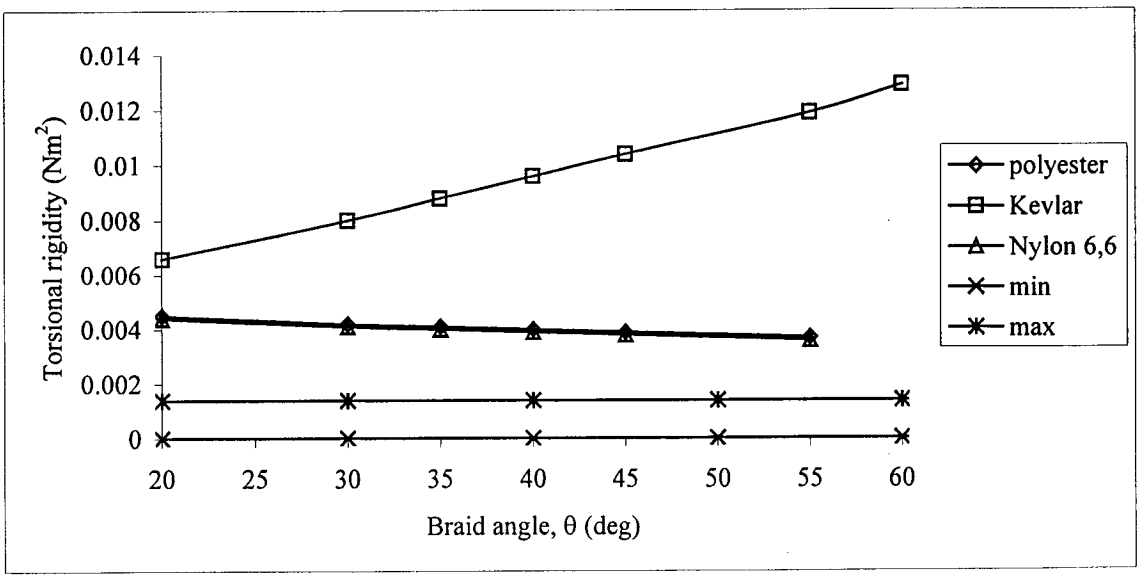

Figure 16: Torsional rigidity of a composite composed of Epon 825/ A1482 resin for all three fibres at various braid angles

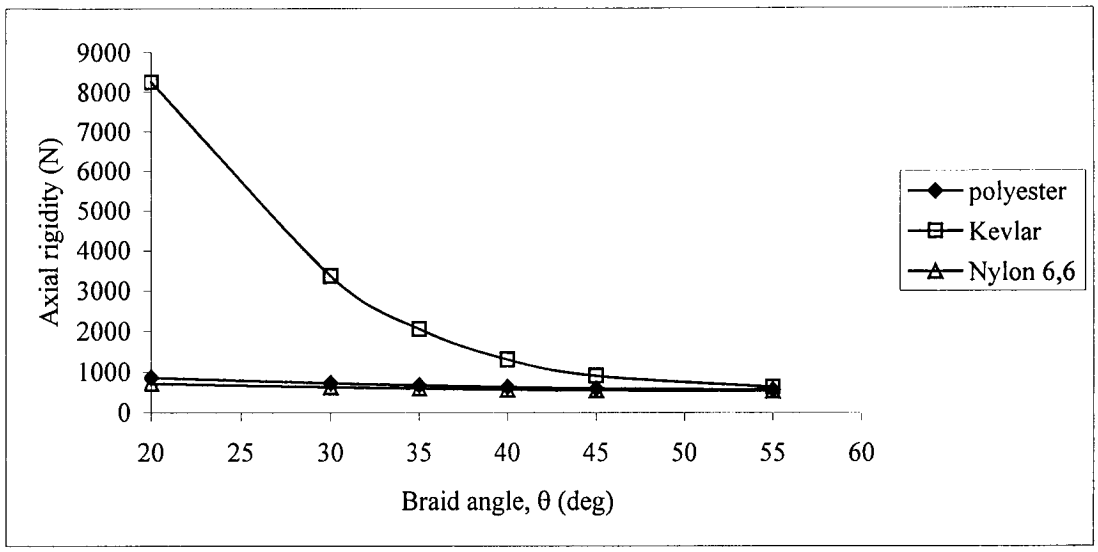

Figure 17: Axial rigidity of a composite composed of Scotchweld 2216 resin for all three fibres at various braid angles

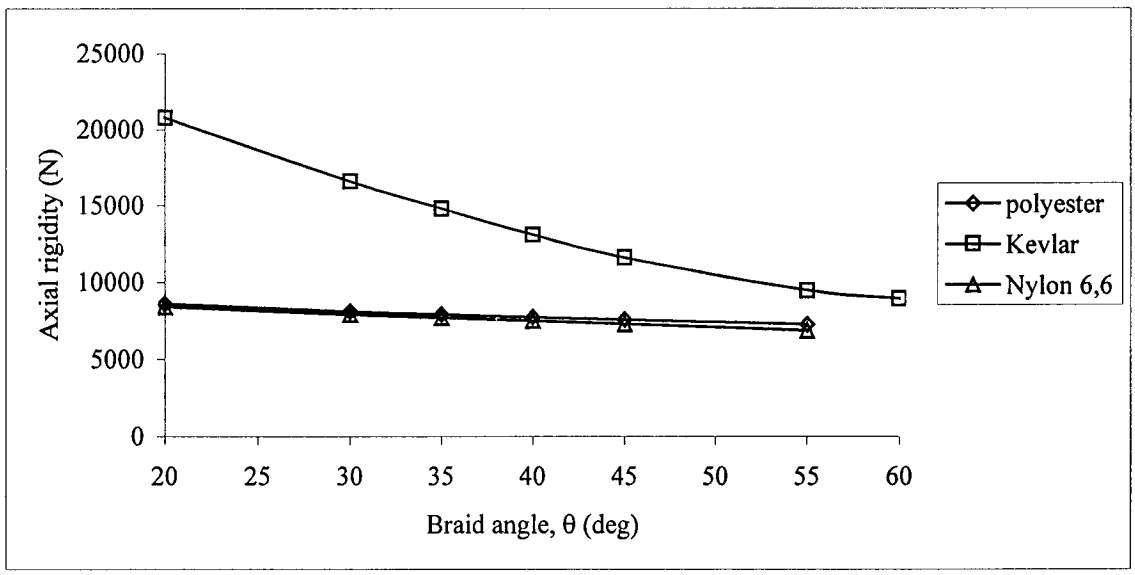

Figure 18: Axial rigidity of a composite composed of Epon 825/A1482 resin for all three fibres at various braid angles

CGWS axial rigidity

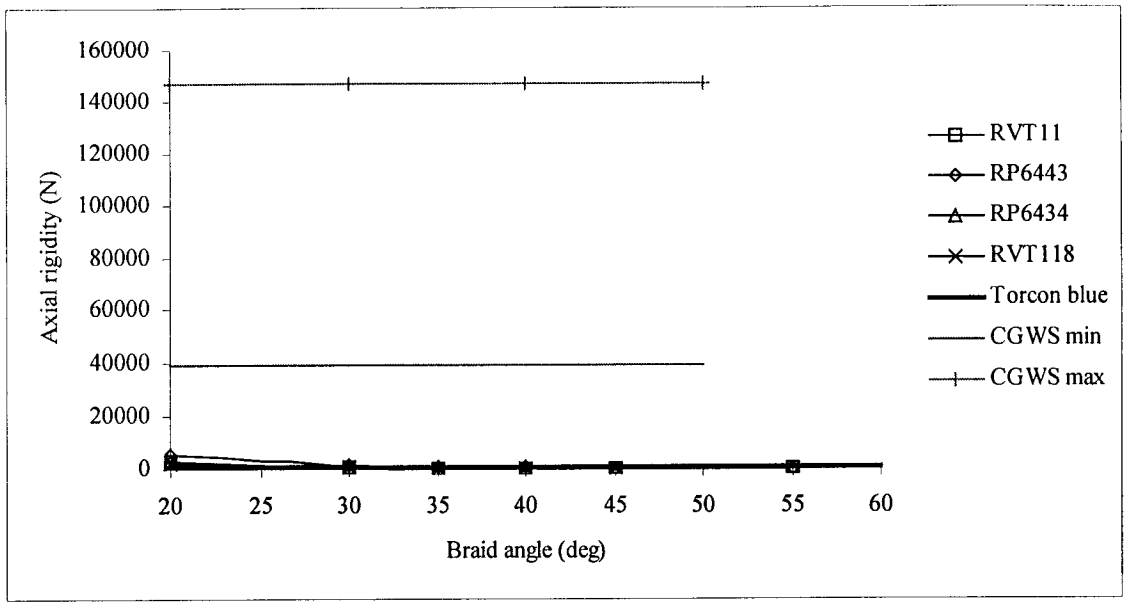

Figure 19: Comparison of the axial rigidity of a composite composed polyurethane and silicone resins with Kevlar 49 fibres and the maximum and minimum axial rigidity of CGWS at various braid angles

APPENDIX 5: REPRESENTATIVE SHEAR MODULUS CALCULATION FOR TORSION TESTS.

Appendix 5 contains representative results of the analysis performed to measure braid shear modulus for RP6443. All following information relates to Section 9.2.1.2. Figure 1 illustrates the linear stress strain behaviour of RP6443.

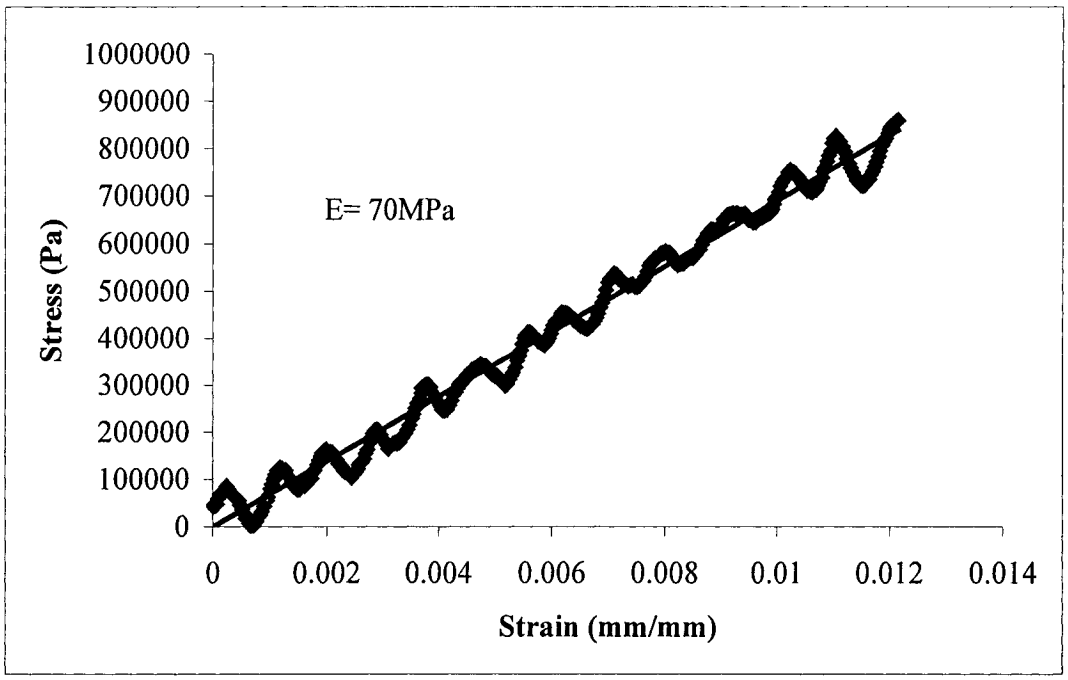

Figure 1: Representative stress strain curve for RP6443 resin. Results are linear but noise is obvious.

During the torsion tests, which were performed in this work, shear modulus was calculated as follows:

$$G_{xy} = \frac{T \cdot L}{J\phi} \qquad (1)$$

Using the three following figures, Gxy is calculated as:

$$G_{xy} = \frac{\Delta T \cdot L}{J(\Delta\phi_2 - \Delta\phi_1)} \tag{2}$$

where L is the distance between point 1 and 2 on the torsion specimen and J is the polar moment inertia of the tube cross-section. The torque difference is calculated as follows:

$$\Delta T = T_{max} - T_{min} \tag{3}$$

and the difference in twist angle is calculated as follows:

$$\Delta\phi_i = \phi_{i\,max} - \phi_{i\,min} \text{ for } i = 1,2 \tag{4}$$

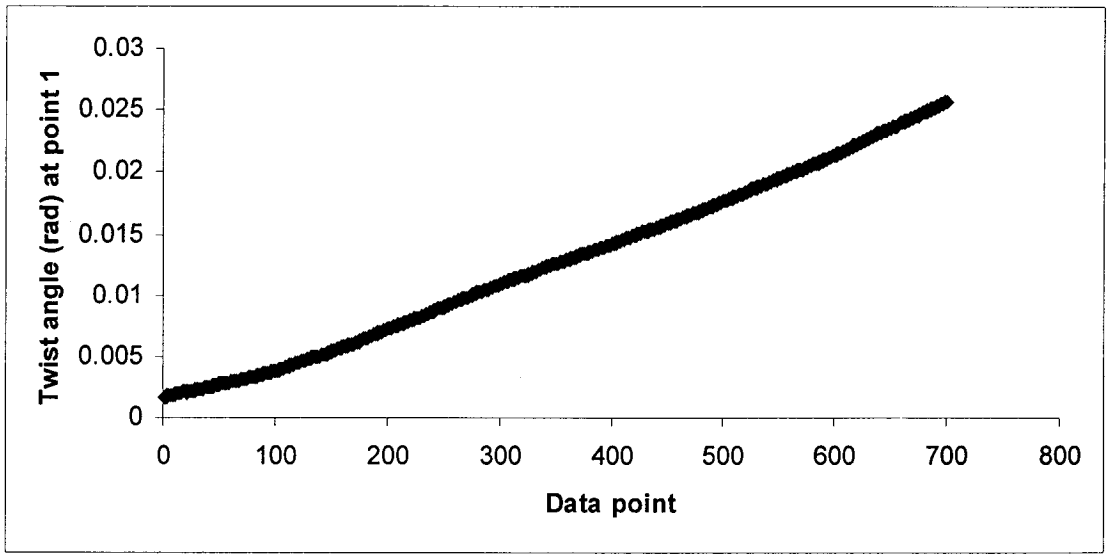

Figure 2: Twist angle at point 1 on torsion specimen.

From Figure 2, it was measured that $\Delta\phi_1 = 0.02192\text{rad}$.

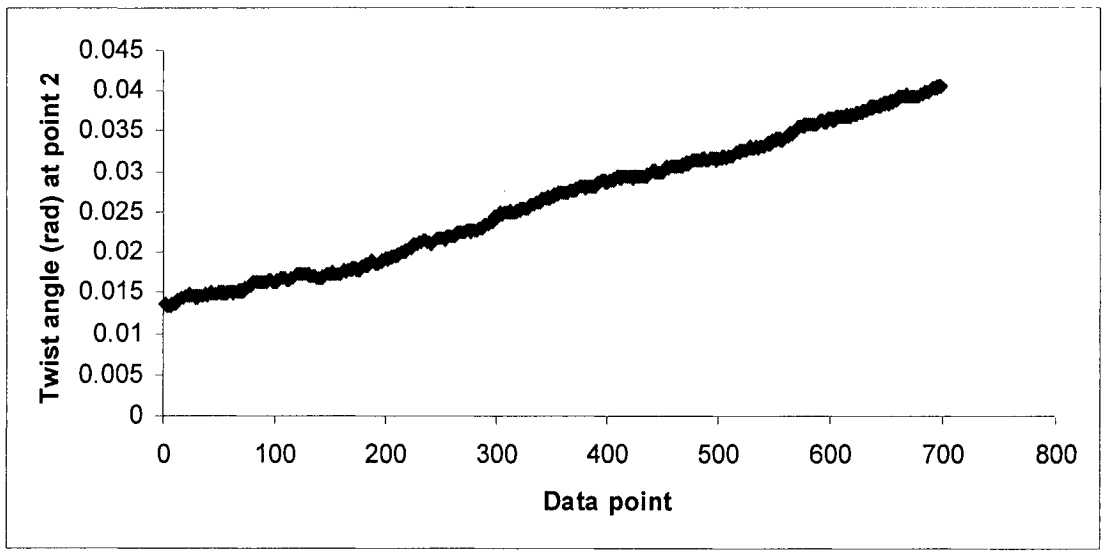

Figure 3: Twist angle at point 2 on torsion specimen.

From Figure 3, it was measured that $\Delta\phi_1 = 0.0242\text{rad}$.

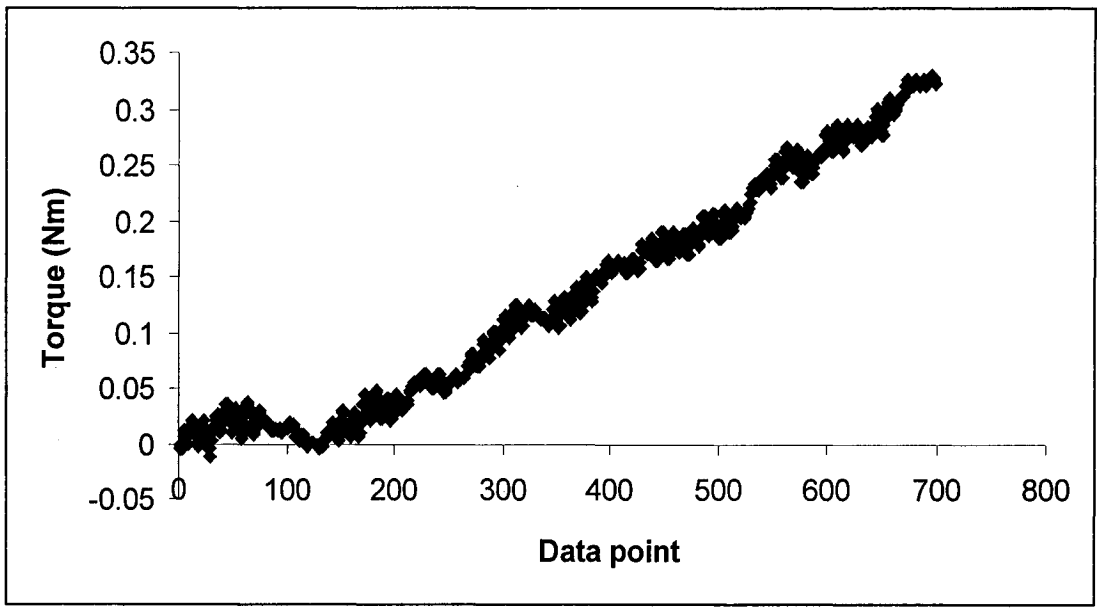

Figure 4: Applied torque to torsion specimen.

Finally, from Figure 4, it was measured that $\Delta T = 0.35\text{rad}$. Therefore, from the above information, the shear modulus is calculated to be 3.9 GPa.